# Interaction of silica nanoparticles with chalk and sandstone minerals

Adsorption, Fluid/Rock Interactions in the absence and presence of hydrocarbons

by

Rockey Abhishek

Thesis submitted in fulfillment of
the requirements for degree of
DOCTOR OF PHILOSOPHY
(Ph.D.)


Faculty of Science and Technology
Department of Energy and Petroleum Technology
2019

University of Stavanger
N-4036 Stavanger
NORWAY
www.uis.no



ISBN: 978-82-7644-839-9

ISSN: 1890-1387

PhD Thesis UiS no. 452

*This work is dedicated with genuine gratitude to my father*

*Mr. Nagendra Yadav*

# Acknowledgments

Writing this PhD thesis has been the most daunting and fulfilling endeavor of academic career and it would not have been possible without the support and encouragement I received from various people along the way.

First and foremost, I would like to express deep gratitude towards my supervisor Prof. Aly A. Hamouda for his constant and unwavering support over the three years it took to execute this PhD project. Without his guidance and critical comments this project would not have been possible. I am also grateful to the University of Stavanger (UiS), Norway for funding this project.

I would like to thank the engineers and technicians at the Department of Energy and Petroleum Technology, UiS for assisting me with building and troubleshooting various experimental setups used in this work. I would like to thank Krzysztof Nowicki in particular for his assistance with building the core flooding setups. I would like to thank Mona W. Minde (UiS) for helping with the SEM imaging and Prof. Lutz Eichacker (UiS) for providing access to the DLS equipment. I am grateful for the enthusiastic cooperation of Ivan Muzin, Amr Ayoub and Faisal Abdulhameed during the course of this work.

I would like to express my gratitude towards my family back in India. My parents Mr. Nagendra Yadav and Mrs. Manju Yadav and my beloved sister Vandana Yadav for supporting and encouraging me throughout the course of this PhD. I am especially grateful to my wife Nikita Karandikar for putting up with me during the extended periods when I had to focus on my work. And finally I would like to thank Deepak Singh, Raj Patil and Pranav Punde for their constant warmth, and friendship.

# Abstract

Conventional oil production from petroleum reservoirs generally leaves more that 50% of the original oil in place unrecovered. This residual oil is the target of various enhanced oil recovery (EOR) techniques that involve fluid injection into the reservoir which supplements oil recovery by interacting with the rock-oil-brine system. Silica nanofluids have emerged as a promising fluid for EOR. Nanofluids are colloidal suspensions of nanoparticles (NP) dispersed in a suitable fluid. Over the past decade, a lot of research has focused on investigating silica nanofluids for EOR applications. This thesis addresses the mechanisms for silica NP adsorption and fluid/rock interactions during nanofluid injection. Understanding these processes would aid efficient design of nanofluid floods.

In chapter 1 of the thesis, a brief background of the research conducted into silica nanofluids for EOR is discussed. Wettability alteration, interfacial tension reduction and structural disjoining pressure due to NP wedge formation are the major mechanisms attributed to incremental oil recovery by silica NPs. However, the adsorption mechanisms of silica NPs and their effect on fluid/rock interactions are not well understood. This thesis focusses on the adsorption of silica NPs for sandstone and chalks mineral surfaces and their effect on fluid/rock interactions. The materials and methods used in this study are presented in chapter 3.

Chapter 4 addresses the surface modification of berea sandstone by the in-house silica nanofluids. Fines migration during water injection, especially in the case of low salinity, is a potential problem in sandstone reservoirs. It is shown that adsorption of silica NPs in berea sandstone reduces production and migration

of fines. This is due to reduction of direct contact between the flooding fluid and rock minerals. The reduction of the fines was indicated by the reduced pressure drop, i.e. reduce the flow resistance of the fluid during the post flush of the NPs' slug. In addition, it was shown that the adsorption of silica NPs modify sandstone surface and make the interaction between the modified surface and the fine particles more attractive. So, modified surface acts as a "collector" for the fines.

The in-house silica nanofluids show limited stability of the dispersed NPs. To proceed with the objectives of this work, it was decided, then, to acquire a more stable commercial silica nanofluid (DP9711 from Nyacol Nano technologies). The nanofluids' stability was confirmed at our laboratory. Two types of adsorption experiments were performed: (1) static adsorption of silica NPs on minerals and (2) dynamic adsorption of silica NPs injected into sandstone and chalk cores. The kinetic aspects of silica NP adsorption were also addressed. The static adsorption was done to address the silica NPs adsorption affinity to the different minerals (calcite, quartz and kaolinite) and the kinetics of the adsorption process (chapter 5). The dynamic adsorption of the injected silica NPs was performed to address the extent of the fluid/rock (sandstone and chalk) interactions in chapter 6. Fluid/rock interactions during oil recovery by continuous injection of silica nanofluids are addressed in chapter 7.

Silica NPs shows high adsorption affinity towards calcite mineral followed by quartz, and the lowest adsorption affinity towards kaolinite. The scanning electron microscopy (SEM) images did not show pore throat blockage. This was also confirmed by the improved injectivity during nanofluids injection. Silica NPs' adsorption process on quartz and calcite was best fitted to pseudo second order kinetic model. Both the rate of adsorption and the level of equilibrium adsorption increases with the salinity.

The adsorption of NPs is largely influenced by the fluid pH for chalk and sandstones. Increased alkalinity during low salinity flooding favours NP desorption. However, dynamic adsorption of NPs injected into chalk and sandstone core showed high irreversible adsorption at elevated salinity (synthetic seawater: SSW).

It is interesting to see that in the limited oil recovery experiments; mineral dissolution, suppression of the ion exchange process and loss of cementing minerals caused by low salinity injection, were reduced by silica nanofluids. It is also shown that the silica NPs modifies the mineral surface and made the interaction energy between the fines and the mineral surface more attractive for both LSW and SSW. In other words, the silica nanofluids reduce the probability for formation damage associated with low salinity water injection in sandstone reservoirs. Some incremental oil recovery was observed with silica NPs. However, limited experiments were performed on oil recovery, hence the recovery by nanofluids has not been optimized in this work.

NP adsorption on chalk significantly reduced calcite dissolution by about 30%. That is the silica nanofluid reduced the detrimental effect of low salinity flooding on chalk matrix integrity which is one of the major concerns in chalk reservoirs. As mentioned earlier oil recovery optimization was not performed. The results from this work identified that silica nanofluids can potentially increase oil recovery from chalks as compared to low salinity injection alone.

The main outcome of this work suggests a synergy between silica NPs and low salinity flooding technique for EOR wherein, addition of silica NPs to low salinity water can reduce formation damage in sandstone reservoirs and reduce the risk of reservoir subsidence due to calcite dissolution in chalk reservoirs.

# List of Publications

Paper I — Abhishek, R**.** and A. A. Hamouda (2017). "**Effect of Various Silica Nanofluids: Reduction of Fines Migrations and Surface Modification of Berea Sandstone.**" Applied Sciences 7(12): 1216. Special issue: Nanotech for Oil and Gas, MDPI Publication.

Paper II — Abhishek, R., A. A. Hamouda and A. Ayoub (2018). "**Effect of Silica Nanoparticles on Fluid/Rock Interactions during Low Salinity Water Flooding of Chalk Reservoirs.**" Applied Sciences 8(7): 1093. Special issue: Nanofluids and Their Applications, MDPI Publications.

Paper III — Abhishek, R., A. A. Hamouda and I. Murzin (2018). "**Adsorption of silica nanoparticles and its synergistic effect on fluid/rock interactions during low salinity flooding in sandstones**." Colloids and Surfaces A: Physicochemical and Engineering Aspects 555: 397-406. Elsevier Publications.

Paper IV — A. A. Hamouda, Abhishek, R. (2019). "**Effect of salinity on Silica Nanoparticle adsorption kinetics and mechanisms for fluid/rock interaction with calcite.**" Nanomaterials, *9*(2): 213. Special issue: Applications of Nano-Technology for Oil Recovery, MDPI Publications.

Paper V — Abhishek, R., A. A. Hamouda and F. Abdulhameed (2019). "**Adsorption kinetics and Enhanced Oil Recovery by Silica nanoparticles in sandstone**." Petroleum Science and Technology, DOI: 10.1080/10916466.2019.1587455.

# Table of Contents

# List of Figures

# List of Tables

# Abbreviations

| | |
|---|---|
| OOIP | Original oil in place |
| IFT | Interfacial tension |
| EOR | Enhanced oil recovery |
| NP | Nanoparticle |
| NF | Nanofluid |
| PMAA | Polymethacrylic acid |
| CSC | Critical salt concentration |
| MPTMS | (3-Mercaptopropyl) trimethoxysilane |
| SA | Stearic acid |
| NN-DMDA | N,N-Dimethyldodecylamine |
| BR | Berea |
| SK | Stevens Klint chalk |
| DIW | Deionised water |
| SSW | Synthetic sea water |
| LSW | Low salinity water |
| DP | Silica Nano particles in DP9711 nanofluid |
| ABS | Absorption |
| UV/Vis | Ultraviolet/visible |
| PV | Pore volume |
| dP | Differential pressure drop |
| PVP | Polyvinylpyrrolidone |

| | |
|---|---|
| IC | Ion chromatograph |
| Swi | Initial water saturation |
| DLS | Dynamic Light Scattering |
| ESA | Electrostatic Attenuation |
| SEM | Scanning electron microscopy |
| EDX | Energy-dispersive X-ray spectroscopy |
| DLVO | Derjaguin-Landau-Verwey-Overbeek |
| $V_t$ | Total interaction potential |
| $V_{LVA}$ | London-van der Waal interaction |
| $V_{EDLR}$ | electric double layer interaction |
| $V_{BR}$ | Born repulsion |
| $V_{t,ND}$ | No dimensional total interaction potential |
| $h$ | Separation distance |
| $T$ | Temperature |
| $K_B$ | Boltzmann constant |
| $a_p$ | Particle radius |
| $A_{132}$ | Hamaker's constant |
| $\varepsilon_0$ | Permittivity of free space |
| $\varepsilon_i$ | Dielectric constant of species i |
| $\zeta_p$ | Surface potentials of particle |
| $\zeta_s$ | Surface potentials of surface |
| $\kappa$ | Inverse Debye length |
| $\sigma$ | Atomic collision diameter |

| | |
|---|---|
| $w_i$ | Weight intensity of each size class |
| $t$ | Time |
| $q(t)$ | Adsorption at time $t$ |
| $q_{eq}$ | Adsorption at equilibrium |
| $k_1$ | Pseudo first order rate |
| $k_2$ | Pseudo second order rate |
| $m$ | Slope |
| $c$ | Intercept |
| $R^2$ | correlation coefficient |
| IPD | Intraparticle diffusion |
| $K$ | Intraparticle diffusion rate |
| $C$ | Boundary layer effect |
| $\eta_i$ | Refractive index of species i |
| $\nu_e$ | Main electron absorption frequency in the ultraviolet region |
| $N_A$ | Avogadro number |
| $I$ | Ionic strength |
| $e$ | Elementary charge of electron |
| $c_i$ | Ion concertation of the $i^{th}$ species |
| $Z_i$ | Valence number of the $i^{th}$ species |
| $R_i$ | Initial adsorption factor |
| $t_{eq}$ | Time to reach equilibrium adsorption |
| $m_{NPi}$ | Total NP injected |
| $m_{Ao}$ | Excess NP produced in region A |

| | |
|---|---|
| $m_{NP}$ | Total NP available for adsorption |
| $m_{Bo}$ | Total NP produced in equilibrium region B |
| $m_{rev}$ | Reversibly adsorbed NP |
| $m_{Co}$ | Total NP produced during desorption phase in region C |
| $m_{irr}$ | Amount of NP irreversibly adsorbed in the core |
| $NP_{Bo}$ | NP production in region B |
| $Dsp_C$ | Desorption in region C |
| $Ads_{irr}$ | Total irreversible adsorption/remained in core |
| $c_{inj}$ | injected concentration of nanofluid |
| $V$ | Volume |
| $V_{sl}$ | Slug volume of nanofluid |
| $c_{oA}(V)$ | Effluent concentration in region A |
| $c_{oB}(V)$ | Effluent concentration in region B |
| $c_{oC}(V)$ | Effluent concentration in region C |
| Co | Outlet concentration |
| Ci | Injected concentration |
| ICP-OES | Inductive coupled plasma and optical emission spectrometry |
| $T_o$ | Interpolation temperature |

# 1 Introduction

According to the World Energy Report (2018), the global energy demand is set to rise by 30% between 2018 and 2040 with most of the demand rise coming from India and China. Fossil fuels will continue to meet a dominant share of the global energy demand, especially in the critical transportation sector. However, conventional oil fields all over the world are reaching the decline phase where the rate of production is falling (Hite and Bondor 2004). Older oil fields face abandonment with more than 50% of original oil in place (OOIP) unrecovered as the residual oil is outside the reach of conventional techniques. The residual oil is trapped due to high capillary forces, poor oil mobility, unfavourable wettability and high interfacial tension (IFT). This residual oil is the target of enhanced oil recovery (EOR) techniques. EOR focuses on developing techniques targeted at overcoming the unfavourable conditions mentioned earlier in order to recover economical quantities of residual oil. Any process that involves fluid injection into the reservoir to supplement oil recovery by interacting with the rock-oil-brine system can be called an EOR process. Examples of well-known EOR methods are chemical flooding (Alkali-Surfactant-Polymer flooding), low salinity flooding, miscible $CO_2$ injection and thermal EOR methods.

Nanotechnology refers to manipulation of matter with at least one dimension in the range of 1 to 100 nm. By its very definition, it is wide field with applications in targeted drug delivery (Farokhzad and Langer 2009), energy storage (Liu et al. 2015), microfabrication (Lyon and Hubler 2013), nano-electronics (Lu and Lieber 2010), $CO_2$ reforming (Lovell, Scott, and Amal 2015), removal of organic and inorganic pollutants (Walcarius and Mercier 2010), and environmental materials (Di Credico et al. 2015), among others. Over the past

decade, many of researches have focused on application of nanoparticles (NP) as an EOR method (Ayatollahi and Zerafat 2012). The small size and high specific surface area of NPs offer unique advantages like allowing them to easily pass through pore throats and enhanced interaction in the reservoir at very low volume concentrations. NPs have displayed the potential to act as surface modifiers that could alter the wettability and reduce the oil/water interfacial tension leading to better mobility of the oil phase (Abhishek, Kumar, and Sapru 2015, Behzadi and Mohammadi 2016, Giraldo et al. 2013, Li and Torsæter 2015, Shahrabadi et al. 2012, Sheshdeh 2015, Zhang, Nikolov, and Wasan 2014) and reduce fines migration (Arab and Pourafshary 2013, Arab et al. 2014).

Recent laboratory studies have indicated that nanofluids, which are colloidal dispersions of NPs in a dispersing medium have the potential to increase oil recovery (Behzadi and Mohammadi 2016, Hendraningrat, Li, and Torsæter 2013, Hendraningrat and Torsæter 2015a, Ogolo, Olafuyi, and Onyekonwu 2012, Suleimanov, Ismailov, and Veliyev 2011, Zhang, Nikolov, and Wasan 2014). Special focus has been directed to silica NPs for EOR due to its hydrophilic nature and ease of functionalization. Hofmann, Endell, and Wilm (1934) postulated the presence of silanol groups (Si–OH) on the silica surface that causes its hydrophilicity as the silanol groups act as binding sites ($H^+$ bonds) for water. These NPs are dispersed in a suitable medium to prepare nanofluids (NF).

## 1.1 Stability of nanofluids

For NFs which are two phase systems, one of the most important issue is their colloidal stability i.e., no or low rate of agglomeration of the NPs. The suspended NPs in fluid have the tendency to aggregate due to the high surface

area to volume ratio leading to high surface energy. Hence they tend to aggregate to minimize the surface energy. Stability of NP is essential for injection application as EOR agents in oil reservoirs. Agglomeration can lead to blockage of micro channels, formation damage, hinder the transport of NPs and the displacing fluid in the reservoir. The main strategies utilized to enhance the stability of nanofluids are: (a) electrostatic stabilization (Ortega et al. 2016) (by varying pH of the nanofluids); (b) employing stabilizing fluid/surfactant (Hendraningrat and Torsæter 2015b); (c) surface modification (functionalization) of the NP (Yang and Liu 2010, Weston et al. 2015).

Electrostatic stabilization (for example by varying the pH) is expected to fail in the presence of dissolved salts. Electrolytes could destabilize particle dispersions by compressing the double layer. As the electrolyte concentration increases, the energy barrier is lowered to an extent that kinetic energy of particles dictates the kinetics of particle aggregation (Metin et al. 2011). For a given surface charge, the aggregation of silica NP occurs because of the presence of electrolytes. Metin et al. (2011) studied the effect of pH, cation type, temperature and electrolyte concentration on the stability of silica dispersions. They found that pH does not have a significant effect on stability in the presence of electrolytes. Surfactants may also be used as a stabilizing fluid (Hwang et al. 2008). Adding surfactants in the two-phase systems is an easy and economic method to enhance the stability of nanofluids. They consists of a hydrophobic tail portion, usually a long-chain hydrocarbon, and a hydrophilic polar head group. The surfactants tends to locate at the interface of the two phases, where it introduces a degree of continuity between the nanoparticles and fluids. Surfactants may be divided into four classes:

(1) Nonionic surfactants (Liz-Marzán and Lado-Touriño 1996)
(2) Anionic surfactants (Kvitek et al. 2008)

(3) Cationic surfactants(Binks, Rodrigues, and Frith 2007)

(4) Amphoteric surfactants (Gao et al. 2009)

Although addition of stabilizing fluid can be an effective way to enhance the dispersion of NP, it might cause several problems like foaming and stabilizing fluid adsorption in porous media leading to loss of the intended stabilization.

Use of functionalized nanoparticles is a promising approach to achieve long-term stability of nanofluid. It has the advantage of being a surfactant-free technique. Joni et al. (2009) made a stable dispersion of titania NPs in an organic solvent. In order to enhance dispersion stability, surface modification of dispersed titania particles was carried out with silane coupling agents. Tang et al. (2006) modified zinc oxide NPs with polymethacrylic acid (PMAA) in aqueous system. The hydroxyl groups on the particle surface interact with carboxyl groups of PMAA and form poly (zinc methacrylate) complex. They found that PMAA enhanced the dispersibility of the NPs. Yang and Liu (2010) presented a work on the synthesis of functionalized silica ($SiO_2$) NPs by grafting silanes directly to the surface of silica NP which showed good stability. Weston et al. (2015) systematically performed surface modification of silica with different silanes and studied the wettability of the modified nanomaterials. However, it is essential to examine the effect these stabilization strategies have on the effectiveness of the nanofluids.

## 1.2 Adsorption

For stable nanofluids, which can be utilized as EOR agents, an important factor is the interaction of the NPs with the rock minerals over a wide area of the reservoir. When NPs are introduced into porous medium, different processes may take place such as adsorption, desorption, blocking, transportation and aggregation (Li and Torsæter 2015). The adsorption could be irreversible or

reversible. Blocking of pore throats may occur if the NPs aggregate in situ so that their size exceeds the pore throat (Wang et al. 2016). The transportation of the NP through the porous medium is governed by advection-diffusion and hydrodynamics once equilibrium adsorption and desorption has been achieved. Silica NPs can alter the wettability of the oil wet rock surface towards more water wet and this has been attributed and studied as the main mechanism that that improves recovery due to application of silica NPs (Hendraningrat, Li, and Torsæter 2013, Li and Torsæter 2015, Abhishek, Kumar, and Sapru 2015, Dehghan Monfared et al. 2016). Hence the adsorption of silica nanoparticles on the mineral surface in sandstones is of prime importance. Literature indicates some debatable with regards to silica NP adsorption on sandstone minerals. Metin, Baran, and Nguyen (2012) reported that the adsorption of surface functionalized silica NPs on quartz mineral surfaces was insignificant. Other researchers reported significant adsorption of silica NPs on sandstones (Li et al. 2013, Yuan, Moghanloo, and Zheng 2016, Zhang et al. 2015).

Yu et al. (2012) investigated the adsorption and transport of silica NPs injected into sandstone, limestone and dolomite cores. They found that the silica NPs did not impair the permeability of sandstone cores, however, they observed severe plugging in dolomite cores. Lecoanet, Bottero, and Wiesner (2004) investigated the adsorption and transport of different NPs with flooding experiments. Among the investigated NPs, the NPs that were surface modified for stability showed the best mobility. The adsorption of NPs is governed by various colloidal forces like: London-van der Waals forces, double layer forces and hydrodynamic forces. Zhang and co-workers (Zhang et al. 2015) performed an extensive series of transport experiment to systematically analyse the effect of injection rate, rock type, NP concentration and porous medium properties on NP adsorption and transport. They reported distinct adsorption and desorption

sites in the porous media and that the adsorption capacity was much lower than that would be expected for monolayer coverage. Most importantly they showed that the adsorption behaviour of NPs in porous medium is unlike typical solute sorption (Yao, Habibian, and O'Melia 1971) wherein the adsorption capacity is a characteristic to the porous medium. Also, the NP adsorption behaviour does not follow classical filtration behaviour (Li et al. 2008). In their follow up work, (Zhang, Murphy, et al. 2016) suggested an independent two-site model. This model includes physically independent sites of fixed capacity for reversible and irreversible adsorption. Monfared et al. (2015) studied the kinetic aspects of silica NP adsorption on calcite surfaces and effect of salinity and pH on the adsorption process. The reported that lowering the pH and increasing the salinity positively impacts the adsorption process. Most of the research effort in the literature has been directed at investigating the adsorption and transport of NPs in sandstones. The adsorption of silica NPs in carbonate minerals is not well addressed.

## 1.3 Surface modification

Low salinity water injection is a popular EOR technique for sandstone reservoirs (Morrow and Buckley 2011, Austad, RezaeiDoust, and Puntervold 2010, Hamouda and Valderhaug 2014). This techniques generally involves altering or lowering the salinity to injection brines. However, lowering the salinity of injection brine can have detrimental effects. Khilar and Fogler (1984) identified the existence of a critical salt concentration (CSC) for permeating fluids in berea sandstones below which clay particles get released and cause formation damage due to fines migration. Fines refer to solid mineral particles of the sandstone minerals that lose their coherence due to fluid/rock interaction and become mobilized with the flowing fluids. Formation damage by lowering

brine salinity has also been reported by other researchers (Kia, Fogler, and Reed 1987, Rosenbrand et al. 2015, Bhattacharya et al. 2016) and choosing optimum brine salinity in low salinity projects is limited by the CSC (Arab and Pourafshary 2013). The adsorption of silica NPs on minerals causes surface modification which may affect the fluid/rock interactions. Arab and Pourafshary (2013) and Arab et al. (2014) studied the surface modification of sandstone by NPs to reduce fines migration and colloid facilitated transport in porous medium modified by NPs. They reported that porous media that has been treated with NPs acts as a strong adsorbent of fine particles. Huang et al. (2015) made a similar observation wherein they observed that for a sand pack treated with silica NPs, the pressure drop across the sand pack was 10% lower than of unmodified sand pack, thereby showing an improvement in water injectivity. Yuan (2017) reported an analytical model for utilizing nanofluids to control fines migration.

In addition to sandstones, low salinity water flooding can also be an effective technique for improving oil recovery from carbonate reservoirs (Hamouda and Rezaei Gomari 2006, Hamouda et al. 2014, Zahid, Shapiro, and Skauge 2012, Mahani et al. 2015, Al-Nofli et al. 2018, Wang and Alvarado 2011, Hamouda and Gupta 2017, Rezaei Gomari and Joseph 2017). However, increased calcite dissolution induced by low salinity interaction with chalk during flooding may lead to loss of rock integrity (Hamouda and Maevskiy 2014). To best of our knowledge, the effect of silica NP adsorption on fluid/rock interactions with carbonate minerals has not been addressed in the literature.

## 1.4 Oil recovery by nanofluids

Various research groups have investigated the potential of silica NPs to increase oil recovery (Behzadi and Mohammadi 2016, Hendraningrat and Torsæter

2015b, Ogolo, Olafuyi, and Onyekonwu 2012, Zhang, Nikolov, and Wasan 2014, Shahrabadi et al. 2012, Ortega et al. 2016, Haroun et al. 2012, Agista, Guo, and Yu 2018). As discussed earlier, NPs are suitable for subsurface porous media applications since they can pass through the pore throats of porous media without blocking them and enhance oil recovery at relatively low volume concentrations (Suleimanov, Ismailov, and Veliyev 2011, Fletcher and Davis 2010) via wettability alteration (Hendraningrat, Li, and Torsæter 2013, Maghzi et al. 2012, Li and Torsæter 2015).

Core flood studies conducted by different research groups have shown the silica NPs can increase recovery in sandstone reservoirs (Hendraningrat, Li, and Torsæter 2013, Torsater, Li, and Hendraningrat 2013, Alomair, Matar, and Alsaeed 2015, Aurand, Dahle, and Torsæter 2014, Ju, Fan, and Ma 2006). Hendraningrat and Torsæter (2015a) investigated the applicability of different metal oxide NPs for EOR. They reported wettability alteration to more water wet by the NPs which corresponded with the increased oil recovery. They suggested that wettability alteration is the dominant mechanism for NPs based EOR. Apart from wettability change, silica NPs have also been shown to reduce oil-water interfacial tension thereby improving the mobility of oil phase (Li, Hendraningrat, and Torsaeter 2013, Sharma, Iglauer, and Sangwai 2016, Al-Anssari, Wang, Barifcani, and Iglauer 2017) and stabilize oil in water emulsions (Xu et al. 2017, Binks and Whitby 2005, Sharma et al. 2015, Sharma, Kumar, and Sangwai 2015). In addition, Wasan and coworkers (Wasan and Nikolov 2003, Zhang, Nikolov, and Wasan 2014) suggested the mechanism of NP wedge formation that drives the detachment of oil from mineral surfaces. The formation of NP wedge like structure due to the self assembly of the NPs in the three-phase contact between the oil, water and mineral raises the structural disjoining pressure (perpendicular to the oil-water interface). This

force enhances the detachment of oil from the mineral surface. The disjoining pressure depends on the particle size and self-assembly of the NPs in the wedge region (Zhang, Ramakrishnan, et al. 2016).

Silica NPs can also be an effective EOR agent in carbonate reservoirs (Al-Anssari, Wang, Barifcani, Lebedev, et al. 2017, Roustaei and Bagherzadeh 2015, Abhishek, Kumar, and Sapru 2015, Abhishek, Bagalkot, and Kumar 2016, Nwidee et al. 2017). Nazari Moghaddam et al. (2015) compared the performance of different types of NPs in altering the wettability of carbonate reservoirs. Al-Anssari et al. (2016) reported that silica NPs adhere to the calcite surface irreversibly and can alter the wettability of oil/mixed-wet to water-wet state. The efficiency of wettability change by silica NPs was shown to be enhanced at higher temperatures (Al-Anssari, Wang, Barifcani, Lebedev, et al. 2017).

# 2 Objectives

The motivation behind this work is to contribute to the emerging field of nanofluid flooding for EOR. In the previous chapter, a brief background of the research conducted on silica nanofluids for EOR was discussed. Wettability alteration, interfacial tension reduction and structural disjoining pressure due to NP wedge formation are the majors mechanisms attributed to incremental oil recovery by silica NPs. However, the adsorption mechanisms of silica NPs and its effect on fluid/rock interactions are not clearly addressed in literature. This thesis focusses on the adsorption of silica NPs for sandstone and chalks mineral surfaces and their effect on fluid/rock interactions.

The main objectives of this work are:

(1) Investigate the stability of silica nanofluids.
(2) Investigate the mechanisms of silica NP for sandstone and chalks mineral surfaces and their effect on fluid/rock interactions at different salinity conditions.
(3) Merging the popular low salinity flooding with silica NPs for EOR.

# 3 Materials and methods

The experimental methods in this work involved nanofluid preparation, nanofluid characterization (particle size and zeta potential measurements), adsorption studies, core flooding studies and SEM imaging. This chapter includes the details of materials, experimental setup and methodology of measurement techniques used in this study. The list of chemicals used and their sources are outlined in Table 3.1.

Table 3.1 List of chemicals

| **Material** | **Properties** | **Source** |
|---|---|---|
| Silicon dioxide nanopowder | Spherical, 5-20 nm, Purity: 99.5% | Sigma- Aldrich (637246) |
| (3-Mercaptopropyl) trimethoxysilane (MPTMS) | Purity: 95 % | Sigma- Aldrich (175617) |
| Quartz mineral powder) | Specific surface area (0.62 $m^2/g$) | Sigma-Aldrich (00653) |
| Kaolinite mineral powder | Specific surface area (8.56 $m^2/g$) | Sigma-Aldrich (03584) |
| Calcite mineral powder | Specific surface area (0.23 $m^2/g$) | Honeywell Riedel-de Haen |
| n-decane | Purity > 99% | Chiron AS |
| Stearic acid (SA) | Grade I, Purity ≥98.5% | Sigma-Aldrich (S4751) |
| N,N-Dimethyldodecylamine (NN-DMDA) | Purity >99% | Fluka Analytical |
| DP9711 Silica nanofluid | 30 wt.% dispersion in DIW (pH 3) | Nyacol Nano Technologies |

## 3.1 Cores

Two types of outcrop cores were used to perform core flooding studies in this work: (1) berea sandstone (BR) cores and (2) Stevens Klint (SK) chalks. The berea sandstone cores work were acquired from Koucurek Industries Inc., Caldwell, TX, USA. The properties and mineral composition of the used cores are listed in Table 3.2.

Table 3.2 Properties and mineral composition of used Berea sandstone

| **Core Properties** | | **Mineral Composition of Berea** | |
|---|---|---|---|
| **Type** | **Berea Sandstone** | **Mineral Name** | **Semi-Quantitative (%)** |
| Length | 8.95 ± 0.08 cm | Quartz | 94 |
| Diameter | 3.78 cm | Kaolinite | 1 |
| Porosity | 20.05 ± 0.76% | Muscovite | 1 |
| Permeability | 200–220 mD | Microline | 1 |

SK chalk is 99% pure biogenic with a high porosity range of 45–50% and a relatively low absolute permeability of ≈4 mD (Hamouda et al. 2014). SK chalk matrix material and its petro-physical properties resembles chalk reservoirs, which makes it useful in the analysis (Frykman 2001).

## 3.2 Brines

Apart from DIW (deionised water), synthetic sea water (SSW) and low salinity water (LSW) at 1:10 SSW dilution with pH 7.45 and 7.32 respectively were the brines used in this study. The LSW dilution ratio of 1:10 was chosen based on previous work in our lab (Hamouda et al. 2014, Hamouda and Gupta 2017, Hamouda and Valderhaug 2014, Hamouda and Maevskiy 2014) where, 1:10

dilution showed best performance. The ionic compositions of SSW and LSW are listed in Table 3.3.

Table 3.3 Ionic composition of SSW and LSW

| Ion | SSW (mol/L) | LSW (mol/L) |
|---|---|---|
| $HCO_3^-$ | 0.002 | 0.0002 |
| $Cl^-$ | 0.525 | 0.0525 |
| $SO_4^{2-}$ | 0.0240 | 0.0024 |
| $Mg^{2+}$ | 0.045 | 0.0045 |
| $Ca^{2+}$ | 0.013 | 0.0013 |
| $Na^+$ | 0.450 | 0.045 |
| $K^+$ | 0.010 | 0.0010 |

## 3.3 Nanofluids

Two types of nanofluids were used in this study. The first set of NFs were prepared in house with silica nanopowder obtained from Sigma Aldrich (Table 3.1). The nanopowder was dispersed in deionized water (DIW) at a predetermined concentration using a magnetic stirrer at 500 rpm for 30 min. To loosen the agglomerates in the nanopowder and disperse it, probe sonication was applied using an ultrasonic processor. Sonication was performed for 120 min (50% amplitude and 0.5 pulse) with breaks every 15 min to avoid overheating. Mondragon et al. (2012) observed that silica nanofluids prepared by dispersing the NPs in DIW using an ultrasonic probe proved to be the most effective technique. Following nanofluids were prepared at varying concentrations of NPs:

(1) Unmodified silica NPs dispersed in DIW.
(2) Sulfonated silica NPs dispersed in DIW (functionalized).

(3) Silica NPs dispersed in DIW with MPTMS stabilizing fluid.

The nanofluids of silica in DIW with MPTMS stabilizing fluid were prepared by dispersing the desired concentration of silica NPs in DIW via ultra-sonication. Thereafter, 1 g of MPTMS was added per 100 mL of the nanofluid under vigorous stirring. To avoid confusion in this text between NP and MPTMS concentration, NP concentration is always stated in g/L units and MPTMS concertation is always stated in g/100 mL units.

Sulfonated silica NPs were prepared by surface functionalization of silanol groups present of the silica surface. Hofmann, Endell, and Wilm (1934) postulated the presence of silanol groups (Si–OH) on the silica surface. The aim of functionalization of silica was to increase the hydrophilicity and stability of the silica NPs. The grafting of silanes on NP leads to steric stabilization. The surface modification was performed based on the method described by Weston et al. (2015). 10 g of silica NP was dispersed in 100 mL toluene by probe sonication. 5 g of MPTMS was added to the dispersed silica in toluene. The solution was stirred for 12 hrs at 35 °C. Particles were removed from the dispersion by centrifugation (7000 rpm for 10 min). Thereafter, the particles were washed 5 times with isopropyl alcohol, after each time, the fluids were centrifuged to separate the particles. The wash with isopropyl alcohol was done to remove excess silane/toluene and followed by washing twice with 70/30 (*v*/*v*) mixture of isopropyl alcohol and DIW. The NPs were dried in a vacuum oven at 120 °C for 24 h. Thereafter, the thiol groups of MPTMS were oxidized based on the technique described by Oh et al. (2006): the dried NPs were dispersed in a solution of 30% $H_2O_2$ and stirred at room temperature for 24 hrs. This results in the formation of sulfonic acid groups on the silica surface. The particles were then washed several times with water and dried. The sulfonic acid groups were converted into sodium sulfonate by dispersing the particles in 0.1 mol/L

solution of NaOH under continuous stirring for 24 hrs. The particles were washed and dried in a vacuum oven for 3 days at 35 °C. These surface modified NPs are referred to as sulfonated NP. Thereafter the sulfonated NPs were dispersed in DIW via ultra-sonication to prepare the nanofluid.

The second type of nanofluids were prepared from DP9711 nanofluid (Table 3.1) which was acquired as dispersion with silica nanoparticles at 30 wt. % concentration dispersed in deionized water (DIW). The DP9711 product has a proprietary surface coating but Singh and Mohanty (2015) reported that DP 9711 is coated with polyethylene glycol. For ease, these NPs are referred to as DP in this study. The NPs as claimed by the manufacturer have an average particle size of 20 nm. As and when required, the NFs used in this study were prepared from the stock fluid by diluting it with appropriate brines.

## 3.4 Model oil

The oil phase used in this study was n-decane. For saturating chalk cores, stearic acid was dissolved into n-decane at 0.005 mol/L concentration. For treating berea sandstone cores, N,N-Dimethyldodecylamine (NN-DMDA) at a concentration of 0.01 mol/L was dissolved with n-decane. Stearic acid and NN-DMDA are polar natural fatty acid and amine used to modify the wettability of chalk and sandstone cores towards oil wet based on previous work in our lab (Gomari, Denoyel, and Hamouda 2006, Hamouda and Tabrizy 2013).

## 3.5 NP adsorption on minerals

Adsorption studies were performed to address the interaction between silica NPs and the major minerals present in chalk and sandstone reservoirs. Two types of adsorption experiments were performed: (1) adsorption on minerals

and (2) dynamic adsorption of silica NPs injected into sandstone and chalk cores (section 3.6.2). The kinetic aspects of silica NP adsorption were also addressed.

During static adsorption experiments, 0.15 g of a particular mineral powder was dispersed in 30 mL of nanofluid. Then the samples were agitated in a rotator agitator for 24 hrs at room temperature. After 24 hrs, the minerals were removed from the dispersion and the remained NP concentration in the fluid was determined (Section 3.5.1). This was used to calculate the amount of NPs adsorbed on the mineral surfaces. The in-house prepared silica nanofluids were much less stable compared to the commercially available (DP9711) nanofluid. In addition, the commercial nanofluid was almost transparent at low concentrations. A different method were developed for determining the remained unabsorbed NP concentration which is outlined in section 3.5.2. The developed methods for determining NP concentration during adsorption tests were also utilized in analyzing NP concentration in the effluents from core flooding experiments outlined in section 3.6.

For investigating the kinetics of silica NP adsorption, 5 grams of mineral powder was dispersed in 30 ml of nanofluid. The nanofluid was prepared at a predetermined NP concertation and salinity. The nanofluid-mineral dispersion was placed in a 50 ml capped centrifuge tube. The tube containing the nanofluid and the mineral was then agitated using a rotary agitator for the desired length of time. At the end of the time period, the mineral was removed from the fluid by centrifuging. The supernatant fluid containing the remained NPs was recovered and filtered. The concentration of the NPs in the supernatant was determined.

### 3.5.1 Measurement of NP concentrations for in-house silica nanofluids.

For in-house silica nanofluids, the samples were centrifuged at low speed (1000 rpm) for 10 min to promote the settling of mineral powders. The liquid was decanted and further centrifuged for 10 min. This supernatant fluid was analyzed for NP concentration by transmissivity measurements. The suspended NP in fluid have the tendency to aggregate due to the large surface area to volume ratio leading to high surface energy, hence they tend to aggregate to minimize the surface energy.

The stability of the nanofluids was investigated. The uniformity of the dispersed NPs was determined by % transmissivity of the nanofluid. TurbiScan Lab instrument by Formulaction Inc was used to measure transmissivity at different points along a vertically mounted tube. Uniform dispersion of the NPs in a fluid, is indicated by stable transmissivity along the vertical length. In general, it was found that the in-house nanofluids were stable for about 24 hrs beyond which the settlement of particles could be visually observed. The nanofluid with sulfonated silica NPs was the most stable. This nanofluid was stable for about one week. For example, the transmissivity measurement of the 1 g/L dispersion of bare silica in DIW was performed along the turbiscan tubes with sample height of 35 mm. The maximum transmissivity measured was 35.67%, the minimum was 34.87% and the mean transmissivity was 35.14%. This indicates that the prepared nanofluid prepared was uniformly dispersed. Further, the nanofluid was diluted to 0.5 g/L and 0.33 g/L NP concentration and the samples were placed in an ultrasonic bath for 1 h after which the transmissivity was measured. These measurements along with the transmissivity of DIW (no NP) was used to make the calibration curve shown in Figure 3.1. The calibration curve was used to quantitatively determine the concentration of NP in

supernatant/effluent samples. For each nanofluid prepared for particular experiment, a calibration curve was constructed following the above process. The transmissivity of the supernatant/effluent samples is measured and compared against the calibration curve to determine the concentration of the NP in the supernatant/effluent samples.

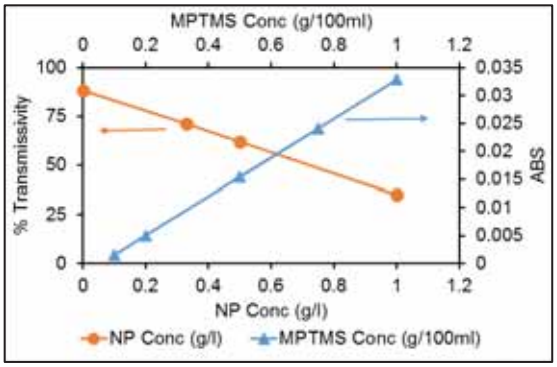


Figure 3.1 Calibration curves for detecting nanoparticle concentration and MPTMS concentration. (ABS: Absorption)

## 3.5.2 Measurement of NP concentration for DP9711 nanofluids.

NP concentration during adsorption tests and in the effluents of flooded cores performed with nanofluids prepared from DP9711 stock fluid were determined using UV-Vis spectroscopy. The mineral was removed from the fluid by centrifuging at 10000 rpm and decanting the supernatant fluid. The supernatant fluid was, then filtered through a 0.22 μm filter which allows the NPs to pass through but not the larger mineral particles. The remaining concentration of the NPs in the supernatant was determined by measuring their absorbance in a dual beam UV/Vis spectrophotometer (UV/Vis 1800 spectrophotometer from Shimadzu Corporation) at 240 nm wavelength against DIW, comparing it with calibration curves and making baseline corrections.

## 3.6 Core flooding

Three types of core flooding experiments are performed in this study to address the effect of silica nanofluids as outlined below.

### 3.6.1 Berea surface modification by in-house nanofluids

These experiments were aimed at addressing the surface modification of berea sandstone by the adsorption/adhesion of silica NPs. For ease of discussion, the NPs retained in the core are henceforth referred to adsorbed NPs. Sandstone surface modification by the in-house prepared nanofluids containing silica NPs, silica NPs with a stabilizer (MPTMS) and sulfonate-functionalized silica NPs in DIW were investigated. Thus two stabilization methods (discussed later): use of stabilizing fluid and NP functionalization were addressed. Silica nanofluid was introduced into the berea sandstone core under vacuum with 1 pore volume of nanofluid, followed by injection of DIW to address the surface modification by the silica NPs.

Berea cores were dried in a vacuum oven at 100° for 24 hrs until stable weight was obtained. The dry weight, length and diameter was noted. The core was vacuum saturated with DIW and the pore volume (PV) of the core was calculated based on the saturated weight of the core. The core was loaded in a core holder and confining pressure of 25 bar was applied. DIW was injected at 0.3 mL/min (≈20 PV/day) to perform pre-flush. Injection was performed at atmospheric pressure (no back pressure). The flooding setup is shown in Figure 3.2. Differential pressure drop across the core (dP) was recorded using Labview 7.1. Upon stabilization of dP, the core was removed from the holder and dried in a vacuum oven at 100 °C until the weight of the core becomes approximately equal to dry core weight previously measured. Thereafter, the core was treated

(vacuum saturated) with 1 PV of a particular nanofluid depending on the experiment and loaded in the core holder with the same inlet-outlet orientation as during pre-flush. Post flush was performed by injecting DIW at 0.3 mL/min (≈20 PV/day). Produced effluent samples were then collected and analyzed. The adsorption/desorption of the NP was addressed by continuous monitoring of the pressure drop and analysing the effluents for produced NPs and stabilizing fluid concentration where applicable.

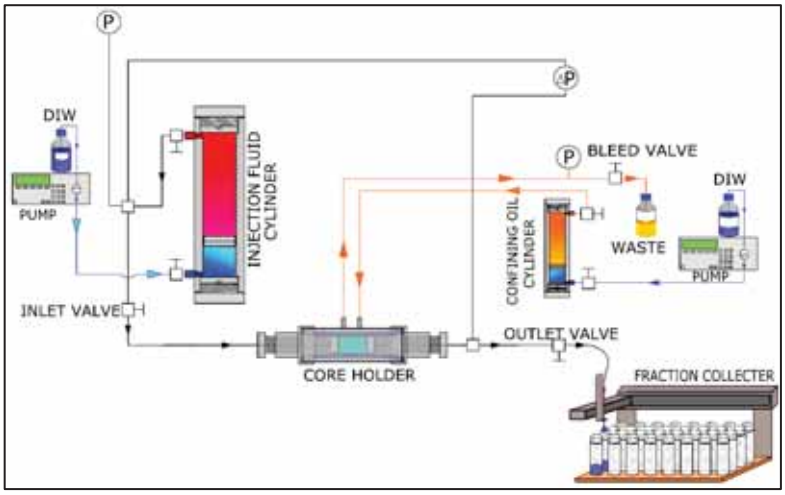


Figure 3.2 Core flooding setup fro in house nanofluids.

As mentioned earlier the NP in the nanofluid tend to aggregate, which may cause resistance to flow. Two strategies were employed to prevent/minimize the agglomeration of NP. Firstly, functionalization or surface modification of the NPs (sulfonated silica). The second is using a stabilizing fluid that keeps the NP suspended. Hendraningrat and Torsæter (2015a) employed Polyvinylpyrrolidone (PVP) at 1% weight concentration in the nanofluid as a stabilizer for silica based nanofluids. However, an important question that arises related to the adsorption of the stabilizing fluid on the mineral during the injection that may take place. This changes the ratio between the fluid and NP,

which may then induce agglomeration of NPs during the injection. In this study a method was developed to determine the adsorption of the stabilizing fluid on the rock surface. The method was based on mass balance calculation, where the effluent was analyzed by UV/Vis spectroscopy. The used wavelength was 300 nm that gave adequate linear relationship between the absorption and concentration of MPTMS (stabilizing fluid). The constructed calibration curve was then used to estimate the loss in the mass balance i.e., related to the adsorbed MPTMS in the core. For each nanofluid containing MPTMS, calibration curve was constructed prior to the injection experiment by measuring the absorption in a dual beam UV/VIS spectrometer at wavelength 300 nm. The removal of the NP from the effluent fluid was achieved by adjusting the pH of the effluent fluid to about 2, then centrifuging the fluid for 60 min at 10,000 rpm to promote the settling of NP. The absorption of the supernatant was determined. As an example, the UV/VIS calibration curve for 1 g/L nanofluid with 1 g/100 mL MPTMS is presented in Figure 3.1. In summary, after measuring the NPs concentration in the effluent samples through transmissivity measurements, the pH of the samples was then adjusted to 2 by dropwise addition of 0.1 M HCl followed by centrifuging for 60 min at 10,000 rpm. The absorption of supernatant was measured relative to a reference of DIW (pH adjusted to about 2) in the double beam UV/VIS spectrometer.

### 3.6.2 Dynamic Adsorption of silica NPs

The objectives of the tests were to study the adsorption profile of the NPs and their interaction with the minerals. The dried berea/chalk cores were vacuum-saturated with DIW or brine (LSW/SSW) and loaded into the core holder. A confining pressure of 25 bar was applied, and injection was performed at a constant flow rate of 10 PV/day at room temperature. After injecting several

PVs of DIW/brine (pre-flush), 1.5 PV of slug with LiCl tracer was injected. Thereafter, the injection was switched to the original fluid to conduct a post-flush. The effluents samples from the core floods were analysed for NP concertation using the method outlined in section 3.5.2 and the pH was recorded. The concentration of cations in effluents produced from core floodings was determined by a Dionex ICS-5000 Ion Chromatograph (IC) from Thermo Fisher Scientific. The schematic of the core flooding setup used in this study is shown in Figure 3.3.

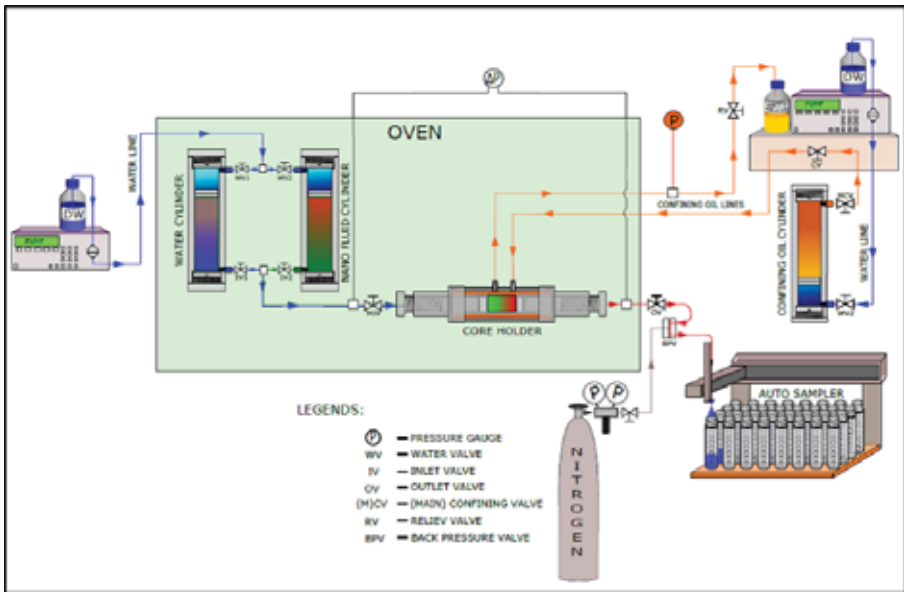


Figure 3.3 Schematic of the core flooding setup.

## 3.6.3 Oil recovery by nanofluids

The berea/chalk cores were dried at 100 °C in a vacuum oven until stable weight was reached. Then the cores were vacuum saturated with SSW and loaded in the core holder. The cores were flooded with model oil (section 3.4) to establish initial water saturation (Swi). Thereafter the cores were aged in model oil for a

period of two weeks at 50 °C to render them oil wet. The flooding experiments were performed at 70 °C under 25 bar confinement pressure and against 10 bar of back pressure in two stages: (1) primary recovery was done by flooding with the particular brine at two flowrates: 4 and 16 PV/day and (2) secondary recovery was done by switching the flood with NF, again the flooding was performed at 4 and 16 PV/day. The amount of oil produced and the differential pressure drop (dP) across the core as flooding progressed were recorded. The concentration of NPs in the produced effluents was determined by the method outlined previously. The pH of the produced water was measured and the concentration of the cations produced as flooding progressed was determined by IC. The experiments were performed in flooding setup shown in Figure 3.3.

## 3.7 Spontaneous imbibition tests

The spontaneous imbibition tests were done briefly to indicate the effect of silica NPs on oil recovery from berea cores. Dried berea cores were vacuum saturated with model oil (section 3.4). Then the cores were aged for two weeks in the model oil at 50 ºC. Thereafter spontaneous imbibition tests were carried in Amott cells at three salinities: deionized water (no added salts), SSW (high salinity) and LSW (low salinity) with and without NPs.

## 3.8 Particle size and zeta potential measurements

All zeta potentials and particle size measurements made in this study were performed using a Zetasizer Nano ZSP from Malvern Instruments based on the principle of Dynamic Light Scattering (DLS). The only exception is the zeta potential measurement of mineral powders in chapter 4 that were measured using Acosustisizer II S/M Flow-through System based on the principle of Electrostatic Attenuation (ESA).

## 3.9 Scanning electron microscopy

Scanning electron microscopy (SEM) imaging was performed to visualize the adsorption/adhesion of the NP on the rock surfaces. “Supra 35VP FE-SEM” instrument with an integrated Energy-dispersive X-ray spectroscopy (EDX) analyzer was used.

# 4 Surface modification by silica NPs

This chapter addresses surface modification of berea sandstone by silica nanofluids (Paper 1). In-house silica nanofluids were used: silica/deionized water (DIW), silica in DIW with a stabilizer fluid MPTMS and sulfonate-functionalized silica in DIW. Hofmann, Endell, and Wilm (1934) postulated the presence of silanol groups (Si–OH) on the silica surface that causes its hydrophilicity, wherein silanol groups act as binding sites ($H^+$ bonds) for water. The protonation and deprotonation of these silanol groups determine the surface charge of silica NP and the extent of the repulsive energy that keep them dispersed in the solution (Metin et al. 2011). Stability of NPs is essential for injection application as EOR agents in oil reservoirs. The main strategies utilized to enhance the stability of nanofluids are: (a) electrostatic stabilization (Ortega et al. 2016) (by varying pH of the nanofluids); (b) employing stabilizing fluid/surfactant (Hendraningrat and Torsæter 2015b); (c) surface modification (Yang and Liu 2010, Weston et al. 2015) (functionalization) of the NP.

Electrostatic stabilization (for example by varying the pH) is expected to fail in the presence of dissolved salts in brines. Electrolytes could destabilize particle dispersions by compressing the electrical double layer. As the electrolyte concentration increases, the energy barrier is lowered to an extent that kinetic energy of particles dictates the kinetics of particle aggregation (Metin et al. 2011). For a given surface charge, the aggregation of silica NPs occurs because of the presence of electrolytes. Metin et al. (2011) studied the effect of pH, cation type, temperature and electrolyte concentration on the stability of silica dispersions. They found that pH does not have a significant effect on stability in the presence of electrolytes. Alternatively, addition of stabilizing fluid can

be an effective way to enhance the dispersion of NPs, but it might cause problems like foaming and stabilizing fluid adsorption in porous media leading to loss of the intended stabilization. Surface modification of NPs (functionalized NP) is a promising approach towards increasing the stability of NPs. Yang and Liu (2010) presented a work on the synthesis of functionalized silica NPs by grafting silanes directly to the surface of silica NP which showed good stability. Weston et al. (2015) systematically performed surface modification of silica with different silanes and studied the wettability of the modified nanomaterials. However, it is essential to examine the effect these stabilization strategies have on the effectiveness of the nanofluids.

For stable nanofluids, which can be utilized as EOR agents, an important factor is the interaction of the NPs with the rock minerals over a wide area of the reservoir. When NPs are introduced into porous medium, different processes may take place such as adsorption, desorption, blocking, transportation and aggregation (Li and Torsæter 2015). The adsorption phenomenon could be reversible (desorption) during the transport of NPs in the porous medium. Blocking of pore throats may occur if the NPs aggregate in situ so that their size exceeds the pore throat (Wang et al. 2016).

Arab and Pourafshary (2013) and Arab et al. (2014) studied the surface modification of sandstone by NPs to reduce fines migration and colloid facilitated transport in porous medium modified by NPs. This chapter addresses the affinity of NPs towards major minerals present in sandstone, adsorption/adhesion of NPs in the porous medium and the influence of nanofluid stabilization on the in-situ surface modification. The core floods performed on berea cores (Table 3.2) are listed in Table 4.1. The methodology used was outlined in section 3.6.1. The results are outlined in the following sections.

Table 4.1 List of core flood experiments performed in this chapter.

| Experiment No. | NP Conc. (g/L) | Type of NP | Dispersing Phase | Comments |
|---|---|---|---|---|
| 1 | 1 | Silica | DIW | |
| 2 | 2.5 | Silica | DIW | |
| 3 | 1 | Silica | DIW | Variable injection rates |
| 4 | 1 | Silica | DIW + MPTMS (1 g/100 mL) | |
| 5 | 2.5 | Silica | DIW + MPTMS (1 g/100 mL) | |
| 6 | 4 | Silica | DIW + MPTMS (1 g/100 mL) | |
| 7 | 1 | Silica | DIW + MPTMS (1 g/100 mL) | Repeated Exp 4 |
| 8 | 2.5 | Silica | DIW + MPTMS (1 g/100 mL) | Repeated Exp 5 |
| 9 | 1 | Sulfonated silica | DIW | |

## 4.1 Unmodified silica nanofluids

Figure 4.1(a) compares effluent NP concentration profiles for cores treated with 1 PV of unmodified silica NP dispersed in DIW. It may be observed that for concentration of 1 and 2.5 g/L, the majority of the NP seized to be produce at about 0.5 and 1 PV, respectively. Long tail in the effluent concentration profile was observed for 2.5 g/L. The percentage of NP adsorbed in the core (calculated from mass balance) as the post flush progressed as shown in Figure 4.1(b). The estimated adsorbed NP was higher for 2.5 g/L nanofluid (88.82%) compared to

that for 1 g/L (85.82%) nanofluid. The recorded pressure drop during these experiments is shown in Figure 4.2.

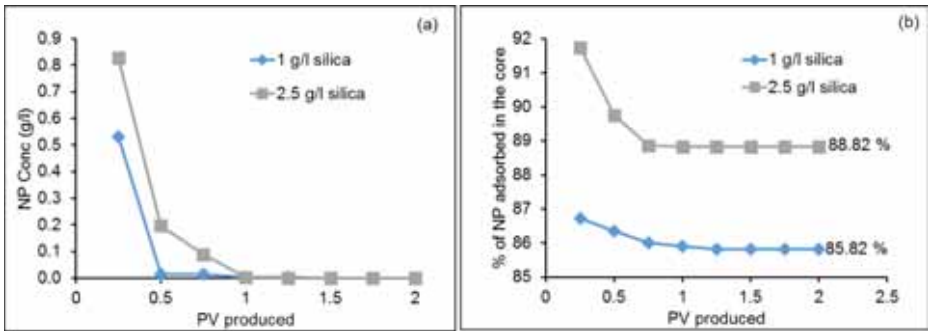


Figure 4.1 (a) Effluent NP concentration profiles; (b) % adsorbed NP during post flush for experiments 1 & 2.

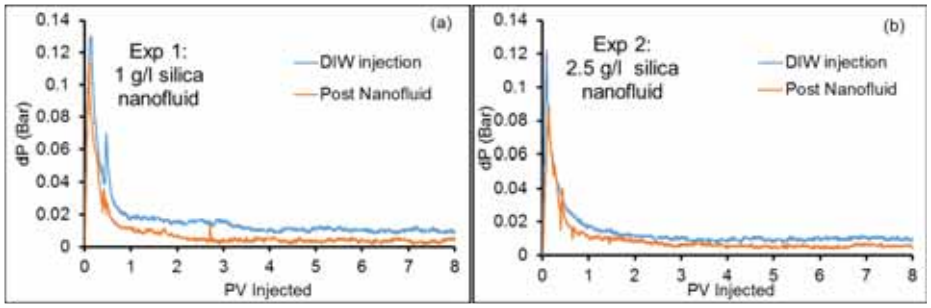


Figure 4.2 Pressure drop profiles for silica dispersed in deionized water (DIW) at (a) 1 g/L in Exp 1 and (b) 2.5 g/L concentration in Exp 2.

Figure 4.2 shows that after treatment with 1 and 2.5 g/L silica NP, pressure drop profiles were lower than that for the initial DIW injection in unmodified berea. The resistance post application of NP was lower than the initial DIW injection as indicated by pressure peak of about 0.12 and about 0.09 bar, for initial DIW injection and post flush respectively (treatment with 2.5 g/L of nanofluid). It may be concluded from Figure 4.2 that using 1 g/L concertation leads to greater improvement in water injectivity.

Fines refer to solid mineral particles of the sandstone minerals that lose their coherence due to fluid/mineral interaction and become mobilized with the flowing fluids. In this study, the injection has been performed with DIW wherein the salinity is lower than the Critical Salt Concentration (CSC). This indices fluid/interaction to produce fines that migrate and increase resistance to flow. This may ultimately lead to formation damage (Yuan and Shapiro 2011). Arab and Pourafshary (2013) studied the applicability of NPs for mitigating fine migration in engineered porous media (glass beads). In their work, they studied the application of different metal oxide NP to mitigate fines migration. They found that treating the porous medium with NPs caused reduction in concentration of fines particles in the effluents as compared to untreated porous media. For example, they observed that treating the porous medium with silica NPs dispersed in DIW led to approximately 20% reduction in effluent fines concentration as compared to the reference case. They observed that porous media that has been treated with NPs acts as a strong adsorbent of fine particles (Arab et al. 2014). Huang et al. (2015) made a similar observation wherein they observed that for a sand pack treated with NP, the pressure drop across the sand pack was 10% lower than of sand pack without NP, showing an improvement in water injectivity.

To verify the effects of surface modification by silica NP and the associated improvement in water injectivity, experiment 3 (Table 4.1) was performed. In experiment 3, the core sample was initially injected with DIW and the stabilized dP was recorded at increasing injection rates. Thereafter the core was unloaded from the core holder, vacuum dried and treated with 1 g/L silica nanofluid prepared in DIW and flushed again with DIW. Stabilized dP was recorded at increasing injection rates. Figure 4.3 shows that saturating the porous medium with the NP improves the water injectivity as indicated by the lower dP (≈8%)

during DIW flooding post treatment with NP. To quantify the remedial effect due to the application of NP, the ratio of the original pressure drop during the initial DIW injection (dPi) to the pressure drop post treatment with nanofluid (dPnp) is shown in Figure 4.3. As shown, the nanofluid treatment was effective at lower injection rates i.e., in reducing pressure drop. This is perhaps due to the increased hydrodynamic forces at higher injection rates

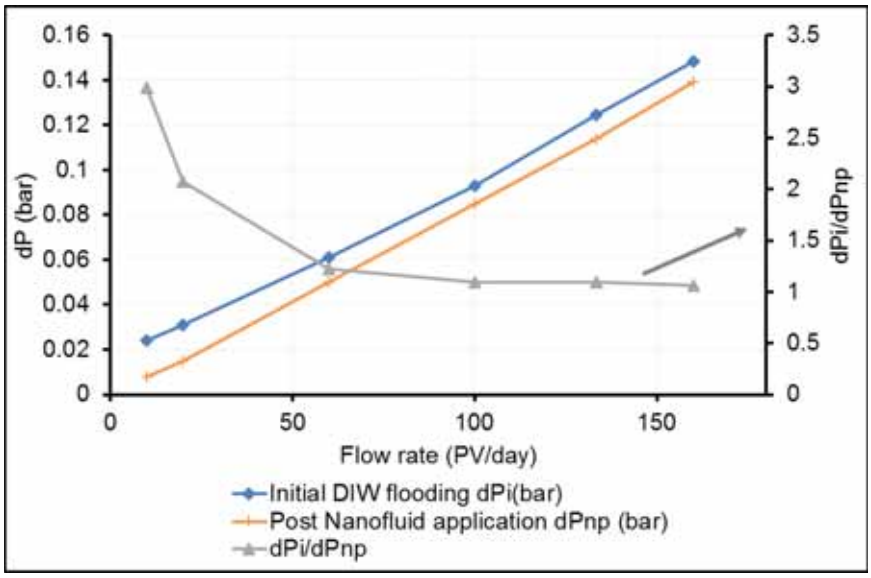


Figure 4.3 Pressure drop as function of injection rates (Exp 3)

SEM imaging was performed to better visualize the adsorption of the NP on the rock surface, which causes the surface modification. Figure 4.4(a) shows the image of a slice of berea core. It may be noted that the slice of the berea core was cleaved along the injection plane approximately at the center of the core. The integrated energy-dispersive X-ray spectroscopy (EDX) analyzer was used to identify the minerals. As shown, the core was mainly composed of well-defined quartz with some feldspar and the core has pores of several microns in diameter. Another cylindrical slice of berea, which was vacuum saturated with

1 g/L silica NP in DIW, was examined using SEM as shown in Figure 4.4(b). The adsorbed NP were clearly shown on the mineral's surface. Figure 4.4(c) is a magnified view of adsorbed silica NP. The adsorbed NP were in successive layers. This might be due to the drying effect. In addition, it was observed that most of the NP adsorption was on quartz mineral. This is an interesting observation and static adsorption test and quantitative analysis based on the theory of surface forces were performed to further test this observation. Thus, it may be concluded that the silica NPs adsorb on the minerals and this may cause in situ surface modification. This modified surface is more effective at capturing fines, which can cause injectivity improvement. To test this, the theory of surface forces was utilized to quantify the interaction between the fines and the mineral before and after the application of NP. This addressed in a latter section.

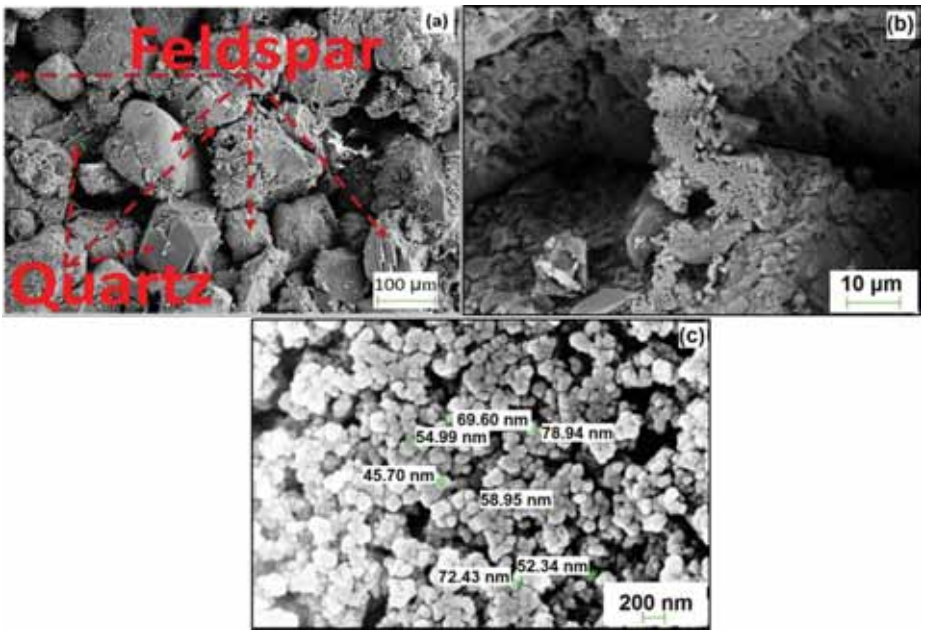


Figure 4.4 SEM image of (a) berea sandstone sample; (b) berea sandstone treated with nanofluid; (c) magnified view of the adsorbed silica.

## 4.2 Nanofluids Stabilized by MPTMS

In this section, surface modification of berea sandstone was performed with nanofluids that were stabilized by addition of MPTMS. As stated previously, to avoid confusion, NP concentration is stated in g/L units and MPTMS concertation is stated in g/100 mL units. The effluent concentration profiles of NP during the post flush (with DIW) for the cores treated with nanofluids at different concentrations (Exp: 4–8 in Table 4.1) are shown in Figure 4.5(a). As shown, the nanofluids with 1 g/L and 2.5 g/L NP concentration show similar profile of NP production. After DIW flush of about 1.5 PV for 2.5 g/L and 1 PV for 1 g/L, the NP production in the effluent stopped. To ensure that this difference did not arise due to dissimilarities in the core, experiments 4 and 5 were repeated. The effluent concentration profiles shown in Figure 4.5 (a) for

the repeated cases are close to the initial experiments 4 and 5. For the nanofluid at 4 g/L concentration, the behaviour is completely different. The percentage of NPs adsorbed in the core (Exp 4–8 in Table 4.1) as the post flush progresses is shown in Figure 4.5(b).

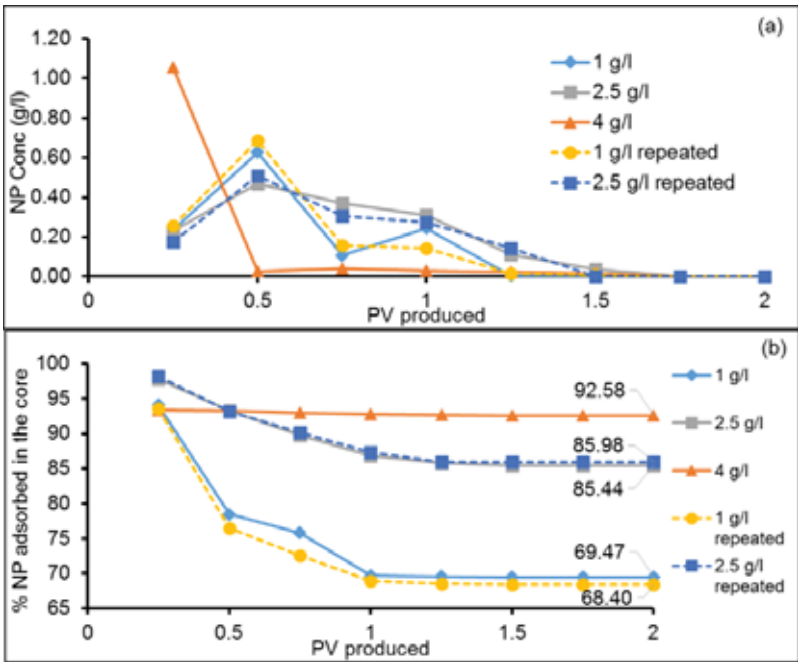


Figure 4.5 (a) Effluent NP concentration profiles and (b) % adsorption of NP during post flush for cores saturated with silica dispersed in DIW with MPTMS stabilizing fluid (Exp: 4–8).

In these experiments, the cores were vacuum saturated with the nanofluid. Therefore, it may be assumed that the spatial distribution of the NPs in the core was uniform. Gradually decreasing retention for the case of 1 g/L and 2.5 g/L possibly suggests desorption of particles in the core or that the adsorbed particles were forced out during the post flush. However, for 4 g/L it can be inferred from the almost flat nature of the curve that perhaps only the NPs near

the outlet of the core were produced and substantial channelling of the fluid may be caused by blockage of some pore throats. This was confirmed by the monitored pressure drop during the experiments (Figure 4.6).

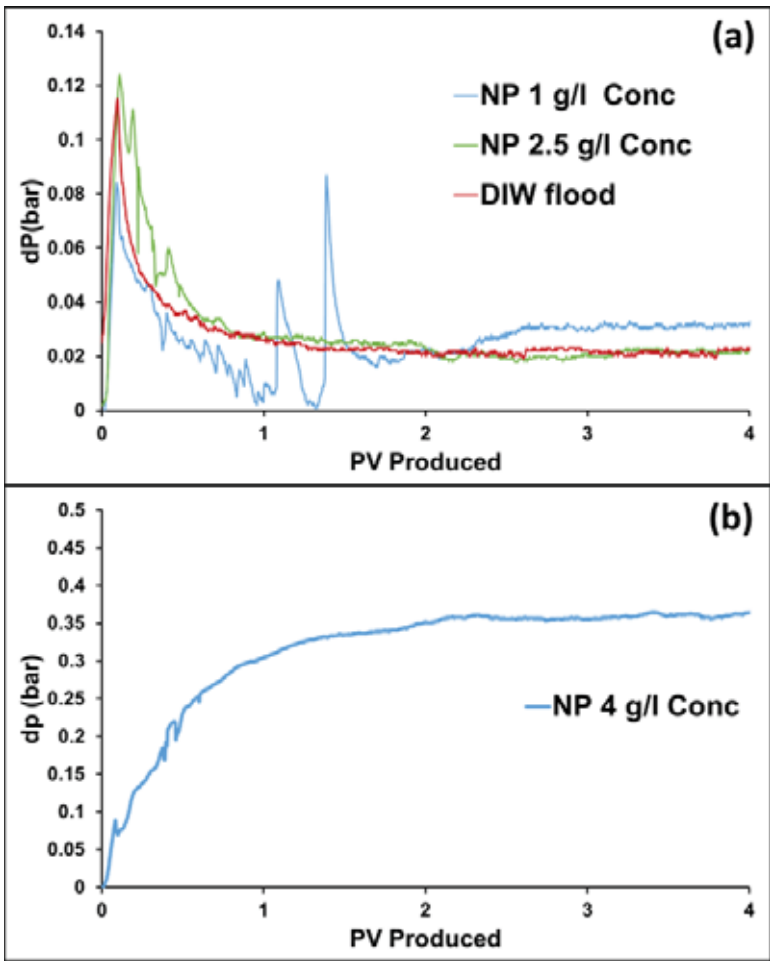


Figure 4.6 Variation of the drop across the core (dP) during post flush with DIW after saturation of the core with MPTMS stabilized nanofluids at NP concentrations (a)1 and 2.5 g/L and (b) 4g/L.

The recorded pressure drop during initial DIW injection was taken as a base line for the pressure drop in Figure 4.6 (a). It is interesting to see that the

pressure drop peaked at about 0.25 PV indicating entry resistance. The lowest pressure drop peak occurred at NP concentration of 1 g/L followed by the base fluid (DIW), then 2.5 g/L. In the case of 4 g/L NP concentration, the pressure drop increased to above 0.3 bar in Figure 4.6(b). For cores saturated with NP concentration of 1 g/L, more fluctuations in dP was observed, followed by two peaks between 1–2 PV, while the others (DIW and 2.5 g/L) dP declined smoothly. It may be concluded that 1 g/L flowed through the core with occasions of resistance to the flow. From mass balance, in the case of 1 g/L, 69.47% (0.01389 g) and for 2.5 g/L, 85.44% (0.044 g) of NPs were adsorbed in the core, i.e., the adsorbed NPs in the core for the case of 2.5 g/L was 3 times higher compared to 1 g/L, yet the dP curves eventually became almost equal to the initial DIW injection, this may indicate that the adsorbed NP did not hinder the flow. However, the surface modification of the surface by this nanofluid does not lead improvement in water injectivity as observed in Figure 4.3 for the case of unmodified silica NPs. In contrast, in the case of 4 g/L NP concentration, the pressure drop increased for more than 2 PV before it stabilized at dP ≈ 0.3 bar, this may indicate possible aggregation of NPs that restricted/blocked some of the pore throats.

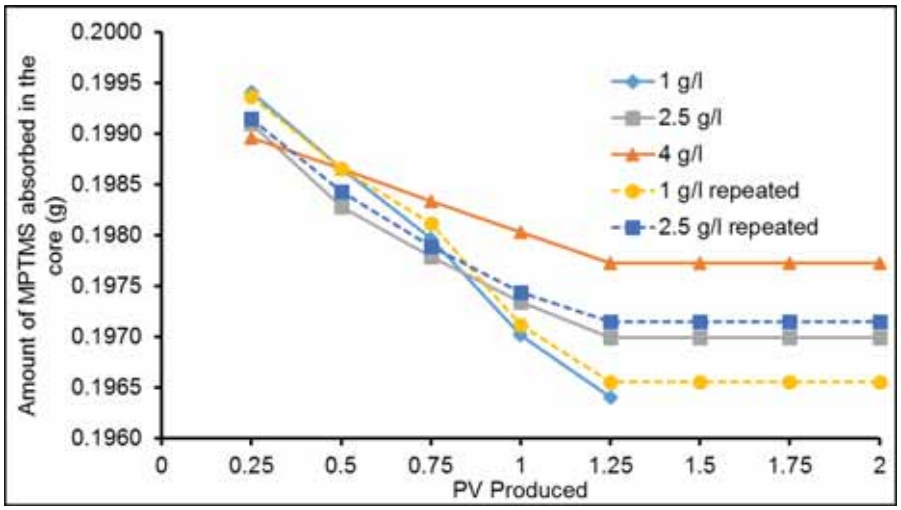


Figure 4.7 Absorbed MPTMS for cores saturated with nanofluid stabilized with MPTMS (Experiments: 4–8).

Figure 4.7 shows the amount of MPTMS adsorbed in the core. The concertation of MPTMS was measured by UV/VIS. The amount of MPTMS retained in the core was calculated from the mass balance. It may be observed that a high amount of the stabilizing fluid is adsorbed in the core. High adsorption of stabilizing fluid (MPTMS) in the porous media suggest that this fluid may not be suitable for subsurface application.

## 4.3 Sulfonated silica nanofluids

The effluent concentration profile during the post flush for core saturated with 1 g/L surface modified (sulfonated) NP in DIW is shown in Figure 4.8(a). For the sake of comparison, the effluent concertation profiles for cores saturated with 1 g/L unmodified NPs and NPs stabilized with MPTMS are also shown in Figure 4.8 (a). It may be observed that the behaviour of sulfonated NP was similar to unmodified silica NPs. That is the majority of the NP were produced in the first 0.5 PV. Contrary to that with MPTMS (stabilizing fluid), the NP

production continues for 1 PV. Based on mass balance it was calculated that 74.6% of the sulfonated NPs were adsorbed in the core. Pressure drop profile recorded with sulfonated NPs is shown in Figure 4.8(b). The entry resistance post application of sulfonated NP was lower than the initial DIW injection. This observation was consistent with the case of the post flushing for cores saturated with unmodified NP. As the NP were being produced, high pressure drop fluctuation occurs. Thereafter the pressure drop profile declined smoother and almost overlaps with the initial DIW injection. In summary, the application of sulfonated NPs did not lead to improvement of water injectivity.

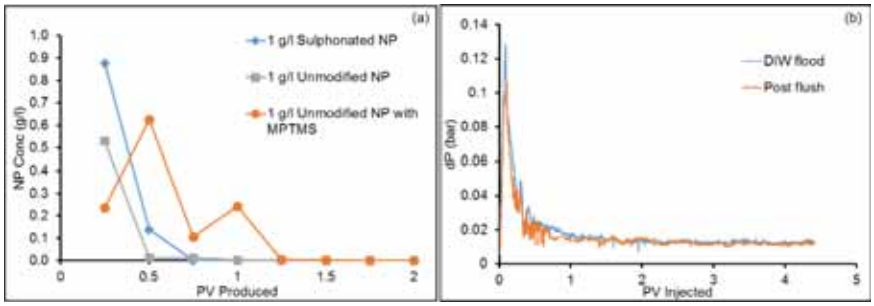


Figure 4.8 (a) Comparison of effluent concentration profiles of the different types of nanofluid (concentration of NP: 1 g/L) silica, sulfonated and silica with stabilizing fluid; (b) Pressure drop profiles for core treated with sulfonated NP.

Two important observations are made by the application of nanofluids and SEM imaging of silica NP adsorption in sandstone cores (1) The preferential adsorption of the silica NPs on quartz mineral, which was not reported pervious to this work and (2) The water injectivity improvement was observed upon the application of unmodified silica NPs. That is, the two nanofluid stabilization methods tend to reduce the effectiveness of the surface modification by the NPs. These observations are further investigated and strengthened in latter sections.

## 4.4 Adsorption of silica NP on Minerals

As mentioned previously, SEM images for cores saturated with silica NPs showed that the adsorption was mostly on quartz. To further investigate this, quartz and kaolinite powders were dispersed in all three kinds of nanofluids and the adsorption of NP per unit surface area of the mineral was determined as outlined in section 3.5.1. The results are shown in Figure 4.9.

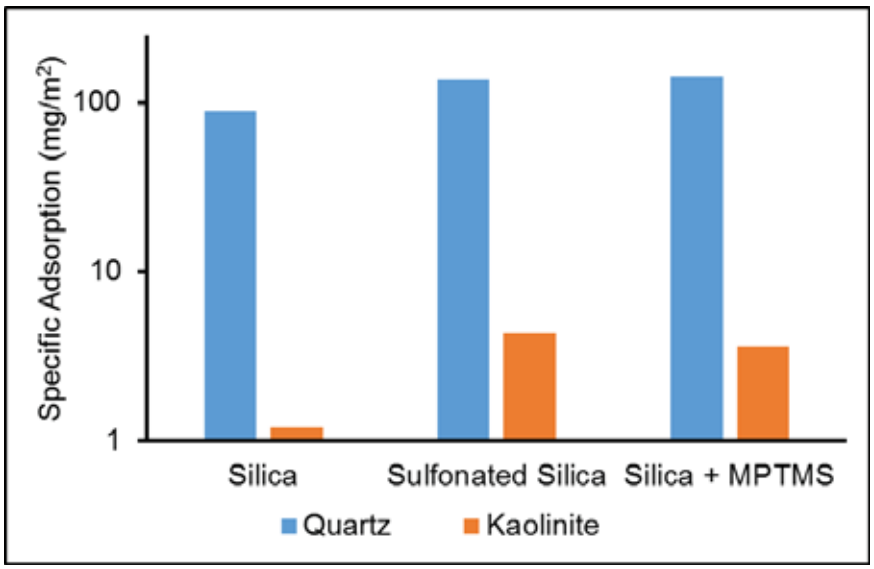


Figure 4.9 Specific adsorption of NP (mg/m$^2$) on quartz and kaolinite.

In addition, surface forces estimation was utilized to characterize the inter-surface interaction between NP-mineral based on the Derjaguin-Landau-Verwey-Overbeek (DLVO) theory. DLVO theory describes the forces between charged surfaces interacting in a medium. The DLVO theory combines the effect of attraction due to van der Waals interaction and the electrostatic repulsion due to the double layer of counter ions around charged surfaces in a medium. Silica NPs in this study have sizes in the order of 100–500 nm (Table 4.2). These are much smaller than the size of the mineral powders. Due to this

size difference, the curvature of the mineral surfaces may be neglected and the interactions can be modelled as Sphere-Plate collector geometry (Seetha et al. 2015, Khilar and Fogler 1998, Arab and Pourafshary 2013, Dunphy Guzman, Finnegan, and Banfield 2006). The forces acting on a particle approaching a mineral surface are the sum of van der Waals attraction, electric double layer repulsion and Born repulsion as follows:

$$V_t(h) = V_{LVA}(h) + V_{EDLR}(h) + V_{BR}(h) \tag{4.1}$$

where $V$ is the potential of interaction as a function of separation distance ($h$) between the particle and the collector surface. The subscripts $t$, $LVA$, $BR$, $EDLR$ denote total, London-van der Waal interaction, electric double layer interaction and Born Repulsion, respectively. The sign of the total interaction potential indicates attractive potential and repulsive potential for negative and positive signs respectively. The interaction potential can be represented in non-dimensional ($ND$) form as follows:

$$V_{t,ND}(h) = \frac{V_t(h)}{k_B \times T} \tag{4.2}$$

where $k_B$ is the Boltzmann constant ($1.38 \times 10^{-23}$ J·K$^{-1}$) and $T$ is temperature. In this study, all the experiments are conducted at room temperature hence $T$ = 297 K. The contributions due to the different types of interactions in Equation (4.1) can be calculated as follows (Khilar and Fogler 1998, Arab and Pourafshary 2013, Seetha et al. 2015):

$$V_{LVA}(h) = -\frac{A_{132}}{6}\left[\frac{2(1+H)}{H(2+H)} + ln\left(\frac{H}{2+H}\right)\right] \tag{4.3}$$

$$V_{EDLR}(h) = \left(\frac{\varepsilon_0 \varepsilon_3 a_p}{4}\right)\left[2\zeta_p\zeta_s\, ln\frac{1+exp(-\kappa h)}{1-exp(-\kappa h)} + \left(\zeta_p^2 + \zeta_P^2\right) ln(1 - exp(-2\kappa h))\right] \quad (4.4)$$

$$V_{BR}(h) = \frac{A_{132}}{7560}\left(\frac{\sigma}{a_p}\right)^6\left[\frac{8+H}{(2+H)^7} + \frac{6-H}{H^7}\right] \quad (4.5)$$

Where,

$$H = \frac{h}{a_p} \quad (4.6)$$

And, $a_p$ is the particle radius (m). $A_{132}$ is Hamaker's constant between the sphere and plate collector which is typically in the range of $10^{-19}$ J. This value of Hamaker's constant is based on the assumption that the van der Waals interactions occurs in vacuum and is not influenced by the presence of surrounding particles. Hence, to account of the intervening fluid and the surrounding particles, Hamaker's constant must be modified based on the Lifshitz theory (Israelachvili 2011). Based on previous work which are in turn based on the expression for modified Hamaker's constant developed by Israelachvili, the Hamaker's constant in this study is taken to be equal to $10^{-21}$ J (Arab and Pourafshary 2013). Also, $\varepsilon_0$ is the permittivity of free space ($8.854 \times 10^{-12}$ $C^2$ $J^{-1}$ $m^{-1}$) and $\varepsilon_3$ is the dielectric constant of water equal to 78 (Khilar and Fogler 1998, Arab and Pourafshary 2013). $\kappa$ is the inverse Debye length. For pure water used in this study, the inverse Debye length is equal to $(9.6 \times 10^{-7})^{-1}$ $m^{-1}$ (Arab and Pourafshary 2013). $\zeta_p$ and $\zeta_s$ are the surface potentials of the particles and the surface respectively which can be replaced by the zeta potential (Khilar and Fogler 1998). In Equation (4.5), $\sigma$ is the atomic collision diameter and is equal to 0.5 nm (Khilar and Fogler 1998). The born repulsive

potentials are formed when the particle approaches point of contact with the mineral resulting in overlap of electron clouds. Hence it is a short range interaction and thus calculated only when the distance of separation is less than 1 nm. $\sigma$ is the atomic collision diameter and is equal to 0.5 nm (Khilar and Fogler 1998). For the various scenarios in this study, the zeta potentials have been experimentally measured. The particle size and surface zeta potential data is shown in Table 4.2. The results for the surface forces estimation between NPs and minerals are shown in Figure 4.10.

Table 4.2 Particle Size and Zeta potential measurements of NP and minerals.

| **Material** | **Conc (g/L)** | **Dispersing Phase** | **Zeta Potential (mV)** | **Particle Radius (nm)** |
|---|---|---|---|---|
| Silica | 1 | DIW | −51.45 | 161.2 |
| Sulfonated silica | 1 | DIW | −44.8 | 182.9 |
| Silica | 1 | DIW + 1 g/100 mL MPTMS | −47.75 | 153.3 |
| Powdered Berea | 10 | DIW | −29.53 | - |
| Quartz powder | 10 | DIW | −5.732 | - |
| Kaolinite powder | 10 | DIW | −9.097 | - |

Figure 4.9 shows higher adsorption of NP on quartz compared to kaolinite. This was supported by Figure 4.10, where the attractive interaction potentials for all three type of NP were greater for quartz as compared to kaolinite. This in in line with SEM images where most of the adsorption of NPs were on the quartz mineral as compared to kaolinite.

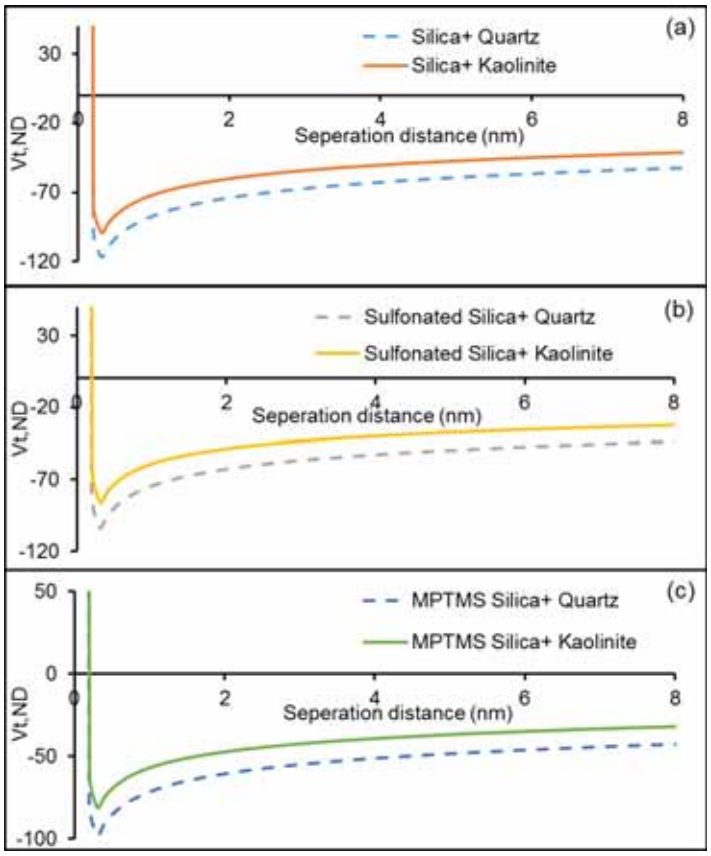


Figure 4.10 Interaction potential between the mineral and (a) unmodified silica; (b) sulfonated silica; and (c) unmodified silica + MPTMS.

In the previous section it was noted that the unmodified silica showed highest adsorption on the berea core (85.82%) followed by sulfonated silica (74.61%) and MPTMS stabilised silica (69.47%), however the stabilized NPs by MPTMS show higher adsorption in the static adsorption tests Figure 4.9. The reason is not known, however, the observation, may be explained by (1) insufficient contact time with minerals, i.e., slower kinetics than the unmodified NPs; (2) influence of the collective neighbouring minerals compared to individual

isolated minerals (static adsorption); (3) weak adsorption on mineral surface, hence desorbed in fluid flow and (4) all the above factors.

## 4.5 Interaction between Fines and Porous Media

The effect of berea surface modification on interaction between the fines and berea was addressed by surface forces estimation. Due to the size difference between the fines and mineral, the sphere plate model presented in section 4.4 was used to estimate the interaction. The surface zeta potential of berea in DIW was determined to be −29.53 mV (Table 4.2). To investigate the modification caused by NP, powdered berea at 10 g/L concentration was added to nanofluids of silica and sulfonated silica prepared in DIW at 1 g/L concentration. This mixture was left under stirring for 12 hrs. Thereafter, the surface zeta potential of the berea powder treated with unmodified and sulfonated silica was measured It was found that the surface zeta potential of treated berea was reduced to −11.4 mV and −20.36 mV in the case of unmodified and sulfonated silica respectively. The fines produced were analysed for the size and surface zeta potential. Specifically, effluent sample from effluent bank collected during DIW injection was collected and analysed. It was found that the zeta potential of the fine particles was −22.9 mV. The measured zeta potential of fines is in close agreement with previous measurements of fines eluted from berea sandstone (Kia, Fogler, and Reed 1987). In addition, the fines produced were in there different size classes (Table 4.3).

Table 4.3 Size classes of the fine particles

| Radius of Fine Particles (nm) | Intensity (%) |
|---|---|
| 233.8 | 73.0 |
| 68.57 | 24.2 |
| 2687 | 2.8 |

Since the fines have separate size classes, the interaction potential was calculated for each size class and summed on a weighted basis as:

$$V_t(h) = \sum_{i=1}^{n} \{V_{t,i}(h) \times w_i\} \tag{4.7}$$

where $w_i$ is the weight intensity of each size class and $V_{t,i}(h)$ is the interaction potential calculated for the specific size class and finite distance of separation ($h$). Thereafter, the non-dimensional interaction energy was determined using Equation (4.2). The interaction potentials between berea mineral and fines calculated for the reference case (no NP) and berea treated with silica and sulfonated silica is shown in Figure 4.11.

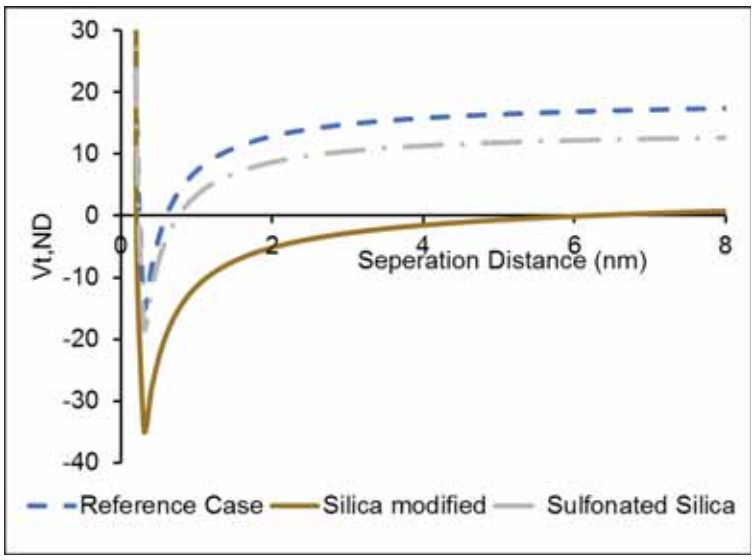


Figure 4.11 Dimensionless Interaction potential between the fines and the berea mineral for reference case (no NP), berea treated with silica and berea treated with sulfonated silica.

In Figure 4.11, it may be observed that in the reference case, there is a net repulsive potential between the fines and the mineral surface. However, for

mineral treated with silica NPs, there is a net attractive potential between the fines and the mineral. This could possibly cause the mineral to act as collectors for capturing fine particles thereby reducing fine migration. This may explain the improvement in water injectivity post application of silica nanofluid as observed in Figure 4.2 and Figure 4.3. In the case where berea was treated with sulfonated NP, there is a reduction in the repulsion (Figure 4.11), however the net potential is still close to the reference case. This may explain the similarity in pressure drops observed during initial DIW injection and post flush after saturating the core with sulfonated NP in Figure 4.8(b). Thus, it maybe concluded that the surface modification caused silica is much more effective at reducing fine migration and thereby improving the water injectivity in berea cores. Li and Torsæter (2015) observed that the injection of colloidal NP into berea sandstone did not lead to permeability impairment. They stated that adsorption of NP on the pore wall act like lubrication reducing the friction between the water and pore walls. However, as discussed in this, this effect may be explained by the surface modification of berea which reduces the fines migration.

## 4.6 Summary

This chapter addressed the surface modification of berea sandstone by the in-house silica nanofluids. Low salinity water flooding is currently a popular method for EOR. However, it suffers from increased fines migration. Excessive fines production may lead to formation damage. It is observed in this work that the adsorption of NPs in berea sandstone could reduce the production and migration of fines. This may be the result of the adsorption of silica NPs on the mineral surfaces, which in turns affects the direct contact between the flooding fluid and rock mineral. The reduction of the fines was indicated by the reduced

pressure drop, i.e. reduce the flow resistance of the fluid during the post flush of the NPs' slug. In addition, it was shown that the adsorption of silica NPs modifies the sandstone surface and makes the interaction between the modified surface and the fine particles attractive. The modified surface acts as a collector for the fines. This may lower the migration of produced fines.

It was observed that the silica NPs have preferential adsorption affinity towards quartz surfaces compared to kaolinite. Unmodified silica nanofluid reduced fine migration and improved water injectivity. Adsorption of NPs on mineral surfaces may be utilized to overcome the problem of formation damage induced during low salinity flooding. Stabilization enhances the static adsorption of NPs on quartz and kaolinite minerals. However, the used stabilization method showed inconsiderable effect compared to nanofluids of unmodified NPs.

These observations form the basis of the investigations in the flowing chapters. Since the in-house nanofluids investigated up to this point in the study are stable only for about 1 day, in the flowing chapters, a stable commercial silica nanofluid (DP 9711) is used to address first the adsorption of the silica NPs followed by transport and oil recovery in sandstone and chalk cores. Throughout the work, the associated fluid/rock interaction are investigated.

# 5 Adsorption of silica NPs on minerals

This chapter addresses the static adsorption and kinetic aspects of silica NP adsorption on major minerals present in chalk and sandstone rocks. The contents of this chapter refer to the work presented in Papers 2-5.

## 5.1 Nanofluids characterization

The NFs used were prepared from the stock fluid (DP9711) by diluting it with different brines. NFs prepared in DIW, LSW and SSW at 1 g/L NP concentration were characterized for particle size and zeta potential at different temperatures. NPs stability at different temperatures were examined by particle size measurements as shown in Figure 5.1. Figure 5.1(a) shows the average hydrodynamic diameter of the NPs. For 1 g/L NP concentration in DIW and LSW, similar particle size (average size about 38.4 ± 0.6 nm) was observed at all three temperatures. However, in SSW the NPs showed higher particle size of around 57 ± 0.5 nm at 25°C and 50 °C and about 88 ±0.1 nm at 80 °C. That is an average size of about 67 ± 0.3 nm, which is approximately 43% higher than the average particle size for all tested temperatures with DIW and LSW. One possible reason for the difference in the measured zeta potential may be the compression of the double layer at higher salinity.

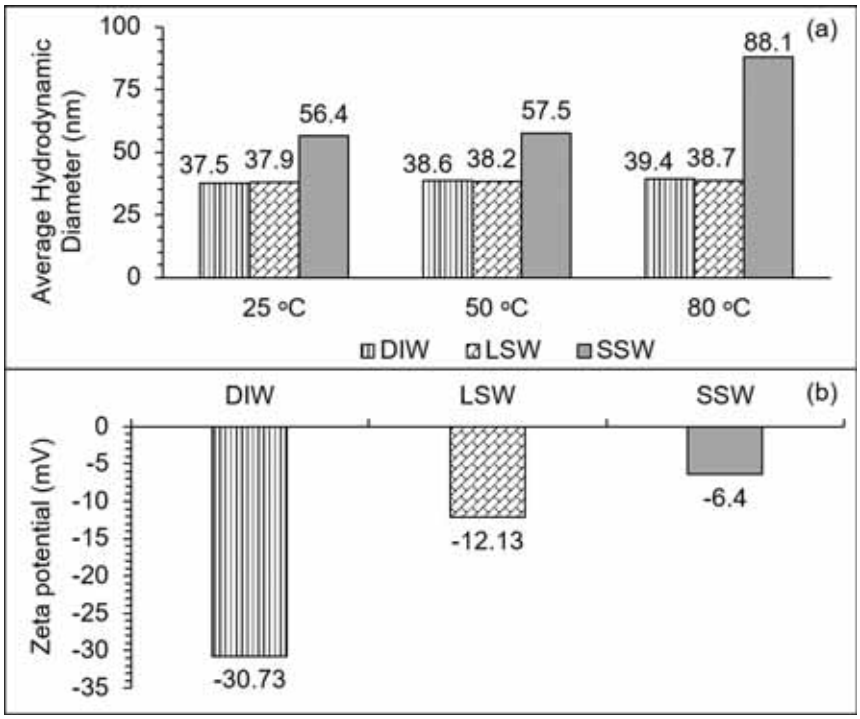


Figure 5.1 (a) Average particle size of the NPs dispersed in DIW, LSW & SSW measured at varying temperatures. (b) Zeta potential measurements (25 °C) of the NPs in DIW, LSW and SSW.

The measured surface zeta potential at 25 °C for the NFs prepared in SSW was about −6.4 mV compared with −30.73 and −12.13 mV for DIW and LSW, respectively. Griffith et al. (2016) stated a similar observation for DP9711 NFs. They observed that increasing the brine salinity did not immediately increase particle size but that, after a certain point in time, a sudden rise in particle size was seen. To address particle size and stability, particle size measurements were repeated after three months. These tests showed that all measurements were close to the initial measured values (within 5 nm). In addition, the NFs remained visually clear with no sign of sedimentation.

## 5.2 Static adsorption of silica NPs on sandstone minerals

Metin, Baran, and Nguyen (2012) reported that the adsorption of surface functionalized silica NPs on quartz mineral surfaces was insignificant. Other researchers reported significant adsorption of silica NPs on sandstones (Li et al. 2013, Yuan, Moghanloo, and Zheng 2016, Zhang et al. 2015). Isothermal static adsorption tests on mineral powders (quartz and kaolinite) were performed at room temperature. The experiments were performed in DIW and SSW media to address the effect of salinity on NPs' adsorption. 0.15 g of mineral was added to NF prepared at 1 and 0.5 g/L NP concentration. The results are shown in Figure 5.2.

Figure 5.2 shows that the NPs have greater affinity to adsorb on quartz than on kaolinite surface which is in line with the observations made in the previous chapter with in-house nanofluids. Figure 5.2 also shows that increasing NPs' concentration increases the adsorbed amount per unit surface area of the minerals. In all experiments, the volume of NF was kept constant (30 ml) and the added amount of mineral was also constant (0.15 g). Higher adsorption occurred in SSW environment. The measured zeta potential of the NPs in SSW was -12.13 mV which is about 2.5 times less negative than that in the case of NPs in DIW (-30.73 mV) as shown in Figure 5.1. The difference in the zeta potential may have been caused by double later compression due to higher ionic strength (SSW). Hence, the electrostatic repulsion between the NP and the mineral decreases enhancing adsorption of NPs.

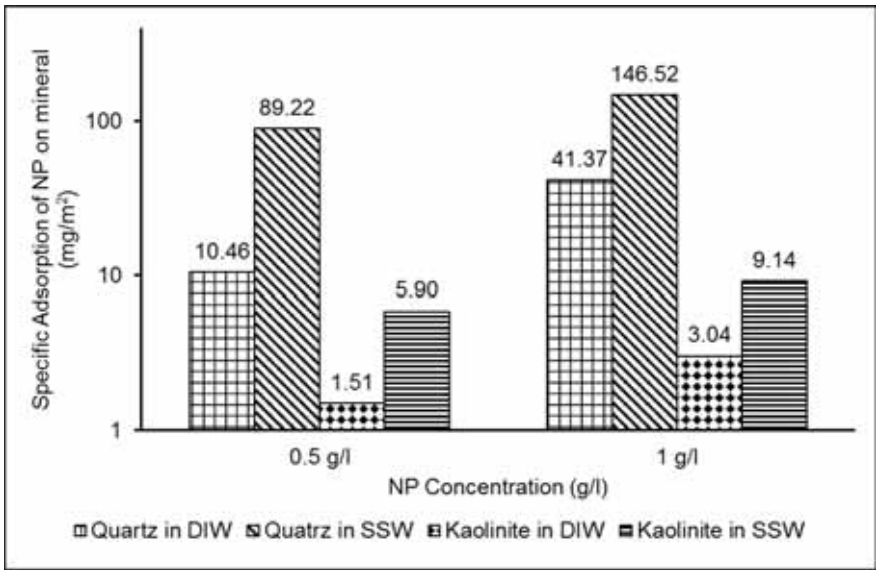


Figure 5.2 Specific adsorption (mg/m$^2$) of two concentrations of NPs (0.5 and 1 g/L) on quartz and kaolinite minerals in DIW and SSW environment.

Zhang et al. (2015) also identified that strong repulsion exists between NPs and sand particles at low salinity. They reported that adsorption of NPs increases with less clay content. The SEM image (Figure 5.3) visually shows that more NPs adsorb on quartz surface compared to kaolinite i.e., SEM image confirmed the preferential adsorption of NPs obtained by the static adsorption tests. Thus increasing the clay content may have affected the overall adsorption of NPs. SEM image is of a berea core treated with 1 g/L NF prepared in DIW. The core was cleaved and imaged along the flooding plane. Adsorption of NPs on the mineral surface was shown to be well spread that may indicate a monolayer like coverage. There was some in situ aggregation of the NP which may be due to drying and handling processes of the core before taking the SEM image. However, the image did not show pore throat blockage hence permeability impairment is not expected.

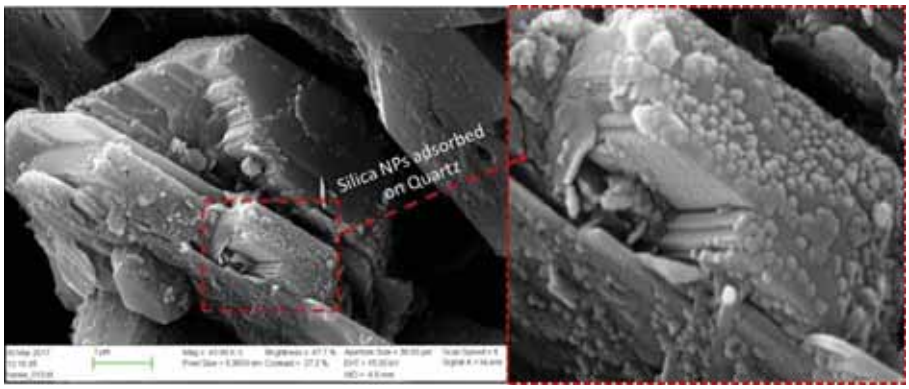


Figure 5.3 SEM image of NP adsorbed on mineral surfaces on a berea core and magnified view of the NP adsorbed on quartz surface on the right.

## 5.3 Static adsorption of silica NPs on calcite

Static adsorption tests of NPs on a calcite surface were conducted with DIW and SSW. Figure 5.4(a) shows that the adsorption of the NPs on the calcite surface increases with the NP concentration. Figure 5.4(a) also shows that at a lower concentration of NPs prepared in SSW, adsorption is higher than in DIW (≈ 40%). At higher NP concentrations, however, the adsorptions in SSW and DIW were almost the same. Monfared et al. (2015) have reported an increase in adsorption of unmodified silica NPs on a calcite surface with increasing salinity (0–0.2 mol/L) of single salt (NaCl) brine at low NP concentrations (0.4 and 0.6 g/L).

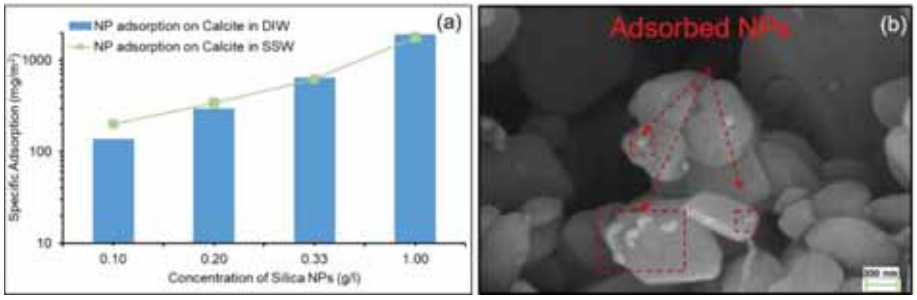


Figure 5.4 (a) Adsorption of silica NPs on Calcite surface. (b) SEM image of NPs adsorbed on chalk core with DP 9711 nanofluid at 1 g/L concentration prepared in DIW.

Zeta potential of the NPs becomes less negative in the presence of SSW ions (Figure 5.1) owing to the compression of the double layer. This would lower the electrostatic repulsion and enhance the adsorption. Figure 5.4(b) shows a SEM image of a chalk core which was vacuum-treated with 1 g/L NF prepared in DIW. The image was taken along the injection plane. In general, NPs are shown to be spread on the chalk surface similar to the observations made by Monfared et al. (2015). No pore throat blockage was observed from SEM imaging. The SEM images were done on spots along horizontally cut core. However, they are small fractions of the whole core.

Comparing the relative adsorption of silica NPs on the tested mineral shows that the NPs' highest adsorption affinity is towards calcite followed by quartz and least adsorption affinity towards kaolinite. In the following sections, the kinetic aspects of silica NP adsorption on quartz and calcite minerals are addressed.

## 5.4 Kinetics of silica NP adsorption on quartz

This section addresses the kinetics of silica NP adsorption on quartz which the major constituent mineral in sandstones. The adsorption was investigated at three salinities: DIW, Synthetic seawater (SSW) and Low salinity water (1:10 SSW). All nanofluids were prepared at 1 g/L concentration. Quartz powder was used as the adsorbate in these experiments. The details are outlined in section 3.5. Pseudo first order and pseudo second order models were used to address the kinetics of the adsorption process. The linearized form of the pseudo first order and second order kinetics models can, respectively be expressed as (Ho and McKay 1999, Monfared et al. 2015):

$$\ln\left(q_{eq} - q(t)\right) = ln(q_{eq}) - k_1 t \tag{5.1}$$

$$\frac{1}{q(t)} = \frac{1}{k_2 q_{eq}^2} + \frac{t}{q_{eq}} \tag{5.2}$$

Where, $q(t)$ and $q_{eq}$ are the experimental data of NP adsorption (mg/g) on quartz at a given time ($t$) and equilibrium, respectively. $k_1$ (1/h) and $k_2$ (g/mg h) are the rate constants. The linear fits for adsorption data in DIW, LSW and SSW are shown in Figure 5.5. In Figure 5.5(a), $ln(q_e\text{-}q(t))$ vs $t$ is shown and in Figure 5.5(b), $t/q(t)$ vs $t$ is shown. They are the performed linear fits (for all three salinities) for pseudo first and second order kinetic model respectively. The fits were used to obtain the slope ($m$) and intercept ($c$) which were used to calculate the rate constants and estimated equilibrium adsorption for both models and they are listed in Table 5.1. The quality of the fit was judged based on the correlation coefficient ($R^2$) and comparing model estimated equilibrium adsorption to the measured value. It is shown in Figure 5.5 (c) and that pseudo first order model does not describe the data well since the $R^2$ values for the fits are low (0.86-0.93) and the model estimated equilibrium adsorption differs

significantly from the measurement. However, for pseudo second order model, the fits are much better ($R^2 \approx 0.99$) and the model estimated adsorption are close to measurements with an average mean deviation of around 0.07 mg/g. Together, this suggests that pseudo second order kinetic model best describes the progression of NP adsorption on quartz. It is also interesting to note that as the salinity increases from DIW to SSW, both the rate and equilibrium adsorption capacity increases. This confirms that salinity has positive effect on the adsorption process. The adsorption data was also fit to the linearized Intraparticle diffusion (IPD) model to address adsorption mechanism as follows (Monfared et al. 2015, Wu, Tseng, and Juang 2009):

$$q(t) = Kt^{1/2} + C \tag{5.3}$$

Where, $K$ (mg/g $h^{1/2}$) is the IPD rate which is related to the transport of adsorbate particles to the adsorptions sites on the adsorbent; $C$ (mg/g) refers to the boundary layer effect which is related to the film diffusion of the adsorbate (NPs) from the solution to the surface of the adsorbent (quartz). $K$ and $C$ estimated from the slope and intercepts in Figure 5.5(c) are shown in Table 5.1

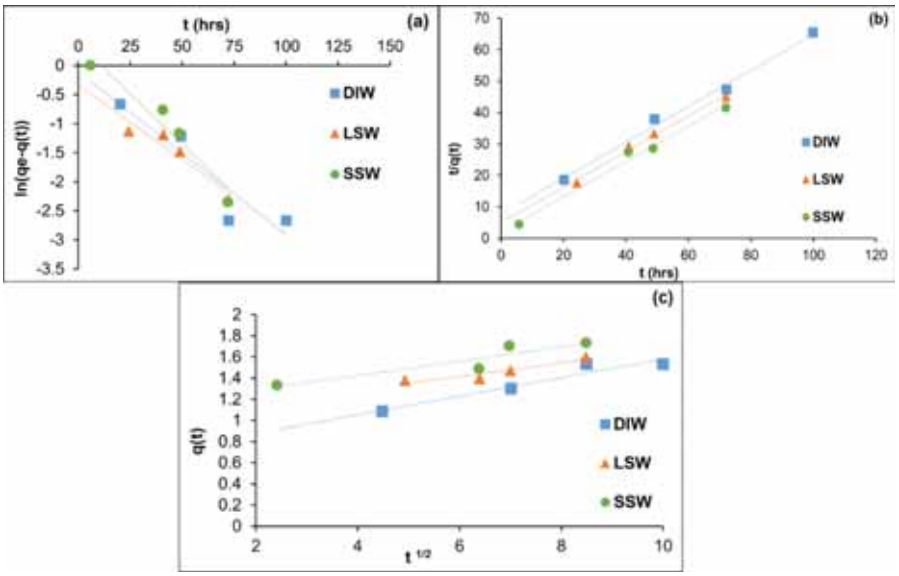


Figure 5.5 Linear fit of adsorption data: (a) Pseudo first order (b) Pseudo second order kinetics model and (c) Intraparticle diffusion model.

For the IPD model, it can be seen that adsorption in DIW shows the best fit ($R^2$= 0.93). In saline environments (LSW/SSW) the quality of the fit falls to around 0.86. None of fits passes through the origin indicating that IPD is not the sole rate controlling mechanism. Thus, the NP adsorption is a combination of film diffusion and IPD. It is shown that as we move from DIW to SSW, the estimated IPD rate falls by around 20 %. The reduction in IPD rate may be due to increased NP particle size when dispersed in SSW (Figure 5.1), which is approximately 1.5 times the size of the NPs in DIW/LSW. The increased size in SSW may hinder the transport of NPs on the adsorbent (quartz) surface. At the same time, the boundary layer effect (film diffusion) which represents the transport of NP from the solution to the mineral surface increases by ≈ 40 % from DIW to LSW and an additional 10 % in SSW. The transport of NP to the mineral surfaces would be affected by the interaction between the NPs and the

mineral. To address this, the DLVO interaction between NP and mineral was estimated.

Table 5.1 Estimated fit parameters for silica NP adsorption data on quartz.

| **Pseudo 1st order Model** | | | | |
|---|---|---|---|---|
| **Medium** | **Exp $q_e$ (mg/g)** | **$R^2$** | **$k_1$: (1/h)** | **Estimated $q_e$: (mg/g)** |
| DIW | 1.6 | 0.8664 | 0.028 | 0.90 |
| LSW | 1.7 | 0.8906 | 0.022 | 0.59 |
| SSW | 1.8 | 0.9388 | 0.035 | 1.46 |
| **Pseudo 2nd order Model** | | | | |
| **Medium** | **Exp $q_e$ (mg/g)** | **$R^2$** | **$k_2$ :(g/mg h)** | **Estimated $q_e$: (mg/g)** |
| DIW | 1.6 | 0.9932 | 0.042 | 1.75 |
| LSW | 1.7 | 0.9909 | 0.065 | 1.77 |
| SSW | 1.8 | 0.9883 | 0.154 | 1.79 |
| **Intraparticle Diffusion Model** | | | | |
| **Medium** | **$R^2$** | **$C$ (mg/g)** | **$K$ (mg/g $h^{1/2}$)** | |
| DIW | 0.9303 | 0.70 | 0.088 | |
| LSW | 0.8786 | 1.03 | 0.065 | |
| SSW | 0.8529 | 1.16 | 0.067 | |

The theory of surface forces can be utilized to calculate interaction energies between the NP and quartz minerals based on the DLVO theory. Due to the size

difference between the NP and mineral the curvature of the mineral surface may be neglected and the interactions can be modelled as Sphere - Plate collector geometry. The net interaction ($V_t$) as a function of separation distance ($h$) is the sum of London-van der Waal interaction and Electric double layer interaction which can be calculated as:

$$V_t(h) = V_{LVA}(h) + V_{EDLR}(h) \tag{5.4}$$

The contributions due to the different interactions in Equation 5.4 based on the constant potential approach can be calculated as follows (Monfared et al. 2015, Dunphy Guzman, Finnegan, and Banfield 2006, Bhattacharjee and Elimelech 1997):

$$V_{LVA}(h) = -\frac{A_{132}}{6}\left[\frac{a_p}{h} + \frac{a_p}{h+2a_p} + ln\left(\frac{h}{h+2a_p}\right)\right] \tag{5.5}$$

$$V_{EDLR}(h) = \pi\varepsilon_0\varepsilon_3\kappa\left(\zeta_p^2 + \zeta_s^2\right)\int_0^{a_p}\left(-coth\left[\kappa\left(h + a_p - a_p\sqrt{1-\left(h/a_p\right)^2}\right)\right] + coth\left[\kappa\left(h + a_p + a_p\sqrt{1-\left(h/a_p\right)^2}\right)\right] + \frac{\zeta_p\zeta_s}{\zeta_p^2+\zeta_s^2}csch\left[\kappa\left(h + a_p - a_p\sqrt{1-\left(h/a_p\right)^2}\right)\right] - \frac{\zeta_p\zeta_s}{\zeta_p^2+\zeta_s^2}csch\left[\kappa\left(h + a_p + a_p\sqrt{1-\left(h/a_p\right)^2}\right)\right]\right)r.dr \tag{5.6}$$

Hamaker's ($A_{132}$) constant was calculated according to Lifshitz theory based on the refractive indices, dielectric constants and the temperature (Israelachvili 2011):

$$A_{132} \approx \frac{3}{4} K_b T \left(\frac{\varepsilon_1 - \varepsilon_3}{\varepsilon_1 + \varepsilon_3}\right)\left(\frac{\varepsilon_2 - \varepsilon_3}{\varepsilon_2 + \varepsilon_3}\right) + \frac{3h_o v_e}{8\sqrt{2}} \left(\frac{(\eta_1^2 - \eta_3^2)(\eta_2^2 - \eta_3^2)}{((\eta_1^2 + \eta_3^2)(\eta_2^2 + \eta_3^2))^{\frac{1}{2}}((\eta_1^2 + \eta_3^2)^{\frac{1}{2}} + (\eta_2^2 + \eta_3^2)^{\frac{1}{2}})}\right) \quad (5.7)$$

Where $\varepsilon_1$(4.5), $\varepsilon_2$(4.5) and $\varepsilon_3$(80) represents the static dielectric constants and $\eta_1$(1.45), $\eta_2$(1.45) and $\eta_3$(1.33) represents the refractive indices at 0.5876 μm wavelength of the interacting species (mineral and NP which are both $SiO_2$) and the intervening media: water, respectively. The refractive index can vary by approximately 7.9 *$10^{-3}$ between fresh water and salt water and hence its effect has been neglected (Temple 2007). $v_e$ is the main electron absorption frequency in the ultraviolet region and its value is between 3-5 ×$10^{15}$$s^{-1}$(Israelachvili 2011). The permittivity of free space $\varepsilon_0$: 8.854 × $10^{-12}$ $C^2$ $J^{-1}$ $m^{-1}$. $\zeta_p$ and $\zeta_s$ are the surface potentials of the NP and minerals respectively which can be considered as the zeta potential. Based on equation 5.7, the Hamaker's constant was estimated as 5.6 × $10^{-21}$ J. The surface forces estimation in this study are performed 25°C. For DIW, the inverse Debye length can be taken as (9.6 × $10^{-7}$) $^{-1}$ $m^{-1}$ (Khilar and Fogler 1998). For saline mediums, the inverse Debye length ($\kappa$) depends on the salinity of the intervening medium (LSW/SSW) and can be calculated as:

$$\kappa^{-1} = \sqrt{\frac{\varepsilon_0 \varepsilon_3 k_B T}{2 N_A e^2 I}} \quad (5.8)$$

Where, $e$ is the elementary charge of an electron (C), $k_B$ is the Boltzmann constant, $N_A$ is the Avogadro number and $I$ is the ionic strength of the medium:

$$I = \frac{1}{2} \sum c_i Z_i^2 \quad (5.9)$$

Where, $c_i$ is the ion concertation of the i$^{th}$ species and $Z_i$ is the valence number of the i$^{th}$ species as listed in Table 3.3. Finally, the total non-dimensionalized interaction energy ($V_{t,ND}$) can be calculated as follows:

$$V_{t,ND}(h) = \frac{(V_{LVA}(h)+V_{EDLR}(h))}{k_B*T} \quad (5.10)$$

The particle size and zeta potential of the NPs in DIW, LSW and SSW have been measured previously (Figure 5.1). Zeta potentials measurements of crushed berea core (which is mostly composed of quartz) dispersed in different waters were used for DLVO calculation. The measurements are shown in Table 5.2. The estimated surface forces are shown in Figure 5.6.

Table 5.2 Zeta potential of crushed berea powder dispersed in different brines.

| **Material** | **Zeta-potential (mV)** |
|---|---|
| Berea in DIW | -29.5 |
| Berea in LSW | -18.1 |
| Berea in SSW | -7.7 |

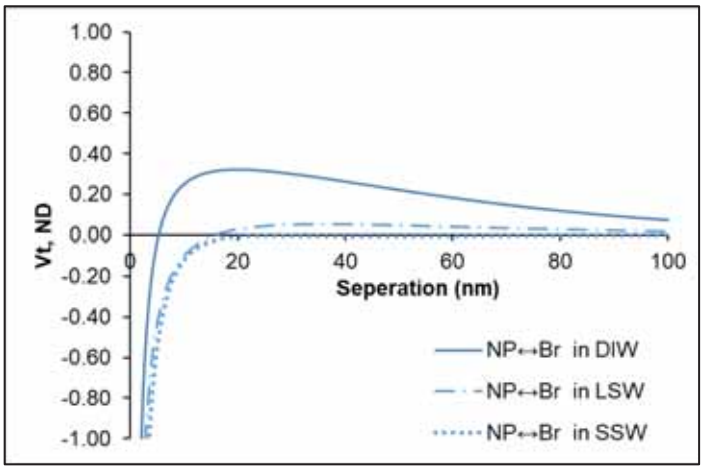


Figure 5.6 Effect of salinity on interaction energies between (a) NP and berea

In Figure 5.6 it is shown that the interaction energy is most repulsive for DIW followed by LSW, while it is slightly attractive for SSW. That is, the interaction between the NPs and the mineral becomes less repulsive as the salinity increases. Lowered repulsion with increasing salinity would enhance transport of NPs from the fluid to the mineral surface thereby increasing film diffusion. This qualitatively supports the observation made earlier regarding the increased contribution of film diffusion to the adsorption as the salinity increases.

## 5.5 Kinetics of silica NP adsorption on calcite

This section addresses the kinetics of silica NP adsorption on calcite and its effect on fluid/mineral interaction. Adsorption of NP dispersed in water at three salinities (DIW, LSW and SSW) and its influence on calcite dissolution was investigated. The used NP concentrations was 1 g/L for all the fluids except an additional concentration of 1.5 g/L that was used in the case of LSW. The NP adsorption data obtained from the experiments described in section 3.5 were fit

to pseudo first order and pseudo second order models to address the order of the adoption process (Eq. 5.1 and 5.2).

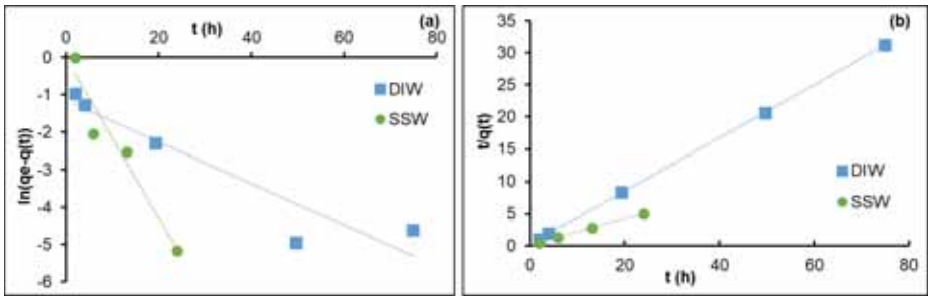


Figure 5.7 Data fit for the adsorption of NP on calcite in DIW and SSW: (a) pseudo first order (b) pseudo second order kinetic models.

The linear fits for adsorption data in DIW and SSW are shown Figure 5.7. The slope and the intercept from the linear fits were used to estimate the rate constants and equilibrium adsorption for both models (Table 5.3). It is shown in Figure 5.7 (a) and Table 5.3 that the $R^2$ correlation values of the linear fits are poor (0.88-0.94) for both DIW and SSW. The model estimated equilibrium adsorption varies significantly from the experimentally observed level of equilibrium adsorption. Therefore, it may be concluded that the pseudo first order model does not describe the adsorption process well. However, the fits for adsorption in both DIW and SSW are excellent for the pseudo second order kinetic model (Figure 5.8b). The $R^2$ values are close to 1 and the model estimated equilibrium adsorption agrees well with the experimental data (Table 5.3). This indicates that the pseudo second order kinetic model best describes the progression of silica NP adsorption on the calcite surface. It is interesting to see that at elevated salinity (SSW) the adsorption rate is ≈ 3 times higher than that for DIW and the equilibrium adsorption almost doubled.

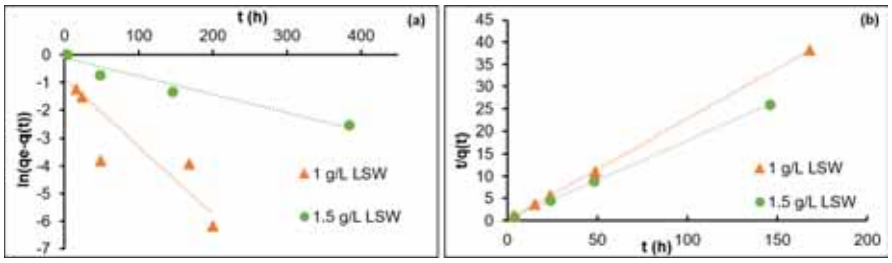


Figure 5.8 Data fit for the adsorption of silica NP on calcite in LSW: (a) pseudo first order (b) pseudo second order kinetic models.

To address the adsorption of NP in LSW, two sets of adsorption experiments are performed at two NP concentrations, 1 and 1.5 g/L. The amount of the calcite was kept constant. Figure 5.8 (b) and Table 5.3 shows the data fit.

Table 5.3 Summary of the fit parameters for progressive silica NP adsorption on calcite.

| **Pseudo 1st order Model** | | | | |
|---|---|---|---|---|
| **Fluid** | **Exp $q_e$ (mg/g)** | **$R^2$** | **$k_1$ :(1/h)** | **Estimated $q_e$: (mg/g)** |
| DIW (NP Conc 1 g/L) | 2.41 | 0.88 | 0.055 | 0.312 |
| SSW (NP Conc 1 g/L) | 4.75 | 0.94 | 0.2132.5 | 0.971 |
| LSW (NP Conc 1 g/L) | 4.4 | 0.9025 | 0.1149 | 1.09 |
| LSW (NP Conc 1.5 g/L) | 4.75 | 0.9378 | 0.0066 | 0.89 |
| **Pseudo 2nd order Model** | | | | |
| **Fluid** | **Exp $q_e$ (mg/g)** | **$R^2$** | **$k_2$ :(g/mg h)** | **Estimated $q_e$: (mg/g)** |
| DIW (NP Conc 1 g/L) | 2.41 | 0.99 | 0.73 | 2.42 |
| SSW (NP Conc 1 g/L) | 4.75 | 1 | 2.5 | 4.77 |
| LSW (NP Conc 1 g/L) | 4.4 | 1 | 0.191 | 4.44 |
| LSW (NP Conc 1.5 g/L) | 4.75 | 0.99 | 0.11 | 5.68 |

It is shown in Figure 5.8 (a) and Table 5.3 that $R^2$ for the first order is poor (0.9-0.93) for both concentration of NP in LSW and the model estimated equilibrium adsorption varies significantly from the experimentally observed level of

equilibrium adsorption. It is therefore, concluded that similar to the adsorption of NP from DIW and SSW, pseudo second order kinetic model describe the adsorption process well with $R^2 \approx 1$ for both the concentrations. It is interesting to note that as NP concertation increases from 1 to 1.5 g/L, the rate of adsorption decreases from 0.191 to 0.11 g/mg hr. In addition, the adsorption rates in LSW (for both concentration) are lower than the rate estimated for DIW and SSW. This observation is discussed latter in this section.

The proposed model by Weber and Morris (1962) has been applied previously in literature to understand adsorption mechanisms. Wu, Tseng, and Juang (2009) used the fractional approach of equilibrium change to determine the IPD contribution to the adsorption as follows:

$$q_{eq} = K\, t_{eq}^{1.5} + C \tag{5.11}$$

Rearrangement of Equations 5.3 and 5.11 yields,

$$\frac{q_t}{q_{eq}} = 1 - R_i \left[1 - \left(\frac{t}{t_{eq}}\right)^{0.5}\right] \tag{5.12}$$

where,

$$R_i = K \frac{{t_{eq}}^{0.5}}{q_{eq}} \tag{5.13}$$

*Here,* $R_i$ is defined as the initial adsorption factor and $t_{eq}$ (hr) is the time to reach equilibrium adsorption. $R_i$ may also be expressed as the ratio of initial adsorption to equilibrium adsorption amounts, which is used in this work:

$$R_i = 1 - \frac{C}{q_{eq}} \tag{5.14}$$

In Equation 5.14, if $C = 0$, means there is no initial adsorption in the system. Figure 5.9 shows characteristic curves for DIW (NP conc 1g/L), LSW (NP conc 1g/L), LSW (NP conc 1.5 g/L) and SSW (NP conc 1g/L) systems. Table 5.4 shows the classified adsorption characteristic according to Wu, Tseng, and Juang (2009). In the case of DIW, LSW (1g/L) and LSW (1.5g/L) adsorption is classified as strong initial adsorption. That is, all the tested systems follow strong initial adsorption behavior except SSW (1g/L), which is shown to be approaching complete initial adsorption, where $q_{eq}$ is almost equal to C (initial adsorption amount). In addition, for SSW, the time to reach equilibrium is almost 50% less than that for the other systems.

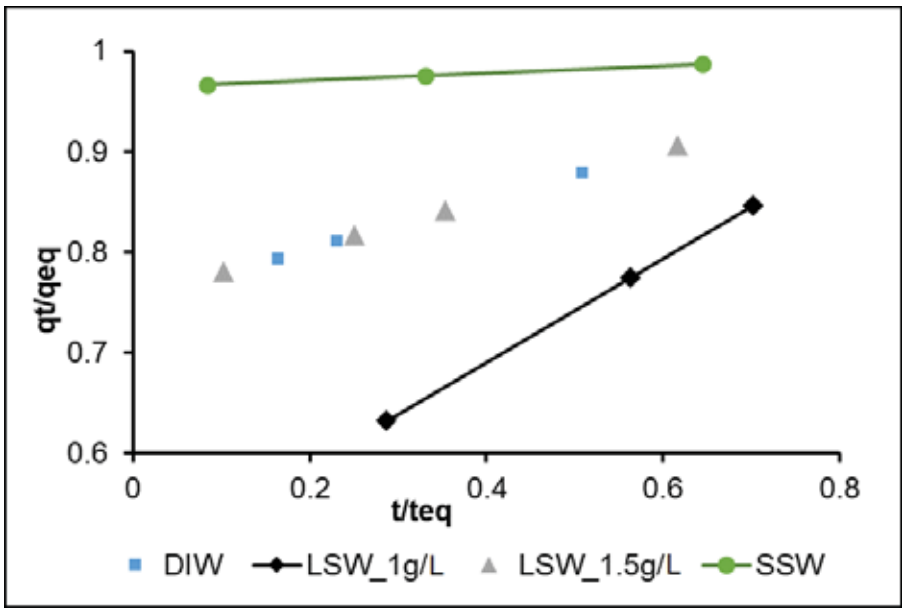


Figure 5.9 Non-dimensional intraparticle diffusion model for adsorption characteristic curves of the four tested systems with dispersed silica NP.

Table 5.4 Summary of initial adsorption of IPD model.

| **Fluid_ NP conc.** | ***C* (mg/g)** | ***K* (mg/g $h^{0.5}$)** | $R_i$ | **$t_{eq}$(hrs)_Adsorption Characterization** |
|---|---|---|---|---|
| DIW_1.0 g/l | 1.8 | 0.16 | 0.25 | 49 (hrs)_ Strong initial adsorption |
| LSW_1.0 g/l | 2.13 | 0.51 | 0.52 | 49(hrs)_Strong initial adsorption |
| LSW_1.5 g/l | 4.29 | 0.19 | 0.24 | 49(hrs)_Strong initial adsorption |
| SSW_1.0 g/l | 4.56 | 0.036 | 0.037 | 16(hrs)_near complete initial adsorption |

The reduced *Ri* in LSW, as the NP concentration increases from 1to 1.5 g/L to almost half may be explained by repulsive forces among the NP as they diffuse from the bulk fluid towards the calcite surface. In other words, the effect of ion charges could help in reducing the repulsive forces; however, the efficiency of the ion charges in shielding NP and reducing the repulsive forces among them is reduced as NP concentration increases. This may also explain the lower adsorption rate observed for LSW with NP at 1.5 g/L during investigation of the adsorption kinetic order in earlier.

Another interesting observation is that *Ri* is almost equal for both DIW and LSW (1.5 g/L), which may support the above hypothesis. That is in the presence of dissolved salts, the ions work as a barrier reducing the adsorption rate and in absence of salt ions (DIW) the repulsive force among NP reduces the adsorption rate. This is an interesting phenomenon worth further investigation.

Figure 5.10 shows the total interaction energies, estimated by DLVO theory based on the model presented in section 5.4 between the silica particles and calcite mineral. The measured zeta potential of calcite mineral is shown in

Table 5.5. It is shown in Figure 5.10 that interaction between NP can calcite in DIW and SSW remains attractive. However, in case of LSW the interaction energy is shown to be less attractive and becomes slightly repulsive at around 30 nm separation. In other words, the LSW system involves more repulsive conditions compared to SSW and DIW systems. This qualitatively support the lower adsorption rate in LSW system.

Table 5.5 Zeta potential measurements of calcite mineral.

| Material | Zeta-potential (mV) |
|---|---|
| Calcite in DIW | -23.4 |
| Calcite in LSW | -8.0 |
| Calcite in SSW | -3.7 |

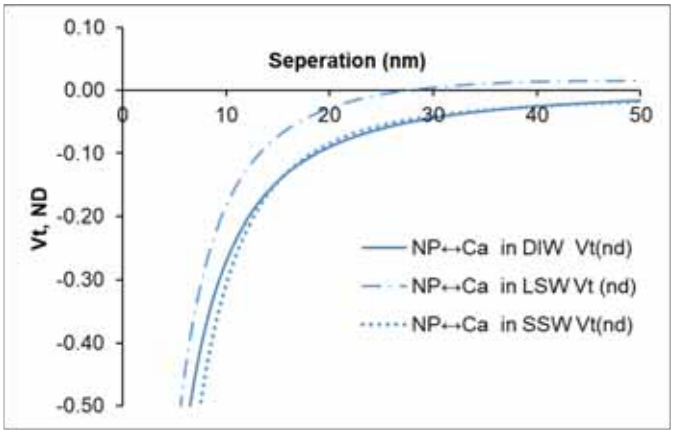


Figure 5.10 DLVO (total interaction energy) between NP and calcite (Ca) mineral interaction in DIW, SSW and LSW

During the adsorption experiments discussed above, the calcium ion concentration and pH were tracked during the adsorption experiments to address the effect of NP adsorption on calcite dissolution. Two main chemical processes (dissolution and adsorption) may have taken place between fluids and mineral ($CaCO_3$) as presented below:

$$CaCO_3 + H_2O \rightleftharpoons Ca^{2+} + HCO_3^- + OH^- \quad (5.15)$$

$$2CaCO_3 + H_2O + NP \rightleftharpoons CaCO_3 - NP + Ca^{2+} + HCO_3^- + OH^- \quad (5.16)$$

As shown in Eq .5.15, dissolution of calcite increases the pH. The adsorption process may be presented by Eq. 5.16, where $OH^-$ and $HCO_3^-$ are among the reaction products. The above two reactions indicate increase of the fluids' pH due to calcite dissolution. The pH values with the dispersed NP in DIW, LSW and SSW are 6.0, 7.2 and 7.3, respectively. The pH was monitored during the progression of NP adsorption (not controlled). The changes in the pH with time during the experiments for the different dispersing fluids without and with NP are shown in Figure 5.11. The order of the pH values from highest to lowest for NP dispersing fluids are DIW>LSW (NP conc 1g/L)>LSW (NP conc 1.5g/L)> SSW. Generally, in all cases during the dissolution/adsorption processes the pH declines, however, the changes are within about 0.3 pH units. The reduction of the pH may be explained by formation of silanol, as a result of the dissociation of water molecules to form silanol groups and reduce the pH (Iler 1979):

$$-SiOH \rightleftharpoons -SiO^- + H^+ \quad (5.17)$$

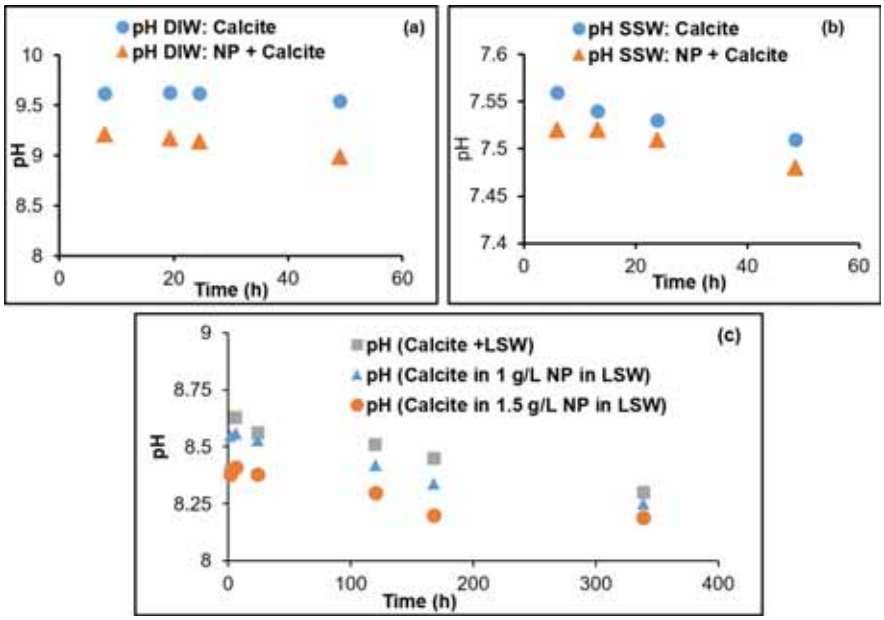


Figure 5.11 pH recorded in (a) DIW, (b) SSW and c) LSW (1 and 1.5g/L) as a function of time during progressive silica NP adsorption on calcite.

In spite of the reduction of pH, the dissolution of calcite is also reduced (discussed later), contrary to what is expected. There are two factors which contribute to less dissolution. The first is that the pH balance between calcite dissolution and formation of silanol shows insignificant decrease of pH. The second factor is adsorption of the NP on the calcite surface which may affect dissolution and formation of silanol.

Figure 5.12 shows the supernatant $Ca^{2+}$ and surface coverage with NP as a function of time in the cases of DIW and SSW. For DIW, as the surface coverage by the NP reached equilibrium, $Ca^{2+}$ concentrations reached a steady state at about 49 hrs. The $Ca^{2+}$ concentration was reduced (from ≈ 0.003 to ≈0.0015 mol/L) by about 50% with NP adsorption. In the case of SSW Figure 5.12(b) shows a reduction of $Ca^{2+}$ (≈ 0.0046 to 0.0041) by about 10% after 16 hrs when the adsorption of the NP reached equilibrium for calcite surface

coverage of about 27%. It is interesting to observe that the $Ca^{2+}$ concentrations decline rather than increase due to solubility.

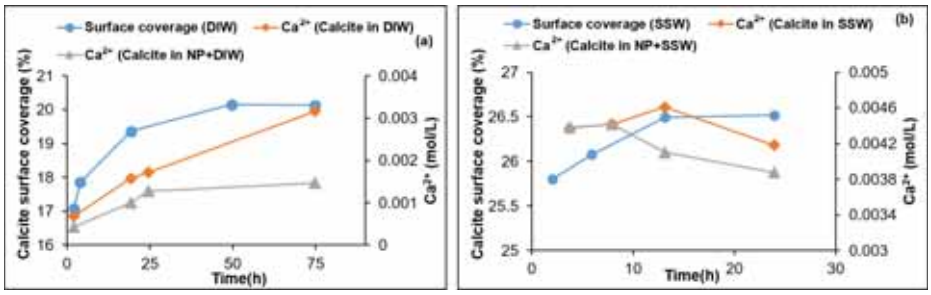


Figure 5.12 Supernatant $Ca^{2+}$ concentrations with and without NP and the estimated surface coverage by NP (a) DIW and (b) SSW fluids.

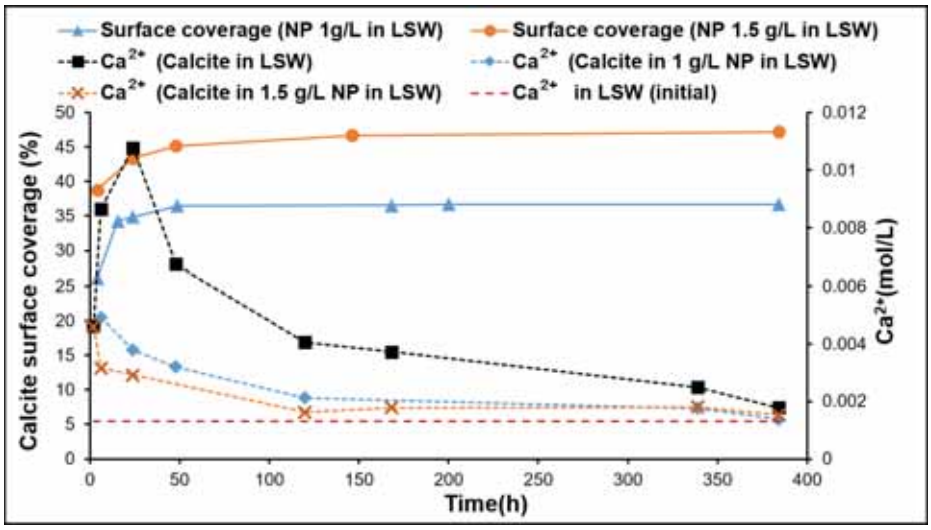


Figure 5.13 Supernatant $Ca^{2+}$ concentrations with and without NP and the estimated surface coverage by NP for LSW fluid.

Figure 5.13 for LSW (1 and 1.5 g/L NP) shows similar observations as for SSW. The $Ca^{2+}$ concentrations declines after a concentration spike (without NP) reaching ≈0.011 mol/L compared to ≈0.0046 mol/L (with NP). It is important to observe that $Ca^{2+}$ shows declining trends in both saline cases: LSW and

SSW, as well as a higher initial spike in $Ca^{2+}$ concentration in the case of LSW compared to SSW. The reduction trend of $Ca^{2+}$ is difficult to explain. However, there are two possible mechanisms. The first is adsorption of $Ca^{2+}$ onto the silica surface according to the following equation (Janusz, Patkowski, and Chibowski 2003):

$$2SiOH + Ca^{2+} \rightleftharpoons (-SiO^{-})_2Ca^{2+} + 2H^{+} \quad (5.18)$$

Equation 5.18 could support the reduction in $Ca^{2+}$. However, Janusz, Patkowski, and Chibowski (2003), previously measured the $Ca^{2+}$ uptake by silica in solutions of ionic strength similar to the LSW used in the present study. They estimated and uptake capacity of ≈0.0016 μmol/L at a pH of 8. This reduction is much lower compared to the reductions in $Ca^{2+}$ concentrations in this study. Therefore, the uptake of calcium is not expected to be the main contributor to the observed $Ca^{2+}$ declining trend. The second hypothesis could be the formation of $CaSO_4$ due to possible reaction with $SO_4^{2-}$ ions present in both fluid cases (LSW and SSW). At the mineral-solution interface, assuming heterogeneous $Ca^{2+}$ distribution, the solubility product of the $CaSO_4$ may be exceeded. The smaller peak in case of SSW (Figure 5.12 (b) may be credited to the higher $SO_4^{2-}$ ions concentration (65% higher than that with LSW). This would kinetically favor faster removal of $Ca^{2+}$ from the fluid in the form of $CaSO_4$, when the thermodynamic solubility product (Ksp) is reached. This may be supported by the case of DIW, where $SO_4^{2-}$ is absent. It is therefore believed that the second mechanism is the cause of the observation.

Figure 5.13 shows that as the NP concentration in LSW was increased from 1 to 1.5 g/L, $Ca^{2+}$ concentration was further reduced at the onset of NP adsorption. It then reached to almost the same concentration as in the case of 1 g/L with time and finally at a close level of $Ca^{2+}$ concentration as in LSW. The observed

decrease of $Ca^{2+}$ concentration may be related to the Intraparticle diffusion phenomenon (discussed earlier) which occours after reaching the maximum calcite surface coverage by the NP. In both cases of NP, $Ca^{2+}$ concentration reduction continues (Figure 5.14) reaching lowest $Ca^{2+}$ concentration almost at the same rate until it reached to the level of $Ca^{2+}$ concentration in LSW. The $Ca^{2+}$ concentration after the NP surface coverage reached maximum (about 49 h, Table 5.4), was about 1.3 times higher for NP 1g/L (≈ 0.0032 mol/L) than that for 1.5g/L (≈ 0.0024 mol/L). The amount of calcite dissolved was estimated from the areas under the produced $Ca^{2+}$ concentration curves in Figure 5.13 (with and without NP). The results are shown in Figure 5.14.

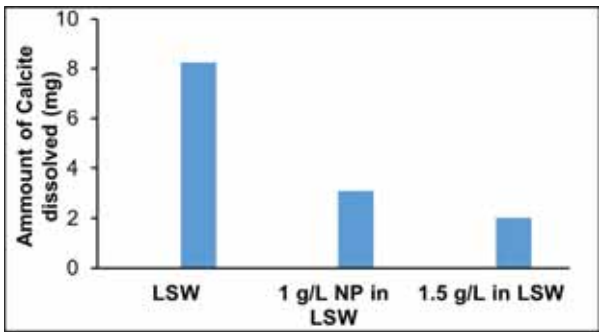


Figure 5.14 Amount on Calcite dissolved in LSW and with NP adsorption on calcite.

Figure 5.14 shows that increasing NP concentration led to lower amount of calcite dissolution. This can have profound implication when designing LSW flooding of chalk reservoirs.

## 5.6 Summary

In his chapter, the static adsorption and the kinetics of silica NP adsorption on major minerals present in sandstone and chalks was addressed. In the first part of the chapter, the nanofluids were characterized for particle size and stability. In DIW and LSW, the silica nanoparticles had particle sizes below 50 nm even at elevated temperature of 80 ºC. In SSW the nanoparticles were 43% larger than the average particle size for all tested temperatures with DIW and LSW. In general, the nanofluids were found to be stable up to 3 months. This is major improvement is stability as compared to in-house silica nanofluids in the previous chapter.

Comparing the relative adsorption of silica NPs on minerals showed that the NPs have highest adsorption affinity on calcite mineral followed by quartz and least kaolinite. The commercial silica NPs used in this chapter shows preferential adsorption affinity similar to the in-house silica NPs in the previous chapter. The rate of adsorption was higher for calcite (0.11-2.5 g/mg h) compared to quartz (0.042-0.15 g/mg h). In addition, it was observed that both rate and equilibrium adsorption of NPs on minerals is enhanced at higher salinity.

SEM images of NP adsorption on sandstone and chalk cores did not show pore throat blockage, hence permeability impairment is not expected. Silica NPs' adsorption process on quartz and calcite was best fitted to pseudo second order kinetic model with $R^2$ close to 1. For NP adsorption on calcite, the adsorption characteristic curves showed high initial adsorption behavior wherein most of the equilibrium adsorption occurred in the initial time period.

Adsorption of silica NP reduces calcite dissolution. This is an important outcome especially when LSW is a candidate for EOR in chalk fields, where less dissolution of chalk would be expected when silica NP are combined with the injection water. It was also observed the progression of NP adsorption influences the pH.

In the following chapters, silica NPs injected into sandstone and chalk cores at different scenarios are investigated to address the influence of pH, salinity and fluid/rock interactions on the adsorption of silica NPs.

# 6 Dynamic adsorption of silica NPs

This chapter addresses the dynamic adsorption of silica NPs injected into sandstone and chalk. The contents of this chapter refer to the work presented in Paper 2-3. In the previous chapter, the adsorption behavior of silica NPs on the quartz and calcite minerals was addressed. This chapter addresses dynamic adsorption of silica NPs during injection into sandstone and chalk cores and its effect on fluid/rock interaction. The methodology used is outlined in section 3.6.2.

## 6.1 Dynamic adsorption of silica NPs in berea sandstone

Two floods were conducted to investigate dynamic adsorption of silica NPs in berea sandstone cores. The details of the floods is listed in Table 6.1.

Table 6.1 List of core flooding for invetigating NP dynamica adsoprtion in berea sanstone.

| Core Id | Porosity (%) | Permeability (mD) | Lenght (cm) | Dia (cm) | Flooding sequence |
|---|---|---|---|---|---|
| BR_SSW | 20.13 | 200 - 220 | 9 | 3.78 | SSW - 1.5 PV Slug (DP 1 g/L + Tracer in SSW) - SSW |
| BR_LSW | 20.24 | 200 - 220 | 9 | 3.78 | LSW - 1.5 PV Slug (DP 1 g/L + Tracer in LSW) - LSW |

As shown in Table 6.1, after pre-flush with several PVs of brine (SSW/LSW), 1.5 PV of nanofluid slug with LiCl tracer was injected. Thereafter, the injection was switched to the original fluid to conduct a post-flush. The effluents samples from the core floods were analysed for NP concertation, pH and cation concentration. Flood BR_SSW was done to establish a baseline for investigating the flood BR_LSW at low salinity conditions. The results are shown in

Figure 6.1. It is shown that the NP production occurs within the tracer production window. From mass balance, it was estimated that approximately 81.6 % of the injected NPs were adsorbed in the core indicating high irreversible adsorption of NPs. Both the recorded pH and cation concertation ratio profiles are stable indicating equilibrium between rock and flooded fluid.

In sharp contrast, dynamic adsorption of NPs dispersed in the low salinity water flooding of berea sandstone is shown in Figure 6.2. Figure 6.2 (a) shows that the breakthrough of the Li tracer and NPs occurred almost simultaneously. The NP concentration profile shows a longer tail compared to the tracer. The amount of NPs irreversibly adsorbed in the core was calculated from the mass balance by integrating the produced area under the NP concentration curve in Figure 6.2(a) and the known injected amount of NPs into the core. The produced concentration profile, may be divided into three regions: A, B and C. Table 6.2 shows the analysis of NP production in these three regions.

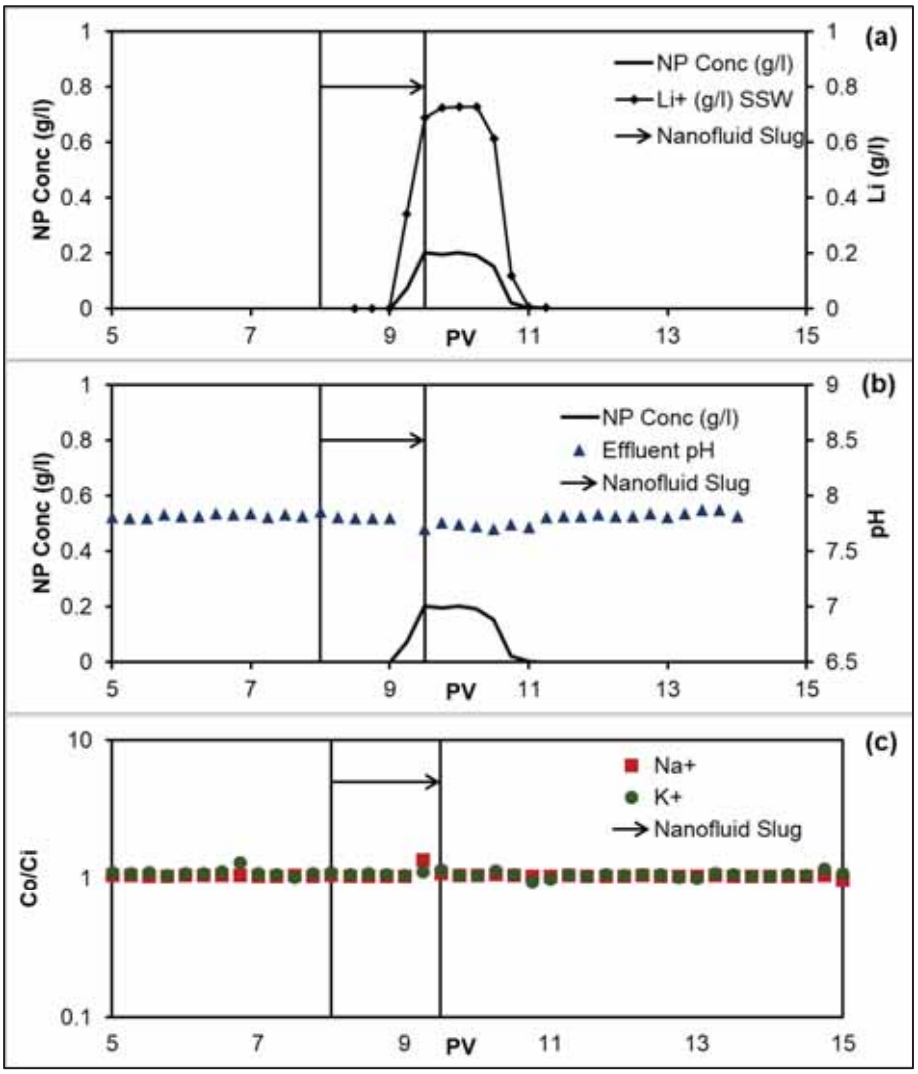


Figure 6.1 (a) NP and tracer concertation (b) Effluent pH profiles and (c) Concertation of cations in effluents from flood BR_SSW.

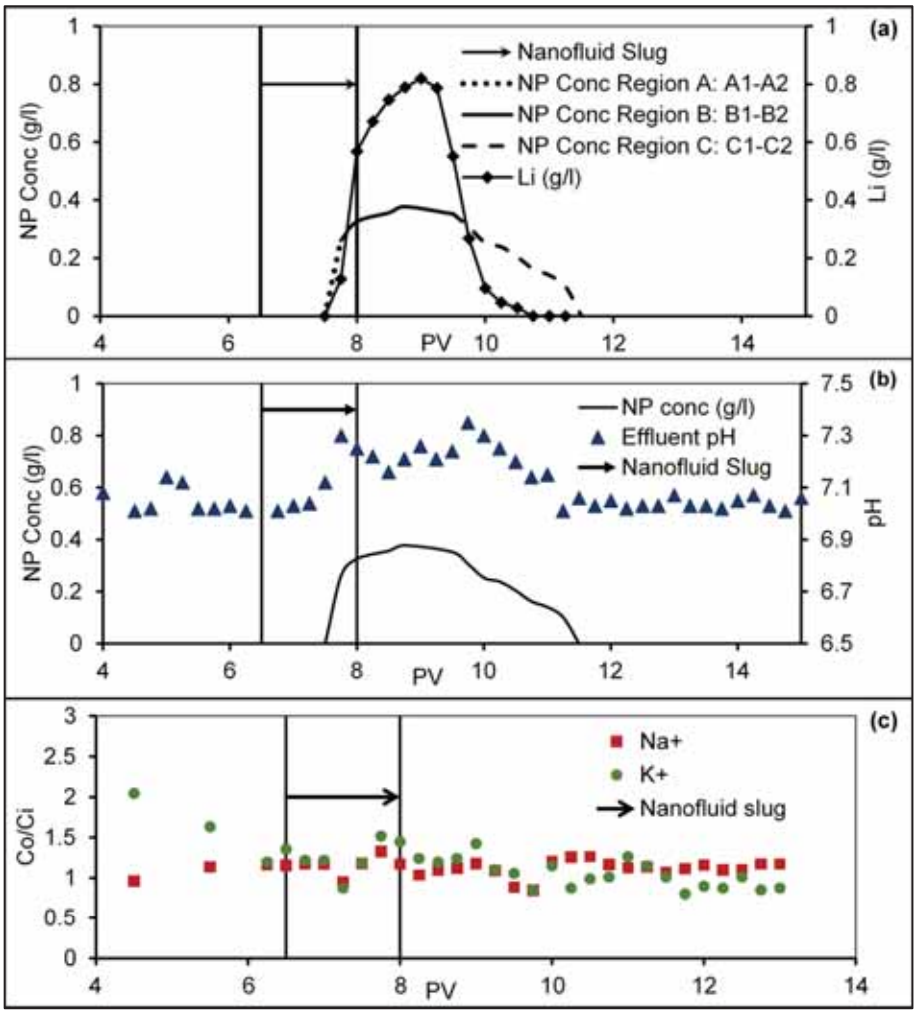


Figure 6.2 (a) NP and tracer concertation (b) Effluent pH profiles and (c) Concertation of cations in effluents from flood BR_LSW.

Table 6.2 Analysis of NPs production in figure 5.2 (a).

| | | | |
|---|---|---|---|
| **Total NP injected (*g*)** | $m_{NPi}$ | $m_{NPi} = c_{inj} * V_{sl}$ | 0.032715 |
| **Excess NP produced in region A (*g*)** | $m_{Ao}$ | $m_{Ao} = \int_{A1}^{A2} c_{oA}(V)dV$ | 0.000712 |
| **Total NP available for adsorption (*g*)** | $m_{NP}$ | $m_{NP} = m_{NPi} - m_{Ao}$ | 0.032003 |
| **Total NP produced in equilibrium region B (*g*)** | $m_{Bo}$ | $m_{Bo} = \int_{B1}^{B2} c_{oB}(V)dV$ | 0.013921 |
| **Total NP adsorbed in core till end of region A (g): reversibly adsorbed NP** | $m_{rev}$ | $m_{rev} = m_{NP} - m_{Bo}$ | 0.018082 |
| **Total NP produced during desorption phase in region C (*g*)** | $m_{Co}$ | $m_{Co} = \int_{C1}^{C2} c_{oC}(V)dV$ | 0.006767 |
| **Amount of NP irreversibly adsorbed in the core (*g*)** | $m_{irr}$ | $m_{irr} = (m_{rev} - m_{Co})$ | 0.011315 |
| **NP production in region B (%)** | $NP_{Bo}$ | $NP_{Bo} = \left(\frac{m_{Bo}}{m_{NP}}\right) * 100$ | 43.49 |
| **Desorption in region C (%)** | $Dsp_C$ | $Dsp_C = \left(\frac{m_{Co}}{m_{NP}}\right) * 100$ | 21.15 |
| **Total irreversible adsorption/remained in core (%)** | $Ads_{irr}$ | $Ads_{irr} = \left(\frac{m_{irr}}{m_{NP}}\right) * 100$ | 35.36 |

In Table 6.2, $c_{inj}$ and $V_{sl}$ refers to the injected concentration and slug volume of the nanofluid. $c_{oA}(V)$, $c_{oB}(V)$ *and* $c_{oC}(V)$ are the produced NP concentration functions with respect to produced effluent volume ($V$) in regions A, B and C

respectively. These were obtained from polynomial regression fitting of the concentration curves in Figure 6.2(a). The $R^2$ for the fits varied between 1-0.99. *A1-A2*, *B1-B2* and *C1-C2* refer to the limits of region A, B and C respectively. In Figure 6.2 (a), the amount of NPs produced in region A is termed as excess NP, since the breakthrough coincided with the breakthrough of the tracer, i.e. un-interacted with the rock minerals ($m_{Ao}$). In region B, a plateau of NP produced concentration is established. This may denote adsorption/desorption equilibrium of the NPs. At equilibrium period by the end of region B, 43.49 % of the total available NPs ($m_{NP}$)were estimated which may be considered to be equal to the adsorbed NPs on the sandstone minerals. That is it may be considered as the maximum reversible adsorption up till end of region B. During NPs' production in region B, the tracer concentration reached a peak. Integrating the area under the tracer production curve showed that almost all the injected amount of the tracer was produced. Further, the tracer production stopped at 10.75 PV while the NP production continued up to 11.5 PV. Combining these two observations, it can be inferred that the NPs produced in region C were, most likely due to desorbed NPs. The NF slug injection length was 1.5 PV. The unreacted tracer production length was 2.75 PV (7.75 to 10.5 PV) and the NPs production length was 3.5 PV (7.75 to 11.25 PV). The ratio of NPs to tracer production volume was approximately 1.3. Thus, NPs production took approximately 30 % longer time to cease after the slug has passed through the core. This further strengthens desorption of NPs in region C. As shown (Table 6.2), 21.15 % or approximately 1/5$^{th}$ of the available NPs were desorbed ($Dsp_c$) in region C. The maximum irreversible adsorption ($Ads_{irr}$) in the core was 35.36 %. This indicates that irreversible adsorption of NPs exceeded the reversible adsorption of NPs.

The pH of the effluent is plotted along with the NP concentration as shown in Figure 6.2 (b). During the initial injection of LSW, the pH remained stable at about 7. The pH, then, increased after NP injection. Thereafter, the pH fell down in the region in which NP desorption is inferred from the difference in NP and Tracer concertation curves (region C). This may be related to the dissolution of adsorbed NPs in accordance with the following equations (Stumm and Morgan 1970):

$$SiO_2\,(s) + 2H_2O \leftrightarrow H_4SiO_4 \quad (6.1)$$

$$H_4SiO_4 \leftrightarrow H_3SiO_4^- + H_3O^+ \quad (6.2)$$

Equation 6.1 shows the dissolution of $SiO_2$. Stumm and Morgan (1970) stated that $SiO_2$ solubility increases at neutral to slightly alkaline pH ranges in accordance with the above equations, silicic acid is produced. This weak acid further dissociates and reduces the pH (Eq. 6.2) which was observed during desorption of NPs. The adsorption/desorption of silica NPs in low salinity environment in chalk showed similar behaviour which is discussed in the following section. Therefore it maybe concluded that the desorption of NPs is influenced by the pH wherein increased alkalinity favours the NP desorption.

The effluents were analysed for the produced cation concentrations for the different injection stages as shown in Figure 6.2 (c). For ease of comparison the effluent cation concentration (Co) have been presented relative to injected concentration (Ci). Hamouda et al. (2014) have previously investigated mechanisms during LSW flooding. They stated that LSW injection leads to mineral dissolution such as for example K-feldspar as presented by the following equation:

$$4\mathrm{KAlSi_3O_8(s)(orthoclase)} + 22\mathrm{H_20(aq)} \rightarrow \mathrm{Al_4Si_4O_{10}(s)(kaolinite)} + 8\mathrm{H_4SiO_4(aq)} + 4\mathrm{K^+(aq)} + 4\mathrm{OH^-(aq)} \quad (6.3)$$

It is shown in Figure 6.2 (c) that during initial LSW injection, $K^+$ in the effluent was high (Co/Ci ≈2). This was followed by a decrease to ≈ 1.35 relative concertation. After injection of NF slug, $K^+$ increased to about 1.5, which coincides with the pH rise in the effluent, which may be explained based on equation 6.2. Thereafter, the $K^+$ concentration showed a downward trend which is accompanied the fall in pH. The pH reduction could be due to the combination of NP dissolution as per equation 6.1-6.2 and reduced mineral dissolution. During the post flush, the $K^+$ concentration stabilized at around 0.8 relative to injected concentration. This may indicate that, the in-situ adsorption of NPs on the berea rock surface may have reduced K-feldspar dissolution thus reducing fines production (Hamouda et al. 2014, Khilar and Fogler 1998, Tang and Morrow 1999) thereby reducing formation damage. Hamouda et al. (2014) also stated that LSW injection leads to possible ion exchange represented by the following equation:

$$4\mathrm{KAlSi_3O_8(s)(orthoclase)} + Na^+(aq) \rightarrow K^+ + NaAlSi_3O_8(s)(albite) \quad (6.4)$$

The above reaction leads to reduction of $Na^+$ during the initial LSW injection. However, after the NF slug injection, the $Na^+$ relative concentration in the effluent was about 1.1. This also indicate suppression of ion exchange based on equation 6.4. Thus, the investigated slug injection of NPs into the berea sandstone suggests that the adsorbed NPs adsorb on the surface of berea affect the fluid/rock interactions during low salinity flooding.

## 6.2 Dynamic adsorption of silica NPs in chalk

Dynamic adsorption of NPs in chalk and its effect on fluid/rock interactions are addressed in this section. Three salinities: DIW, LSW and SSW were used in the dynamic tests as outlined in section 3.6.2. To the best our knowledge, the adsorption behavior of silica NPs on chalk and its effect on fluid/rock interactions has not been addressed previously. The list of experiments are shown in Table 6.3.

Table 6.3 List of experiments to test dynamic adsorption of nanoparticles (NPs) in chalk.

| Core Id | Porosity (%) | Permeability (mD) | Length (cm) | Dia (cm) | Pre/Post Flush Fluid | Slug Composition |
|---|---|---|---|---|---|---|
| SK1 | 48.10 | 3.9 | 5.31 | 3.78 | DIW | 1 (g/L) DP in DIW + tracer |
| SK2 | 49.00 | 3.9 | 7.80 | 3.78 | DIW | 90 μL 0.1M HCl + tracer in DIW |
| SK3 | 51.71 | 3.9 | 3.9 | 3.78 | SSW | 1 g/L DP in SSW +tracer |
| SK4 | 47.38 | 3.9 | 3.35 | 3.78 | LSW | 1 g/L DP in LSW + tracer |

The first flood SK1 was performed with DIW as the base fluid. The effluent fluid was analyzed for the concentrations of NP, calcium and Li (tracer). Inductive coupled plasma and optical emission spectrometry (ICP-OES) was carried out to quantitatively determine the trace amounts of elements eluted and to determine the NP concentration in the effluent for chalk cores injected with DIW. The results are shown in Figure 6.3.

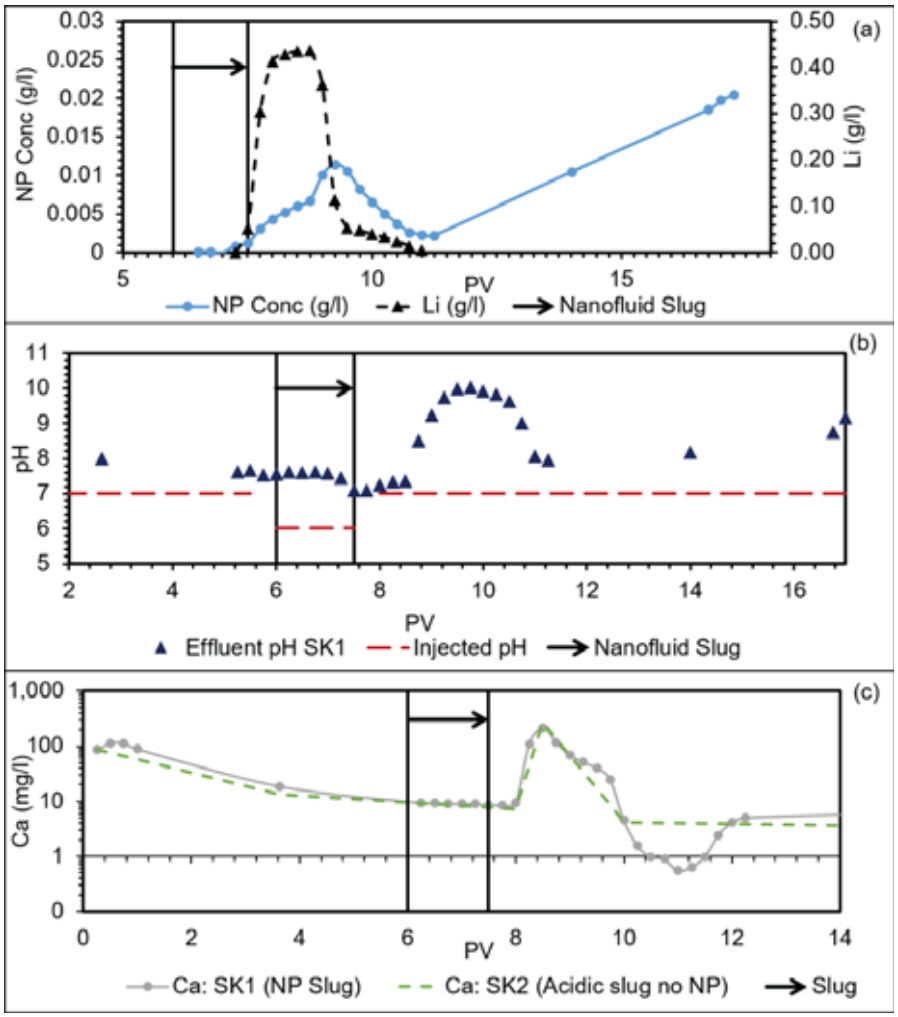


Figure 6.3 (a) NP and tracer concentration profile for SK1. (b) Effluent pH profile for SK1 (c) Effluent Ca concentration for SK1 (with NPs) and SK2 (without NPs).

A difference of about 1 PV between the peak concentration of the tracer and the peak concentration of NPs was observed. It was also observed that the tracer peak concentration declined faster than that for the NPs. The delay of NP decline may indicate interaction between the NP and core surface. After about 11 PV of injection (from the start), the NP concentration showed a linear

increase, while the tracer production ceased. The increase of NPs' concentration after 11 PV, may indicate NP desorption

Now the question is, why did the NP concentration decline below 0.01 g/L before the start of the desorption process (at approximately 11 PV)? The adsorption/desorption process may be related to the pH of post flowing fluid in contact with calcite surface and adsorbed NPs. The effluent pH profile for the effluents of SK1 are shown in Figure 6.3(b). It is shown that the pH after nanofluid slug increased steadily for approximately 1 PV, then steeply increased to a pH of about 10, before it started to decline to reach a pH of about 8.6. The highest pH coincided with the peak concentration of NP in the effluent and the desorption of NP from 11 PV in Figure 6.3(a) coincided with the steady increase of the pH from about 8 to about 9. Equation (5.15) may explain the associated increase of pH with calcite dissolution.

Therefore, as calcite dissolves, the pH increases. Increase of the pH increases the dissolution of NPs according to the equations 6.1 and 6.2. The progression of equation 6.1 and 6.2 may explain the pH reduction in Figure 6.3(b). The reduction of the pH to 8, would negatively affect the dissolution of NPs since equation 6.1 and 6.2 require a high pH environment. Hence reduced the produced NPs in the effluent. The increase of the pH from about 8 at approximately 11 PV till about 9 at the termination point of the experiment (PV ≈ 18) may be caused by calcite dissolution by Equation 5.15. This rise in pH would favor the desorption of NPs observed in this region. That is as the pH started to increase, desorption of NPs increases.

These observations may be summarized as: maximum NP concentration in the effluent occurred at the highest pH (≈10) of this experiment. As the pH declined, less concentration of NPs was detected in the effluent until NPs

reached minimum at 11 PV (pH ≈ 8), after which, NP started to rise again and to reach 0.03 g/L (at the time of the experimental termination). This counts for about 50% higher than the peak concentration of 0.02 g/L. The dissolution of calcite can be inferred from the effluent calcium concentration profiles. Since the injected fluid did not contain any calcium, the effluent calcium observed may be attributed to the calcite dissolution by Equation (4.15). A second test (SK2) was done without NPs to provide a baseline for comparing the calcite dissolution in SK1. The pH of the slug without NPs in SK2 was adjusted to be approximately same as that of nanofluid in SK1. The calcium concentration in the effluent from test SK1 (with NP) and SK2 (without NP) is shown in Figure 6.3(c). In Figure 6.3(c), there is no significant difference between the Ca in the two cases during DIW pre-flush. However, after the slug injection, the difference in the Ca trend for the two experiments started to increase. At 10–12 PV in the case of test fluid with NP the calcium concentration was about 80% less than that for the fluid without NP.

The general mechanism may, then, be deduced as follow: the dissolution of calcite increases the pH, which in turn reduces NP adsorption on the calcite surface. Monfared et al. (2015) have made similar observation where increasing the pH from around 7.5 to 10 reduced the adsorption of silica NPs on the calcite surface by about 33.33%. As mentioned earlier, effluent calcium was reduced by about 80% for fluid with NPs. As the pH increases, the calcite surface becomes less positive, so that NP adsorption decreases. As observed, more NPs were produced when the pH increased, with peak concentration at pH ≈ 10. Since $SiO_2$ dissolves in the alkaline range of the pH (Equation 6.1). Dissociation of silicic acid (Equation 6.2) increases the negative ions and thereby adsorption. The dissociation of (weak) silicic acid slightly increases the acidity of the solution, which may again increase the adsorption of NPs. Figure

6.3(a) shows the relation between pH and adsorption. As the desorption process proceeded, the pH steadily increased until it reached about 9, which was the point where the experiment was terminated. The estimated adsorbed NPs on the chalk is about 0.46 mg per gram of chalk. This was obtained from the integrated area under the curve in Figure 6.3(a) and the mass balance with known injected NPs. The effect of saline environment on adsorption of silica NPs was investigated where SSW and LSW were used in floods SK3 and SK4 respectively. For SK3, both the pre-flush and post-flush was performed with SSW. The nanofluid slug with tracer was also prepared in SSW. The results for the test SK3 are shown in Figure 6.4.

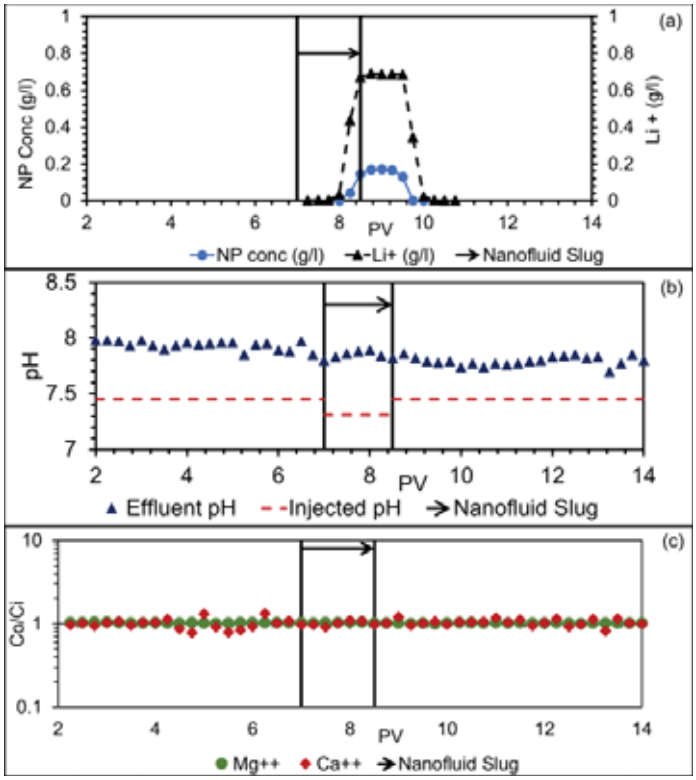


Figure 6.4 (a) NP and tracer concentration profile, (b) effluent pH profile and (c) effluent $Ca^{2+}$ and $Mg^{2+}$ concentration for SK3 in SSW.

It can be seen in Figure 6.4(a) that unlike in test SK1, the NP concentration profile for test SK3 follows the tracer profile closely. In addition, the NP production stopped at about 0.25 PV before the tracer. That is unlike SK1, no NP was detected in the effluent after the tracer has passed through the chalk core. This together with high adsorption of the NPs observed in SSW during static adsorption experiments may indicate strong irreversible adsorption of the NPs on the chalk surface. Integrating the area under the curve in Figure 6.4 (a) and the computing mass balance by known amount of injected NPs showed that about 86% of NPs were adsorbed on the chalk surface. Further, the effluent pH and relative ion concentration profiles for test SK3 in SSW are shown in Figure 6.4(b), (c) respectively. It can be seen that pH remains almost constant throughout test SK3 and the ion ($Ca^{2+}$ and $Mg^{2+}$) concentration in the effluents remain close to injected concentration. This makes the baseline for comparing the behavior at low salinity condition in the next test SK4. In test SK4, both the pre-flush and post flush was performed with LSW. The nanofluid slug with tracer was also prepared in LSW. The results for test SK4 are shown in Figure 6.5.

It can be seen in Figure 6.5(a) that with LSW, the NP breakthrough is delayed by 0.25 PV compared to the tracer. In addition, the NP production continues after the tracer production stops. This is similar to test SK1 (ion free) and may indicate desorption of the NPs. It was estimated that 67.2% of the NPs were adsorbed in the core in SK4 (LSW) as compared to 86.2% in SK3 (SSW). At low salinity conditions in SK4, the NP concentration profile is similar to DIW. This together with the high irreversible adsorption observed with SSW indicates that salinity strongly influences the adsorption behavior of the NPs on the chalk surface which supports the adsorption analysis in the previous chapter.

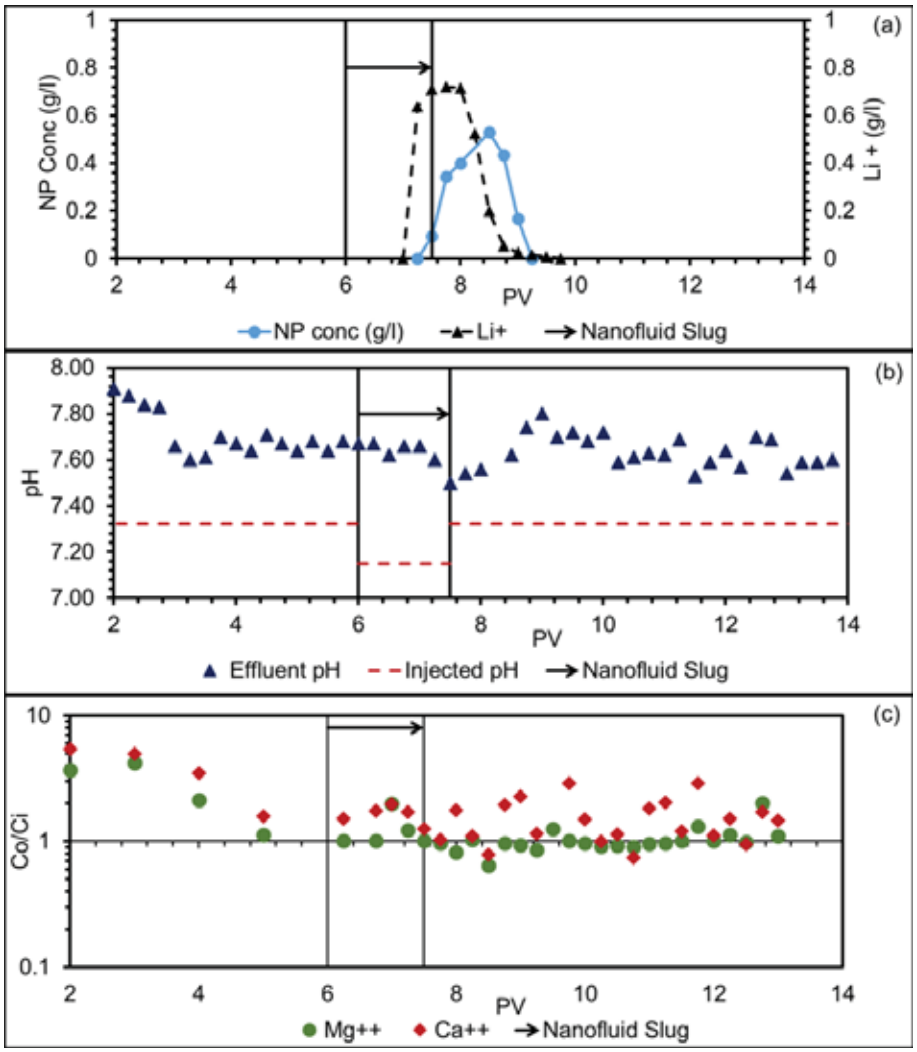


Figure 6.5 (a) NP and tracer concentration profile, (b) effluent pH profile and (c) effluent $Ca^{2+}$ and $Mg^{2+}$ concentration for SK4 in LSW.

The effluent pH profile for test SK4 (Figure 6.5(c)) shows a sharp rise in pH with NP production and the pH peak coincides with peak NP production. Thereafter the desorption of NPs during the decline phase can be attributed to the dissolution of the NPs which produces a weak silicic acid as per Equations 6.1 and 6.2 This supports the proposed NP adsorption/desorption mechanism.

However, the linear rise of NPs production in the effluents as observed with DIW in Figure 6.3(a) was not observed with LSW in SK4. This may be due the heavy dissolution of chalk due to DIW in SK1 which significantly raised the pH to 10, whereas in SK4 the pH remained below 8. The effluent $Ca^{2+}$ and $Mg^{2+}$ profiles shown in Figure 6.5(c). The high levels of $Ca^{2+}$ in the pre flush stage suggest high calcite dissolution. However, after the adsorption of NPs on the chalk surface, the $Ca^{2+}$ fell by about 30%. In addition, the $Mg^{2+}$ levels fell below the injected concentration during the post flush. This may be due to the incorporation of magnesium into the calcite structure. This is discussed in detail in the next chapter.

Dynamic adsorption of NPs on chalk surface (in the absence of oil phase) indicated that NP adsorption in chalk could significantly reduce calcite dissolution induced by low salinity injection. However, for the application of NPs to petroleum reservoirs, it is essential to study the effect of NPs on chalk surface that is oil wet and the effect of NPs in the presence of oil phase. This is addressed in the following chapter.

## 6.3 Summary

This chapter addressed dynamic adsorption of silica NPs injected into sandstone and chalk cores and its effect on fluid/rock interactions. At high salinity (SSW), silica NPs show irreversible adsorption in both berea sandstone and chalk cores. In contrast, NP desorption was observed in LSW for both berea and chalk.

The estimated desorption in LSW was about 21.2% in berea cores. The adsorption/desorption of silica NPs is influenced by the pH wherein increased alkalinity during LSW injection enhances NP desorption. The injected NPs

adsorb on the sandstone surfaces and reduce mineral dissolution and suppressed ion exchange due to LSW injection. This may explain the reduction of fines migration observed in chapter 4. NP adsorption during the oil recovery process and its effects on fines migration is addressed in the following chapter.

Similar to the observations for berea, in chalk cores desorption of NPs was observed in low salinity condition. Adsorption/desorption mechanisms for the NPs related to pH have been proposed. Dynamic adsorption of NPs on chalk surface showed that NP adsorption reduced calcite dissolution by about 30% during by low salinity injection, which supports the results reported in chapter 5. Thus silica NPs combined with low salinity EOR technique could reduce the risk of matrix integrity loss and the subsidence of water flooded chalk. The effect of silica NPs adsorption oil wet chalk surface during oil recovery by continuous injection of nanofluids is addressed in the following chapter.

# 7 Oil recovery by silica NPs

This chapter addresses the effect of continuous silica NPs flooding fof fluid/rock interaction in sandstone and chalk. The contents of this chapter refer to the results presented in paper 2 and 3.

Nanofluids are prepared in brines and some studies (Hendraningrat and Torsæter 2016, Ding et al. 2019, Hosseini, Hajivand, and Yaghodous 2018) have investigated the combined role of salinity and NPs on the wettability alteration and NP adsorption on mineral surfaces (Dehghan Monfared et al. 2016, Monfared et al. 2015, Zhang, Murphy, et al. 2016, Zhang et al. 2015). Hendraningrat and Torsæter (2016) stated that nanofluid flooding is sensitive to water salinity especially in the presence of divalent ion ($Ca^{2+}$ and $Mg^{2+}$). The effect of injection brine salinity on oil recovery process is well documented in literature (Austad et al. 2011, Chukwudeme and Hamouda 2009, Yi and Sarma 2012, Tang and Morrow 1997, Hamouda et al. 2014, Al-Nofli et al. 2018). However, the effect of silica NP on fluid /rock interaction during oil recovery is not well addressed.

As discussed in the previous chapter, the adsorption of NPs on the mineral surface alters the rock surface and affects fluid/rock interactions. To address the effect of salinity and NPs, flooding experiments are divided into two stages (1) brine alone and (2) NPs dispersed in the selected brine.

## *7.1 Oil recovery from berea cores*

Many researchers have identified that; injection of low salinity brine may lead to enhanced release of fines which can cause formation damage (Akhmetgareev and Khisamov 2015, Zeinijahromi, Ahmetgareev, and Bedrikovetsky 2015,

Merdhah and Yassin 2009). The flooding was divided into two stages: primary recovery (brine alone) and secondary recovery (NP dispersed in brine). Table 7.1, summarizes the flooding schemes for the three cases (BR2, BR3 and BR4). Two flow rates 4 PV/day (0.06 ml/min) and 16 PV/day (0.24 ml/min) were used. The oil recovery profiles for floods BR2-4 are plotted in Figure 7.1.

Table 7.1 List of core properties and flooding details

| Core Id | Porosity (%) | Permeability (mD) | Lenght (cm) | Dia (cm) | Swi | Primary recovery fluid | Secondary recovery fluid |
|---|---|---|---|---|---|---|---|
| BR2 | 20.9 | 200 - 220 | 9 | 3.78 | 0.250 | SSW | DP (1g/L) in SSW |
| BR3 | 20.6 | 200 - 220 | 9 | 3.78 | 0.293 | LSW | DP (1g/L) in LSW |
| BR4 | 20.25 | 200 - 220 | 9 | 3.78 | 0.218 | SSW | DP (1g/L) in LSW |

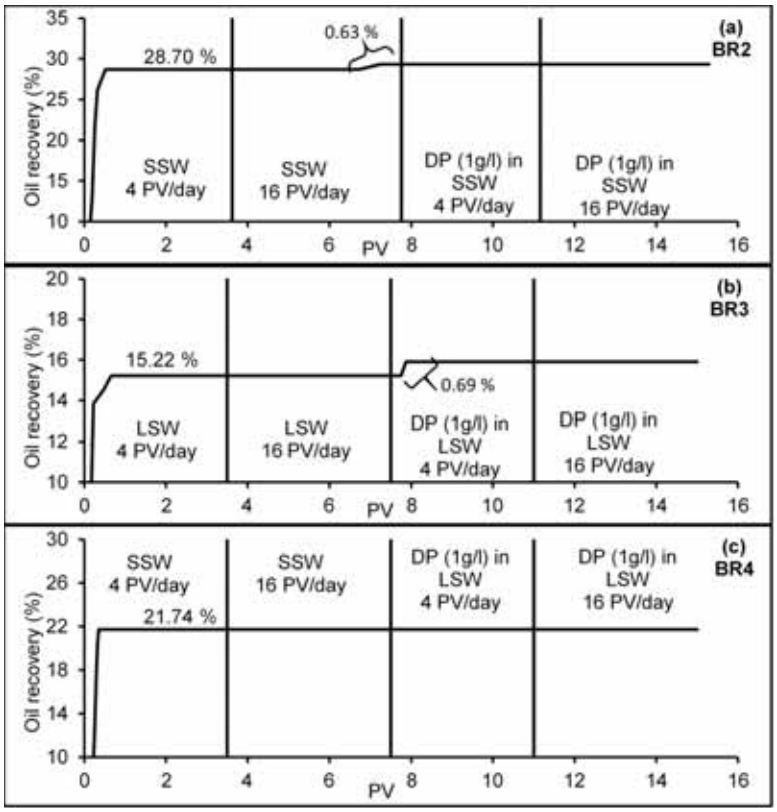


Figure 7.1 Oil recovery profiles for floods (a) BR2, (b) BR3 and BR4 (c).

Incremental oil recovery by silica NFs in sandstones have been reported by several researchers (Hendraningrat, Li, and Torsater 2013, Joonaki and Ghanaatian 2014, Aurand, Dahle, and Torsæter 2014). These studies were performed at higher flow rates and low Swi to enhance sweep and test incremental recovery by NFs. The objective of this work is to addresses the effect of NP on fluid/rock interactions. It was therefore decided during the core preparation process (establishing Swi) to minimize possible modification of the core mineral surface with oil. The oil injection was done at low rate and only from one direction which resulted in relatively high Swi ranging from 0.21-0.29 in (Table 7.1). High Swi allows larger surface area of the cores to be

available for NP adsorption and fluid/rock interactions during flooding. Flooding was done at lower rates to be closer to field cases and to increase residence time of the fluid. A possible shortcoming of using lower flow rates is less swept zone, especially with high permeability cores like berea, as evidenced by the low overall recovery (average recovery of about 20% in Figure 7.1) shown in floods BR 2-4. It is shown in Figure 7.1 that for all the flooding experiments, most of the oil was recovered within the first PV of injected water at 4 PV/day injection rate. Increasing the rate to 16 PV/day led to incremental recovery of ≈ 0.63% in BR2 experiment with SSW but not for experiments BR3 and BR4. For primary recovery (without NPs) SSW was shown to be more effective compared to primary recovery by LSW (BR3). Even for flooding with SSW in BR2 and BR4 there was about 7 % difference in primary oil recovery. Previous work in our lab (Hamouda et al. 2014, Hamouda and Valderhaug 2014) and by other researchers (Tang and Morrow 1997, Austad, RezaeiDoust, and Puntervold 2010, Tang and Morrow 1999) has identified that low salinity water injection is in general more effective at oil recovery. The deviation observed in Figure 7.1 may be attributed to the core preparation described earlier with high and non-uniform Swi. Hence, the oil recovery profiles from these experiment cannot not be directly compared. Spontaneous imbibition test were performed to address the effect fluid salinity and silica NPs on oil recovery. For spontaneous imbibition, the core preparation process was comparable since all the cores were saturated with 1 PV of synthetic oil and aged for the same time period (2 weeks). Figure 7.2 show that in the absence of NPs, DIW and LSW shows higher oil recovery (55% and 48% respectively) than that for SSW (24.5%).

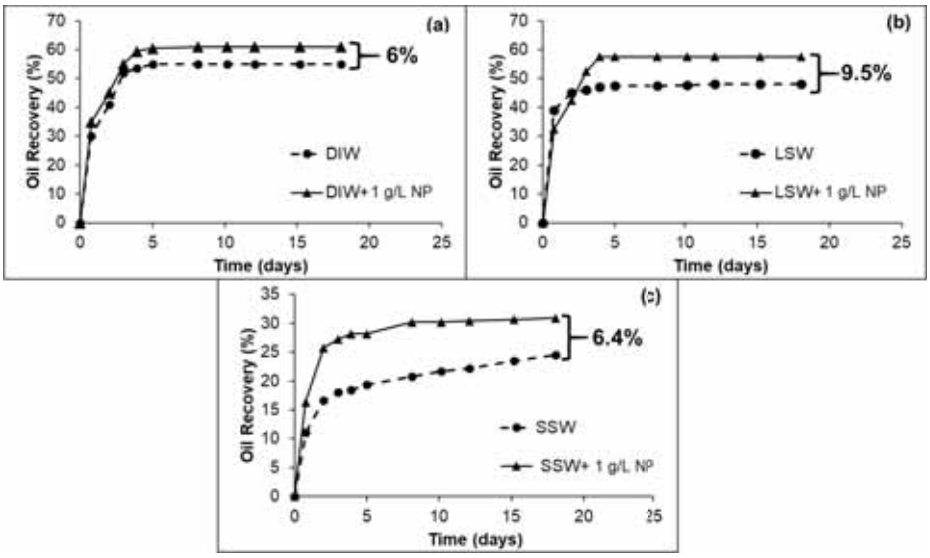


Figure 7.2 Effect of nanoparticles on spontaneous imbibition of oil from the berea cores.

In all cases, the oil recovery increases when NPs are dispersed. In LSW an incremental recovery of about 9.5% was observed with NPs, whereas NPs in DIW and SSW showed incremental recovery of about 6 %. Imbibition of water into a porous medium is driven by reduction in capillary pressure which is dependent on oil water interfacial tension and wettability. Wasan and coworkers (Wasan and Nikolov 2003, Zhang, Nikolov, and Wasan 2014) suggested that NP wedge formation is the mechanism that detaches oil from mineral surfaces. The formation of NP wedge like structure at the three-phase contact between the oil, water and mineral raises the structural disjoining pressure (perpendicular to the oil-water interface). This force enhances the detachment of oil from the mineral surface in the presence of NPs. The disjoining pressure depends on the particle size and self-assembly of the NPs in the wedge region (Zhang, Ramakrishnan, et al. 2016). The self assembly of the NPs depends on the NP size (Figure 5.1) and repulsion between the NPs.

The interaction between the NPs was estimated based on the sphere-sphere interaction (Kovalchuk and Starov 2012) as follows:

$$V_{LVA}(h) = -\frac{A_{132}}{6}\left[\frac{2\,a_p^2}{h\,(4a_p+h)} + \frac{2\,a_p^2}{(2a_p+h)^2} + ln\left(\frac{h((4a_p+h)}{(2a_p+h)^2}\right)\right] \quad (7.1)$$

$$V_{EDLR}(h) = 2\pi\varepsilon_0\varepsilon_3\zeta_p^2 a_p \frac{2a_p}{(2a_p+h)}\exp(-\kappa h) \quad (7.2)$$

Hamaker's constant for NP-NP interaction was calculated as per equation 5.7. For DIW, the inverse Debye length can be taken as $(9.6 \times 10^{-7})^{-1}m^{-1}$(Khilar and Fogler 1998). For saline mediums, the inverse Debye length was calculated as per equation 5.8. The London's van der Waals interaction and electric double layer interaction estimated from equation 7.1 and 7.2 are non dimensional (equation 5.10). The results are shown in Figure 7.3.

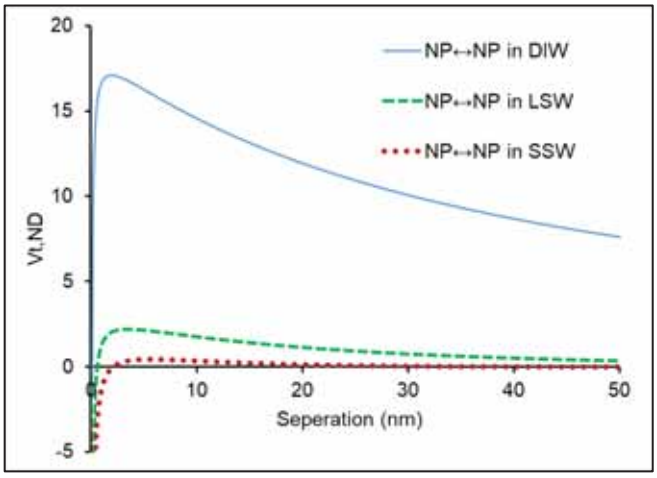


Figure 7.3 Effect of salinity on interaction energies between NP-NP

In DIW, the NPs exhibit lowest average size (37.5 nm) however it is shown Figure 7.3 that the estimated interaction energy is most repulsive in case of DIW. Due to high repulsion, lower quantity of NPs would occupy the wedge

area. In SSW, the effect of higher average particle size (56.4 nm) on the quantity of NPs in the wedge region may be compensated by lower repulsive interaction between the NPs (Figure 7.3). In LSW however, the average NP particle size (37.9 nm) is almost equal to particle size in DIW and at the same time the repulsive interaction is much lower in LSW compared to DIW. This may lead to higher quantity of NPs assembling in the wedge area thereby increasing the structural disjoining pressure. That is, in the case of NP dispersed in LSW, both NP size and inter-particle interaction increase the oil detachment from mineral surface caused by structural disjoining pressure. This may explain the higher incremental recovery observed from NPs dispersed in LSW compared to DIW and SSW and indicate a synergy between silica NPs and low salinity water for enhancing oil recovery from sandstones reservoirs. The effluent fluids from floods BR2-4 were analysed for: (1) pH (2) NP concertation and (3) concentration of cations. In the previous chapter, it was indicated that combining LSW with silica NPs may reduce fines migration and formation damage.

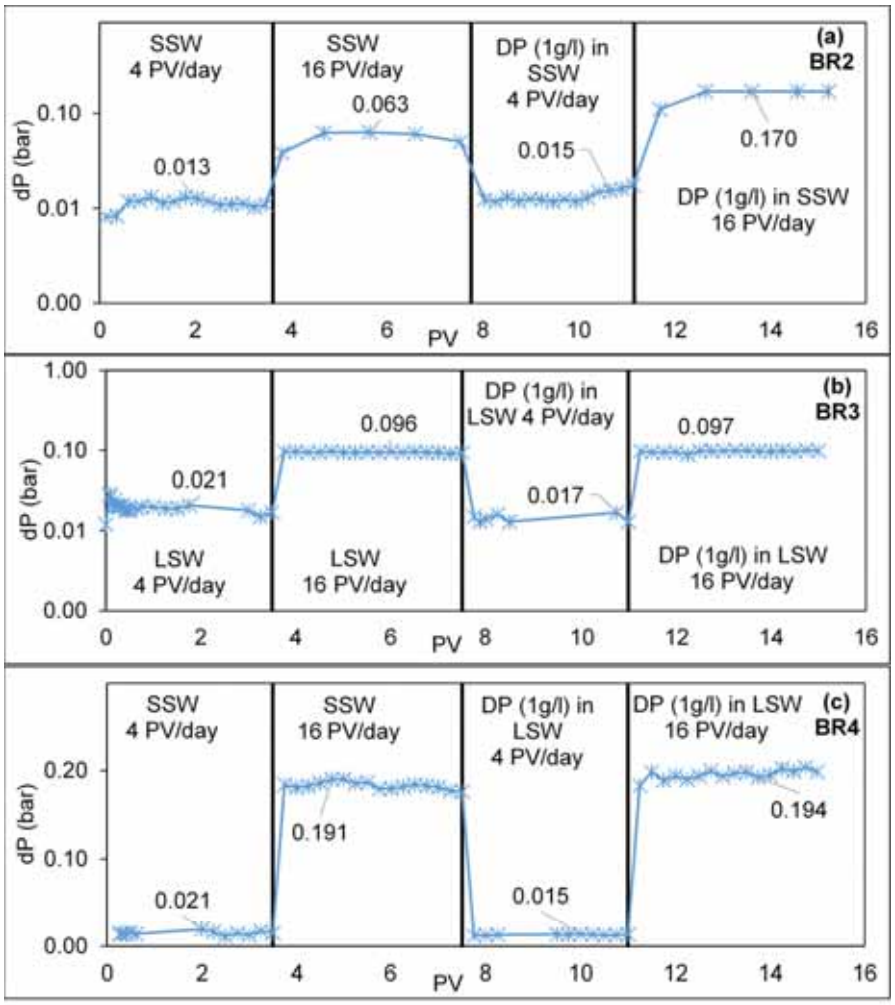


Figure 7.4 Differential pressure drop profiles for floods (a) BR2, (b) BR3 and (c) BR4.

Figure 7.4 shows that the monitored pressure drop during primary recovery is lower for experiment BR2 (SSW) compared to BR3 (LSW). The cores used were outcrops having almost similar dimension and PVs to ensure reasonable comparison. High pressure drop associated with LSW injection could thus be an indication of increased release of fines. Hamouda and Valderhaug (2014) made a similar observation of increased pressure drop during low salinity

injection. Switching the flood to NF in BR2 at flow rate of 4 PV/day, the pressure drop increases slightly to 0.015 bar from 0.013 bar. At 16 PV/day the recorded pressure drops with and without NPs were about the same: 0.097 and 0.096 bar, respectively.

SEM imaging in Figure 5.3 showed that the NP adsorption did not lead to blockage of pore throats. In case of SSW, larger particle size (Figure 5.1) could resist the flow of NPs through the core, therefore a slightly higher pressure drop was observed in BR2. On switching the flood to NF in BR3, the pressure drop fluctuated between 0.013 and 0.017 bar, which was lower than the pressure drop during primary recovery at 4 PV/day (0.021 bar). This may, qualitatively indicate reduction of the produced fines. Finally, for combined flooding BR4 in Figure 7.4(c), the recorded pressure drop was lower during NF injection at 4 PV/day. It was estimated that the water injectivity improved by about 19% and 28 % for flood BR 3 and 4 respectively. At 16 PV/day injection rate in BR3 and BR4, the pressure drops during primary and secondary recovery were almost equal. Thus, the recorded pressure drops in Figure 7.4 may indicate a reduction in the produced fines by combining low salinity and NPs. The NP concentrations in the effluents during floods BR 2-4 is shown in Figure 7.5.

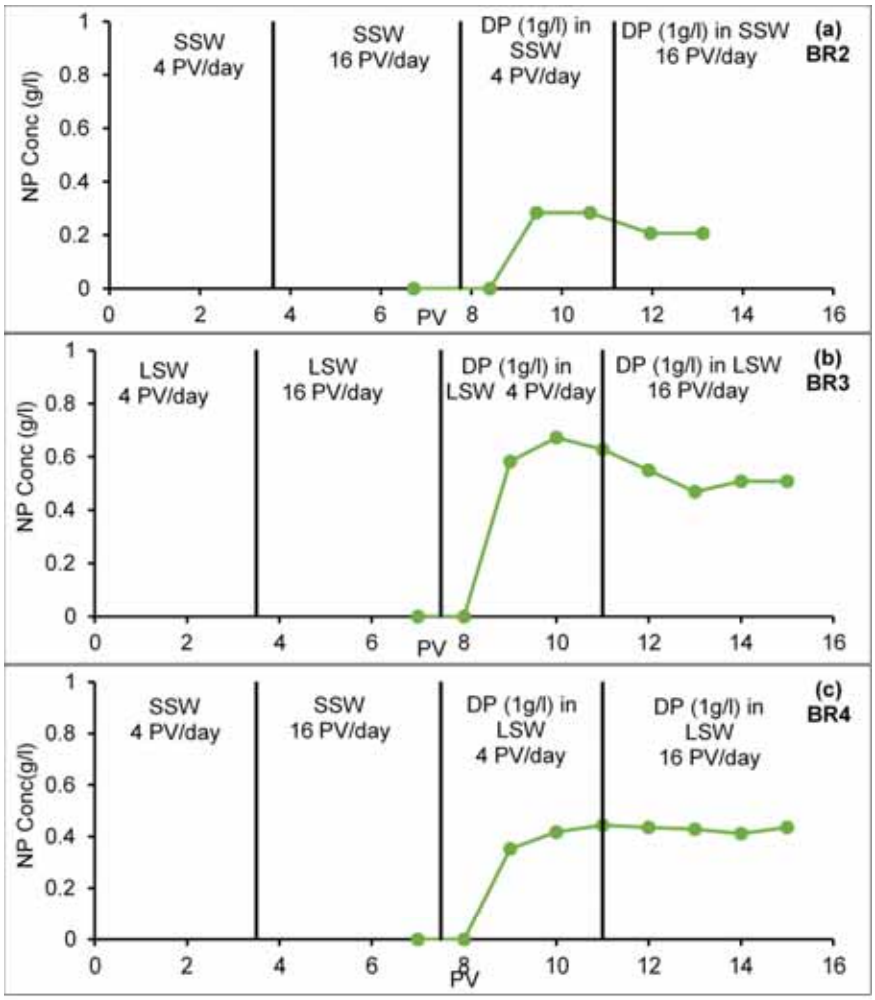


Figure 7.5 Effluent NP concentration profile for floods (a) BR2, (b) BR3 and (c) BR4.

Figure 7.5 shows that for BR2 (NF in SSW) the effluent NP concentration reached a peak of 0.28 g/L as compared to the peak of 0.67 g/L for BR3 (NF in LSW). This indicates higher adsorption of NP on mineral surface at elevated salinity confirming the observations made for adsorption in chapter 5. Increasing NF injection rate to 16 PV/day, the effluent NP concentration fell for both BR2 and BR3 which suggests that NP adsorption increases with higher

injection rate. This may be due to diversion of flow to un swept parts of the core. For combined flooding in BR4, the NP effluent concentration was around 0.5 g/L which is intermediate between BR 2-3. This may partially be effect of to residual SSW from the primary stage on the adsorption of NPs. The pH of the effluents are shown in Figure 7.6.

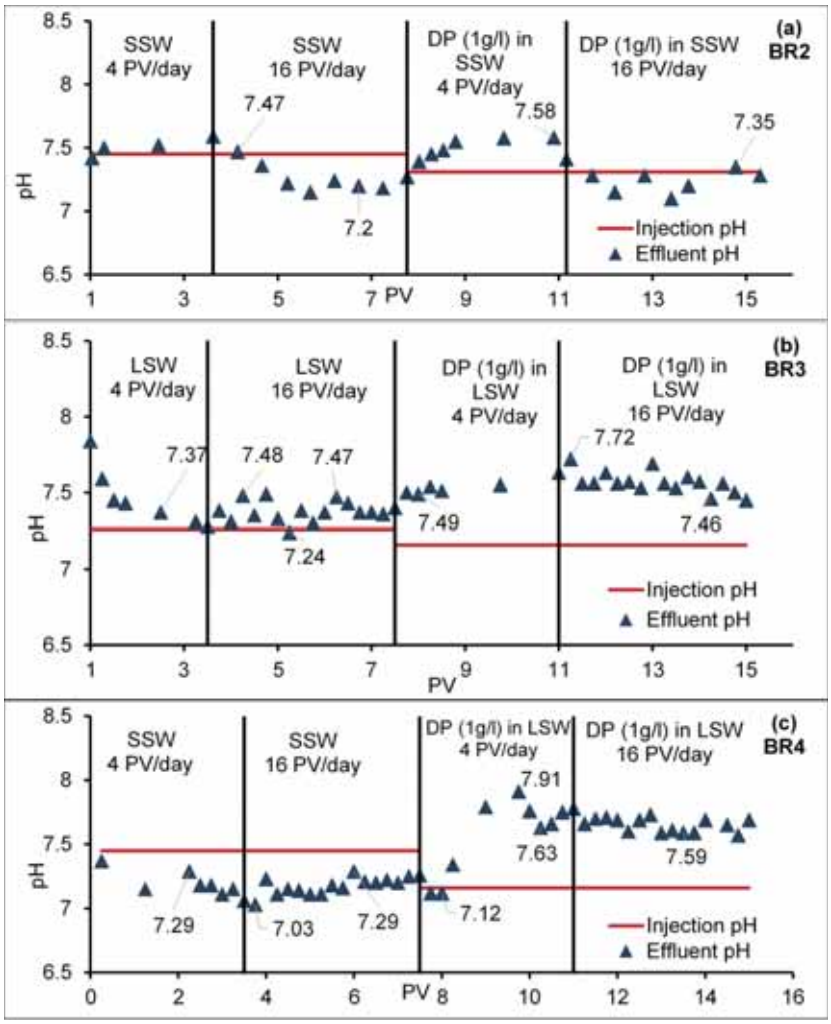


Figure 7.6 Effluent pH profiles for flood (a) BR2, (b) BR3 and (c) BR4.

During primary recovery by SSW (BR2), effluent pH was slightly lower than injected pH. This reduction in pH has been reported by other researchers earlier (RezaeiDoust et al. 2009, Fjelde, Asen, and Omekeh 2012). The observed pH during flood BR3 (all LSW) is slightly higher than the injected pH. This behaviour is typical to low salinity floods and has been reported previously (Hamouda and Valderhaug 2014). On switching to NF in SSW in case of BR2, pH rose. A similar rise in pH was also observed for flood BR3 with NF in LSW. For flood BR 4, the pH remained lower than injected pH for primary recovery by SSW. Thereafter, the pH rose when the flood was switched to NF prepared in LSW. The cations produced during floods BR2-4 are shown in Figure 7.7.

In the case of BR2 (SSW), the effluent cation concentrations did not show much fluctuation, which may indicate equilibrium between rock and the fluid was established. In the case of BR3 (LSW), high initial relative concentrations of $Na^+$, $K^+$ and $Ca^{2+}$ was produced perhaps due to residual SSW in the core during core preparation for establishing initial water saturation. After some fluctuations at the start of the flood, $Mg^{2+}$ relative concentration stabilized and remained close to 1 during remainder of the flooding. As the primary flood progressed in BR3 (LSW), $K^+$ relative concentration stabilized at 1.6 and 1.37 at 4 and 16 PV/day respectively. This together with the increase in pH observed during these stages in Figure 7.6 (b) supports dissolution of K-feldspar (equation 6.3) as discussed in the previous chapter. Additionally, during this stage the $Na^+$ concentration was lower than the injected concentration by about 20 %. This may indicate ion exchange process according to equation 6.4. However, when the flood was switched to NF, the $K^+$ relative concentration fell and stabilized at around 0.85 and 0.66 at injection rate of 4 and 16 PV/day respectively. Further the $Na^+$ relative concertation also rose to 0.94 and 0.95 at injection rate of 4 and 16 PV/day respectively. These observations suggest that

both mineral dissolution and ion exchange were reduced by the NF i.e., reduced direct contact between the injected fluid and mineral. The reduction was observed to be enhanced at higher flowrate which coincides with increased NP adsorption in Figure 7.5(b).

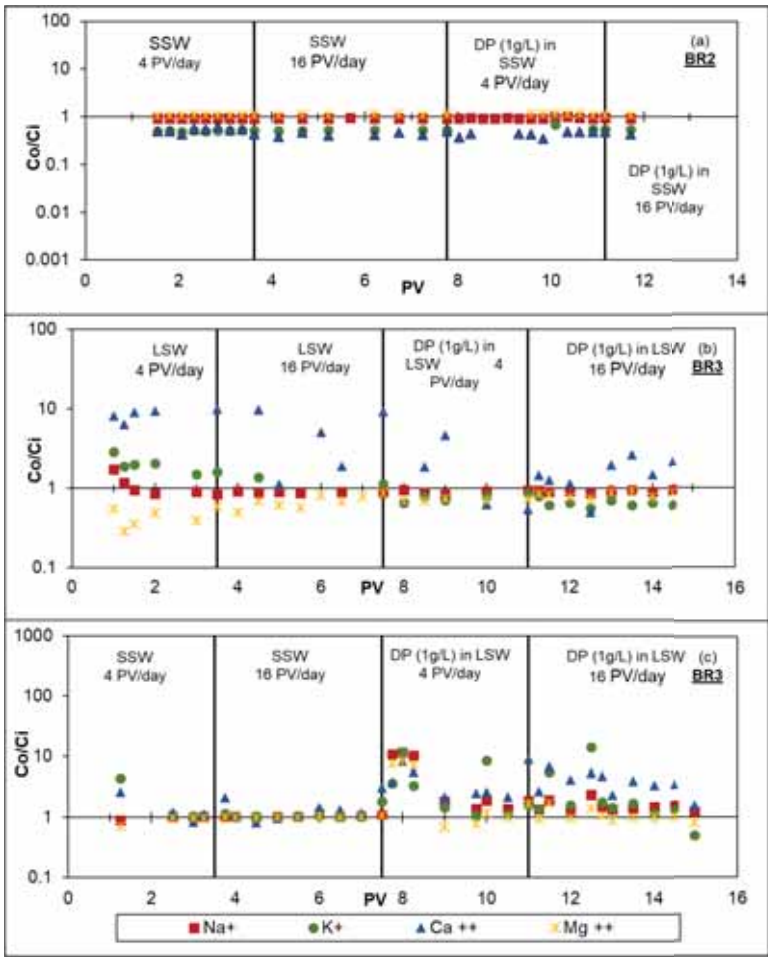


Figure 7.7 Relative concertation of $K^+$ and $Na^+$ and $Ca^{2+}$ in effluents for floods (a) BR2, (b) BR3 and (c) BR4.

Unlike BR2 (all SSW) where an equilibrium like condition was indicated, high $Ca^{2+}$ production was observed during primary recovery by LSW in BR3. Hamouda and Valderhaug (2014) reported similar observations for low salinity flooding of berea and attributed the increased $Ca^{2+}$ production to the dissolution of cementing material ($CaCO_3$) in the core. In the previous chapter, it was shown that silica NPs can significantly lower the dissolution of calcite and the silica NPs have a high affinity of adsorption on calcite. During secondary recovery by NFs in BR3, the $Ca^{2+}$ levels fell and fluctuated between 4.65 and 0.62. Further reduction in $Ca^{2+}$ levels was observed when NF injection rate was increased to 16 PV/day (fluctuation between 2.64 and 0.49). This confirms the previously stated observation of increasing effect of NP at higher flowrate. Thus, combining LSW with the used NPs reduces the mineral dissolution induced by injecting LSW alone and also reduces loss of cementing mineral. This may explain the reduction in pressure drop observed in Figure 7.4 (b) due to lesser production of fines caused by adsorption of NP of berea surface. During combined flooding in BR4, the relative concentrations of all the ions were close to 1 during primary recovery by SSW. During secondary recovery by NF in LSW, initially the ions are high perhaps due to residual SSW from previous stage. Thereafter both $K^+$ and $Ca^{2+}$ showed a decreasing trend and the $Na^+$ stabilizes at about 1.2. This confirms the conclusions made from BR3 that the silica NFs reduced mineral dissolution, ion exchange and loss of cementing minerals due to low salinity flooding.

The adsorption of NPs can modify the berea surface as discussed in chapter 4. The effect of the surface modification on the interaction between the fines and berea was modelled based on the DLVO theory as outlined in section 4.5. The zeta potential of berea powder aged in synthetic oil and dispersed in SSW and LSW corresponds to the primary recovery in floods BR2 and BR3, respectively.

The oil aged berea was further treated with NF at 1 g/L concentration in SSW and LSW. The modified mineral was recovered and dispersed in SSW and LSW after which zeta potential measurements were performed to correspond to the secondary recovery stage of floods BR2 and BR3. The size of the fines eluted from flooding berea are reported in Table 7.2. The zeta potential measurements are listed in Table 7.2 and the sizes of the fine particles are listed in Table 4.3. Hamaker's constant was calculated from equation 5.7. The surface forces estimation here are performed at 70º C. Therefore the measured zeta potential values at room temperature are corrected to 70ºC based on correlation for common minerals from previous studies (Schembre, Tang, and Kovscek 2006, Karoussi and Hamouda 2007) :

$$\zeta(T) = (0.01712(T - T_0) + 1) \cdot \zeta(T_0) \qquad (7.3)$$

Where, $T$ and $T_o$ are interpolation and measurement temperature respectively in Kelvin. $\zeta(T_o)$ is the zeta potential measured at $T_o$. The inverse Debye lengths in LSW and SSW were calculated from equation 5.8 and 5.9. The calculated interaction potentials are shown in Figure 7.8.

Table 7.2 Zeta potential measurements for crushed berea mineral and fines.

| Mineral | Zeta potential (mV) |
|---|---|
| Berea aged in oil and dispersed in SSW | -7.67 |
| Berea aged in oil and dispersed in LSW | -18.1 |
| Berea aged in oil and then treated with dispersed NP in SSW | -8.91 |
| Berea aged in oil then treated with dispersed NP in LSW | -21.2 |
| Fines in SSW | -5.89 |
| Fines in LSW | -13.7 |

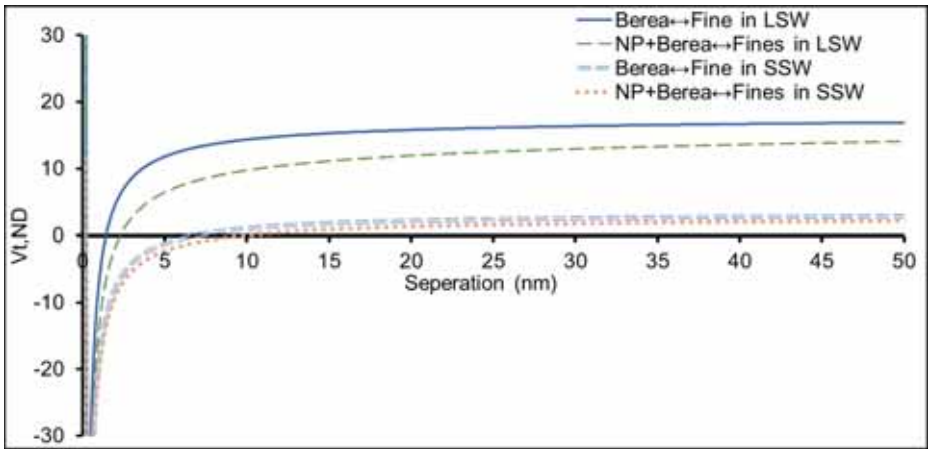


Figure 7.8 Calculated interaction potential between the fines and the mineral at 70ºC.

Figure 7.8 shows that the interaction is more repulsive in LSW compared to SSW, indicating that flooding with LSW could lead to greater fines release/migration. Modifying the rock with NPs make the interaction energy less repulsive for both LSW and SSW. However, the change is greater in the case of LSW compared to SSW. These results are supported by the lower

pressure drop observed during secondary recovery in BR3 (NP+LSW) as compared to primary recovery by brine alone in Figure 7.4(b). In addition, Figure 7.4(c) shows that secondary recovery by LSW+NP has lower pressure drop than primary recovery by SSW. This may be due to adsorption of NPs on minerals. Thus the adsorption of silica NPs on the rock makes the interaction between fines and rock less repulsive. This would hinder the migration of produced fines.

## 7.2 Oil recovery from chalk cores

This section addresses the incremental oil recovery by silica NPs and the interaction of NPs with mineral surface in presence of oil. In order to mimic the field status (water flooding), different scenarios were studied as shown in Table 7.3. The injection rates were small to be able to account for the kinetics of the interaction. From our previous studies with LSW alone (Hamouda and Maevskiy 2014), two flow rates were used 4 and 16 PV/day. Thereafter, the injection was switched to NF and the flow was at 4 and 16 PV/day. The details of the experimental tests are listed in Table 7.3. The experiments were divided into two stages with brine alone and NPs dispersed in the selected brine. The injection was performed at lower flowrates that are closer to real field cases and to give the injected fluid sufficient residence time in the core for the interaction. Hamouda and Maevskiy (2014) and Hamouda and Gupta (2017) previously studied the effect of low salinity composition on primary and secondary recovery in SK chalk by systematically diluting the SSW. They found that LSW at a 1:10 SSW dilution was the optimum for the investigated brines for EOR. Therefore, LSW 1:10 dilution of SSW was used here.

Table 7.3 List of oil recovery experiments with chalk.

| Core Id | Porosity (%) | Permeability (mD) | Length (cm) | Dia (cm) | Swi | Primary Recovery Fluid | Secondary Recovery Fluid |
|---|---|---|---|---|---|---|---|
| SK5 | 50.7 | 3.9 | 8.83 | 3.785 | 0.13 | SSW | DP (1 g/L) in SSW |
| SK6 | 50 | 3.9 | 5.96 | 3.785 | 0.28 | LSW | DP (1 g/L) in LSW |
| SK7 | 50.24 | 3.9 | 4.658 | 3.785 | 0.275 | SSW | DP (1 g/L) in LSW |

In the SK5 case, both primary and secondary used SSW. For the secondary, however, silica NPs (DP 1 g/L) was dispersed in SSW. In SK6, primary flooding was with LSW followed by injection of NF (DP 1 g/L) in LSW. The third scenario was for SK7, where SSW was used in primary stage, followed by NF (DP 1 g/L) in LSW. These three scenarios represent the various possible combinations. Incremental oil obtained from nanofluid injection in SK5-7 are shown in Figure 7.9.

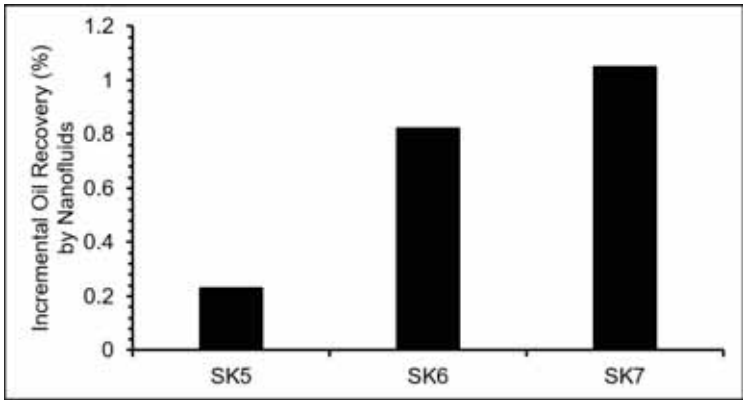


Figure 7.9 Incremental recovery from SK5-SSW, SK6-LSW and SK7-mixed.

As mentioned earlier, the recovery here is not optimized to account properly for EOR, but compared to our previous studies with LSW alone (Hamouda and Maevskiy 2014). The incremental recovery was greater in the case of SK6 (0.824%) than with SK5 (0.15%). The highest incremental recovery was observed when the fluid was switched to NF prepared in LSW (1.05% for SK7 experiment). The effluent pH profiles were recorded for the SK5, SK6 and SK7 and are shown in Figure 7.10.

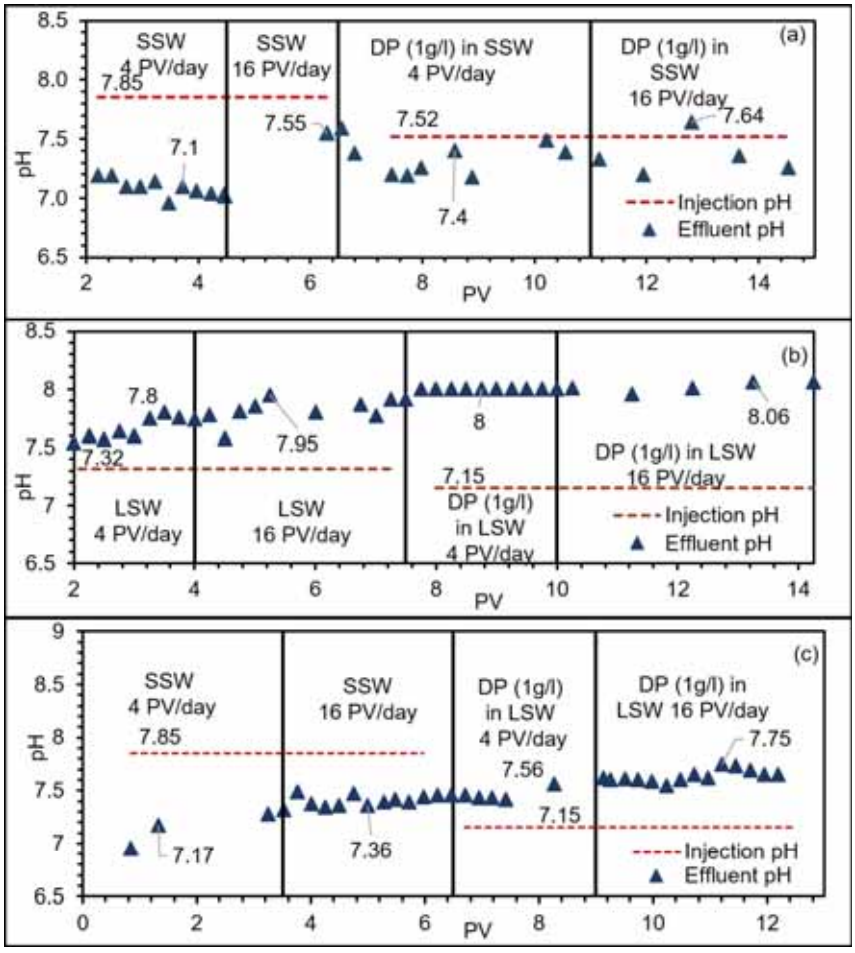


Figure 7.10 Effluent pH profiles SK5-SSW (a), SK6-LSW (b) and SK7-mixed (**c**).

For SK5 (all SSW), the effluent pH during primary and secondary stages were lower than the pH of the injected SSW. This observation is similar to that previously made by Hamouda and Maevskiy (2014). In the case of SK6 (LSW and LSW with NPs) however, interesting behavior was observed. The effluent pH was higher than the injection pH and continued rising until it stabilized at about 7.8. Increasing the flow rate to 16 PV/day led to a slight increase in pH to around 7.95, after which it stabilized at around 7.91. The increase in pH may be explained by calcite dissolution, in accordance with the Equation 5.15.

The pH in the case of SK7 (SSW and LSW with NPs) shows that the pH remained below the injected pH in primary stage. However, the pH increased slightly to about 7.56 when the injection was switched to LSW with NF. When the NF injection rate was increased to 16 PV/day, the pH of SK6 and SK7 stabilized at about 8.06 and 7.75, respectively. As expected, the pH was higher for SK6 case than in the case of SK7. The concentrations of $Ca^{2+}$ and $Mg^{2+}$ in the effluents of SK5-7 are plotted in Figure 7.11.

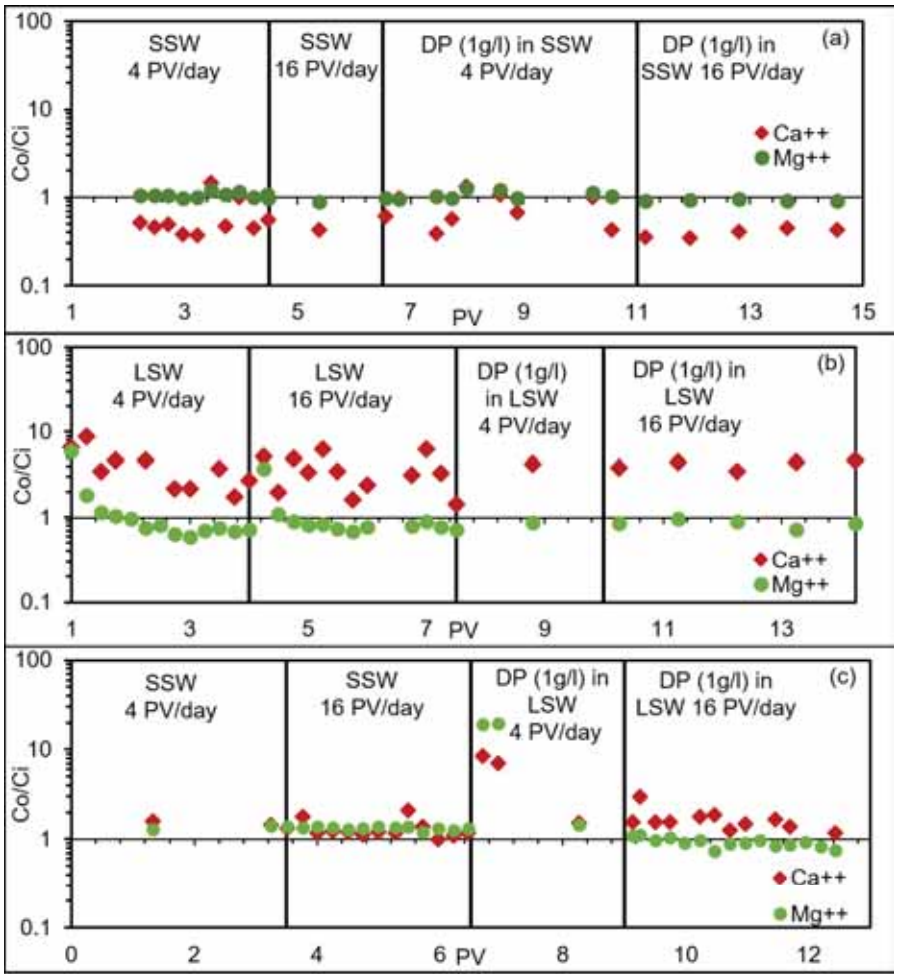


Figure 7.11 Effluent $Ca^{2+}$ and $Mg^{2+}$ concentrations for SK5-SSW (a), SK6-LSW (b) and SK7-mixed (c).

Figure 7.11(a) shows that the $Ca^{2+}$ effluent in SK5 was lower than the injected concentration during primary stage and even more so during secondary stage. This may indicate slight calcite dissolution with high injection salinity (SSW). This observation was also supported by the low pH recorded for this SK5 in Figure 7.10(a). $Mg^{2+}$ concentration in the effluent was close to the injected

concentration. Where the SK6 (all LSW) is concerned, however, the $Ca^{2+}$ ion concentration during primary stage by LSW was consistently higher, indicating calcite dissolution similar to the observation made during dynamic adsorption experiments in SK4. This observation is supported by the high effluent pH in Figure 7.10(b). Along with the excess $Ca^{2+}$, there was a deficiency in $Mg^{2+}$ in the effluent. It is well established that calcite has a tendency to accommodate $Mg^{2+}$ in its structure (Stumm and Morgan 1970). The exchange between $Ca^{2+}$ and $Mg^{2+}$ may lead to the formation of complex calcium/magnesium minerals with different ratios. The following reaction is for a 1:1 ratio (dolomite):

$$2CaCO_{3(s)} + Mg^{2+} \rightarrow CaMg(CO_3)_2 + Ca^{2+} \quad (7.4)$$

Dolomitization has been previously observed by Petrovich and Hamouda (1998) in the chalk formations of the Ekofisk field. During primary stage by LSW, the ratio of the effluent ion concentration to the injected concentration reached 6.267 and 0.686 for $Ca^{2+}$ and $Mg^{2+}$ respectively at 16 PV/day. When SK6 was switched to NF prepared in LSW, the ratio of $Ca^{2+}$ to injected concentrations fell to 4.26 at the injection rate of 4 PV/day. Increasing the rate to 16 PV/day raised the $Ca^{2+}$ concentration slightly to 4.63, which is still below the $Ca^{2+}$ concentration during primary stage by LSW. This reduction in $Ca^{2+}$ during NF injection (almost 30%) coincided with a comparative increase in levels of $Mg^{2+}$ to 0.86 at 4 PV/day and 0.85 at 16 PV/day. These observations may indicate a reduction in calcite dissolution and the formation of calcium/magnesium minerals. The increased amount of $Mg^{2+}$ was not significant enough to indicate reduced magnesium/calcium exchange. It is therefore possible that the reduction in $Ca^{2+}$ was caused by reduced calcite dissolution during NF injection. Increasing the rate to 16 PV/day, the $Ca^{2+}$ concentration stabilized at around 4.6. This also represents a 25% reduction of $Ca^{2+}$ production compared with the 4 PV/day flow rate during primary stage.

With primary stage in the SK7 case, the effluent ion concentration profiles were close to the injected concentration. When the SK7 was switched to NF prepared in LSW, the $Ca^{2+}$ and $Mg^{2+}$ ions were initially high. Two main possibilities exist for the increase of $Ca^{2+}$ and $Mg^{2+}$: (1) production of trapped SSW from the first stage and/or (2) dissolution of possible calcium sulfate formed during the first stage. The latter may sound more realistic because of a rapid reduction in $Ca^{2+}$ and $Mg^{2+}$ concentrations. Thereafter, the $Ca^{2+}$ concentration was around 1.5 at 4 PV/day. The $Ca^{2+}$ concentration during this stage is almost three times lower than at the same stage in SK6. When increasing the injection rate to 16 PV/day, the $Ca^{2+}$ concentration fluctuates between 2.9 and 1.16. This concentration at 4 PV/day is almost three times lower than during the same stage in SK6.

The differential pressure drop (dP) data recorded for SK5-7 is shown in Figure 7.12. At 4 PV/day with SSW injection in SK5, the pressure drop stabilized at about 1.79 bar. When the injection rate was increased to 16 PV/day, the dP increased and stabilized at around 3.70 bar. After the injection fluid was switched to NF prepared in SSW, the pressure rose steadily from 0.68 to 2.17 bar.

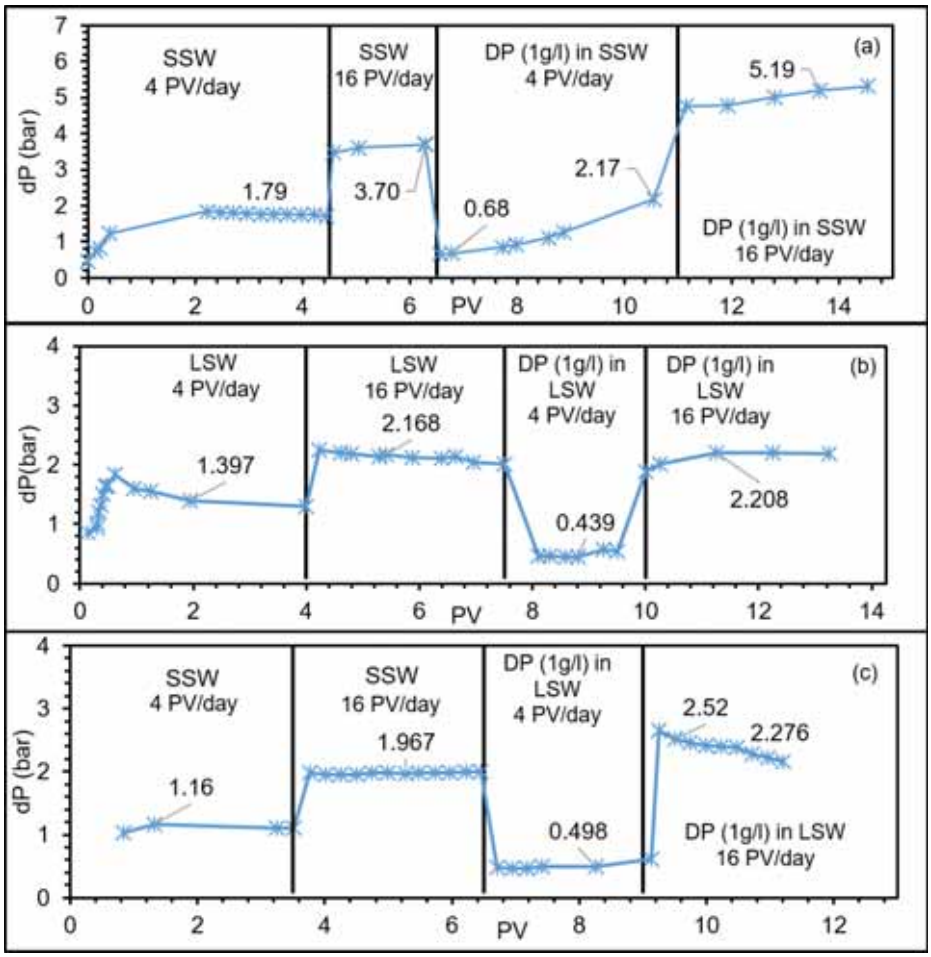


Figure 7.12 Differential pressure drop (dP) profile for SK5-SSW (a), SK6-LSW (b) and SK7-mixed (c).

van Oort, Van Velzen, and Leerlooijer (1993) stated a general rule of thumb that, if the particle size of the suspended solids exceeds one-third of the pore diameter, the particles will cause plugging behavior. The average pore size of the SK chalk used in this study is around 200 nm (Jolma et al. 2017). The size of the NPs in SSW was shown earlier to be 88.1 nm at 80 °C. It is possible that some of the smaller pore throats are blocked by the NPs. For SK6 however, the

recorded dP for NF (in LSW) was 0.439 bar, which is almost three times lower than the dP recorded for LSW injection in the first stage. The measured particle size of the NPs in LSW is about 38 nm, which is significantly lower than the average pore throat of the chalk used. The recorded dP at 16 PV/day was slightly higher for the NF compared with LSW alone. However, the difference (≈0.04 bar) is within the uncertainty range of the measured dP (±0.1 bar). The resistance to flow was therefore lower at the low flow rate. A similar observation was made with SK7 where, at the lower flow rate (4 PV/day), the dP during NF injection was less than half that from SSW injection. However, the pressure drop at the higher flow rate was slightly (≈0.5 bar) higher during NF injection, with a decreasing trend. The decreasing pressure trend observed in SK7 during 16 PV/day injection of nanofluid was not observed for the same stages in flood SK5 and 6 wherein the salinity of the fluid was constant throughout the experiment, with only addition of NPs. However, in SK7, the fluid salinity is switched from SSW to LSW (with NP). Two mechanisms take place: (1) adsorption of NP on the chalk surface, hence reduced calcite dissolution and (2) disturbance of fluid rock equilibrium due to low salinity. As the injection rate is increased to 16 PV/day, the swept region with LSW + NPs increased, hence reduced pressure. This is evident in Figure 7.11(c) wherein at 16 PV/day, a decreasing trend in $Ca^{2+}$ production was observed. The decrease in $Ca^{2+}$ may be explained based on reduced dissolution of calcite and dilution factor due to increased sweep.

## 7.3 Summary

This chapter addressed the interaction of silica NPs with mineral in the presence of hydrocarbon. This was done to compare the interaction between NP and mineral surface in the presence and absence of oil phase (chapter 6). Three cases were investigated, with silica NPs mixed with SSW and LSW. In the first two cases, the primary injection was performed with either SSW or LSW followed by secondary injection of silica nanofluids prepared in the same brine as in primary injection phase. In the third case, the primary recovery was performed by SSW followed by injection of silica NPs dispersed in LSW. This represents a more realistic case where most fields are flooded with seawater and low salinity injections are being considered for the following phase.

Secondary recovery by NFs in sandstones showed that NP adsorption reduces mineral dissolution, suppresses ion exchange process and loss of cementing minerals caused by LSW injection. Lower pressure drop and surface forces estimation confirmed that silica NPs reduces formation damage associated with low salinity water injection in sandstone reservoirs. The silica NFs improved water injectivity by about 20%. Since neither the core preparation nor the nanofluid injection was optimised, the incremental recovery and the potential for EOR by silica nanofluids is indicated by spontaneous imbibition tests. Spontaneous imbibition test showed that NPs dispersed in LSW led to higher incremental oil recovery (≈9.5%) than in case of DIW/SSW(≈6%). Particle size measurements and surface forces estimation between the NPs suggests that dispersing NPs in LSW could increase the structural disjoining pressure, which would enhance the removal of oil from the mineral surface.

In chalk cores, the silica NPs reduced calcite dissolution by about 25 % during the oil recovery. However without oil (chapter 6) the reduction of calcite

dissolution was about 30 %. The lower reduction in the presence of oil may be due to less available sites for NP to adsorb on mineral surface. Injection of silica nanofluid prepared in LSW at low rate reduced resistance to flow in chalk core. While some incremental oil recovery by nanofluid injection was observed, tests for oil recovery ware not optimised in the current work.

The outcome from this chapter confirms the observation made in the previous chapter that combining silica NPs with low salinity flooding could reduce formation damage in sandstone reservoirs and lower the risk of matrix integrity loss and the subsidence degree of the water-flooded chalk. This suggests a potential synergy between the silica NPs and low salinity for EOR.

# 8 Concluding remarks

This thesis addressed the effect of silica NP adsorption on fluid/rock interaction in sandstone and chalk reservoirs. In-house silica nanofluids and commercial silica nanofluids were investigated. The adsorption of silica NPs was addressed by two methods: (1) static adsorption of silica NPs on minerals and (2) dynamic adsorption of silica NPs injected into sandstone and chalk cores. The kinetic aspects of silica NP adsorption were also addressed. In addition, the fluid/rock interactions during dynamic adsorption and oil recovery by silica nanofluids were addressed. Based on the work, the following are the main conclusions:

(1) The in-house silica nanofluids showed limited stability of the dispersed NPs. However, the nanofluids prepared from commercial silica NPs showed good stability and may be considered for flooding.
(2) Silica NPs show high adsorption affinity towards calcite mineral followed by quartz, and the lowest adsorption affinity was towards kaolinite. The rate of adsorption was higher for calcite (0.11-2.5 g/mg h) compared to quartz (0.042-0.15 g/mg h). In addition, it was observed that both rate and equilibrium adsorption of NPs on minerals are enhanced at higher salinity. SEM imaging did not show pore throat blockage, in fact the injectivity improves with nanofluid injection. The silica NFs prepared in LSW improved water injectivity by about 20% in sandstones. Injection of silica nanofluid prepared in LSW significantly reduced resistance to flow in chalk core.
(3) Silica NPs' adsorption process on quartz and calcite was best fitted to pseudo second order kinetic model with $R^2$ close to 1. For NP adsorption on calcite, the adsorption characteristic curves showed high initial

adsorption behavior wherein most of the equilibrium adsorption occurred in the initial time period.

(4) The adsorption of NPs is largely influenced by the fluid pH for chalk and sandstones. Increased alkalinity during low salinity flooding favours NP desorption. Dynamic adsorption of NPs injected into chalk and sandstone core showed high irreversible adsorption at elevated salinity and desorption in low salinity conditions. NP adsorption/desorption mechanisms related to pH for chalk and sandstones have been proposed.

(5) Silica NFs injection during secondary recovery in sandstones showed that NP adsorption reduces mineral dissolution, suppresses ion exchange process and loss of cementing minerals caused by LSW injection. This reduces the production of fines. In addition, silica NP adsorption modifies the mineral surface and makes its interaction with produced fines less repulsive. Together these two mechanisms reduce the formation damage caused by low salinity injection. Spontaneous imbibition tests showed that NPs dispersed in LSW showed higher incremental oil recovery of about 9.5% than in case of DIW/SSW where in the incremental recovery was about 6%. Particle size measurements and surface forces estimation between the NPs suggests that dispersing NPs in LSW could increase the structural disjoining pressure, which would enhance the removal of oil from the mineral surface.

(6) NP adsorption on chalk significantly reduces calcite dissolution by about 30%. That is the silica nanofluid reduced the detrimental effect of low salinity flooding on chalk matrix integrity which is one of the major concerns in chalk reservoirs. While some incremental oil recovery by nanofluid injection was observed, tests for oil recovery were not optimised in the current work. The results from this work identified that silica

nanofluids can potentially increase oil recovery from chalks as compared to low salinity injection alone.

In summary the main outcome of this work suggests a synergy between silica NPs and low salinity flooding for EOR wherein, dispersing of silica NPs in low salinity water can reduce the risk of formation damage in sandstones and reduce the risk of reservoir subsidence due to calcite dissolution in chalks.

**Future works**

This study investigated the fluid/rock interactions during combined silica NP and nanofluid flooding. Multicomponent brines (SSW/LSW) apart from DIW were used to prepare the nanofluids. Further optimization of the processes identified in this study would require investigation into the effect of NPs dispersed in single component brines. Using techniques like XRD and SEM mapping can help identify the mineralogical changes associated with the application of silica NPs.

In this study, the oil recovery due to the Silica NPs has not been optimized. Further work needs to be done to investigate the oil recovery mechanisms by silica NPs. Contact angle measurements and interfacial tension studies could be used to investigate mechanisms for enhanced oil recovery by silica nanoparticles. The work also indicates a possible combined effect of silica NPs and LSW in increasing the structural disjoining pressure which can cause detachment of oil from mineral surface. This need to be investigated further.

# 9 Bibliography

2018. World Energy Outlook. International Energy Agency.

Abhishek, R, G Suresh Kumar, and RK Sapru. 2015. "Wettability alteration in carbonate reservoirs using nanofluids." *Petroleum Science and Technology* 33 (7):794-801.

Abhishek, Rockey, Nikhil Bagalkot, and G Suresh Kumar. 2016. "Effect of transverse forces on velocity of nanoparticles through a single fracture in a fractured petroleum reservoir." *International Journal of Oil, Gas and Coal Technology* 12 (4):379-395.

Agista, Madhan, Kun Guo, and Zhixin Yu. 2018. "A State-of-the-Art Review of Nanoparticles Application in Petroleum with a Focus on Enhanced Oil Recovery." *Applied Sciences* 8 (6):871.

Akhmetgareev, Vadim, and Rais Khisamov. 2015. "40 Years of Low-Salinity Waterflooding in Pervomaiskoye Field, Russia: Incremental Oil." SPE European Formation Damage Conference and Exhibition.

Al-Anssari, Sarmad, Ahmed Barifcani, Shaobin Wang, and Stefan Iglauer. 2016. "Wettability alteration of oil-wet carbonate by silica nanofluid." *Journal of colloid and interface science* 461:435-442.

Al-Anssari, Sarmad, Shaobin Wang, Ahmed Barifcani, and Stefan Iglauer. 2017. "Oil-water interfacial tensions of silica nanoparticle-surfactant formulations." *Tenside Surfactants Detergents* 54 (4):334-341.

Al-Anssari, Sarmad, Shaobin Wang, Ahmed Barifcani, Maxim Lebedev, and Stefan Iglauer. 2017. "Effect of temperature and SiO 2 nanoparticle size on wettability alteration of oil-wet calcite." *Fuel* 206:34-42.

Al-Nofli, Kholood, Peyman Pourafshary, Nader Mosavat, and Ali Shafiei. 2018. "Effect of Initial Wettability on Performance of Smart Water Flooding in Carbonate Reservoirs—An Experimental Investigation with IOR Implications." *Energies* 11 (6):1394.

Alomair, Osamah Ali, Khaled M Matar, and Yousef H Alsaeed. 2015. "Experimental study of enhanced-heavy-oil recovery in Berea sandstone cores by use of nanofluids applications." *SPE Reservoir Evaluation & Engineering* 18 (03):387-399.

Arab, D, P Pourafshary, Sh Ayatollahi, and A Habibi. 2014. "Remediation of colloid-facilitated contaminant transport in saturated porous media treated by nanoparticles." *International Journal of Environmental Science and Technology* 11 (1):207-216.

Arab, Danial, and Peyman Pourafshary. 2013. "Nanoparticles-assisted surface charge modification of the porous medium to treat colloidal particles migration induced by low salinity water flooding." *Colloids and Surfaces A: Physicochemical and Engineering Aspects* 436:803-814.

Aurand, Katherine R, Gunnar Sie Dahle, and Ole Torsæter. 2014. "Comparison of oil recovery for six nanofluids in Berea sandstone cores." International Symposium of the Society of Core Analysts, September.

Austad, T, SF Shariatpanahi, S Strand, CJJ Black, and KJ Webb. 2011. "Conditions for a low-salinity enhanced oil recovery (EOR) effect in carbonate oil reservoirs." *Energy & fuels* 26 (1):569-575.

Austad, Tor, Alireza RezaeiDoust, and Tina Puntervold. 2010. "Chemical mechanism of low salinity water flooding in sandstone reservoirs." SPE improved oil recovery symposium.

Ayatollahi, Shahab, and Mohammad M Zerafat. 2012. "Nanotechnology-assisted EOR techniques: New solutions to old challenges." SPE International Oilfield Nanotechnology Conference and Exhibition.

Behzadi, Abed, and Aliasghar Mohammadi. 2016. "Environmentally responsive surface-modified silica nanoparticles for enhanced oil recovery." *Journal of Nanoparticle Research* 18 (9):1-19.

Bhattacharjee, Subir, and Menachem Elimelech. 1997. "Surface Element Integration: A Novel Technique for Evaluation of DLVO Interaction between a Particle and a Flat Plate." *Journal of Colloid and Interface Science* 193 (2):273-285. doi: https://doi.org/10.1006/jcis.1997.5076.

Bhattacharya, SS, J Paitaridis, A Pedler, A Badalyan, Y Yang, T Carageorgos, P Bedrikovetsky, D Warren, and N Lemon. 2016. "Fines Mobilisation by Low-Salinity Water Injection: 3-Point-Pressure Tests." SPE International Conference and Exhibition on Formation Damage Control.

Binks, Bernard P, Jhonny A Rodrigues, and William J Frith. 2007. "Synergistic interaction in emulsions stabilized by a mixture of silica nanoparticles and cationic surfactant." *Langmuir* 23 (7):3626-3636.

Binks, Bernard P, and Catherine P Whitby. 2005. "Nanoparticle silica-stabilised oil-in-water emulsions: improving emulsion stability." *Colloids and Surfaces A: Physicochemical and Engineering Aspects* 253 (1-3):105-115.

Chukwudeme, EA, and AA Hamouda. 2009. "Oil recovery from polar components (asphaltene and SA) treated chalk rocks by low salinity water and water containing SO42− and Mg2+ at different temperatures." *Colloids and Surfaces A: Physicochemical and Engineering Aspects* 336 (1-3):174-182.

Dehghan Monfared, Abolfazl, Mohammad Hossein Ghazanfari, Mohammad Jamialahmadi, and Abbas Helalizadeh. 2016. "Potential Application of Silica Nanoparticles for Wettability Alteration of Oil–Wet Calcite: A Mechanistic Study." *Energy & Fuels* 30 (5):3947-3961.

Di Credico, B., I. R. Bellobono, M. Arienzo, D. Fumagalli, M. Redaelli, R. Scotti, and F. Morazzoni. 2015. "Efficacy of the Reactive Oxygen Species Generated by Immobilized TiO2 in the Photocatalytic Degradation of Diclofenac " *International Journal of Photoenergy* 2015:13. doi: 10.1155/2015/919217.

Ding, Yanan, Sixu Zheng, Xiaoyan Meng, and Daoyong Yang. 2019. "Low Salinity Hot Water Injection With Addition of Nanoparticles for Enhancing Heavy Oil Recovery." *Journal of Energy Resources Technology* 141 (7):072904.

Dunphy Guzman, Katherine A, Michael P Finnegan, and Jillian F Banfield. 2006. "Influence of surface potential on aggregation and transport of titania nanoparticles." *Environmental Science & Technology* 40 (24):7688-7693.

Farokhzad, Omid C, and Robert Langer. 2009. "Impact of nanotechnology on drug delivery." *ACS nano* 3 (1):16-20.

Fjelde, Ingebret, Siv Marie Asen, and Aruoture Voke Omekeh. 2012. "Low salinity water flooding experiments and interpretation by simulations." SPE Improved Oil Recovery Symposium.

Fletcher, Alistair, and John Davis. 2010. "How EOR can be transformed by nanotechnology." SPE Improved Oil Recovery Symposium.

Frykman, Peter. 2001. "Spatial variability in petrophysical properties in Upper Maastrichtian chalk outcrops at Stevns Klint, Denmark." *Marine and Petroleum Geology* 18 (10):1041-1062.

Gao, Gui-Mei, Hai-Feng Zou, Da-Rui Liu, Li-Na Miao, Gui-Juan Ji, and Shu-Cai Gan. 2009. "Influence of surfactant surface coverage and aging time on physical properties of silica nanoparticles." *Colloids and Surfaces A: Physicochemical and Engineering Aspects* 350 (1-3):33-37.

Giraldo, Juliana, Pedro Benjumea, Sergio Lopera, Farid B Cortés, and Marco A Ruiz. 2013. "Wettability alteration of sandstone cores by alumina-based nanofluids." *Energy & Fuels* 27 (7):3659-3665.

Gomari, KA Rezaei, R Denoyel, and AA Hamouda. 2006. "Wettability of calcite and mica modified by different long-chain fatty acids (C18 acids)." *Journal of colloid and interface science* 297 (2):470-479.

Griffith, Nicholas, Yusra Ahmad, Hugh Daigle, and Chun Huh. 2016. "Nanoparticle-stabilized natural gas liquid-in-water emulsions for residual oil recovery." SPE Improved Oil Recovery Conference.

Hamouda, AA, and V Alipour Tabrizy. 2013. "The effect of light gas on miscible CO2 flooding to enhance oil recovery from sandstone and chalk reservoirs." *Journal of Petroleum Science and Engineering* 108:259-266.

Hamouda, AA, OM Valderhaug, R Munaev, and H Stangeland. 2014. "Possible mechanisms for oil recovery from chalk and sandstone rocks by low salinity water (LSW)." SPE Improved Oil Recovery Symposium.

Hamouda, Aly A., and Sachin Gupta. 2017. "Enhancing Oil Recovery from Chalk Reservoirs by a Low-Salinity Water Flooding Mechanism and Fluid/Rock Interactions." *Energies* 10 (4):576.

Hamouda, Aly Anis, and Evgeny Maevskiy. 2014. "Oil recovery mechanism (s) by low salinity brines and their interaction with chalk." *Energy & Fuels* 28 (11):6860-6868.

Hamouda, Aly Anis, and Karam Ali Rezaei Gomari. 2006. "Influence of temperature on wettability alteration of carbonate reservoirs." SPE/DOE Symposium on Improved Oil Recovery.

Hamouda, Aly Anis, and Ole Martin Valderhaug. 2014. "Investigating enhanced oil recovery from sandstone by low-salinity water and fluid/rock interaction." *Energy & Fuels* 28 (2):898-908.

Haroun, Muhammad Raeef, Saeed Alhassan, Arsalan Arshad Ansari, Nabeela Abdul Munim Al Kindy, Nada Abou Sayed, Abdul Kareem, Basma Ali, and Hemanta Kumar Sarma. 2012. "Smart nano-EOR process for Abu Dhabi carbonate reservoirs." Abu Dhabi International Petroleum Conference and Exhibition.

Hendraningrat, Luky, Shidong Li, and Ole Torsæter. 2013. "A coreflood investigation of nanofluid enhanced oil recovery." *Journal of Petroleum Science and Engineering* 111:128-138. doi: 10.1016/j.petrol.2013.07.003.

Hendraningrat, Luky, Shidong Li, and Ole Torsater. 2013. "Effect of some parameters influencing enhanced oil recovery process using silica nanoparticles: An experimental investigation." SPE Reservoir Characterization and Simulation Conference and Exhibition.

Hendraningrat, Luky, and Ole Torsæter. 2015a. "Metal oxide-based nanoparticles: revealing their potential to enhance oil recovery in different wettability systems." *Applied Nanoscience* 5 (2):181-199.

Hendraningrat, Luky, and Ole Torsæter. 2015b. "A Stabilizer that Enhances the Oil Recovery Process Using Silica-Based Nanofluids." *Transport in Porous Media* 108 (3):679-696.

Hendraningrat, Luky, and Ole Torsæter. 2016. "A study of water chemistry extends the benefits of using silica-based nanoparticles on enhanced oil recovery." *Applied Nanoscience* 6 (1):83-95. doi: 10.1007/s13204-015-0411-0.

Hite, J. Roger, and Paul L. Bondor. 2004. "Planning EOR Projects." SPE International Petroleum Conference in Mexico, Puebla Pue., Mexico, 2004/1/1/.

Ho, Yuh-Shan, and Gordon McKay. 1999. "Pseudo-second order model for sorption processes." *Process biochemistry* 34 (5):451-465.

Hofmann, Ulrich, Kurd Endell, and Diederich Wilm. 1934. "Röntgenographische und kolloidchemische Untersuchungen über Ton." *Angewandte Chemie* 47 (30):539-547. doi: 10.1002/ange.19340473002.

Hosseini, Erfan, Farzad Hajivand, and Ali Yaghodous. 2018. "Experimental investigation of EOR using low-salinity water and nanoparticles in one of southern oil fields in Iran." *Energy Sources, Part A: Recovery, Utilization, and Environmental Effects* 40 (16):1974-1982.

Huang, T, J Han, G Agrawal, and PA Sookprasong. 2015. "Coupling nanoparticles with waterflooding to increase water sweep efficiency for high

fines-containing reservoir-lab and reservoir simulation results." SPE Annual Technical Conference and Exhibition.

Hwang, Yujin, Jae-Keun Lee, Jong-Ku Lee, Young-Man Jeong, Seong-ir Cheong, Young-Chull Ahn, and Soo H Kim. 2008. "Production and dispersion stability of nanoparticles in nanofluids." *Powder Technology* 186 (2):145-153.

Iler, Ralph K. 1979. "Chemistry of Silica--Solubility, Polymerization, Colloid and Surface Properties, and Biochemistry."

Israelachvili, Jacob N. 2011. *Intermolecular and surface forces*: Academic press.

Janusz, Władysław, Jacek Patkowski, and Stanisław Chibowski. 2003. "Competitive adsorption of Ca2+ and Zn(II) ions at monodispersed SiO2/electrolyte solution interface." *Journal of Colloid and Interface Science* 266 (2):259-268. doi: https://doi.org/10.1016/S0021-9797(03)00469-7.

Jolma, IW, D Strand, A Stavland, I Fjelde, and D Hatzignatiou. 2017. "When Size Matters-Polymer Injectivity in Chalk Matrix." IOR 2017-19th European Symposium on Improved Oil Recovery.

Joni, I Made, Agus Purwanto, Ferry Iskandar, and Kikuo Okuyama. 2009. "Dispersion stability enhancement of titania nanoparticles in organic solvent using a bead mill process." *Industrial & Engineering Chemistry Research* 48 (15):6916-6922.

Joonaki, E, and S Ghanaatian. 2014. "The application of nanofluids for enhanced oil recovery: effects on interfacial tension and coreflooding process." *Petroleum Science and Technology* 32 (21):2599-2607.

Ju, Binshan, Tailiang Fan, and Mingxue Ma. 2006. "Enhanced oil recovery by flooding with hydrophilic nanoparticles." *China Particuology* 4 (1):41-46.

Karoussi, Omid, and Aly A Hamouda. 2007. "Imbibition of sulfate and magnesium ions into carbonate rocks at elevated temperatures and their influence on wettability alteration and oil recovery." *Energy & fuels* 21 (4):2138-2146.

Khilar, Kartic C, and H Scott Fogler. 1984. "The existence of a critical salt concentration for particle release." *Journal of Colloid and Interface Science* 101 (1):214-224.

Khilar, Kartic C, and H Scott Fogler. 1998. *Migrations of fines in porous media*. Vol. 12: Springer Science & Business Media.

Kia, SF, HS Fogler, and MG Reed. 1987. "Effect of pH on colloidally induced fines migration." *Journal of colloid and interface science* 118 (1):158-168.

Kovalchuk, NM, and VM Starov. 2012. "Aggregation in colloidal suspensions: Effect of colloidal forces and hydrodynamic interactions." *Advances in Colloid and Interface Science* 179:99-106.

Kvitek, Libor, Aleš Panáček, Jana Soukupova, Milan Kolář, Renata Večeřová, Robert Prucek, Mirka Holecova, and Radek Zbořil. 2008. "Effect of surfactants and polymers on stability and antibacterial activity of silver nanoparticles (NPs)." *The Journal of Physical Chemistry C* 112 (15):5825-5834.

Lecoanet, Hélène F, Jean-Yves Bottero, and Mark R Wiesner. 2004. "Laboratory assessment of the mobility of nanomaterials in porous media." *Environmental science & technology* 38 (19):5164-5169.

Li, Shidong, Luky Hendraningrat, and Ole Torsaeter. 2013. "Improved oil recovery by hydrophilic silica nanoparticles suspension: 2 phase flow experimental studies." IPTC 2013: International Petroleum Technology Conference.

Li, Shidong, Anne Tinnen Kaasa, Luky Hendraningrat, and Ole Torsæter. 2013. "Effect of silica nanoparticles adsorption on the wettability index of Berea sandstone." Paper SCA2013-059 presented at the international symposium of the society of core analysts held in Napa Valley, California, USA.

Li, Shidong, and Ole Torsæter. 2015. "Experimental investigation of the influence of nanoparticles adsorption and transport on wettability alteration for oil wet Berea sandstone." SPE Middle East Oil & Gas Show and Conference.

Li, Yusong, Yonggang Wang, Kurt D Pennell, and Linda M Abriola. 2008. "Investigation of the transport and deposition of fullerene (C60) nanoparticles in quartz sands under varying flow conditions." *Environmental science & technology* 42 (19):7174-7180.

Liu, Jun, Peter Kopold, Peter A van Aken, Joachim Maier, and Yan Yu. 2015. "Energy Storage Materials from Nature through Nanotechnology: A Sustainable Route from Reed Plants to a Silicon Anode for Lithium-Ion Batteries." *Angewandte Chemie* 127 (33):9768-9772.

Liz-Marzán, Luis M, and Isabel Lado-Touriño. 1996. "Reduction and stabilization of silver nanoparticles in ethanol by nonionic surfactants." *Langmuir* 12 (15):3585-3589.

Lovell, C. Emma, Jason Scott, and Rose Amal. 2015. "Ni-SiO2 Catalysts for the Carbon Dioxide Reforming of Methane: Varying Support Properties by Flame Spray Pyrolysis." *Molecules* 20 (3). doi: 10.3390/molecules20034594.

Lu, Wei, and Charles M Lieber. 2010. "Nanoelectronics from the bottom up." In *Nanoscience And Technology: A Collection of Reviews from Nature Journals*, 137-146. World Scientific.

Lyon, D., and A. Hubler. 2013. "Gap size dependence of the dielectric strength in nano vacuum gaps." *IEEE Transactions on Dielectrics and Electrical Insulation* 20 (4):1467-1471. doi: 10.1109/TDEI.2013.6571470.

Maghzi, Ali, Saber Mohammadi, Mohammad Hossein Ghazanfari, Riyaz Kharrat, and Mohsen Masihi. 2012. "Monitoring wettability alteration by silica nanoparticles during water flooding to heavy oils in five-spot systems: A pore-level investigation." *Experimental Thermal and Fluid Science* 40:168-176.

Mahani, Hassan, Arsene Levy Keya, Steffen Berg, Willem-Bart Bartels, Ramez Nasralla, and William R Rossen. 2015. "Insights into the mechanism of wettability alteration by low-salinity flooding (LSF) in carbonates." *Energy & Fuels* 29 (3):1352-1367.

Merdhah, ABB, and A Yassin. 2009. "Scale formation due to water injection in Berea sandstone cores." *J. Appl. Sci* 9 (18):3298-3307.

Metin, Cigdem O, Jimmie R Baran, and Quoc P Nguyen. 2012. "Adsorption of surface functionalized silica nanoparticles onto mineral surfaces and decane/water interface." *Journal of Nanoparticle Research* 14 (11):1246.

Metin, Cigdem O., Larry W. Lake, Caetano R. Miranda, and Quoc P. Nguyen. 2011. "Stability of aqueous silica nanoparticle dispersions." *Journal of Nanoparticle Research* 13 (2):839-850. doi: 10.1007/s11051-010-0085-1.

Mondragon, Rosa, J Enrique Julia, Antonio Barba, and Juan Carlos Jarque. 2012. "Characterization of silica–water nanofluids dispersed with an ultrasound

probe: a study of their physical properties and stability." *Powder technology* 224:138-146.

Monfared, A Dehghan, MH Ghazanfari, M Jamialahmadi, and A Helalizadeh. 2015. "Adsorption of silica nanoparticles onto calcite: Equilibrium, kinetic, thermodynamic and DLVO analysis." *Chemical Engineering Journal* 281:334-344.

Morrow, Norman, and Jill Buckley. 2011. "Improved oil recovery by low-salinity waterflooding." *Journal of Petroleum Technology* 63 (05):106-112.

Nazari Moghaddam, Rasoul, Alireza Bahramian, Zahra Fakhroueian, Ali Karimi, and Sharareh Arya. 2015. "Comparative study of using nanoparticles for enhanced oil recovery: wettability alteration of carbonate rocks." *Energy & Fuels* 29 (4):2111-2119.

Nwidee, Lezorgia N., Sarmad Al-Anssari, Ahmed Barifcani, Mohammad Sarmadivaleh, Maxim Lebedev, and Stefan Iglauer. 2017. "Nanoparticles influence on wetting behaviour of fractured limestone formation." *Journal of Petroleum Science and Engineering* 149:782-788. doi: https://doi.org/10.1016/j.petrol.2016.11.017.

Ogolo, NA, OA Olafuyi, and MO Onyekonwu. 2012. "Enhanced oil recovery using nanoparticles." SPE Saudi Arabia Section Technical Symposium and Exhibition.

Oh, Young-Kwon, Lan-Young Hong, Yamini Asthana, and Dong-Pyo Kim. 2006. "Synthesis of super-hydrophilic mesoporous silica via a sulfonation route." *Journal of Industrial and Engineering Chemistry* 12 (6):911-917.

Ortega, Daniel J Sivira, Han Byal Kim, Lesley A James, Thormod E Johansen, and Yahui Zhang. 2016. "The Effectiveness of Silicon Dioxide SiO 2 Nanoparticle as an Enhanced Oil Recovery Agent in Ben Nevis Formation, Hebron Field, Offshore Eastern Canada." Abu Dhabi International Petroleum Exhibition & Conference.

Petrovich, R, and AA Hamouda. 1998. "Dolomitization of Ekofisk oil field reservoir chalk by injected seawater." Ninth International Symposium on Water–Rock Interactions, Taupo, New Zealand, March 30th–April 3rd.

Rezaei Gomari, Sina, and Nikhil Joseph. 2017. "Study of the Effect of Clay Particles on Low Salinity Water Injection in Sandstone Reservoirs." *Energies* 10 (3):322.

RezaeiDoust, A, T Puntervold, S Strand, and T Austad. 2009. "Smart water as wettability modifier in carbonate and sandstone: A discussion of similarities/differences in the chemical mechanisms." *Energy & fuels* 23 (9):4479-4485.

Rosenbrand, Esther, Claus Kjøller, Jacob Fabricius Riis, Frans Kets, and Ida Lykke Fabricius. 2015. "Different effects of temperature and salinity on permeability reduction by fines migration in Berea sandstone." *Geothermics* 53:225-235.

Roustaei, Abbas, and Hadi Bagherzadeh. 2015. "Experimental investigation of SiO2 nanoparticles on enhanced oil recovery of carbonate reservoirs." *Journal of Petroleum Exploration and Production Technology* 5 (1):27-33. doi: 10.1007/s13202-014-0120-3.

Schembre, JM, G-Q Tang, and AR Kovscek. 2006. "Wettability alteration and oil recovery by water imbibition at elevated temperatures." *Journal of Petroleum Science and Engineering* 52 (1-4):131-148.

Seetha, N, S Majid Hassanizadeh, Mohan Kumar, and Amir Raoof. 2015. "Correlation equations for average deposition rate coefficients of nanoparticles in a cylindrical pore." *Water Resources Research* 51 (10):8034-8059.

Shahrabadi, Abbas, Hadi Bagherzadeh, Abbas Roostaie, and Hassan Golghanddashti. 2012. "Experimental investigation of HLP nanofluid potential to enhance oil recovery: A mechanistic approach." SPE International Oilfield Nanotechnology Conference and Exhibition.

Sharma, Tushar, Stefan Iglauer, and Jitendra S Sangwai. 2016. "Silica nanofluids in an oilfield polymer polyacrylamide: interfacial properties, wettability alteration, and applications for chemical enhanced oil recovery." *Industrial & Engineering Chemistry Research* 55 (48):12387-12397.

Sharma, Tushar, G Suresh Kumar, Bo Hyun Chon, and Jitendra S Sangwai. 2015. "Thermal stability of oil-in-water Pickering emulsion in the presence of nanoparticle, surfactant, and polymer." *Journal of Industrial and Engineering Chemistry* 22:324-334.

Sharma, Tushar, G Suresh Kumar, and Jitendra S Sangwai. 2015. "Comparative effectiveness of production performance of Pickering emulsion stabilized by nanoparticle–surfactant–polymerover surfactant–polymer (SP) flooding for enhanced oil recoveryfor Brownfield reservoir." *Journal of Petroleum Science and Engineering* 129:221-232.

Sheshdeh, Milad Jokari. 2015. "A Review Study of Wettability Alteration Methods with Regard to Nano-Materials Application." SPE Bergen One Day Seminar.

Singh, Robin, and Kishore K Mohanty. 2015. "Synergy between nanoparticles and surfactants in stabilizing foams for oil recovery." *Energy & Fuels* 29 (2):467-479.

Stumm, Werner, and James J Morgan. 1970. *Aquatic chemistry; an introduction emphasizing chemical equilibria in natural waters*.

Suleimanov, BA, FS Ismailov, and EF Veliyev. 2011. "Nanofluid for enhanced oil recovery." *Journal of Petroleum Science and Engineering* 78 (2):431-437.

Tang, Erjun, Guoxiang Cheng, Xiaolu Ma, Xingshou Pang, and Qiang Zhao. 2006. "Surface modification of zinc oxide nanoparticle by PMAA and its dispersion in aqueous system." *Applied Surface Science* 252 (14):5227-5232.

Tang, GQ, and Norman R Morrow. 1997. "Salinity, temperature, oil composition, and oil recovery by waterflooding." *SPE Reservoir Engineering* 12 (04):269-276.

Tang, Guo-Qing, and Norman R Morrow. 1999. "Influence of brine composition and fines migration on crude oil/brine/rock interactions and oil recovery." *Journal of Petroleum Science and Engineering* 24 (2):99-111.

Temple, SE 2007. "Effect of salinity on the refractive index of water: considerations for archer fish aerial vision." *Journal of Fish Biology* 70 (5):1626-1629.

Torsater, Ole, Shidong Li, and Luky Hendraningrat. 2013. "A coreflood investigation of nanofluid enhanced oil recovery in low-medium permeability Berea sandstone." SPE International Symposium on Oilfield Chemistry.

van Oort, Eric, JFG Van Velzen, and Klaas Leerlooijer. 1993. "Impairment by suspended solids invasion: testing and prediction." *SPE Production & Facilities* 8 (03):178-184.

Walcarius, Alain, and Louis Mercier. 2010. "Mesoporous organosilica adsorbents: nanoengineered materials for removal of organic and inorganic pollutants." *Journal of Materials Chemistry* 20 (22):4478-4511.

Wang, Wendong, Bin Yuan, Yuliang Su, Kai Wang, Miaolun Jiang, Rouzbeh Ghanbarnezhad Moghanloo, and Zhenhua Rui. 2016. "Nanoparticles Adsorption, Straining and Detachment Behavior and its Effects on Permeability of Berea Cores: Analytical Model and Lab Experiments." SPE Annual Technical Conference and Exhibition, UAE.

Wang, Xiuyu, and Vladimir Alvarado. 2011. "Kaolinite and Silica Dispersions in Low-Salinity Environments: Impact on a Water-in-Crude Oil Emulsion Stability." *Energies* 4 (10):1763.

Wasan, Darsh T, and Alex D Nikolov. 2003. "Spreading of nanofluids on solids." *Nature* 423 (6936):156.

Weber, W. J., and J. C. S. Morris. 1962. "Advances in water pollution research: removal of biologically-resistant polluants from waste waters by adsorption." *Advances in Water Pollution Research: Proceedings of the International Conference*:231-266.

Weston, J. S., R. E. Jentoft, B. P. Grady, D. E. Resasco, and J. H. Harwell. 2015. "Silica Nanoparticle Wettability: Characterization and Effects on the Emulsion Properties." *Industrial & Engineering Chemistry Research* 54 (16):4274-4284. doi: 10.1021/ie504311p.

Wu, Feng-Chin, Ru-Ling Tseng, and Ruey-Shin Juang. 2009. "Initial behavior of intraparticle diffusion model used in the description of adsorption kinetics." *Chemical Engineering Journal* 153 (1-3):1-8.

Xu, Ke, Peixi Zhu, Tatiana Colon, Chun Huh, and Matthew Balhoff. 2017. "A Microfluidic Investigation of the Synergistic Effect of Nanoparticles and Surfactants in Macro-Emulsion-Based Enhanced Oil Recovery." *SPE Journal* 22 (02):459-469.

Yang, Xuefei, and Zhen-hua Liu. 2010. "A kind of nanofluid consisting of surface-functionalized nanoparticles." *Nanoscale research letters* 5 (8):1324.

Yao, Kuan-Mu, Mohammad T Habibian, and Charles R O'Melia. 1971. "Water and waste water filtration. Concepts and applications." *Environmental Science & Technology* 5 (11):1105-1112.

Yi, Zhang, and Hemanta Kumar Sarma. 2012. "Improving Waterflood Recovery Efficiency in Carbonate Reservoirs through Salinity Variations and Ionic Exchanges: A Promising Low-Cost "Smart-Waterflood" Approach." Abu Dhabi International Petroleum Conference and Exhibition, Abu Dhabi, UAE, 2012/1/1/.

Yu, Jianjia, Cheng An, Di Mo, Ning Liu, and Robert L Lee. 2012. "Study of adsorption and transportation behavior of nanoparticles in three different porous media." SPE improved oil recovery symposium.

Yuan, Bin. 2017. "Modeling Nanofluid Utilization to Control Fines Migration."

Yuan, Bin, Rouzbeh Ghanbarnezhad Moghanloo, and Da Zheng. 2016. "Analytical evaluation of nanoparticle application to mitigate fines migration in porous media." *SPE Journal* 21 (06):2,317-2,332.

Yuan, Hao, and Alexander A. Shapiro. 2011. "Induced migration of fines during waterflooding in communicating layer-cake reservoirs." *Journal of Petroleum Science and Engineering* 78 (3–4):618-626. doi: http://dx.doi.org/10.1016/j.petrol.2011.08.003.

Zahid, Adeel, Alexander A Shapiro, and Arne Skauge. 2012. "Experimental studies of low salinity water flooding carbonate: A new promising approach." SPE EOR Conference at Oil and Gas West Asia.

Zeinijahromi, A, V Ahmetgareev, and P Bedrikovetsky. 2015. "Case Study of 25 Years of Low Salinity Water Injection." SPE/IATMI Asia Pacific Oil & Gas Conference and Exhibition.

Zhang, Hua, Alex Nikolov, and Darsh Wasan. 2014. "Enhanced oil recovery (EOR) using nanoparticle dispersions: underlying mechanism and imbibition experiments." *Energy & Fuels* 28 (5):3002-3009.

Zhang, Hua, TS Ramakrishnan, Alex Nikolov, and Darsh Wasan. 2016. "Enhanced oil recovery driven by nanofilm structural disjoining pressure: flooding experiments and microvisualization." *Energy & Fuels* 30 (4):2771-2779.

Zhang, Tiantian, Michael J Murphy, Haiyang Yu, Hitesh G Bagaria, Ki Youl Yoon, Bethany M Nielson, Christopher W Bielawski, Keith P Johnston, Chun

Huh, and Steven L Bryant. 2015. "Investigation of nanoparticle adsorption during transport in porous media." *SPE Journal* 20 (04):667-677.

Zhang, Tiantian, Michael Murphy, Haiyang Yu, Chun Huh, and Steven L Bryant. 2016. "Mechanistic model for nanoparticle retention in porous media." *Transport in Porous Media* 115 (2):387-406.

**Effect of Various Silica Nanofluids: Reduction of Fines Migrations and Surface Modification of Berea Sandstone**.

Abhishek, R**.** and A. A. Hamouda (2017).

Applied Sciences 7(12): 1216. Special issue: Nanotech for Oil and Gas, MDPI Publication.

Paper I

applied sciences

MDPI

Article

# Effect of Various Silica Nanofluids: Reduction of Fines Migrations and Surface Modification of Berea Sandstone

**Rockey Abhishek and Aly A. Hamouda ***

Institute of Petroleum Technology, University of Stavanger, 4036 Stavanger, Norway; rockey.abhishek@uis.no
* Correspondence: aly.hamouda@uis.no; Tel.: +47-9570-2604

Received: 7 November 2017; Accepted: 21 November 2017; Published: 24 November 2017

**Abstract:** This work is aimed at addressing surface modification of berea sandstone by silica nanofluids (NFs). Three types of nanofluids were used: silica/deionized water (DIW), silica in DIW with a stabilizer fluid (3-Mercaptopropyl Trimethoxysilane) and sulfonate-functionalized silica in DIW. Core flood studies showed that application of silica nanoparticles (NPs) improved water injectivity in sandstone. The change in the measured zeta potential indicated surface modification of sandstone by application of NPs. Computation of the surface forces showed that the modified berea sandstone has net attractive potential with fines (obtained from water/rock interaction) leading to reduction of fines migration, hence improvement of water injectivity. It was also observed that the silica NPs have greater affinity to adhere/adsorb on quartz surfaces than kaolinite in berea core. This was confirmed by scanning electron microscope imaging and isothermal static adsorption tests. Although the stabilizing of NFs almost did not reduce the fine migration, as was qualitatively indicated by the pressure drop, it enhanced the NPs adsorption on the minerals as obtained by isothermal static adsorption tests. The reduction of fines migration due surface modification by silica NP suggests that NPs can be utilized to overcome the problem of formation damage induced during low salinity flooding in sandstones.

**Keywords:** silica nanoparticle; nanofluid stabilization; surface modification; adsorption; fines migration; berea sandstone; low salinity

## 1. Introduction

With the rising demand for energy and fast approaching end of the era of easy oil, the petroleum industry today faces unique challenges especially in the Enhanced Oil Recovery (EOR) area. Over the past decade, many of researches have focused on application of nanoparticles (NP) as an EOR method. The small size and high specific surface area of NP offer unique advantages like allowing them to easily pass through pore throats and enhanced interaction in the reservoir even with a small quantity of NP. NPs have displayed the potential to act as surface modifiers that could alter the wettability and reduce the oil/water interfacial tension leading to better mobility of the oil phase [1–7] and reduce fines migration [8,9]. Recent laboratory studies have indicated that nanofluids, which are colloidal dispersions of NP in a dispersing medium have the potential to increase oil recovery [2,7,10–13]. Over the past decade, special focus has been directed to silica NPs for EOR due to its hydrophilic nature and ease of functionalization.

Hofmann et al. [14] postulated the presence of silanol groups (Si–OH) on the silica surface that causes its hydrophilicity, wherein silanol groups act as binding sites ($H^+$ bonds) for water. The protonation and deprotonation of these silanol groups determine the surface charge of silica NP and the extent of the repulsive energy that keep them dispersed in the solution [15]. For two-phase systems like nanofluids, one of the most important issue is their colloidal stability i.e., no or low rate

of agglomeration of the NP. Stability of NP is essential for injection application as EOR agents in oil reservoirs. Agglomeration can lead to blockage of micro channels, formation damage, hinder the transport of NP and the displacing fluid in the reservoir. The main strategies utilized to enhance the stability of nanofluids are: (a) electrostatic stabilization [16] (by varying pH of the nanofluids); (b) employing stabilizing fluid/surfactant [17]; (c) surface modification [18,19] (functionalization) of the NP. Electrostatic stabilization (for example by varying the pH) is expected to fail in the presence of dissolved salts in brines. Electrolytes could destabilize particle dispersions by compressing the electrical double layer. As the electrolyte concentration increases, the energy barrier is lowered to an extent that kinetic energy of particles dictates the kinetics of particle aggregation [15]. For a given surface charge, the aggregation of silica NP occurs because of the presence of electrolytes. Metin, Lake, Miranda and Nguyen [15] studied the effect of pH, cation type, temperature and electrolyte concentration on the stability of silica dispersions. They found that pH does not have a significant effect on stability in the presence of electrolytes. Although addition of stabilizing fluid can be an effective way to enhance the dispersion of NP, it might cause several problems like foaming and stabilizing fluid adsorption in porous media leading to loss of the intended stabilization. Surface modification of NPs (functionalized NP) is a promising approach towards increasing the stability of NPs. Yang and Liu [18] presented a work on the synthesis of functionalized silica ($SiO_2$) NP by grafting silanes directly to the surface of silica NP which showed good stability. Weston, Jentoft, Grady, Resasco and Harwell [19] systematically performed surface modification of silica with different silanes and studied the wettability of the modified nanomaterials. However, it is essential to examine the effect these stabilization strategies have on the effectiveness of the nanofluids.

For stable nanofluids, which can be utilized as EOR agents, an important factor is the interaction of the NPs with the rock minerals over a wide area of the reservoir. When NPs are introduced into porous medium, different processes may take place such as adsorption, desorption, blocking, transportation and aggregation [4]. The adsorption phenomenon could be reversible (desorption) during the transport of NP in the porous medium [20]. Blocking of pore throats may occur if the NPs aggregate in situ so that their size exceeds the pore throat [21]. The transportation of the NP through the porous medium is governed by advection-diffusion and hydrodynamics once equilibrium adsorption and desorption has been achieved.

This work is aimed at studying the surface modification of berea sandstone by the adsorption/adhesion of silica NPs. Arab and Pourafshary [8] and Arab, Pourafshary, Ayatollahi and Habibi [9] studied the surface modification of sandstone by NPs to reduce fines migration and colloid facilitated transport in porous medium modified by NPs. However, affinity of NPs towards major minerals present in sandstone, adsorption/adhesion of NPs in the porous medium and the influence of nanofluid stabilization on the in-situ surface modification has been addressed in this study. Three types of nanofluids containing silica, silica with a stabilizer (3-Mercaptopropyl Trimethoxysilane) and sulfonate-functionalized silica in deionized water (DIW) were investigated. Thus two stabilization methods: the use of stabilizing fluid and NP functionalization have been investigated. The dynamic adsorption/desorption of the NP was addressed by continuous monitoring of the pressure drop and analysing the effluents produced during injection of DIW into nanofluid modified berea, for produced NP and the stabilizing fluid concentration were determined. It was found that application of silica NP could improve water injectivity in the porous medium by reducing fine migration. Zeta potential measurements indicated surface modification of sandstone by application of silica NPs. Calculated surface forces showed that modified berea has net attractive potential with fines leading to reduction of fines migration, hence improvement of water injectivity. It was also observed that silica NP tend to preferentially adsorb/adhere on quartz as compared to kaolinite.

## 2. Materials and Methods

The silicon dioxide NP (637246 Aldrich) used in this study were acquired from Sigma Aldrich, Drammensveien, Oslo, Norway. As reported by manufacturer, the Silica NP had a primary particle

size of 10–15 nm (spherical). The NP were dispersed in DIW and DIW containing 3-Mercaptopropyl Trimethoxysilane (MPTMS) as stabilizing fluid. MPTMS (175617 Aldrich) was also acquired from Sigma Aldrich. Berea sandstone (outcrops) cores used in this work were acquired from Koucurek Industries Inc., Caldwell, TX, USA. The properties and mineral composition of the used cores are listed in Table 1. Quartz (00653 Sigma-Aldrich) and kaolinite (03584 Sigma-Aldrich) mineral powders were acquired from Sigma Aldrich with chemical compositions: $SiO_2$ and $Al_2O_3 \cdot 2SiO_2 \cdot 2H_2O$, respectively. The specific surface area of the mineral powders are 0.62 $m^2/g$ and 8.56 $m^2/g$, respectively [22] previously determined by nitrogen adsorption.

The nanofluid preparation was done using ultrasonic processor: UP400S (400 watts, 24 kHz) by Hielscher Ultrasonics. A TurbiScan Lab instrument by Formulaction Inc. (Worthington, OH, USA) was used to determine the stability and concertation of silica nanofluids. A dual beam UV/Vis spectrophotometer: UV 1700 PharmaSpec by Shimadzhu Corporation (Nakagyo-ku, Kyoto, Japan) was used to determine the concentration of the stabilizing fluids in the effluents. The particle size and zeta potentials of the NP in the prepared nanofluids were measured using a Zetasizer Nano ZSP from Malvern Instruments (Malvern, Worcestershire, UK). The zeta potential of the mineral powders was measured using an Acosustisizer II S/M Flow-through System by Colloidal Dynamics. Scanning Electron Microscope (SEM) imaging of the barea cores saturated with the nanofluids was performed on a SUPRA 35 VP instrument by Zeiss with an integrated energy-dispersive X-ray spectroscopy (EDX) analyzer by EDAX. Core flood studies were conducted to study the adsorption and transport of NP in the porous medium. A schematic of the core flood apparatus is shown in Figure 1. The setup consists of a core holder connected to a piston cylinder filled with injection fluid. The prepared core was wrapped in a plastic sleeve. The wrapped core with the plastic sleeve was inserted in a cylindrical rubber sleeve and loaded into the core holder. As shown in Figure 1, another pump and cylinder filled with confining oil (Tellus S2 V 32) was used for applying confining pressure. The outlet valve of the core was connected to automated liquid handler (GX-271 by Gilson Inc. Middleton, WI, USA) to collect the effluent at regular intervals. Pressure gauges are connected at the inlet and outlet valve to record the differential pressure drop across the core. The experimental methods used in in this study are explained in detail in the following sections.

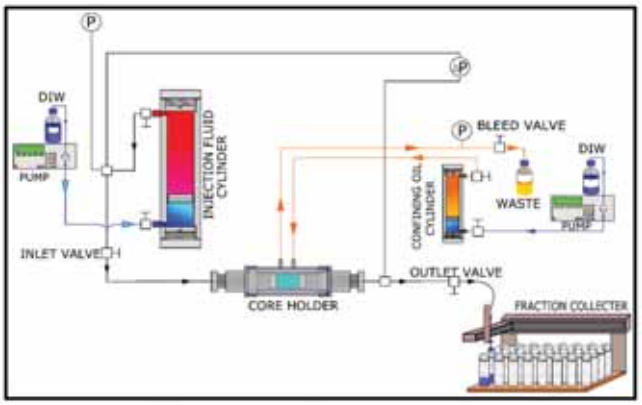


**Figure 1.** Schematic of the core flood setup. DIW: Deionized water; P: Pressure.

**Table 1.** Properties and mineral composition of used Berea sandstone.

| Core Properties | | Mineral Composition of Berea | |
|---|---|---|---|
| **Type** | **Berea Sandstone** | **Mineral Name** | **Semi-Quantitative (%)** |
| Length | 8.95 ± 0.08 cm | Quartz | 94 |
| Diameter | 3.78 cm | Kaolinite | 1 |
| Porosity | 20.05 ± 0.76% | Muscovite | 1 |
| Permeability | 200–220 mD | Microline | 1 |

### 2.1. Nanofluid Preparation

The NP were dispersed in deionized water (DIW) at a predetermined concentration using a magnetic stirrer at 500 rpm for 30 min. To loosen the agglomerates in the nanopowder and disperse it, probe sonication was applied using an ultrasonic processor. Sonication was performed for 120 min (50% amplitude and 0.5 pulse) with breaks every 15 min to avoid overheating. Mondragon et al. [23] observed that silica nanofluids prepared by dispersing the NP in DIW using an ultrasonic probe proved to be the most effective technique. Three types of nanofluids were prepared at varying concentrations of NP:

1. Silica dispersed in DIW.
2. Sulfonated silica dispersed in DIW (functionalized).
3. Silica dispersed in DIW with MPTMS stabilizing fluid.

Two types of NP were used in this study: firstly, silica acquired from Sigma-Aldrich and surface modified NP. The modification procedure is described in the following section. The nanofluids of silica in DIW with MPTMS stabilizing fluid were prepared by dispersing the desired concentration of silica in DIW via ultrasonication. Thereafter, 1 g of MPTMS was added per 100 mL of the nanofluid under vigorous stirring. To avoid confusion in this text between NP and MPTMS concentration, NP concentration is always stated in g/L units and MPTMS concertation is always stated in g/100 mL units.

### 2.2. NP Functionalization

The aim of functionalization of silica was to increase the hydrophilicity and stability of the silica NPs. The grafting of silanes on NP leads to steric stabilization. The surface modification was performed based on the method described by Weston, Jentoft, Grady, Resasco and Harwell [19]. 10 g of silica NP was dispersed in 100 mL toluene by probe sonication. 5 g of MPTMS was added to the dispersed silica in toluene. The solution was stirred for 12 h at 35 °C. Particles were removed from the dispersion by centrifugation (7000 rpm for 10 min). Thereafter, the particles were washed 5 times with isopropyl alcohol, after each time, the fluids were centrifuged to separate the particles. The wash with isopropyl alcohol was done to remove excess silane/toluene and followed by washing twice with 70/30 ($v/v$) mixture of isopropyl alcohol and DIW. The NP were dried in a vacuum oven at 120 °C for 24 h. Thereafter, the thiol groups of MPTMS were oxidized based on the technique described by Oh et al. [24]: the dried NP were dispersed in a solution of 30% $H_2O_2$ and stirred at room temperature for 24 h. This results in the formation of sulfonic acid groups on the silica surface. The particles were then washed several times with water and dried. The sulfonic acid groups were converted into sodium sulfonate by dispersing the particles in 0.1 M solution of NaOH under continuous stirring for 24 h. The particles were washed and dried in a vacuum oven for 3 days at 35 °C. These surface modified NP are referred to as sulfonated NP.

### 2.3. Particle Size and Zeta Potential Measurement

The particle size and zeta potentials of the NP in the prepared nanofluids were measured using a Zetasizer Nano ZSP instrument based on the principle of Dynamic Light Scattering (DLS). The zeta

potential of the mineral powders was determined by an Acosustisizer II S/M Flow-through System based on the principle of Electrostatic Attenuation (ESA). The measurement are listed in Table 2.

**Table 2.** Particle Size and Zeta potential measurements. DIW: Deionized water; MPTMS 3-Mercaptopropyl Trimethoxysilane; NA: Not Applicable; DLS: Dynamic Light Scattering; ESA: Electrostatic Attenuation.

| Material | Conc (g/L) | Dispersing Phase | Zeta Potential (mV) | Particle Radius (nm) | Method |
|---|---|---|---|---|---|
| Silica | 1 | DIW | −51.45 | 161.2 | DLS |
| Sulfonated Silica | 1 | DIW | −44.8 | 182.9 | DLS |
| Silica | 1 | DIW + 1 g/100 mL MPTMS | −47.75 | 153.3 | DLS |
| Powdered Berea | 10 | DIW | −29.53 | NA | ESA |
| Quartz powder | 10 | DIW | −5.732 | NA | ESA |
| Kaolinite powder | 10 | DIW | −9.097 | NA | ESA |

### *2.4. Introduction of Silica Nanofluids to the Porous Medium*

Silica nanofluid was introduced into the berea sandstone core under vacuum with 1 pore volume of nanofluid (nanofluid slug), followed by injection of DIW to address the effects of NPs assisted surface modification. The produced effluents were analyzed and the differential pressure drop was recorded. The list of injection experiments conducted is shown in Table 3.

**Table 3.** List of injection experiments performed in this study.

| Experiment No. | NP Conc. (g/L) | Type of NP | Dispersing Phase | Comments |
|---|---|---|---|---|
| 1 | 1 | Silica | DIW | |
| 2 | 2.5 | Silica | DIW | |
| 3 | 1 | Silica | DIW | Performed at varying injection rates |
| 4 | 1 | Silica | DIW + MPTMS (1 g/100 mL) | |
| 5 | 2.5 | Silica | DIW + MPTMS (1 g/100 mL) | |
| 6 | 4 | Silica | DIW + MPTMS (1 g/100 mL) | |
| 7 | 1 | Silica | DIW + MPTMS (1 g/100 mL) | Repeated Experiment 4 |
| 8 | 2.5 | Silica | DIW + MPTMS (1 g/100 mL) | Repeated Experiment 5 |
| 9 | 1 | Sulfonated | DIW | |

The core was dried in a vacuum oven at 100° for 24 h until its weight stabilizes. The dry weight, length and diameter was noted. The core was vacuum saturated with DIW and the pore volume (PV) of the core was calculated based on the saturated weight of the core. The core was loaded in a core holder and confining pressure of 25 bar was applied. DIW was injected at 0.3 mL/min (≈20 PV/day). Injection was performed at atmospheric pressure (no back pressure). Differential pressure drop across the core (dP) was recorded using Labview 7.1. Upon stabilization of dP, the core was removed from the holder and dried in a vacuum oven at 100 °C until the weight of the core becomes equal to dry core weight previously measured. Thereafter, the core was treated (vacuum saturated) with 1 PV of a particular nanofluid depending on the experiment and loaded in the core holder with the same inlet-outlet orientation as before. Post flush was performed by injecting DIW at 0.3 mL/min (≈20 PV/day). Produced effluent samples were collected and analyzed. In this part of the study, the effect of surface modification by the different nanofluids was analyzed. Also, the adsorption of NP and determination of possible absorption of the stabilizing fluid (MPTMS) in the berea sandstone cores was studied. The experiments are listed in Table 3. Two experiments performed with nanofluids containing MPTMS (Experiment 4 and 5 in Table 3) have been performed again (Experiment 7 and 8 in Table 3) to determine the repeatability of the results.

### *2.5. Nanofluid Stability and Determination of NP Concentration*

The suspended NP in fluid have the tendency to aggregate due to the large surface area to volume ratio leading to high surface energy, hence they tend to aggregate to minimize the surface energy.

The stability of the nanofluids was investigated. Measurement of transmissivity of nanofluids at different points (along the vertical height) in a sample is a method that addresses the uniformity of dispersion of the NP in the fluid. The used instrument was TurbiScan Lab by Formulaction Inc. The instrument measures, among other things, the % transmissivity with predetermined scanning time and duration. Uniform dispersion of the NP in a fluid, is indicated by stable transmissivity along the vertical length. The results for the prepared nanofluid showed that it was stable and uniformly dispersed for up to 24 h. In general, from this work it was found that the tested nanofluids were stable for about 24 h beyond which the settlement of particles could be visually observed. The nanofluid with sulfonated silica NP was the most stable. This nanofluid was stable for about one week. All the experiments were performed within 10 h to ensure that the experiments were within the stability period.

The effluent was analyzed for the concentrations of the NP and the stabilizing fluid. Transmissivity calibration curve (Figure 2) was constructed by dispersing NP in a corresponding fluid. In this case was done with deionized water (DIW) with different concentrations of NP. For example, the transmissivity measurement of the 1 g/L dispersion of bare silica in DIW was performed along the turbiscan tubes with sample height of 35 mm. The maximum transmissivity measured was 35.67%, the minimum was 34.87% and the mean transmissivity was 35.14%. This indicates that the prepared nanofluid prepared was uniformly dispersed. Further, the nanofluid was diluted to 0.5 g/L and 0.33 g/L NP concentration and the samples were placed in an ultrasonic bath for 1 h after which the transmissivity was measured. These measurements along with the transmissivity of DIW (no NP) was used to make the calibration curve shown in Figure 2. The calibration curve was used to determine the concentration of NP in effluent samples. For each nanofluid prepared for particular experiment, a calibration curve was constructed following the above process. The transmissivity of the effluent samples is measured and compared against the calibration curve to determine the concentration of the NP in the effluent. The total amount of NP adsorbed/retained in the core was calculated via mass balance of the amount of NP introduced (calculated from the pore volume of the core and the concentration of the nanofluid introduced in the core) into the porous medium and the amount of NP produced determined from the concentration and the volume of the effluents.

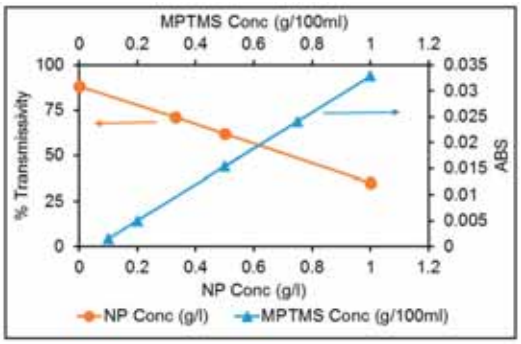


**Figure 2.** Calibration curves for detecting nanoparticle (NP) concentration and 3-Mercaptopropyl Trimethoxysilane (MPTMS) concentration. ABS: Absorption.

### *2.6. Determination of MPTMS Concentration in Effluent*

As mentioned earlier the NP in the nanofluid tend to aggregate, which may lead to resisting the flow. Two strategies were employed to prevent/minimize the agglomeration of NP. Firstly, functionalization or surface modification of the NP. The second is by using a stabilizing fluid that keeps the NP suspended. Hendraningrat and Torsæter [11] employed Polyvinylpyrrolidone (PVP) at 1% weight concentration in the nanofluid as a stabilizer for silica based nanofluids. However,

an important question that arises is the adsorption of the stabilizing fluid on the mineral during the injection that may take place. This changes the ratio between the fluid and NP, which may induce agglomeration of NP during the injection. In this study a method was developed to determine the adsorption of the stabilizing fluid in the rock during the injection. The method was based on mass balance calculation, where the effluent was analyzed by Ultraviolet light (UV). The used wavelength was 300 nm that gives adequate linear relationship between the absorption and concentration of MPTMS (stabilizing fluid). The constructed calibration curve was then used to estimate the loss in the mass balance i.e., related to the adsorbed MPTMS in the core. For each nanofluid containing MPTMS, calibration curve was constructed prior to the injection experiment by measuring the absorption in a dual beam UV/VIS spectrometer at wavelength 300 nm. Absorption of the MPTMS was measured referenced to DIW (with pH adjusted to 2 by dropwise addition of 0.1 M HCl). The removal of the NP from the effluent fluid was achieved by adjusting the pH of the effluent fluid to about 2, then centrifuging the fluid for 60 min at 10,000 rpm to promote the settling of NP. The absorption of the supernatant was determined. As an example, the UV/VIS calibration curve for 1 g/L nanofluid with 1 g/100 mL MPTMS is presented in Figure 3. In summary, after measuring the NPs concentration in the effluent samples through transmissivity measurements, the pH of the samples was then adjusted to 2 by dropwise addition of 0.1 M HCl followed by centrifuging for 60 min at 10,000 rpm. The absorption of supernatant was measured relative to a reference of DIW (pH adjusted to about 2) in the double beam UV/VIS spectrometer.

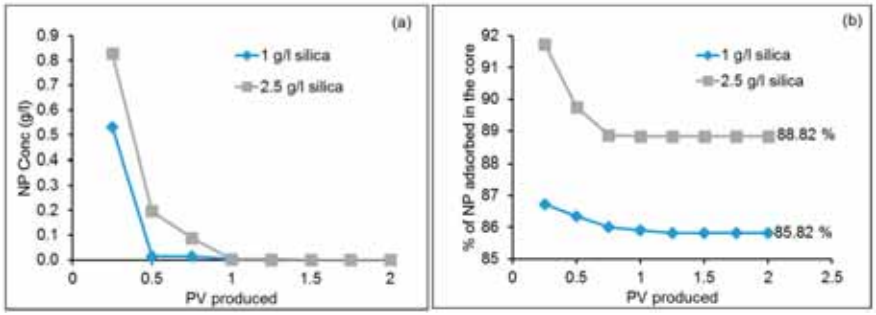


**Figure 3.** (**a**) Effluent NP concentration profiles; (**b**) % adsorbed NP during post flush. PV: Pore Volume.

### 2.7. Isothermal Static Adsorption Experiments

Berea sandstone cores are composed mostly of quartz and kaolinite. Adsorption tests were run on samples of 0.15 g of the individual minerals separately. The mineral powder were dispersed in 30 mL of nanofluid (1 g/L in DIW), the mass ratio between the minerals and the NP was kept constant at 5:1 mineral/NP. The minerals were dispersed in the three types of nanofluids. The samples were agitated in a rotator agitator for 24 h at room temperature. Thereafter the samples were centrifuged at low speed (1000 rpm) for 10 min to promote the settling of mineral powders. The liquid was decanted and further centrifuged for 10 min. The transmissivity of the supernatant was measured. To establish base line, samples containing minerals only were prepared in similar manner and their transmissivity were measured. The baseline corrected transmissivity was used to determine the concentration of NP in the supernatant liquid. The adsorbed NP were calculated from the change in concentration, and the volume of the fluid. Based on the specific surface area of the mineral powders, the amount of NP (mg) adsorbed per unit surface area of the mineral powders was determined.

### 2.8. Surface Forces

The theory of surface forces has been utilized to characterize the inter-surface interaction between NP-mineral and fine-mineral based on the Derjaguin-Landau-Verwey-Overbeek (DLVO) theory. It describes the forces between charged surfaces interacting in a medium. The DLVO theory combines the effect of attraction due to van der Waals interaction and the electrostatic repulsion due to the double layer of counter ions around charged surfaces in a medium. Silica NP and fines have sizes in the order of 100–500 nm and 0.1–5 μm respectively. These are much smaller than the size the pore throats of the porous medium. Due to this size difference, the curvature of the mineral surfaces may be neglected and the interactions can be modelled as Sphere-Plate collector geometry [8,20,25–27]. The forces acting on a particle approaching a mineral surface are the sum of van der Waals attraction, electric double layer repulsion and Born repulsion.

$$V_t(h) = V_{LVA}(h) + V_{EDLR}(h) + V_{BR}(h) \tag{1}$$

where $V$ is the potential of interaction as a function of separation distance ($h$) between the particle and the collector surface. The subscripts $t$, $LVA$, $BR$, $EDLR$ denote total, London-van der Waal interaction, electric double layer interaction and Born Repulsion, respectively. The sign of the total interaction potential indicates attractive potential and repulsive potential for negative and positive signs respectively. The interaction potential can be represented in non-dimensional ($ND$) form as follows:

$$V_{t,ND}(h) = \frac{V_t(h)}{k_B \times T} \tag{2}$$

where $k_B$ is the Boltzmann constant ($1.38 \times 10^{-23}$ J·K$^{-1}$) and $T$ is temperature. In this study, all the experiments are conducted at room temperature hence $T$ = 297 K. The contributions due to the different types of interactions in Equation (1) can be calculated as follows [8,25,26]:

$$V_{LVA}(h) = -\frac{A_{132}}{6}\left[\frac{2(1+H)}{H(2+H)} + ln\left(\frac{H}{2+H}\right)\right] \tag{3}$$

$$V_{EDLR}(h) = \left(\frac{\varepsilon_0 D_e a_p}{4}\right)\left[2\zeta_p\zeta_s\, ln\frac{1+exp(-\kappa h)}{1-exp(-\kappa h)} + \left(\zeta_p^2 + \zeta_P^2\right) ln(1-exp(-2\kappa h))\right] \tag{4}$$

$$V_{BR}(h) = \frac{A_{132}}{7560}\left(\frac{\sigma}{a_p}\right)^6\left[\frac{8+H}{(2+H)^7} + \frac{6-H}{H^7}\right] \tag{5}$$

where

$$H = \frac{h}{a_p} \tag{6}$$

And, $a_p$ is the particle radius (m). $A_{132}$ is the Hamaker's constant between the sphere and plate collector which is typically in the range of $10^{-19}$ J. This value of the Hamaker's constant is based on the assumption that the van der Waals interactions occurs in vacuum and is not influenced by the presence of surrounding particles. Hence, to account of the intervening fluid and the surrounding particles, the Hamaker's constant must be modified based on the Lifshitz theory [28]. Based on previous works which are in turn based on the expression for modified Hamaker's constant developed by Israelachvili, the Hamaker's constant in this study is taken to be equal to $10^{-21}$ J [8]. Also, $\varepsilon_0$ is the permittivity of free space ($8.854 \times 10^{-12}$ C$^2$ J$^{-1}$ m$^{-1}$) and $D_e$ is the dielectric constant of water equal to 78 [8,26]. $\kappa$ is the inverse Debye length. For pure water used in this study, the inverse Debye length is equal to $(9.6 \times 10^{-7})^{-1}$ m$^{-1}$ [8]. $\zeta_p$ and $\zeta_s$ are the surface potentials of the particles and the surface respectively which can be replaced by the zeta potential [26]. In Equation (5), $\sigma$ is the atomic collision diameter and is equal to 0.5 nm [26]. The born repulsive potentials are formed when the particle approaches point of contact with the mineral resulting in overlap of electron clouds. Hence it is a short range interaction and thus calculated only when the distance of separation is less than 1 nm. For the various scenarios in

this study, the zeta potentials have been experimentally measured. $\sigma$ is the atomic collision diameter and is equal to 0.5 nm [26].

## 3. Results and Discussion

Injection experiments were performed with three kind of nanofluids: silica dispersed in DIW, silica dispersed in DIW containing MPTMS (1 g/100 mL) stabilizing fluid and sulfonated silica NP, dispersed in DIW. The effect of application (by vacuum treatment as outlined in Section 2.4) of each of these three nanofluids on berea sandstone are discussed in the following sections.

### *3.1. Unmodified Silica Nanofluids*

Figure 3a compares effluent NP concentration profiles for cores treated with 1 PV of unmodified silica NP dispersed in DIW. It may be observed that for both 1 and 2.5 g/L, the majority of the NP seized to be produce at about 0.5 and 1 PV, respectively. Long tail in the effluent concentration profile was observed for 2.5 g/L. The percentage of NP adsorbed in the core (calculated from mass balance) as the post flush progressed is plotted in Figure 3b. The estimated adsorbed NP was higher for 2.5 g/L nanofluid (88.82%) as compared to that for 1 g/L (85.82%) nanofluid. The recorded pressure drop during these experiments is shown in Figure 4.

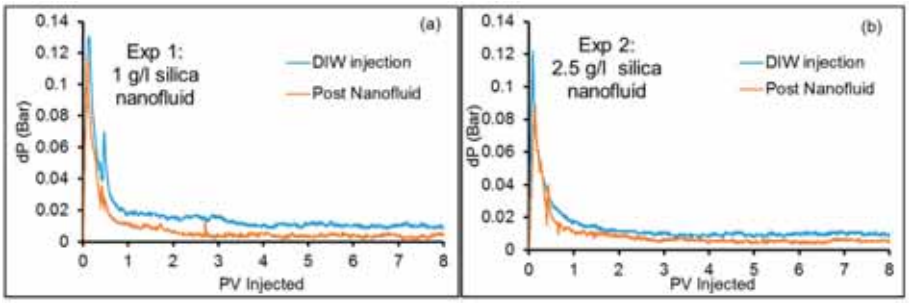


**Figure 4.** Pressure drop profiles for silica dispersed in deionized water (DIW) at (**a**) 1 g/L and (**b**) 2.5 g/L concentration.

Figure 4 shows that after treatment with 1 and 2.5 g/L silica NP, pressure drop profiles were lower than that for the initial DIW injection in unmodified berea. It may be observed that the entry resistance post application of NP was lower than the initial DIW injection as indicated by pressure peak of about 0.12 and about 0.09 bar, for initial DIW injection and post flush respectively (treatment with 2.5 g/L of nanofluid). It may be concluded from Figure 4a,b that using 1 g/L concertation leads to greater improvement in water injectivity, as there is a greater difference between the pressure drop for initial DIW injection and post flush after treatment with NP. Fines refer to solid mineral particles of the sandstone minerals that lose their coherence due to fluid/mineral interaction and become mobilized with the flowing fluids. In this study, the injection has been performed with DIW wherein the salinity is almost zero hence lower than the Critical Salt Concentration (CSC), which may induce interaction with minerals and produces fines that migrate and increase resistance to flow which may ultimately lead to formation damage [29]. Arab and Pourafshary [8] studied the applicability of NP for mitigating fine migration in engineered porous media (glass beads). In their work, they studied the application of different metal oxide NP to mitigate fines formation. They found that treating the porous medium with NP caused reduction in concentration of fines particles in the effluents as compared to untreated porous media. For example, they observed that treating the porous medium with silica dispersed in DIW led to approximately 20% reduction in effluent fines concentration as compared to the reference case. They observed that porous media that has been treated with NPs acts as a strong adsorbent

of fine particles [9]. Huang et al. [30] made a similar observation wherein they observed that for a sand pack treated with NP, the pressure drop across the sand pack was 10% lower than of sand pack without NP, showing an improvement in water injectivity.

To verify the effects of surface modification by silica NP and the associated improvement in water injectivity, experiment 3 was performed. In experiment 3, the core sample was initially injected with DIW and the stabilized dP was recorded at increasing injection rates. Thereafter the core was unloaded from the core holder, vacuum dried and treated with 1 g/L silica nanofluid prepared in DIW and flushed again with DIW. Stabilized dP was recorded at increasing injection rates. The results are shown in Figure 5. It can be observed that saturating the porous medium with the NP improves the water injectivity as indicated by lower dP (≈8%) during DIW flooding post treatment with NP. To quantify the remedial effect due to the application of NP, the ratio of the original pressure drop during the initial DIW injection (dPi) to the pressure drop post treatment with nanofluid (dPnp) was estimated and plotted as shown in Figure 5. As shown, the nanofluid treatment was effective at lower injection rates i.e., in reducing pressure drop. This is perhaps due to the increased hydrodynamic forces at higher injection rates.

SEM imaging was performed to better visualize the adsorption/adhesion of the NP on the rock surface, which causes the surface modification. Figure 6a shows the image of a slice of berea core. It may be noted that the slice of the berea core was cleaved along the injection plane approximately at the center of the core. The integrated energy-dispersive X-ray spectroscopy (EDX) analyzer was used to identify the minerals. As shown, the core was mainly composed of well-defined quartz with some feldspar and the core has pores of several microns in diameter. Another cylindrical slice of berea, which was vacuum saturated with 1 g/L silica NP in DIW, was examined using SEM (Figure 6b). The adsorbed/adhered NP were clearly shown on the mineral's surface. Figure 6c is a magnified view where the adsorbed/adhered silica NP is present. The adhered NP were in successive layers. This might be due to the drying effect. In addition, it was observed that most of the NP adsorption/adhesion was on quartz mineral. This is an interesting observation and static adsorption test and quantitative analysis based on the theory of surface forces were performed to further test this observation. Thus, it may be concluded that the NP adhere/adsorb on the minerals and this perhaps causes in situ surface modification. This modified surface is more effective at capturing fines, which can cause injectivity improvement. To test this, the theory of surface forces was utilized to quantify the interaction between the fines and the mineral before and after the application of NP. This addressed in a latter section.

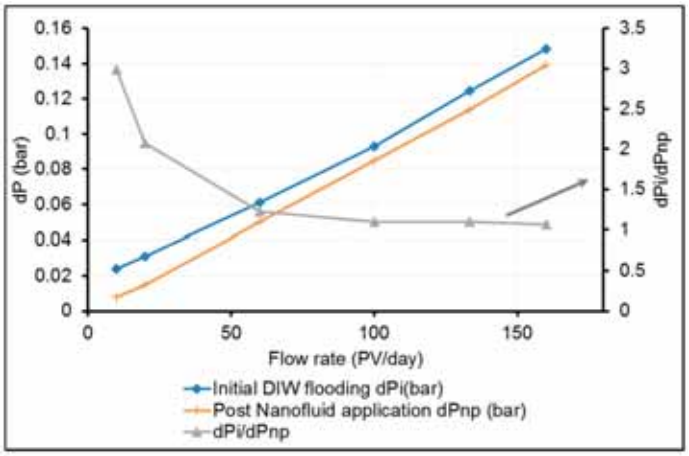


**Figure 5.** Pressure drop as function of injection rates (Experiment 3).

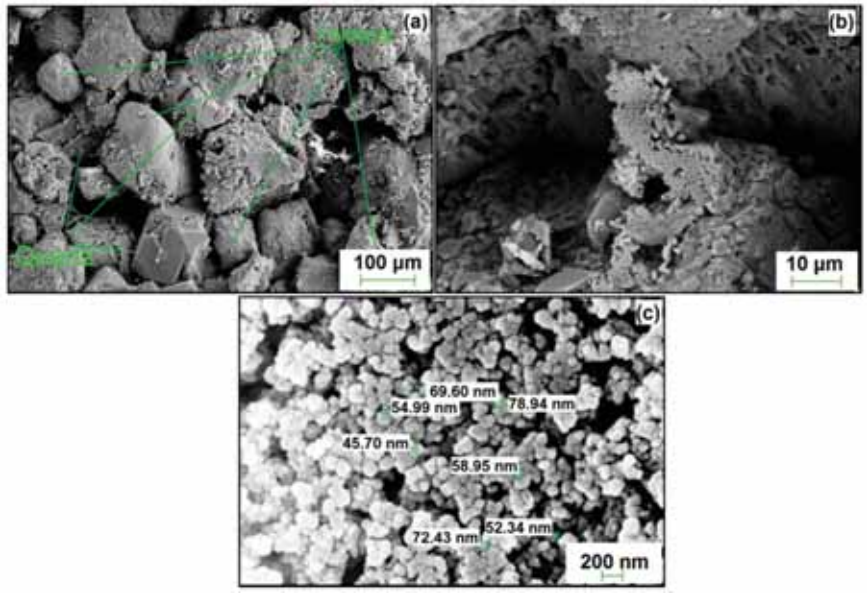


**Figure 6.** SEM image of (**a**) berea sandstone sample; (**b**) berea sandstone treated with nanofluid; (**c**) magnified look at the adsorbed/adhered silica.

### *3.2. Nanofluids Stabalized by MPTMS*

In this part of the study, surface modification of the porous medium was performed with nanofluids that were stabilized by addition of MPTMS. As stated previously, to avoid confusion, NP concentration is stated in g/L units and MPTMS concertation is stated in g/100 mL units. The effluent concentration profiles of NP during the post flush (with DIW) for the cores treated with nanofluids at different concentrations (Experiment: 4–8) are shown in Figure 7a. As shown, the nanofluids with 1 g/L and 2.5 g/L NP show similar profile of NP production. After DIW flush of about 1.5 PV for 2.5 g/L and 1 PV for 1 g/L the NP production in the effluent stopped. To ensure that this difference does not arise due to dissimilarities in the core, experiments 4 and 5 were repeated. The effluent concentration profiles shown in Figure 7a for the repeated cases are close to the initial experiments 4 and 5. For the nanofluid at 4 g/L concentration, the behaviour is completely different. The percentage of NP adsorbed in the core (Experiment 4–8) as the post flush progresses is shown in Figure 7b. In these experiments, the cores were vacuum saturated with the nanofluid. Therefore, it may be assumed that the spatial distribution of the NP in the core was uniform. Gradually decreasing retention for the case of 1 g/L and 2.5 g/L possibly suggests desorption of particles in the core or that the retained particles were forced out during the post flush. However, for 4 g/L it can be inferred from the almost flat nature of the curve that possibly only the NP near the outlet of the core were produced and substantial channelling of the fluid may be caused by blockage of some pore throats. This was confirmed by the monitoring the corresponding pressure drop during the experiments (Figure 8).

Figure 8 shows the recorded pressure drop (dP) during the post flush with DIW after application of nanofluid (Experiments 4–6). The recorded pressure drop during initial DIW injection was taken as a base line for the pressure drop. It is interesting to see that the pressure drop peaked at about 0.25 PV indicating entry resistance. The lowest pressure drop peak occurred for 1 g/L followed by the base fluid (DIW), then 2.5 g/L. In the case of 4 g/L, the pressure drop increased to above 0.3 bar. For cores saturated with NP concentration of 1 g/L, more fluctuations in dP was observed, followed by two

peaks between 1–2 PV, while the others (DIW and 2.5 g/L) dP declined smother. It may be concluded that 1 g/L flowed through the core with occasions of resistance to the flow. From mass balance, in the case of 1 g/L, 69.47% (0.01389 g) and for 2.5 g/L, 85.44% (0.044 g) of NP were adsorbed/retained in the core, i.e., the loss of the NP in the core for the case of 2.5 g/L exceeded 3 times higher compared to 1 g/L, yet the dP curves eventually became almost equal to the initial DIW injection, this may indicate that the retained/adsorbed NP did not hinder the flow. However, the surface modification of he surfaced by this nanofluid does not lead improvement in water injectivity. In contrast, for the 4 g/L, where the pressure drop increased for more than 2 PV before it was stabilized at dP > 0.3 bar, this may indicate possible aggregation of NPs that restricted/blocked some of the pore throats.

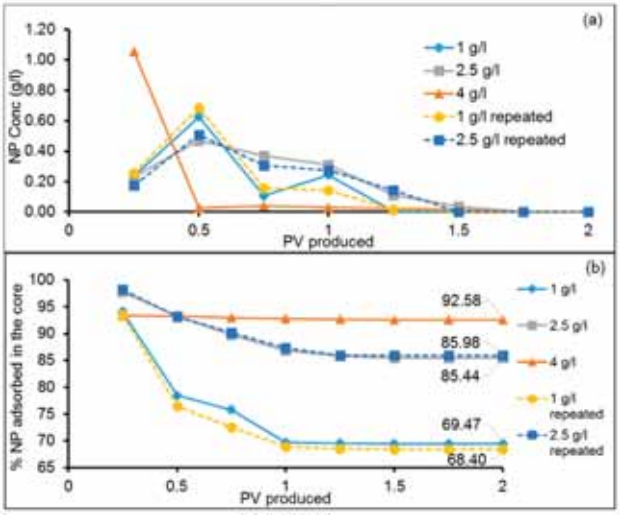


**Figure 7.** (**a**) Effluent NP concentration profiles and (**b**) % adsorption of NP during post flush for cores saturated with silica dispersed in DIW with MPTMS stabilizing fluid (Experiments: 4–8).

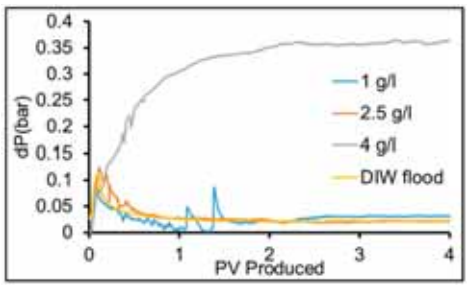


**Figure 8.** Variation of the drop across the core (dP) during post flush with DIW after saturation of the core with MPTMS stabilized nanofluids at different NP concentrations of NP (Experiments 4–6).

Figure 9 shows the amount of MPTMS adsorbed in the core. The concertation of MPTMS was measured by UV/VIS. The amount of MPTMS retained in the core was calculated from the mass balance. It may be observed that a high amount of the stabilizing fluid in adsorbed in the core. High adsorption of NP stabilizing fluid (MPTMS) in the porous media suggest that this method may not be suitable for subsurface application.

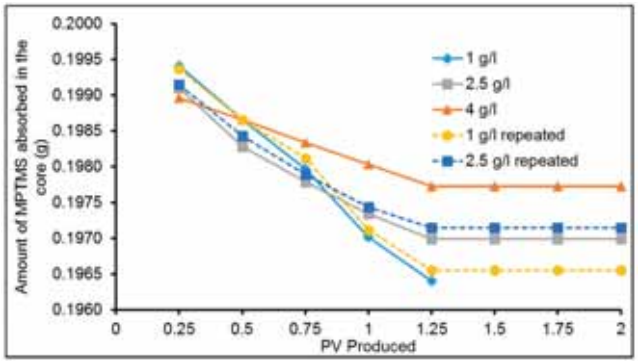


**Figure 9.** Absorbed MPTMS for cores saturated with nanofluid stabilized with MPTMS (Experiments: 4–8).

### *3.3. Sulfonated Silica Nanofluids*

This section addresses the behaviour of sulfonated silica. Sulfonated silica NP were prepared by the method described earlier Section 2.2 and dispersed at 1 g/L concentration in DIW. The effluent concentration profile during the post flush for core saturated with 1 g/L surface modified (sulfonated) NP in DIW is shown in Figure 10a. For the sake of comparison, the effluent concertation profiles for cores saturated with 1 g/L unmodified NP and NP stabilized with MPTMS are also shown in Figure 10a. It may be observed that the behaviour of sulfonated NP was similar to silica NP. That is the majority of the NP were produced in the first 0.5 PV. Contrary to that with MPTMS (stabilizing fluid), the NP production continues for 1 PV. Based on mass balance it was calculated that 74.6% of the sulphonated NPs were adsorbed in the core. Pressure drop profile recorded with sulphonated NP is shown in Figure 10b. As may be observed that the entry resistance post application of sulfonated NP was lower than the initial DIW injection. This observation was consistent with the case of the post flushing for cores saturated with unmodified NP. As the NP were being produced, high variation frequency was observed in the pressure drop. Thereafter the pressure drop profile declined smoother and almost overlaps with the initial DIW injection. In summary, the application of sulfonated NP did not lead improvement of water injectivity.

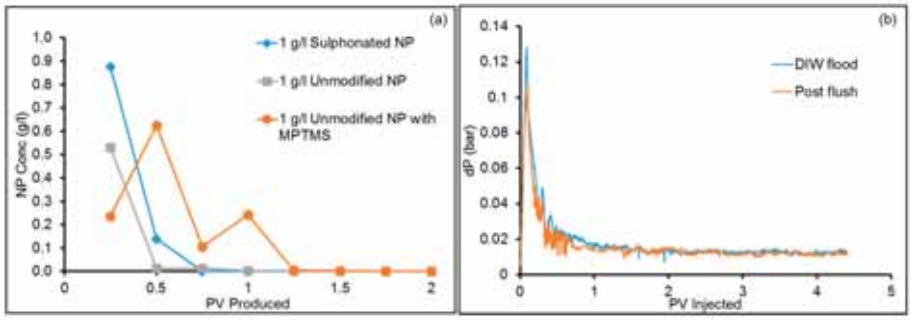


**Figure 10.** (**a**) Comparison of effluent concentration profiles of the different types of nanofluid (concentration of NP: 1 g/L) silica, sulfonated and silica with stabilizing fluid; (**b**) Pressure drop profiles for core treated with sulfonated NP.

Two important observations are made from the application of nanofluids and SEM imaging conducted: (1) The preferential adsorption of the silica NPs on quartz mineral, which to the best knowledge of the authors have not been reported previously and (2) The water injectivity improvement was observed upon the application of silica NPs only. That is, the two nanofluid stabilization methods tend to reduce the effectiveness of the surface modification by the NPs. These observations are further investigated and strengthened in latter sections.

### *3.4. Adsorption of NP on Minerals*

SEM imaging for cores saturated with silica NP showed that the adsorption was mostly on quartz. Isothermal static adsorption tests and calculation of interaction potential between the NP and the mineral powders were performed to investigate the affinity of the NP to quartz and kaolinite mineral powders. Metin et al. [31] have previously studied the adsorption of silica NP onto representative mineral surfaces. SEM imaging for cores saturated with silica NP showed that the adsorption was mostly on quartz. To further investigate this, quartz and kaolinite were dispersed in all three kinds of nanofluids and the adsorption of NP per unit surface area of the mineral was determined. The results are shown in Figure 11. In addition, the interaction potentials between the minerals and NP was calculated by the model presented in Section 2.8 based on the particle size and zeta potential data presented in Table 2. The results are plotted in Figure 12.

Figure 11 shows higher adsorption of NP on quartz compared to kaolinite. As shown, Figure 11, the adsorption of NP is higher for stabilized nanofluids (with MPTMS and modified by sulphonated material). This was supported by Figure 12, where the attractive interaction potentials for all three type of NP were greater for quartz as compared to kaolinite. This validates SEM images where most of the adhesion/adsorption of NPs/nanofluids were on the quartz mineral as compared to kaolinite.

In the previous section it was noted that the unmodified silica showed highest adsorption on the berea core (85.82%) followed by sulfonated silica (74.61%) and MPTMS stabilised silica (69.47%), however the stabilized NPs by MPTMS show higher adsorption in the static adsorption tests. The reason is not known, however, the observation, may be explained by (1) insufficient contact time with minerals, i.e., slower kinetics than the unmodified NPs; (2) influence of the collective neighbouring minerals compared to individual isolated minerals (static adsorption); (3) weak adsorption on mineral surface, hence desorbed in fluid flow and (4) all the above factors. More work is ongoing on this observation.

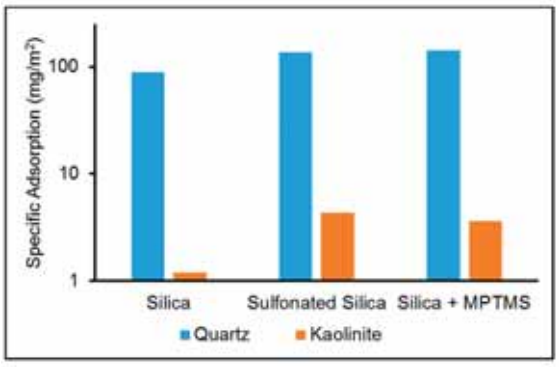


**Figure 11.** Specific adsorption of NP (mg/m$^2$) on quartz and kaolinite.

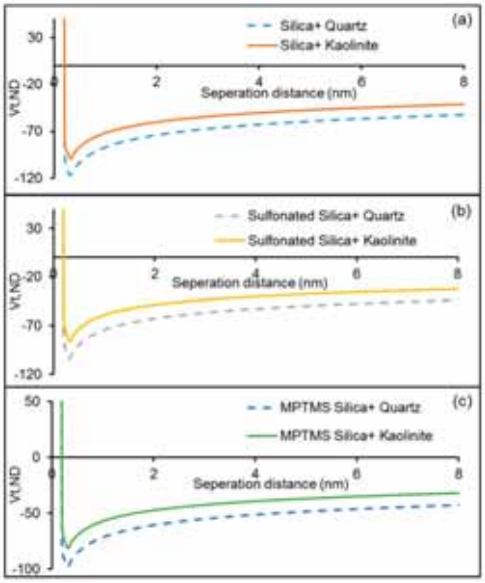


**Figure 12.** Interaction potential between the mineral and (**a**) unmodified silica; (**b**) sulfonated silica; and (**c**) unmodified silica + MPTMS.

### *3.5. Interaction between Fines and Porous Media*

The surface charge of berea in DIW was determined to be −29.53 mV (Table 2). To investigate the surface charge modification caused by NP, powdered berea at 10 g/L concentration was added to nanofluids of silica and sulfonated silica prepared in DIW at 1 g/L concentration. This mixture was left under stirring for 12 h. Thereafter, the surface charge of the barea powder treated with unmodified and sulfonated silica was measured using Acosustisizer II S/M Flow-through System. It was found that the surface charge of treated barea was reduced to −11.4 mV and −20.36 mV in the case of unmodified and sulfonated silica respectively. The fines produced were analysed for the size and zeta potential. Specifically, effluent sample from effluent bank collected during DIW injection was collected and analysed in the Zetasizer Nano ZSP (Malvern instruments). It was found that the zeta potential of the fine particles was −22.9 mV. The measured zeta potential of fines is in close agreement with previous measurements of fines eluted from berea sandstone [32]. In addition, the fines produced were in there different size classes (Table 4).

**Table 4.** Size classes of the fine particles.

| Radius of Fine Particles (nm) | Intensity (%) |
|---|---|
| 233.8 | 73.0 |
| 68.57 | 24.2 |
| 2687 | 2.8 |

The interaction potential between the fine particles and the porous media was calculated based on the sphere plate collector model presented in Section 2.8. Since the fines have separate size classes, the interaction potential was calculated for each size class and summed on a weighted basis:

$$V_t(h) = \sum_{i=1}^{n} \{V_{t,i}(h) \times w_i\} \quad (7)$$

where $w_i$ is the weight intensity of each size class and $V_{t,i}(h)$ is the interaction potential calculated for the specific size class and finite distance of separation ($h$). Thereafter, the non-dimensional interaction energy was determined using Equation (2). The interaction potentials between berea mineral and fines calculated for the reference case (no NP) and berea treated with silica and sulfonated silica is shown in Figure 13.

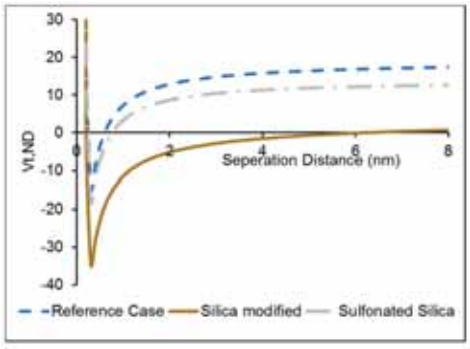


**Figure 13.** Dimensionless form of Interaction potential for interaction between the fines and the berea mineral for reference case (no NP), berea treated with silica and berea treated with sulfonated silica.

In Figure 13, it may be observed that in the reference case, there is a net repulsive potential (energy barrier) between the fines and the mineral surface. However, for mineral treated with silica, there is a net attractive potential (no energy barrier) between the fines and the mineral. This could possibly cause the mineral to act as collectors for capturing fine particles thereby reducing fine migration. This may explain the improvement in water injectivity post application of silica nanofluid as observed in Figures 4 and 5. In the case where berea was treated with sulfonated NP, there a reduction in the energy barrier (Figure 13), however the net potential is still repulsive and close to the reference case. This may explain the similarity in pressure drops observed during initial DIW injection and post flush after saturating the core with sulfonated NP in Figure 10. Thus, it maybe concluded that the surface modification caused silica is much more effective at reducing fine migration and thereby improving the water injectivity in berea cores. Li and Torsæter [4] observed that the injection of colloidal NP into berea sandstone did not lead to permeability impairment. They stated that adsorption of NP on the pore wall act like lubrication reducing the friction between the water and pore walls. However as discussed earlier, this effect may be explained based on reduction of the fine migration rather than direct influence on flow. Reduction of fine production may overcome the problem of formation damage induced during low salinity flooding in sandstones.

## 4. Conclusions

Low salinity water (LSW) flooding is currently a popular method for EOR. However, it suffers from the results of water/mineral interaction and production of fines. Excessive fines production may lead to formation damage. This work addressed the potential of different silica nanofluids as surface modifying agents for berea sandstone, hence reduced fines migration. The reduction of the fines was indicated by the reduced pressure drop during the post flush of the NPs' slug. This supports the reduction of fines, which may be explained based on NPs' adsorption on berea surface, i.e., reduction of direct contact between water and minerals.

Silica NPs have shown to have a higher affinity to adhere/adsorb on quartz surface compared to kaolinite minerals.

Unmodified silica nanofluid reduced fine migration and improved water injectivity. Adsorption of NPs on mineral surfaces may be utilized to overcome the problem of formation damage induced during low salinity flooding.

The used stabilizing methods for the NPs almost did not reduce the fine migration, which was qualitatively indicated by the pressure drop across the porous media. The used stabilizing fluids enhances the static adsorption of NPs on quartz and kaolinite minerals. However, as discussed earlier, may not be strong enough to resist the dynamic fluid forces, their effect on fines, hence are not as effective as the unmodified NPs.

**Acknowledgments:** The authors would like to thank the University of Stavanger (UiS), Norway for funding this work. We also like to thank Mona W. Minde (UiS) for helping with the SEM imaging and Lutz Eichacker (UiS) for providing access to the DLS equipment. The authors would like to thanks Inger Johanne M-K Olsen (UiS) for acquiring the chemical used in this study. In addition, the authors would like to thank Kim Andre Vorland (UiS) and Krzysztof I Nowicki (UiS) for helping with the setup.

**Author Contributions:** Rockey Abhishek and Aly A. Hamouda conceived and designed the experiments; Rockey Abhishek performed the experiments; Rockey Abhishek and Aly A. Hamouda analyzed the data; Rockey Abhishek and Aly A. Hamouda wrote the paper.

**Conflicts of Interest:** The authors declare no conflict of interest. The funding sponsors had no role in the design of the study; in the collection, analyses, or interpretation of data; in the writing of the manuscript, and in the decision to publish the results.

## References

1. Abhishek, R.; Kumar, G.S.; Sapru, R. Wettability alteration in carbonate reservoirs using nanofluids. *Pet. Sci. Technol.* **2015**, *33*, 794–801. [CrossRef]
2. Behzadi, A.; Mohammadi, A. Environmentally responsive surface-modified silica nanoparticles for enhanced oil recovery. *J. Nanopart. Res.* **2016**, *18*, 1–19. [CrossRef]
3. Giraldo, J.; Benjumea, P.; Lopera, S.; Cortés, F.B.; Ruiz, M.A. Wettability alteration of sandstone cores by alumina-based nanofluids. *Energy Fuels* **2013**, *27*, 3659–3665. [CrossRef]
4. Li, S.; Torsæter, O. Experimental investigation of the influence of nanoparticles adsorption and transport on wettability alteration for oil wet berea sandstone. In Proceedings of the SPE Middle East Oil & Gas Show and Conference, Manama, Bahrain, 8–11 March 2015; Society of Petroleum Engineers: Richardson, TX, USA, 2015.
5. Shahrabadi, A.; Bagherzadeh, H.; Roostaie, A.; Golghanddashti, H. Experimental investigation of hlp nanofluid potential to enhance oil recovery: A mechanistic approach. In Proceedings of the SPE International Oilfield Nanotechnology Conference and Exhibition, Noordwijk, The Netherlands, 12–14 June 2012; Society of Petroleum Engineers: Richardson, TX, USA, 2012.
6. Sheshdeh, M.J. A review study of wettability alteration methods with regard to nano-materials application. In Proceedings of the SPE Bergen One Day Seminar, Bergen, Norway, 22 April 2015; Society of Petroleum Engineers: Richardson, TX, USA, 2015.
7. Zhang, H.; Nikolov, A.; Wasan, D. Enhanced oil recovery (EOR) using nanoparticle dispersions: Underlying mechanism and imbibition experiments. *Energy Fuels* **2014**, *28*, 3002–3009. [CrossRef]
8. Arab, D.; Pourafshary, P. Nanoparticles-assisted surface charge modification of the porous medium to treat colloidal particles migration induced by low salinity water flooding. *Colloids Surf. A Physicochem. Eng. Asp.* **2013**, *436*, 803–814. [CrossRef]
9. Arab, D.; Pourafshary, P.; Ayatollahi, S.; Habibi, A. Remediation of colloid-facilitated contaminant transport in saturated porous media treated by nanoparticles. *Int. J. Environ. Sci. Technol.* **2014**, *11*, 207–216.
10. Hendraningrat, L.; Li, S.; Torsæter, O. A coreflood investigation of nanofluid enhanced oil recovery. *J. Pet. Sci. Eng.* **2013**, *111*, 128–138.
11. Hendraningrat, L.; Torsæter, O. Metal oxide-based nanoparticles: Revealing their potential to enhance oil recovery in different wettability systems. *Appl. Nanosci.* **2015**, *5*, 181–199. [CrossRef]
12. Ogolo, N.; Olafuyi, O.; Onyekonwu, M. Enhanced oil recovery using nanoparticles. In Proceedings of the SPE Saudi Arabia Section Technical Symposium and Exhibition, Al-Khobar, Saudi Arabia, 8–11 April 2012; Society of Petroleum Engineers: Richardson, TX, USA, 2012.

13. Suleimanov, B.; Ismailov, F.; Veliyev, E. Nanofluid for enhanced oil recovery. *J. Pet. Sci. Eng.* **2011**, *78*, 431–437. [CrossRef]
14. Hofmann, U.; Endell, K.; Wilm, D. Röntgenographische und kolloidchemische untersuchungen über ton. *Angew. Chem.* **1934**, *47*, 539–547. [CrossRef]
15. Metin, C.O.; Lake, L.W.; Miranda, C.R.; Nguyen, Q.P. Stability of aqueous silica nanoparticle dispersions. *J. Nanopart. Res.* **2011**, *13*, 839–850. [CrossRef]
16. Ortega, D.J.S.; Kim, H.B.; James, L.A.; Johansen, T.E.; Zhang, Y. The effectiveness of silicon dioxide $SiO_2$ nanoparticle as an enhanced oil recovery agent in ben nevis formation, hebron field, offshore eastern canada. In Proceedings of the Abu Dhabi International Petroleum Exhibition & Conference, Abu Dhabi, UAE, 7–10 November 2016; Society of Petroleum Engineers: Richardson, TX, USA, 2016.
17. Hendraningrat, L.; Torsæter, O. A stabilizer that enhances the oil recovery process using silica-based nanofluids. *Transp. Porous Media* **2015**, *108*, 679–696. [CrossRef]
18. Yang, X.; Liu, Z.-H. A kind of nanofluid consisting of surface-functionalized nanoparticles. *Nanoscale Res. Lett.* **2010**, *5*, 1324. [CrossRef] [PubMed]
19. Weston, J.S.; Jentoft, R.E.; Grady, B.P.; Resasco, D.E.; Harwell, J.H. Silica nanoparticle wettability: Characterization and effects on the emulsion properties. *Ind. Eng. Chem. Res.* **2015**, *54*, 4274–4284. [CrossRef]
20. Zhang, T.; Murphy, M.J.; Yu, H.; Bagaria, H.G.; Yoon, K.Y.; Nielson, B.M.; Bielawski, C.W.; Johnston, K.P.; Huh, C.; Bryant, S.L. Investigation of nanoparticle adsorption during transport in porous media. *SPE J.* **2014**. [CrossRef]
21. Wang, W.; Yuan, B.; Su, Y.; Wang, K.; Jiang, M.; Moghanloo, R.G.; Rui, Z. Nanoparticles adsorption, straining and detachment behavior and its effects on permeability of berea cores: Analytical model and lab experiments. In Proceedings of the SPE Annual Technical Conference and Exhibition, Dubai, UAE, 26–28 September 2016; Society of Petroleum Engineers: Richardson, TX, USA, 2016.
22. Tabrizy, V.A.; Denoyel, R.; Hamouda, A. Characterization of wettability alteration of calcite, quartz and kaolinite: Surface energy analysis. *Colloids Surf. A Physicochem. Eng. Asp.* **2011**, *384*, 98–108. [CrossRef]
23. Mondragon, R.; Julia, J.E.; Barba, A.; Jarque, J.C. Characterization of silica–water nanofluids dispersed with an ultrasound probe: A study of their physical properties and stability. *Powder Technol.* **2012**, *224*, 138–146. [CrossRef]
24. Oh, Y.-K.; Hong, L.-Y.; Asthana, Y.; Kim, D.-P. Synthesis of super-hydrophilic mesoporous silica via a sulfonation route. *J. Ind. Eng. Chem.* **2006**, *12*, 911–917.
25. Seetha, N.; Majid Hassanizadeh, S.; Kumar, M.; Raoof, A. Correlation equations for average deposition rate coefficients of nanoparticles in a cylindrical pore. *Water Resour. Res.* **2015**, *51*, 8034–8059. [CrossRef]
26. Khilar, K.C.; Fogler, H.S. *Migrations of Fines in Porous Media*; Springer Science & Business Media: New York, NY, USA, 1998; Volume 12.
27. Dunphy Guzman, K.A.; Finnegan, M.P.; Banfield, J.F. Influence of surface potential on aggregation and transport of titania nanoparticles. *Environ. Sci. Technol.* **2006**, *40*, 7688–7693. [CrossRef]
28. Israelachvili, J.N. *Intermolecular and Surface Forces*; Academic Press: Cambridge, MA, USA, 2011.
29. Yuan, H.; Shapiro, A.A. Induced migration of fines during waterflooding in communicating layer-cake reservoirs. *J. Pet. Sci. Eng.* **2011**, *78*, 618–626. [CrossRef]
30. Huang, T.; Han, J.; Agrawal, G.; Sookprasong, P. Coupling nanoparticles with waterflooding to increase water sweep efficiency for high fines-containing reservoir-lab and reservoir simulation results. In Proceedings of the SPE Annual Technical Conference and Exhibition, Houston, TX, USA, 28–30 September 2015; Society of Petroleum Engineers: Richardson, TX, USA, 2015.
31. Metin, C.O.; Baran, J.R.; Nguyen, Q.P. Adsorption of surface functionalized silica nanoparticles onto mineral surfaces and decane/water interface. *J. Nanopart. Res.* **2012**, *14*, 1246. [CrossRef] [PubMed]
32. Kia, S.; Fogler, H.; Reed, M. Effect of ph on colloidally induced fines migration. *J. Colloid Interface Sci.* **1987**, *118*, 158–168. [CrossRef]


**Effect of Silica Nanoparticles on Fluid/Rock Interactions during Low Salinity Water Flooding of Chalk Reservoirs.**

Abhishek, R., A. A. Hamouda and A. Ayoub (2018)

Applied Sciences 8(7): 1093. Special issue: Nanofluids and Their Applications, MDPI Publications.

Paper II

applied sciences

MDPI

Article

# Effect of Silica Nanoparticles on Fluid/Rock Interactions during Low Salinity Water Flooding of Chalk Reservoirs

**Rockey Abhishek, Aly A. Hamouda * and Amr Ayoub**

Institute of Energy and Petroleum Technology, University of Stavanger, 4036 Stavanger, Norway; rockey.abhishek@uis.no (R.A.); eng.amrayoup@gmail.com (A.A.)

* Correspondence: aly.hamouda@uis.no; Tel.: +47-95-702-604

Received: 11 June 2018; Accepted: 2 July 2018; Published: 5 July 2018


**Abstract:** The main objective of this work is to address the adsorption of Silica nanoparticles (NPs) dispersed in different brines on chalk surfaces and their effect on fluid/rock interaction. Isothermal static and dynamic adsorption on chalk are addressed here. Isothermal static adsorption showed increased adsorption of NPs at higher salinity. The tests were performed to cover wide range of injection scenarios with synthetic seawater (SSW) and low salinity water (LSW). The selected LSW composition here is based on 1:10 diluted SSW, which has shown to have superior performance compared to other ion compositions. The dynamic adsorption tests of NPs showed reduction of calcite dissolution of about 30% compared to LSW alone. That is, silica nanofluid hinders calcite dissolution i.e., has less effect on chalk matrix integrity which is a major concern in chalk reservoir, if low salinity is employed for enhanced oil recovery. Both scanning electron microscope images and pressure drop across the core during nanofluid injection indicated no throat blockage. Based on ion tracking and the monitored pH, the mechanism(s) for NP adsorption/desorption are suggested. The results from this study suggests a synergy wherein adding relatively small amount of silica NPs can improve the performance of low salinity floods.

**Keywords:** silica nanofluid; chalk; fine production; low salinity water flooding; EOR

## 1. Introduction

Nanofluids (NFs) have recently attracted attention from researchers in different disciplines. One of their fields of application is enhanced oil recovery (EOR) from petroleum reservoirs [1–4]. With sizes below 100 nm and high specific surface area, nanoparticles (NPs) are suitable for subsurface porous media applications since they can pass through the pore throats of porous media without blocking them and enhance oil recovery at relatively low volume concentrations [5,6] via wettability alteration [7–9].

The work here is performed using silica NPs. Many researchers have conducted core flooding studies and demonstrated the potential of silica NPs to increase oil recovery [2,10–16]. Adsorption and transport of nanoparticles in porous media is of primary importance for subsurface applications as this determines the effectiveness of the nanofluid injection. However, most of the work has been focused on the adsorption and transport behaviour of NPs in sandstones [17–19]. Few investigations have addressed the applicability of NPs to carbonate reservoirs [20–24]. Nazari Moghaddam, et al. [25] compared the performance of different types of NPs in altering the wettability of carbonate reservoirs. Al-Anssari, et al. [26] reported that silica NPs adhere to the calcite surface irreversibly and can alter the wettability of oil/mixed-wet to water-wet state. The efficiency of wettability change by silica NPs was shown to be enhanced at higher temperatures [20]. Apart from wettability change, silica NPs have also been shown to reduce oil-water interfacial tension thereby improving the mobility of oil phase [27–29]

and stabilize oil in water emulsions [30–33] for EOR application. Monfared, et al. [34] studied the adsorption of silica NPs on calcite surfaces. They reported that salinity has a positive effect on the adsorption process. However, adsorption of silica NPs on the chalk surface is not well understood.

Chalk reservoirs are generally speaking tight, with permeabilities ranging from 1–7 mD and porosity of about 50%. Low salinity water flooding has emerged as an effective technique for improving oil recovery from some reservoirs [35–42]. However, increased calcite dissolution induced by low salinity interaction with chalk during flooding may lead to loss of rock integrity [43]. Previous work in our lab investigated the adsorption different silica NPs on sandstone minerals and its effect on fines migration [44]. We found the silica NPs modifies the sandstones minerals and it can be utilized to overcome the problem of formation damage induced during low salinity flooding in sandstones.

To best of our knowledge, the adsorption behaviour of silica NPs on chalk and its effect on fluid/rock interactions has not been addressed previously. This work aims to address the adsorption desorption mechanisms of silica NPs at different salinity conditions and suggest a synergy between silica NPs and low salinity water flooding of chalk reservoirs. The first part of the study addresses the stability of the used nanofluids. Thereafter, static adsorption of the NPs on calcite at different salinities is addressed. The adsorption of silica NPs on chalk surface is visualized by performing scanning electron microscopy (SEM). Dynamic adsorption of NPs during injection into chalk and its effect on fluid/rock interaction was investigated. Finally, the effect of NP on the fluid/rock interactions during continuous nanofluid injection in the presence of hydrocarbons is addressed. Three types of cases are investigated, with silica NPs mixed with seawater or low salinity water (LSW) and with mix injection as the third case. The last of these represents the situation for most oil fields, especially those in the North Sea where primary flooding has been with seawater. The fluid/rock interaction has been addressed here to shed light on the possible mechanisms, which may help in deciding when to apply the technology. The results from this study suggests a synergy wherein adding a small amount of silica NPs can improve the performance of low salinity floods by reducing the risk of matrix integrity loss and reservoir subsidence in chalk reservoirs.

## 2. Materials and Methods

The silica NPs used in this study were provided by Nyacol Nano Technologies Inc. (Ashland, MA, USA). The DP 9711 product was acquired at a 30 wt. % concentration in deionized water (DIW) and with a pH of 3. The DP9711 product has a proprietary surface coating but Singh and Mohanty [45] reported that DP 9711 is coated with polyethylene glycol. For ease, these NPs are referred to as DP in this study. The NPs as claimed by the manufacturer have an average particle size of 20 nm. As and when required, the NFs used in this study were prepared from the stock fluid by diluting it with appropriate brines. Stevns Klint (SK) outcrop chalk cores were used as the porous media. SK chalk is 99% pure biogenic with a high porosity range of 45–50% and a relatively low absolute permeability of ≈4 mD [36]. SK chalk matrix material and its petro-physical properties resembles chalk reservoirs, which makes it useful in the analysis [46]. Calcite mineral powder acquired from Honeywell Riedel-de Haen was of analysis grade with a surface area of 0.23 ($m^2/g$) calculated previously by the water adsorption isotherm [47]. The model oil used in this study was n-decane (n-C10) acquired from Merck (Drammensveien, Oslo, Norway). Stearic acid (SA) was added to n-decane at a concentration of 0.005 mol/L to prepare the synthetic oil. The properties of the synthetic oil are listed in Table 1, estimated from PVT Sim.

**Table 1.** Synthetic oil properties.

| Temperature °C | Viscosity (cP) | Density (g/mL) |
|---|---|---|
| 20 | 0.92 | 0.73 |
| 50 | 0.5802 | 0.7683 |
| 70 | 0.4812 | 0.7525 |

Zetasizer Nano ZSP from Malvern Instruments (Malvern, Worcestershire, UK) was used to characterize the average hydrodynamic diameter and zeta potential of the NPs. Scanning electron microscopy was performed on a Supra 35 VP SEM by Ziess (Oberkochen, Baden-Württemberg, Germany) with an integrated EDXRF analyzer to visualize the adsorption of the NPs on the SK chalk samples treated with NF. NP concentration during isothermal static adsorption tests and NP dynamic adsorption in brines was measured using a dual beam UV-Vis 1700 spectrophotometer from Shimadzu Corporation (Nakagyo-ku, Kyoto, Japan). The schematic of the core flooding setup used in this study is shown in Figure 1. The concentration of the cations in the effluents was determined by a Dionex ICS-5000 ion chromatograph from Thermo Fisher Scientific (Waltham, MA, USA). Inductive coupled plasma and optical emission spectrometry (ICP-OES) was carried out by an Optima 4300 DV from PerkinElmer (Waltham, MA, USA)to quantitatively determine the trace amounts of elements eluted and to determine the NP concentration in the effluent for chalk cores injected with DIW.

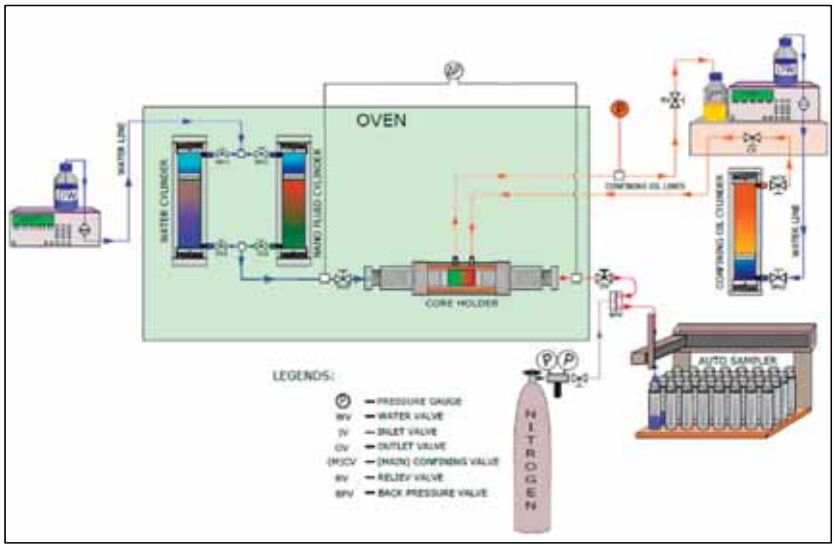


**Figure 1.** Schematic of the core flooding setup.

## 2.1. Brines

Synthetic seawater (SSW) and LSW produced by a 1:10 dilution of SSW with DIW were the brines used in this study. The ionic compositions of the brines are listed in Table 2.

**Table 2.** Ion concentration in the brines.

| Ion | SSW (mol/L) | LSW (mol/L) |
|---|---|---|
| $HCO^{3-}$ | 0.002 | 0.0002 |
| $Cl^{-}$ | 0.525 | 0.0525 |
| $SO_4^{2-}$ | 0.0240 | 0.0024 |
| $Mg^{2+}$ | 0.045 | 0.0045 |
| $Ca^{2+}$ | 0.013 | 0.0013 |
| $Na^{+}$ | 0.450 | 0.045 |
| $K^{+}$ | 0.010 | 0.0010 |

### 2.2. Isothermal Static Adsorption

A series of batch adsorption experiments were performed at room temperature to address the adsorption of the silica NPs on the calcite surface. The concentration of NPs was systematically varied to address the effect of NPs' concentration on the adsorption process. The experiments were performed in DIW and SSW as the media for studying the effect of salinity on the adsorption process. A known amount of mineral was added to NF at a predetermined concentration. The dispersion was agitated on a rotary agitator for 24 h. Thereafter, the mineral was removed from the dispersion and the concentration of the NPs in the fluid was determined by measuring their absorption in a dual beam spectrophotometer at 240 nm, comparing it with the constructed calibration curve and making baseline corrections.

### 2.3. Dynamic Adsorption of NPs in Chalk Core

The objectives of the tests were to study the adsorption profile of the NPs and their interaction with the minerals (mainly calcite). The dried chalk cores were vacuum-saturated with DIW or brine (LSW/SSW) and loaded into the core holder. A confining pressure of 25 bar was applied, and injection was performed at a constant flow rate of 10 PV/day at room temperature. After injecting several PVs of DIW/brine (pre-flush), 1.5 pore volume (PV) of slug with LiCl tracer was injected. Thereafter, the injection was switched to the original fluid to conduct a post-flush. For the tests SK1 & 2, the DIW (ions free) was injected and the effluent was analyzed for Ca to follow the calcite dissolution. Tests SK3 and 4 were performed with SSW and LSW, respectively. Details of the experiment are listed in Table 3.

**Table 3.** List of experiments to test dynamic adsorption of nanoparticles (NPs) in chalk.

| Core Id | Porosity (%) | Permeability (mD) | Length (cm) | Dia (cm) | Pre/Post Flush Fluid | Slug Composition |
|---|---|---|---|---|---|---|
| SK1 | 48.10 | 3.9 | 5.31 | 3.78 | DIW | 1 (g/L) DP in DIW with 0.1M LiCl tracer |
| SK2 | 49.00 | 3.9 | 7.80 | 3.78 | DIW | 90 µL 0.1M HCl + 0.1M LiCl in DIW |
| SK3 | 51.71 | 3.9 | 3.9 | 3.78 | SSW | 1 g/L DP in SSW + 0.1M LiCl |
| SK4 | 47.38 | 3.9 | 3.35 | 3.78 | LSW | 1 g/L DP in LSW + 0.1M LiCl |

### 2.4. Effect of Oil on the Interaction of the NPs and Mineral

The purpose of these tests to confirm the interaction of NPs with mineral surface in presence of synthetic oil (n-C10+ 0.005 M SA). The cores were first dried at 100 °C in a vacuum oven until the weight stabilized. The cores were then vacuum-saturated with SSW and loaded in the core holder. Several PVs of synthetic oil were flooded into the core until initial water saturation (Swi) was obtained. Thereafter, the cores were aged in synthetic oil for a period of two weeks at 50 °C to render them oil-wet. The experiments were performed at 70 °C under a confined pressure of 25 bar and against 10 bar of back pressure in two stages. In order to mimic the field status (water flooded), different scenarios were studied as shown in Table 4. The injection rates were small to be able to account for the kinetics of the interaction. From our previous studies with LSW alone [43], two flow rates were used 4 and 16 PV/day. Thereafter, the injection was switched to NF and the flow was at 4 and 16 PV/day. The details of the experimental tests are listed in Table 4.

**Table 4.** List of nanofluid experiments with hydrocarbons.

| Core Id | Porosity (%) | Permeability (mD) | Length (cm) | Dia (cm) | Swi | Primary Fluid | Secondary Fluid (Nanofluid) |
|---|---|---|---|---|---|---|---|
| SK5 | 50.7 | 3.9 | 8.83 | 3.785 | 0.13 | SSW | DP (1 g/L) in SSW |
| SK6 | 50 | 3.9 | 5.96 | 3.785 | 0.28 | LSW | DP (1 g/L) in LSW |
| SK7 | 50.24 | 3.9 | 4.658 | 3.785 | 0.275 | SSW | DP (1 g/L) in LSW |

The effluent fluids were collected and analyzed for pH and ion concentration. The pressure drop across the core was monitored. Since oil was produced, a rough estimation of potential recovery was estimated. However, the recovered oil is not optimized but is just given as indication.

## 3. Results and Discussion

This section is divided into subsections to fulfil the objectives of this work. The subsections are: (1) NF characterization to address their sizes and stability with different injection fluids, the effect of temperature on size, their zeta potential in the different waters. (2) Adsorption of NP onto the calcite surface in different waters—i.e., the effect of the salinity on the adsorption. (3) Dynamic adsorption of NPs during injection into chalk and its effect on fluid/rock interaction and (4) Effect of NP on the fluid/rock interactions during continuous nanofluid injection in the presence of hydrocarbons.

### *3.1. NF Characterization*

NFs were characterized for particle size and zeta potential at different temperatures and in various brines. The NFs were prepared in DIW, LSW and SSW. Particle-size measurements at different temperatures and the zeta potential measurements at 25 °C are presented in Figure 2. Figure 2a shows the average hydrodynamic diameter of the NP, which was diluted with DIW, LSW and SSW to obtain 1 g/L NP concentration. NFs prepared in DIW and LSW showed almost similar particle size (the average size for the three temperatures, 25, 50 and 80 °C was about 38.4 ± 0.6 nm). In SSW, NPs displayed higher particle size of around 57 nm (25 and 50 °C) and about 88 nm at 80 °C. For higher salinity (SSW), the average size at all temperatures was about 67 ± 0.3 nm, which is approximately 43% higher than the average particle size for all tested temperatures with DIW and LSW. One possible reason for the difference in the measured zeta potential may be the compression of the double layer at higher salinity. The measured surface zeta potential at 25 °C for the NFs prepared in SSW was about −6.4 mV compared with −30.73 and −12.13 mV for DIW and LSW, respectively. Griffith, et al. [48] stated a similar observation for DP9711 NFs. They observed that increasing the brine salinity did not immediately increase particle size but that, after a certain point in time, a sudden rise in particle size was seen. To address particle size and stability, DLS measurements were repeated after three months from the preparation time. These tests showed that all measurements were close to the initial measured values (within 5 nm). In addition, the NFs remained visually clear with no sign of sedimentation.

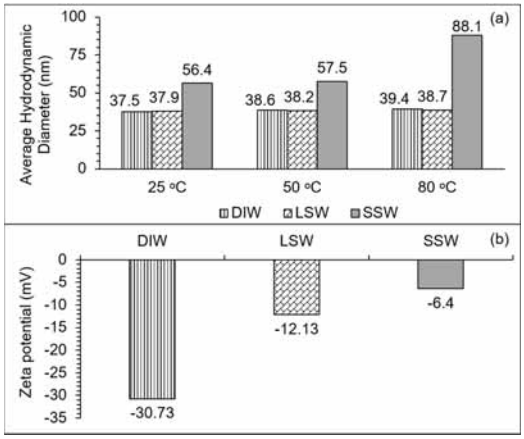


**Figure 2.** (**a**) Average particle size of the NPs dispersed in deionized water (DIW), low salinity water (LSW) and synthetic seawater (SSW) measured at varying temperatures. (**b**) Zeta potential measurements (25 °C) of the NPs in DIW, LSW and SSW.

### *3.2. Isothermal Static Adsorption*

Static adsorption tests of NPs on a calcite surface were conducted with DIW and SSW. Figure 3a shows that the adsorption of the NPs on the calcite surface increases with the NP concentration. Figure 3a also shows that at a lower concentration of NPs prepared in SSW, adsorption is higher than in DIW (≈40%). At higher NP concentrations, however, adsorption in SSW and DIW was almost the same. Monafred, et al. [34] have reported an increase in adsorption of unmodified silica NPs on a calcite surface with increasing salinity (0–0.2 M) of single salt (NaCl) brine at low NP concentrations (0.4 and 0.6 g/L).

Zeta potential of the NPs becomes less negative in the presence of SSW ions (Figure 2) owing to the compression of the double layer. This would lower the electrostatic repulsion and enhance the adsorption. Figure 3b shows an SEM image of a chalk core which was vacuum-treated with 1 g/L NF prepared in DIW. The image was taken along the injection plane. In DIW, the average size of NPs is about 38 nm (at 25 °C). However, some of the NPs may have been agglomerated during handling. In general, NPs are shown to be spread on the chalk surface in a similar way to the observations made by Monafred, et al. [34]. No pore throat blockage was observed from SEM imaging. The SEM images were done on spots along horizontally cut core. However, they are small fractions of the whole core.

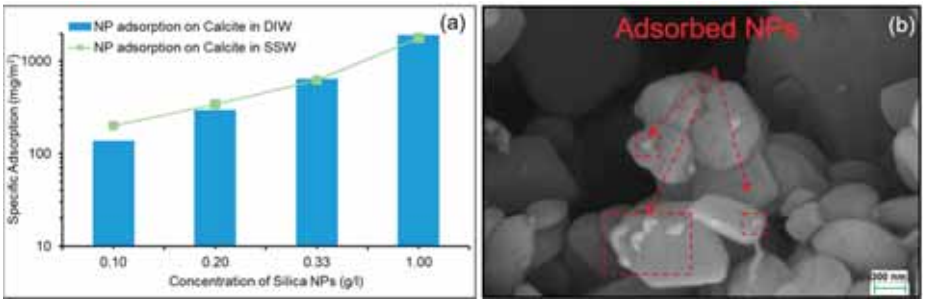


**Figure 3.** (**a**) Adsorption of silica NPs on Calcite surface. (**b**) SEM image of NPs adsorbed on chalk core with DP 9711 nanofluid at 1 g/L concentration prepared in DIW.

### *3.3. Dynamic Adsorption*

This section deals with the dynamic adsorption of NPs in chalk and its effect on fluid/rock interactions. Three salinities: DIW, LSW and SSW were used in the dynamic tests as outlined in Section 2.3. The adsorption/transport behavior of the used Silica NPs (DP9711) in sandstones has been addressed previously by some researchers [17,45,49]. They generally reported low adsorption of NPs on sandstone minerals. To best our knowledge, the adsorption behavior of Silica NPs in chalk and its effect on fluid rock interactions has not been addressed previously. The first test (SK1), was done with a core saturated with DIW. After several PVs pre-flush with DIW, a 1.5 PV slug containing LiCl tracer (0.1 M) and NPs (1 g/L) was injected into the core, followed by post-flush with DIW. The effluent fluid was analyzed for the concentrations of NP, Ca and Li (tracer). The results are presented in Figure 4. As shown, a difference of about 1 PV between the peak concentration of the tracer and the peak concentration of NPs. It was also observed that the tracer peak concentration declined faster than that for the NPs. The delay of NP decline may indicate interaction between the NP and core surface. After about 11 PV of injection (from the start), the NP concentration showed a linear increase, while the Li declined to a level close to zero concentration. The increased of NPs' concentration after 11 PV, may indicate the NPs' desorption.

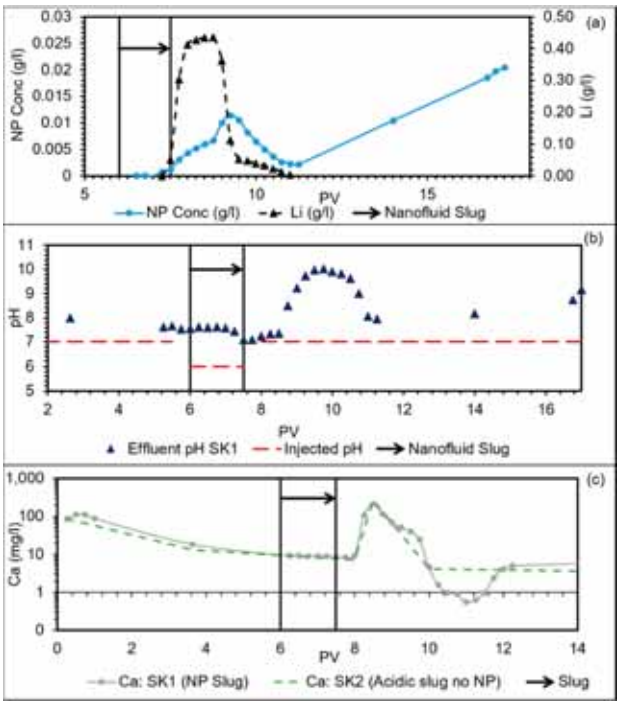


**Figure 4.** (**a**) NP and tracer concentration profile for SK1. (**b**) Effluent pH profile for SK1 (**c**) Effluent Ca concentration for SK1 (with NPs) and SK2 (without NPs).

Now the question is, why did the NP concentration decline below 0.01 g/L before the start of the desorption process (at ≈11 PV)? The adsorption/desorption process may be related to the pH of post flowing fluid in contact with calcite surface and adsorbed NPs. The effluent pH profile for core SK1 is shown in Figure 4b. It is shown that the pH after nanofluid slug increased steadily for approximately 1 PV, and then steeply increased to a pH of about 10, before it started to decline to reach

a pH of about 8.6. The highest pH coincided with the peak concentration of NP in the effluent and the desorption of NP from 11 PV (Figure 4a) coincided with the steady increase of the pH from about 8 to about 9. Equation (1) may explain the associated increase of pH with calcite dissolution.

$$CaCO_3(\text{calcite}) + H_2O \rightarrow Ca^{2+} + HCO_3^- + OH^- \quad (1)$$

Therefore, as calcite dissolves, the pH increases. Increase of the pH increases the dissolution of NPs ($SiO_2$) according to the following equations:

$$SiO_2(s) + 2H_2O \leftrightarrow H_4SiO_4 \quad (2)$$

$$H_4SiO_4 \leftrightarrow H_3SiO_4^- + H_3O^+ \quad (3)$$

Equation (2) shows the dissolution of $SiO_2$. Stumm and Morgan [50] stated that $SiO_2$ solubility increases at neutral to slightly alkaline pH ranges according to the above equation, producing silicic acid, which is a weak acid. Silicic acid further dissociates and reduces the pH (Equation (3)). The progression of this equation may have reduced the effluent pH, as shown in Figure 4b. The reduction of the pH to 8, may have resulted in more adsorption of NP on the calcite surface, hence reduced the produced NPs in the effluent (Figure 4a). As the pH started to increase, desorption of NPs increased.

The increase of the pH from about 8 till about 9 at the termination point of the experiment (PV $\approx$ 18) may be caused by calcite dissolution by Equation (1). These observations may be summarized as: maximum NP concentration in the effluent occurred at the highest pH ($\approx$10) of this experiment. As the pH declined, less concentration of NPs were detected in the effluent until NPs reached minimum at 11 PV (pH $\approx$ 8), after which, NP started to rise again and to reach 0.03 g/L (at the time of the experimental termination). This counts for about 50% higher than the peak concentration of 0.02 g/L. The dissolution of calcite can be inferred from the effluent calcium concentration profiles. Since the injected fluid did not contain any calcium, the effluent calcium observed may be attributed to the calcite dissolution by Equation (1). A second test (SK2) was done without NPs to provide a baseline for comparing the calcite dissolution in SK1. The pH of the slug without NPs in SK2 was adjusted to be at the same pH level as that of nanofluid in SK1. The calcium concertation in the effluent from test SK1 (with NP) and SK2 (without NP) is shown in Figure 4c. Calcite dissolution could be detrimental to chalk matrix integrity, causing severe subsidence and this is a major concern for the operators of chalk reservoirs. It is interesting to observe that calcium concentration during tests of SK1 and SK2, Figure 4c, there is no significant difference between the Ca in the two cases during DIW pre-flush. However, after the slug injection, the difference in the trend of Ca for the two experiments started to increase. At 10–12 PV in the case of test fluid with NP the calcium concentration was about 80% less than that for the fluid without NP.

The general mechanism may, then, be deduced as follow: the dissolution of calcite increases the pH, which in turn reduces NP adsorption on the calcite surface. Monfared, Ghazanfari, Jamialahmadi and Helalizadeh [34] have made similar observation where increasing the pH from around 7.5 to 10 reduced the adsorption of silica NPs on the calcite surface by about 33.33%. As mentioned earlier, effluent calcium was reduced by about 80% for brine with NPs. As the pH increases, the layer closer to the calcite surface becomes less positive, so that NP adsorption decreases. As observed, more NPs were produced when the pH reached about 10, with peak concentration at pH $\approx$ 10. $SiO_2$ dissolves in the alkaline range of the pH (Equation (2)). Dissociation of silicic acid (Equation (3)) increases the negative ions and thereby reduces the adsorption process. In addition, the dissociation of (weak) silicic acid slightly increases the acidity of the solution, which may again increase the adsorption of NPs. The greater the NPs' adsorption, the faster the pH decline, as observed in Figure 4a. As the desorption process proceeded, the pH steadily increased until it reached about 9, which was the point where the experiment was terminated. It is estimated that the adsorbed on the chalk about 0.46 mg per gram of

chalk. This was obtained from the integrated area under the curve (Figure 4a) and the injected NPs. This process was investigated further in saline environments by injecting SSW as base fluid in SK3 and LSW as base fluid in SK4. In SK3 test, both the pre-flush and post-flush was performed with SSW. The nanofluid slug with tracer was also prepared in SSW. The results for the test SK3 are shown in Figure 5.

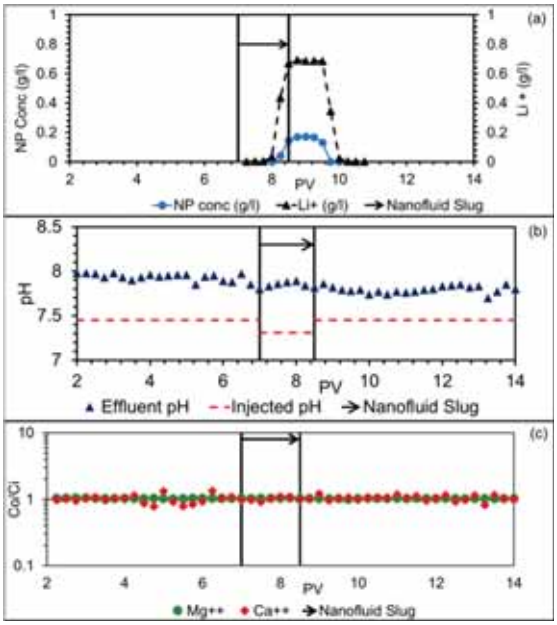


**Figure 5.** (**a**) NP and tracer concentration profile, (**b**) effluent pH profile and (**c**) effluent $Ca^{2+}$ and $Mg^{2+}$ concentration for SK3 in SSW.

It can be seen in Figure 5a that unlike in test SK1, the NP concentration profile for test SK3 follows the tracer profile closely. In addition, the NP production stops about 0.25 PV before the tracer. That is unlike SK1, no NP was detected in the effluent after the unreacted tracer has passed through the chalk core. This together with high adsorption of the NPs observed in SSW during static adsorption experiments may indicate strong irreversible adsorption of the NPs on the chalk surface. Integrating the area under the curve in Figure 5a and comparing it to the known amount of NPs injected into the core showed that about 86% of NPs were adsorbed on the chalk surface. Further, the effluent pH and ion concentration profiles for test SK3 in SSW are shown in Figure 5b,c respectively. At elevated salinity conditions in SK3, the chalk surface and the contacting fluid is at equilibrium [43] and therefore ionic activity due to fluid/rock interaction was expected to be low. For ease of comparison, the effluent concentration (Co) was normalized with respect to the injected concentration (Ci). It can be seen that pH remains almost constant throughout test SK3 and the ion ($Ca^{2++}$ and $Mg^{2++}$) concentration in the effluents remain close to injected concentration. This forms the baseline for comparing the behavior at low salinity condition in the next test SK4. In test SK4, both the pre-flush and post flush was performed with LSW. The nanofluid slug with tracer was also prepared in LSW. The results for test SK4 are shown in Figure 6.

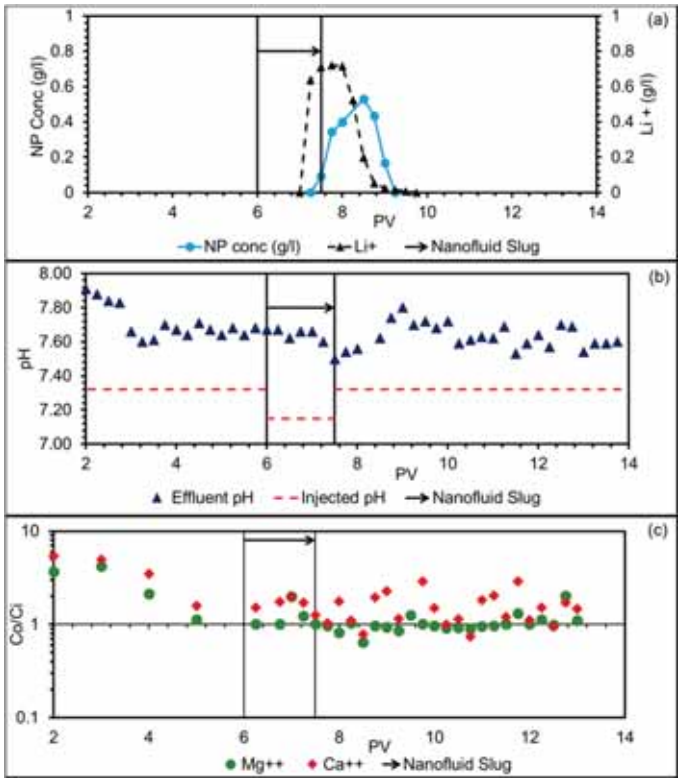


**Figure 6.** (**a**) NP and tracer concentration profile, (**b**) effluent pH profile and (**c**) effluent $Ca^{2+}$ and $Mg^{2+}$ concentration for SK4 in LSW.

It can be seen in Figure 6a that with LSW, the NP breakthrough is delayed by 0.25 PV as compared to the unreacted tracer. In addition, the NP production continues after the tracer production stops. This is similar to test SK1 (ion free) and may indicate desorption of the NPs. It was estimated that 67.2% of the NPs were adsorbed in the core in SK4 as compared to 86.2% in SK3. At low salinity conditions in SK4, the NP concentration profile is similar to DIW. This together with the high irreversible adsorption observed with SSW indicates that salinity strongly influences the adsorption behavior of the NPs on the chalk surface. The effluent pH profile for test SK4 shown in Figure 4c shows a sharp rise in pH with NP production and the pH peak coincides with peak NP production. Thereafter the desorption of NPs during the decline phase can be attributed to the dissolution of the NPs which produces a weak silicic acid as per Equations (2) and (3). This supports the NP adsorption/desorption mechanism proposed previously. However, the linear rise of NPs production in the effluents as observed with DIW (Figure 4a) was not observed with LSW in SK4. This may be due the heavy dissolution of chalk due to DIW in SK1 which significantly raised the pH to 10. The effluent $Ca^{2+}$ and $Mg^{2+}$ profiles shown in Figure 6c. The high levels of $Ca^{2+}$ in the pre flush stage suggest high calcite dissolution. However, after the adsorption of NPs on the chalk surface, the $Ca^{2+}$ falls by about 30%. In addition, the $Mg^{2+}$ levels fall below the injected concentration during the post flush. This may be due to the incorporation of magnesium into the calcite structure. This is discussed in detail in the later section.

From the results so far from static and dynamic adsorption of NPs on chalk surface (in the absence of oil phase) indicated that NP adsorption in chalk could significantly reduce calcite dissolution

induced by low salinity injection. However, for the application of NPs to petroleum reservoirs, it is essential to study the effect of NPs on chalk surface that is oil wet and the effect of NPs in the presence of oil phase. This is addressed in the following section.

### *3.4. NPs Interaction with Chalk Mineral in Presence of Hydrocarbon*

Nanofluid are prepared in brines and some studies have investigated the combined role of salinity and NPs on the wettability change process [51] and NP adsorption on mineral surfaces [52]. Hendraningrat and Torsæter [51] stated that nanofluid flooding is sensitive to water salinity especially in the presence of divalent ion ($Ca^{2+}$ and $Mg^{2+}$). The effect of injection brine salinity on the recovery process has been well documented in the literature [36,39,53–56]. As discussed in the previous section, the adsorption of NPs on the mineral surface alters the rock surface hence fluid/rock interactions. The experiments were divided into two stages with brine alone and NPs dispersed in the selected brine. The injection was performed at lower flowrates that are closer to real field cases and to give the injected fluid sufficient residence time in the core for the interaction. Hamouda and Maevskiy [43] and Hamouda and Gupta [41] previously studied the effect of low salinity composition on primary and secondary recovery in SK chalk by systematically diluting the SSW. They found that LSW at a 1:10 SSW dilution was the optimum for the investigated brines for EOR. Therefore, LSW 1:10 dilution of SSW is used here.

In the SK5 case, both primary and secondary stage the injection of the fluid was SSW. For the secondary stage, however, silica NPs (DP 1 g/L) was mixed with SSW. In SK6, primary stage was performed with LSW followed by injection of NF (DP 1 g/L) prepared in LSW. The third scenario was for SK7, where primary stage SSW was used, followed by NF prepared in LSW (DP 1 g/L). Those three scenarios represent the various possible combinations.

The effluent pH profiles were recorded for the SK5, SK6 and SK7 and are shown in Figure 7. For SK5 (all SSW), the effluent pH during primary and secondary stages were lower than the pH of the injected SSW. This observation is similar to that previously made by Hamouda and Maevskiy [43]. In the case of SK6 (LSW and LSW with NPs) however, an interesting behavior was observed. The effluent pH was higher than the injection pH and continued rising until it stabilized at about 7.8. Increasing the flow rate to 16 PV/day led to a slight increase in pH to around 7.95, after which it stabilized at around 7.91. The increase in pH may be explained by calcite dissolution, in accordance with the Equation (1).

The pH in the case of SK7 (SSW and LSW with NPs) shows that the pH remained below the injected pH in primary stage. However, the pH increased slightly to about 7.56 when the injection was switched to LSW with NF. When the NF injection rate was increased to 16 PV/day, the pH of SK6 and SK7 stabilized at about 8.06 and 7.75, respectively. As expected, the pH was higher for SK6 case than in the case of SK7.

The concentrations of $Ca^{2+}$ and $Mg^{2+}$ in the effluents of SK5-7 are plotted in Figure 8. For ease of comparison, effluent concentration (Co) was normalized with respect to the injected concentration (Ci). Figure 8a shows that the $Ca^{2+}$ effluent in SK5 was lower than the injected concentration during primary stage and even more so during secondary stage. This may indicate slight calcite dissolution with high injection salinity (SSW). This observation was also supported by the low pH recorded for this SK5 in Figure 7a. The $Mg^{2+}$ concentration in effluent was close to the injected concentration. Where the SK6 (all LSW) is concerned, however, the $Ca^{2+}$ ion concentration during primary stage by LSW was consistently higher, indicating calcite dissolution similar to the observation made during dynamic adsorption experiments in SK4. This observation is supported by the high pH recorded during this stage in Figure 7b. Along with the excess $Ca^{2+}$, there was a deficiency of $Mg^{2+}$ in the effluent. It is well established that calcite has a tendency to accommodate $Mg^{2+}$ in its structure [50]. The exchange

between $Ca^{2+}$ and $Mg^{2+}$ may lead to the formation of complex calcium/magnesium minerals with different ratios. The following reaction is for a 1:1 ratio (dolomite):

$$2CaCO_{3(s)} + Mg^{2+} \rightarrow CaMg(CO_3)_2 + Ca^{2+} \quad (4)$$

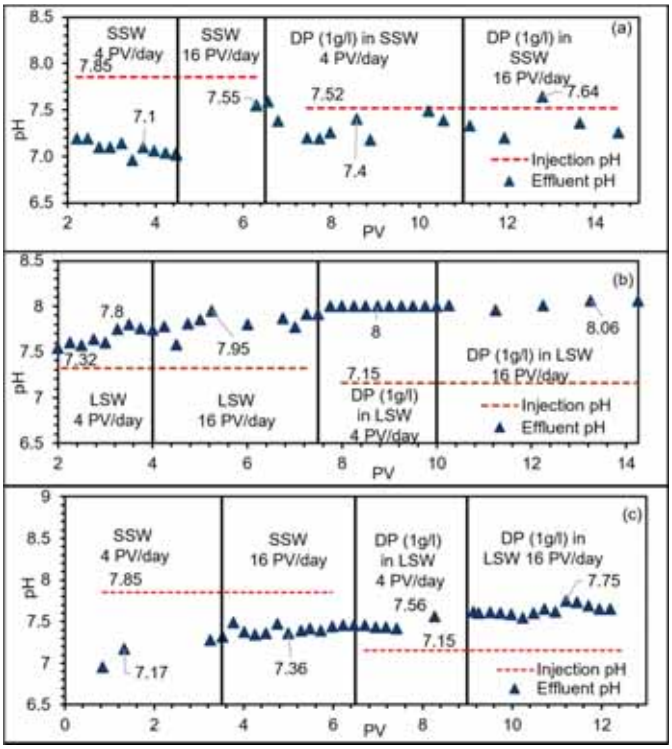


**Figure 7.** Effluent pH profiles for SK5-SSW (**a**), SK6-LSW (**b**) and SK7-mixed (**c**).

Dolomitization has been previously observed by Petrovich and Hamouda [57] in the chalk formations of the Ekofisk field. During primary stage by LSW, the ratio of the effluent ion concentration to the injected concentration reached 6.267 and 0.686 for $Ca^{2+}$ and $Mg^{2+}$ respectively at 16 PV/day. When SK6 was switched to NF prepared in LSW, the ratio of $Ca^{2+}$ to injected concentrations fell to 4.26 at the injection rate of 4 PV/day. Increasing the rate to 16 PV/day raised the $Ca^{2+}$ concentration slightly to 4.63, which is still below the $Ca^{2+}$ concentration during primary stage by LSW. This reduction in $Ca^{2+}$ during NF injection (almost 30%) coincided with a comparative increase in levels of $Mg^{2+}$ to 0.86 at 4 PV/day and 0.85 at 16 PV/day. These observations may indicate a reduction in calcite dissolution and the formation of calcium/magnesium minerals. The increased amount of $Mg^{2+}$ was not significant enough to indicate reduced magnesium/calcium exchange. It is therefore possible that the reduction in $Ca^{2+}$ was caused by reduced calcite dissolution during NF injection. Increasing the rate to 16 PV/day, the $Ca^{2+}$ concentration stabilized at around 4.6. This also represents a 25% reduction of $Ca^{2+}$ production compared with the 4 PV/day flow rate during primary stage. With primary stage in the SK7 case, the effluent ion concentration profiles were close to the injected concentration. When the SK7 was switched to NF prepared in LSW, the $Ca^{2+}$ and $Mg^{2+}$ ions were initially high. Two main possibilities exist for the increase of $Ca^{2+}$ and $Mg^{2+}$: (1) production of trapped SSW from the first stage

and/or (2) dissolution of possible calcium sulfate formed during the first stage. The latter may sound more realistic because of a rapid reduction in $Ca^{2+}$ and $Mg^{2+}$ concentrations. Thereafter, the $Ca^{2+}$ concentration was around 1.5 at 4 PV/day. The $Ca^{2+}$ concentration during this stage is almost three times lower than at the same stage in SK6. When increasing the injection rate to 16 PV/day, the $Ca^{2+}$ concentration fluctuates between 2.9 and 1.16. This concentration at 4 PV/day is almost three times lower than during the same stage in SK6. The differential pressure drop (dP) data recorded for SK5-7 is shown in Figure 9.

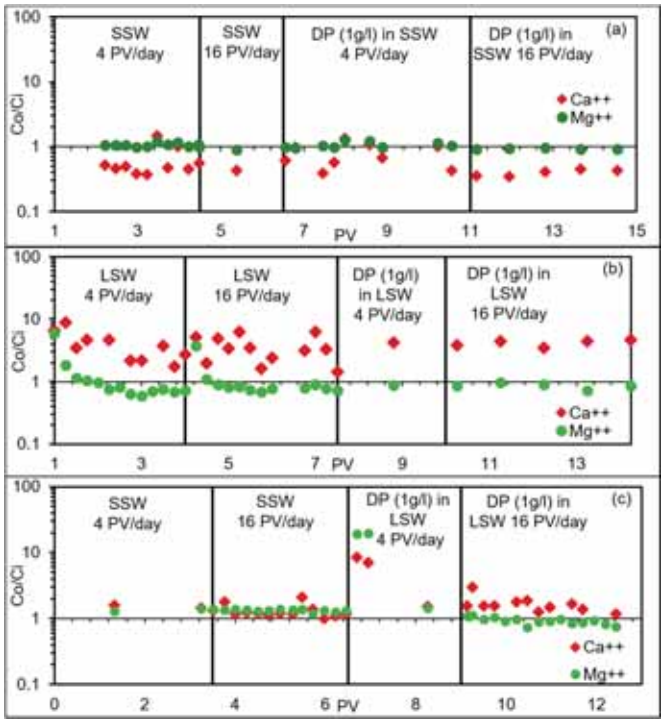


**Figure 8.** Effluent $Ca^{2+}$ and $Mg^{2+}$ concentrations for SK5-SSW (**a**), SK6-LSW (**b**) and SK7-mixed (**c**).

At 4 PV/day with SSW injection in SK5, the pressure drop stabilized at about 1.79 bar. When the injection rate was increased to 16 PV/day, the dP increased and stabilized at around 3.70 bar. After the injection fluid was switched to NF prepared in SSW, the pressure rose steadily from 0.68 to 2.17 bar. van Oort, et al. [58] stated a general rule of thumb that, if the particle size of the suspended solids exceeds one-third of the pore diameter, the particles will cause plugging behavior. The average pore size of the SK chalk used in this study is around 200 nm [59]. The size of the NPs in SSW was shown earlier to be 88.1 nm at 80 °C. It is possible that some of the smaller pore throats are blocked by the NPs. For SK6 however, the recorded dP for NF (in LSW) was 0.439 bar, which is almost three times lower than the dP recorded for LSW injection in the first stage. The measured particle size of the NPs in LSW is about 38 nm, which is significantly lower than the average pore throat of the chalk used. The recorded dP at 16 PV/day was slightly higher for the NF compared with LSW alone. However, the difference ($\approx$0.04 bar) is within the uncertainty range of the measured dP ($\pm$0.1 bar). The resistance to flow was therefore lower at the low flow rate. A similar observation was made with SK7 where, at the lower flow rate (4 PV/day), the dP during NF injection was less than half that from SSW injection.

However, the pressure drop at the higher flow rate was slightly (≈0.5 bar) higher during NF injection, with a decreasing trend. The decreasing pressure trend observed in SK7 during 16 PV/day injection of nanofluid was not observed for the same stages in flood SK5 and 6 wherein the salinity of the fluid was constant throughout the experiment, with only addition of NPs. However, in SK7, the fluid salinity is switched from SSW to LSW (with NP). Two mechanisms take place: (1) adsorption of NP on the chalk surface, hence reduced calcite dissolution and (2) disturbance of fluid rock equilibrium due to low salinity. As the injection rate is increased to 16 PV/day, the swept region with LSW + NPs increased, hence reduced pressure. This is evident in Figure 8c wherein at 16 PV/day, a decreasing trend in $Ca^{2+}$ production was observed. The decrease in $Ca^{2+}$ may be explained based on reduced dissolution of calcite and dilution factor due to increased sweep. In addition to the main objective, an incremental oil obtained from nanofluid injection in SK5-7 as shown in Figure 10. As mentioned earlier, the recovery here is not optimized to account properly for EOR, but as a matter of observation compared to our previous studies with LSW alone.

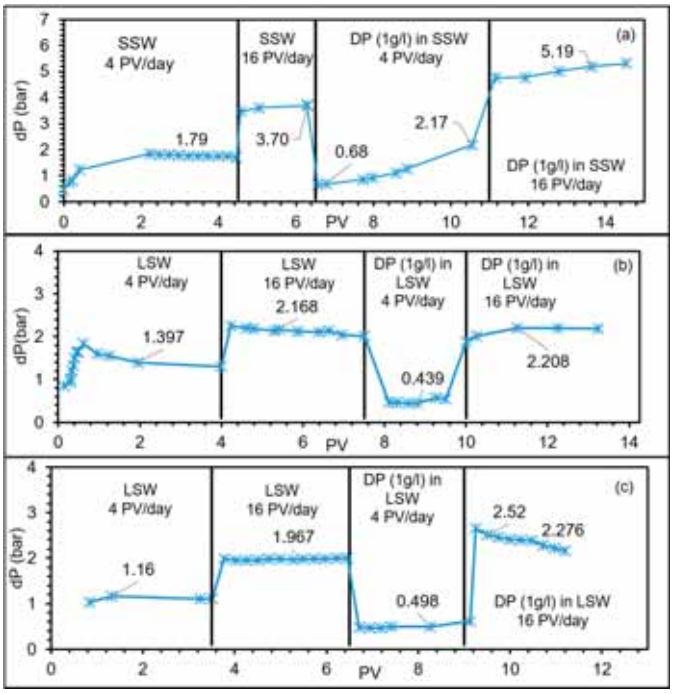


**Figure 9.** Differential pressure drop (dP) profile for SK5-SSW (**a**), SK6-LSW (**b**) and SK7-mixed (**c**).

The incremental recovery was greater in the case of SK6 (0.824%) than with SK5 (0.15%). The highest incremental recovery was observed when the fluid was switched to NF prepared in LSW (1.05% for SK7 experiment).

In summary, the results from this work suggests a possible synergistic effect between low salinity flooding and silica nanoparticles wherein adding a relatively small amount of silica nanoparticles to the injected water can improve the flood performance and reduce the risk of disturbing the integrity of the chalk. Seawater has been injected as a primary recovery EOR method in most of North Sea oil fields. LSW injection for enhanced oil recovery could disturb the chalk integrity due to calcite dissolution. This is a major concern for chalk reservoir operators. As outcome of this work by incorporating silica NPs in the injected water encourages applying LSW. The current work is done with model oil in order

to investigate the potential for field application. However, as demonstrated here it is dependent on fluid composition i.e., we recommend test related to each individual field fluid.

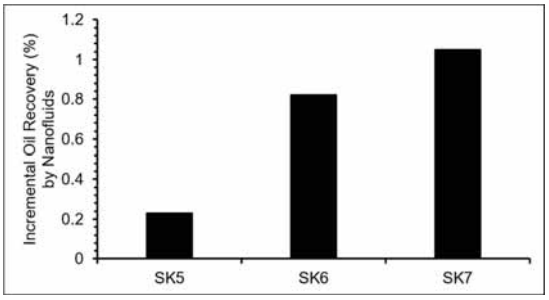


**Figure 10.** Tentative observation of incremental recovery from SK5-SSW, SK6-LSW and SK7-mixed.

## 4. Conclusions

This work addresses static and dynamic adsorption of silica NPs on chalks and their fluid/rock interactions during low salinity flowing tests. Based on the results from this study the following conclusions can be stated:

1. Silica NPs showed an adsorption affinity to calcite surface. Salinity was shown to enhance the adsorption by about 40%.
2. Dynamic adsorption of the NPs in the chalk core showed high irreversible adsorption at elevated salinity (SSW) and desorption of NPs was observed in low salinity and ion free condition.
3. Adsorption/desorption mechanisms for the NPs have been proposed. Further, it can be concluded that NPs adsorption during these experiments led to significant reduction of calcite dissolution both in DIW and LSW.
4. In spite of the NPs affinity to adsorb on the chalk surface, no pore throat blockage was observed from SEM imaging. The SEM images were done on spots along horizontally cut core. However, they are small fractions of the whole core. Further the differential pressure drop across the chalk core during nanofluid injection also indicated reduced resistance to flow wherein lower pressure drop was recorded, compared to with injection of LSW alone.
5. The nanofluid at 1 g/L prepared in LSW reduced the produced calcium ion concentration by about 30% as compared to the case of LSW alone. This indicates that silica NF hinders calcite dissolution i.e., has less effect on chalk matrix integrity which is one of the major concern in chalk reservoir, if low salinity for EOR is to be employed.
6. The combination of silica NPs with low salinity EOR technique reduces the risk of matrix integrity loss and the subsidence degree of the water flooded chalk.

**Author Contributions:** A.A.H. and R.A. designed the study. The experiments were performed by A.A. and R.A. The analysis was done by all three authors. The manuscript was written by A.A.H. and R.A.

**Funding:** This research received no external funding.

**Acknowledgments:** The authors would like to thank the University of Stavanger (UiS), Norway, for funding this work. The authors thank Mona W. Minde (UiS) for help with SEM imaging, Lutz Eichacker (UiS) for providing access to DLS equipment. The authors would like to thank Inger Johanne M.-K. Olsen (UiS) for acquiring chemicals used in this study. In addition, the authors would like to thank Kim Andre Vorland and Krzysztof I. Nowicki (both UiS) for helping with the flooding setup. Finally, the authors would like to thank NYACOL® Nano Technologies Inc for supplying the nanofluid used in this study.

**Conflicts of Interest:** The authors declare no conflict of interest. The funding sponsors had no role in the design of the study; in the collection, analyses, or interpretation of data; in the writing of the manuscript, and in the decision to publish the results.

## References


1. Ayatollahi, S.; Zerafat, M.M. Nanotechnology-Assisted Eor Techniques: New Solutions to Old Challenges. In Proceedings of the SPE International Oilfield Nanotechnology Conference and Exhibition, Noordwijk, The Netherlands, 12–14 June 2012; Society of Petroleum Engineers: Richardson, TX, USA, 2012.
2. Zhang, H.; Nikolov, A.; Wasan, D. Enhanced oil recovery (eor) using nanoparticle dispersions: Underlying mechanism and imbibition experiments. *Energy Fuels* **2014**, *28*, 3002–3009. [CrossRef]
3. Saboorian-Jooybari, H.; Dejam, M.; Chen, Z. Heavy oil polymer flooding from laboratory core floods to pilot tests and field applications: Half-century studies. *J. Pet. Sci. Eng.* **2016**, *142*, 85–100. [CrossRef]
4. Chávez-Miyauchi, T.S.E.; Firoozabadi, A.; Fuller, G.G. Nonmonotonic elasticity of the crude oil–brine interface in relation to improved oil recovery. *Langmuir* **2016**, *32*, 2192–2198. [CrossRef] [PubMed]
5. Suleimanov, B.; Ismailov, F.; Veliyev, E. Nanofluid for enhanced oil recovery. *J. Pet. Sci. Eng.* **2011**, *78*, 431–437. [CrossRef]
6. Fletcher, A.; Davis, J. How eor can be transformed by nanotechnology. In Proceedings of the SPE Improved Oil Recovery Symposium, Tulsa, OK, USA, 24–28 April 2010; Society of Petroleum Engineers: Richardson, TX, USA, 2010.
7. Hendraningrat, L.; Li, S.; Torsæter, O. A coreflood investigation of nanofluid enhanced oil recovery. *J. Pet. Sci. Eng.* **2013**, *111*, 128–138. [CrossRef]
8. Maghzi, A.; Mohammadi, S.; Ghazanfari, M.H.; Kharrat, R.; Masihi, M. Monitoring wettability alteration by silica nanoparticles during water flooding to heavy oils in five-spot systems: A pore-level investigation. *Exp. Therm. Fluid Sci.* **2012**, *40*, 168–176. [CrossRef]
9. Li, S.; Torsæter, O. Experimental investigation of the influence of nanoparticles adsorption and transport on wettability alteration for oil wet berea sandstone. In Proceedings of the SPE Middle East Oil & Gas Show and Conference, Manama, Bahrain, 8–11 March 2015; Society of Petroleum Engineers: Richardson, TX, USA, 2015.
10. Behzadi, A.; Mohammadi, A. Environmentally responsive surface-modified silica nanoparticles for enhanced oil recovery. *J. Nanopart. Res.* **2016**, *18*, 1–19. [CrossRef]
11. Hendraningrat, L.; Torsæter, O. A stabilizer that enhances the oil recovery process using silica-based nanofluids. *Transp. Porous Media* **2015**, *108*, 679–696. [CrossRef]
12. Ogolo, N.; Olafuyi, O.; Onyekonwu, M. Enhanced oil recovery using nanoparticles. In Proceedings of the SPE Saudi Arabia Section Technical Symposium and Exhibition, Al-Khobar, Saudi Arabia, 8–11 April 2012; Society of Petroleum Engineers: Richardson, TX, USA, 2012.
13. Shahrabadi, A.; Bagherzadeh, H.; Roostaie, A.; Golghanddashti, H. Experimental investigation of hlp nanofluid potential to enhance oil recovery: A mechanistic approach. In Proceedings of the SPE International Oilfield Nanotechnology Conference and Exhibition, Noordwijk, The Netherlands, 12–14 June 2012; Society of Petroleum Engineers: Richardson, TX, USA, 2012.
14. Ortega, D.J.S.; Kim, H.B.; James, L.A.; Johansen, T.E.; Zhang, Y. The effectiveness of silicon dioxide sio 2 nanoparticle as an enhanced oil recovery agent in ben nevis formation, hebron field, offshore eastern canada. In Proceedings of the Abu Dhabi International Petroleum Exhibition & Conference, Abu Dhabi, UAE, 7–10 November 2016; Society of Petroleum Engineers: Richardson, TX, USA, 2016.
15. Haroun, M.R.; Alhassan, S.; Ansari, A.A.; Al Kindy, N.A.M.; Abou Sayed, N.; Kareem, A.; Ali, B.; Sarma, H.K. Smart nano-eor process for abu dhabi carbonate reservoirs. In Proceedings of the Abu Dhabi International Petroleum Conference and Exhibition, Abu Dhabi, UAE, 11–14 November 2012; Society of Petroleum Engineers: Richardson, TX, USA, 2012.
16. Agista, M.; Guo, K.; Yu, Z. A state-of-the-art review of nanoparticles application in petroleum with a focus on enhanced oil recovery. *Appl. Sci.* **2018**, *8*, 871. [CrossRef]
17. Zhang, T.; Murphy, M.J.; Yu, H.; Bagaria, H.G.; Yoon, K.Y.; Nielson, B.M.; Bielawski, C.W.; Johnston, K.P.; Huh, C.; Bryant, S.L. Investigation of nanoparticle adsorption during transport in porous media. *SPE J.* **2015**, *20*, 667–677. [CrossRef]
18. Zhang, T.; Murphy, M.; Yu, H.; Huh, C.; Bryant, S.L. Mechanistic model for nanoparticle retention in porous media. *Transp. Porous Media* **2016**, *115*, 387–406. [CrossRef]
19. Li, S.; Torsæter, O. The impact of nanoparticles adsorption and transport on wettability alteration of water wet berea sandstone. In Proceedings of the SPE/IATMI Asia Pacific Oil & Gas Conference and Exhibition, Nusa Dua, Bali, Indonesia, 20–22 October 2015; Society of Petroleum Engineers: Richardson, TX, USA, 2015.

20. Al-Anssari, S.; Wang, S.; Barifcani, A.; Lebedev, M.; Iglauer, S. Effect of temperature and sio 2 nanoparticle size on wettability alteration of oil-wet calcite. *Fuel* **2017**, *206*, 34–42. [CrossRef]
21. Roustaei, A.; Bagherzadeh, H. Experimental investigation of sio2 nanoparticles on enhanced oil recovery of carbonate reservoirs. *J. Pet. Explor. Prod. Technol.* **2015**, *5*, 27–33. [CrossRef]
22. Abhishek, R.; Kumar, G.S.; Sapru, R. Wettability alteration in carbonate reservoirs using nanofluids. *Pet. Sci. Technol.* **2015**, *33*, 794–801. [CrossRef]
23. Abhishek, R.; Bagalkot, N.; Kumar, G.S. Effect of transverse forces on velocity of nanoparticles through a single fracture in a fractured petroleum reservoir. *Int. J. Oil Gas Coal Technol.* **2016**, *12*, 379–395. [CrossRef]
24. Nwidee, L.N.; Al-Anssari, S.; Barifcani, A.; Sarmadivaleh, M.; Lebedev, M.; Iglauer, S. Nanoparticles influence on wetting behaviour of fractured limestone formation. *J. Pet. Sci. Eng.* **2017**, *149*, 782–788. [CrossRef]
25. Nazari Moghaddam, R.; Bahramian, A.; Fakhroueian, Z.; Karimi, A.; Arya, S. Comparative study of using nanoparticles for enhanced oil recovery: Wettability alteration of carbonate rocks. *Energy Fuels* **2015**, *29*, 2111–2119. [CrossRef]
26. Al-Anssari, S.; Barifcani, A.; Wang, S.; Iglauer, S. Wettability alteration of oil-wet carbonate by silica nanofluid. *J. Colloid Interface Sci.* **2016**, *461*, 435–442. [CrossRef] [PubMed]
27. Li, S.; Hendraningrat, L.; Torsaeter, O. Improved oil recovery by hydrophilic silica nanoparticles suspension: 2 phase flow experimental studies. In Proceedings of the IPTC 2013: International Petroleum Technology Conference, Beijing, China, 26 March 2013.
28. Sharma, T.; Iglauer, S.; Sangwai, J.S. Silica nanofluids in an oilfield polymer polyacrylamide: Interfacial properties, wettability alteration, and applications for chemical enhanced oil recovery. *Ind. Eng. Chem. Res.* **2016**, *55*, 12387–12397. [CrossRef]
29. Al-Anssari, S.; Wang, S.; Barifcani, A.; Iglauer, S. Oil-water interfacial tensions of silica nanoparticle-surfactant formulations. *Tenside Surfactants Deterg.* **2017**, *54*, 334–341. [CrossRef]
30. Xu, K.; Zhu, P.; Colon, T.; Huh, C.; Balhoff, M. A microfluidic investigation of the synergistic effect of nanoparticles and surfactants in macro-emulsion-based enhanced oil recovery. *SPE J.* **2017**, *22*, 459–469. [CrossRef]
31. Binks, B.P.; Whitby, C.P. Nanoparticle silica-stabilised oil-in-water emulsions: Improving emulsion stability. *Coll. Surf. A Physicochem. Eng. Asp.* **2005**, *253*, 105–115. [CrossRef]
32. Sharma, T.; Kumar, G.S.; Chon, B.H.; Sangwai, J.S. Thermal stability of oil-in-water pickering emulsion in the presence of nanoparticle, surfactant, and polymer. *J. Ind. Eng. Chem.* **2015**, *22*, 324–334. [CrossRef]
33. Sharma, T.; Kumar, G.S.; Sangwai, J.S. Comparative effectiveness of production performance of pickering emulsion stabilized by nanoparticle–surfactant–polymerover surfactant–polymer (sp) flooding for enhanced oil recoveryfor brownfield reservoir. *J. Pet. Sci. Eng.* **2015**, *129*, 221–232. [CrossRef]
34. Monfared, A.D.; Ghazanfari, M.H.; Jamialahmadi, M.; Helalizadeh, A. Adsorption of silica nanoparticles onto calcite: Equilibrium, kinetic, thermodynamic and dlvo analysis. *Chem. Eng. J.* **2015**, *281*, 334–344. [CrossRef]
35. Hamouda, A.A.; Rezaei Gomari, K.A. Influence of temperature on wettability alteration of carbonate reservoirs. In Proceedings of the SPE/DOE Symposium on Improved Oil Recovery, Tulsa, OK, USA, 22–26 April 2006; Society of Petroleum Engineers: Richardson, TX, USA, 2006.
36. Hamouda, A.; Valderhaug, O.; Munaev, R.; Stangeland, H. Possible mechanisms for oil recovery from chalk and sandstone rocks by low salinity water (lsw). In Proceedings of the SPE Improved Oil Recovery Symposium, Tulsa, OK, USA, 12–16 April 2014; Society of Petroleum Engineers: Richardson, TX, USA, 2014.
37. Zahid, A.; Shapiro, A.A.; Skauge, A. Experimental studies of low salinity water flooding carbonate: A new promising approach. In Proceedings of the SPE EOR Conference at Oil and Gas West Asia, Muscat, Oman, 16–18 April 2012; Society of Petroleum Engineers: Richardson, TX, USA, 2012.
38. Mahani, H.; Keya, A.L.; Berg, S.; Bartels, W.-B.; Nasralla, R.; Rossen, W.R. Insights into the mechanism of wettability alteration by low-salinity flooding (lsf) in carbonates. *Energy Fuels* **2015**, *29*, 1352–1367. [CrossRef]
39. Al-Nofli, K.; Pourafshary, P.; Mosavat, N.; Shafiei, A. Effect of initial wettability on performance of smart water flooding in carbonate reservoirs—An experimental investigation with ior implications. *Energies* **2018**, *11*, 1394. [CrossRef]
40. Wang, X.; Alvarado, V. Kaolinite and silica dispersions in low-salinity environments: Impact on a water-in-crude oil emulsion stability. *Energies* **2011**, *4*, 1763. [CrossRef]
41. Hamouda, A.A.; Gupta, S. Enhancing oil recovery from chalk reservoirs by a low-salinity water flooding mechanism and fluid/rock interactions. *Energies* **2017**, *10*, 576. [CrossRef]

42. Rezaei Gomari, S.; Joseph, N. Study of the effect of clay particles on low salinity water injection in sandstone reservoirs. *Energies* **2017**, *10*, 322. [CrossRef]
43. Hamouda, A.A.; Maevskiy, E. Oil recovery mechanism (s) by low salinity brines and their interaction with chalk. *Energy Fuels* **2014**, *28*, 6860–6868. [CrossRef]
44. Abhishek, R.; Hamouda, A.A. Effect of various silica nanofluids: Reduction of fines migrations and surface modification of berea sandstone. *Appl. Sci.* **2017**, *7*, 1216. [CrossRef]
45. Singh, R.; Mohanty, K.K. Synergy between nanoparticles and surfactants in stabilizing foams for oil recovery. *Energy Fuels* **2015**, *29*, 467–479. [CrossRef]
46. Frykman, P. Spatial variability in petrophysical properties in upper maastrichtian chalk outcrops at stevns klint, denmark. *Mar. Pet. Geol.* **2001**, *18*, 1041–1062. [CrossRef]
47. Tabrizy, V.A.; Denoyel, R.; Hamouda, A. Characterization of wettability alteration of calcite, quartz and kaolinite: Surface energy analysis. *Coll. Surf. A Physicochem. Eng. Asp.* **2011**, *384*, 98–108. [CrossRef]
48. Griffith, N.; Ahmad, Y.; Daigle, H.; Huh, C. Nanoparticle-stabilized natural gas liquid-in-water emulsions for residual oil recovery. In Proceedings of the SPE Improved Oil Recovery Conference, Tulsa, OK, USA, 11–13 April 2016; Society of Petroleum Engineers: Richardson, TX, USA, 2016.
49. Murphy, M.J. Experimental Analysis of Electrostatic and Hydrodynamic Forces Affecting Nanoparticle Retention in Porous Media. Ph.D. Thesis, The University of Texas at Austin Department of Petroleum and Geosystems Engineering, Austin, TX, USA, 2012.
50. Stumm, W.; Morgan, J.J. Aquatic chemistry. In *An Introduction Emphasizing Chemical Equilibria in Natural Waters*; Wiley-Interscience: New York, NY, USA, 1970.
51. Hendraningrat, L.; Torsæter, O. A study of water chemistry extends the benefits of using silica-based nanoparticles on enhanced oil recovery. *Appl. Nanosci.* **2016**, *6*, 83–95. [CrossRef]
52. Dehghan Monfared, A.; Ghazanfari, M.H.; Jamialahmadi, M.; Helalizadeh, A. Potential application of silica nanoparticles for wettability alteration of oil–wet calcite: A mechanistic study. *Energy Fuels* **2016**, *30*, 3947–3961. [CrossRef]
53. Austad, T.; Shariatpanahi, S.; Strand, S.; Black, C.; Webb, K. Conditions for a low-salinity enhanced oil recovery (eor) effect in carbonate oil reservoirs. *Energy Fuels* **2011**, *26*, 569–575. [CrossRef]
54. Chukwudeme, E.; Hamouda, A. Oil recovery from polar components (asphaltene and sa) treated chalk rocks by low salinity water and water containing $so_4^{2-}$ and $mg^{2+}$ at different temperatures. *Coll. Surf. A Physicochem. Eng. Asp.* **2009**, *336*, 174–182. [CrossRef]
55. Yi, Z.; Sarma, H.K. Improving waterflood recovery efficiency in carbonate reservoirs through salinity variations and ionic exchanges: A promising low-cost "smart-waterflood" approach. In Proceedings of the Abu Dhabi International Petroleum Conference and Exhibition, Abu Dhabi, UAE, 11–14 November 2012; Society of Petroleum Engineers: Abu Dhabi, UAE, 2012.
56. Tang, G.; Morrow, N.R. Salinity, temperature, oil composition, and oil recovery by waterflooding. *SPE Reserv. Eng.* **1997**, *12*, 269–276. [CrossRef]
57. Petrovich, R.; Hamouda, A. Dolomitization of ekofisk oil field reservoir chalk by injected seawater. In Proceedings of the Ninth International Symposium on Water–Rock Interactions, Taupo, New Zealand, 30 March–3 April 1998.
58. Van Oort, E.; Van Velzen, J.; Leerlooijer, K. Impairment by suspended solids invasion: Testing and prediction. *SPE Prod. Facil.* **1993**, *8*, 178–184. [CrossRef]
59. Jolma, I.; Strand, D.; Stavland, A.; Fjelde, I.; Hatzignatiou, D. When size matters-polymer injectivity in chalk matrix. In Proceedings of the IOR 2017-19th European Symposium on Improved Oil Recovery, Stavanger, Norway, 24–27 April 2017.


**Adsorption of silica nanoparticles and its synergistic effect on fluid/rock interactions during low salinity flooding in sandstones.**

Abhishek, R., A. A. Hamouda and I. Murzin (2018).

Colloids and Surfaces A: Physicochemical and Engineering Aspects 555: 397-406. Elsevier Publications.

Paper III

Colloids and Surfaces A 555 (2018) 397–406

Contents lists available at ScienceDirect

Colloids and Surfaces A

journal homepage: www.elsevier.com/locate/colsurfa

# Adsorption of silica nanoparticles and its synergistic effect on fluid/rock interactions during low salinity flooding in sandstones

Rockey Abhishek, Aly. A. Hamouda*, Ivan Murzin

*Department of Energy and Petroleum Engineering, University of Stavanger, Stavanger, 4036, Norway*

## GRAPHICAL ABSTRACT

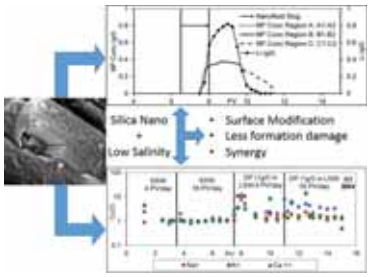


## ARTICLE INFO

*Keywords:*
Adsorption
Silica nanoparticles
Sandstone
fluid/rock interaction
EOR
Fines migration
LSW

## ABSTRACT

Several research works have shown the potential of incremental oil recovery by low salinity water (LSW) injection. The research in this area has also shown that LSW interaction with rock's mineral (sandstone and chalk) raises the potential for formation damage by produced fines. The objectives of this work are to address the adsorption of silica nanoparticles (NPs) on sandstone and their effect on fluid/rock interaction during LSW flooding. Isothermal static adsorption of NPs on sandstone minerals surfaces showed a higher adsorption affinity on quartz surface compared to kaolinite. This was also shown by scanning electron microscope images. The adsorption of NPs was enhanced by increasing salinity. To investigate the dynamic adsorption, a co-injection of about 0.033 g NPs slug with tracer (about 0.13 g of $LiCl_2$) as a reference. The estimated irreversible adsorption of NPs in the berea flooding of core was about 35%. While estimated desorption of the flooded core was about 21.2%. Detailed mass balance analysis is included. It was observed that the adsorption/desorption processes of silica NPs are influenced by the pH wherein increased alkalinity favors NP desorption. NP adsorption on the mineral surface during combined LSW and NP flooding was shown to reduce mineral dissolution, ion exchange, loss of cementing mineral and reduced resistance to flow compared to LSW alone. Surface forces estimation showed that combining LSW with NPs reduced the repulsion between fines and berea. The work here demonstrated the synergistic effect of combining the two technologies of LSW and nanoparticles where the probability of formation damage in sandstone reservoirs is reduced.

* Corresponding author.
*E-mail addresses:* rockey.abhishek@uis.no (R. Abhishek), aly.hamouda@uis.no (A.A. Hamouda), murziivan@gmail.com (I. Murzin).

https://doi.org/10.1016/j.colsurfa.2018.07.019
Received 8 March 2018; Received in revised form 13 July 2018; Accepted 13 July 2018

## 1. Introduction

Use of nanoparticles (NPs) has emerged as an Enhanced Oil Recovery (EOR) technique during the past decade. Nanofluids (NF) which are dispersions of NPs typically under the size of 100 nm in a base fluid have been studied as an injection fluid for improving oil recovery from petroleum reservoirs. The main advantage of NPs is their size and high surface area which allows them to pass through the pore network in the reservoirs and be effective at relatively low volume concentration as compared to other EOR agents [1]. Among the various type of NPs, special attention has been paid to silica NPs due to their hydrophilic nature and ease of surface functionalization [2]. Silica NPs can alter the wettability of the oil wet rock surface towards more water wet and this has been attributed and studied as the main mechanism that improves recovery due to application of Silica NPs [3–6]. In addition, core flood studies conducted by different research groups have shown the silica NPs can increase recovery in sandstone reservoirs [3,7–10]. Another popular EOR technique for sandstone reservoirs is use of low salinity water injection [11–13]. This techniques generally involves altering or lowering the salinity to injection brines. However, lowering the salinity of injection brine can have detrimental effects. Khilar and Fogler [14] identified the existence of a Critical Salt Concentration (CSC) for permeating fluids in berea sandstones below which clay particles get released and cause formation damage. Formation damage by lowering brine salinity has also been reported and studied by other researchers [15–17] and thus choosing optimum brine salinity in low salinity projects is limited by the CSC [18]. Thus fluid/rock interactions are very important during low salinity flooding. Arab and Pourafshary [18] investigated different NPs as surface modifiers by soaking the porous medium in NFs and then testing the ability of the modified porous medium to hinder the transport of artificial fines in water saturated porous medium. They suggest that combining low salinity and with NPs may help overcome the detrimental effects of formation damage associated with low salinity flooding. The current study investigates the adsorption of silica NPs on sandstone minerals and its effect on fluid/rock interactions during oil recovery by low salinity flooding. It has been shown that the adsorption of silica NPs on sandstone mineral surface can reduce mineral dissolution and formation damage in berea sandstones.

## 2. Materials and methods

The Silica NPs (DP 9711) used in this study were provided by Nyacol Nanotechnologies. The NPs were obtained at 30% wt. concentration, dispersed in Deionized Water (DIW) and pH 3. For ease, these NPs are referred to as DP in this study. The NPs are spherical and surface functionalized with a proprietary coating. The NPs have an average particle size of 20 nm as claimed by the manufacturer. The NFs used in this study were prepared from the stock fluid by diluting it with appropriate brines. Berea outcrop cores were used as the porous media. The mineral composition of the used cores is listed in Table 1. Analysis grade quartz and kaolinite mineral powders were acquired from Sigma–Aldrich with chemical compositions: $SiO_2$ and $Al_2O_7Si_2{\cdot}2H_2O$, respectively. The specific surface area of the used mineral powders are 0.62 $m^2/g$ and 8.56 $m^2/g$, respectively which has been calculated previously by the water adsorption isotherm [19]. The model oil used in this study was n-decane acquired from Merck. N,*N*-Dimethyldodecylamine (NN-DMDA) was added to n-decane at a concentration of 0.01 mol/l to prepare the synthetic oil. The properties of the synthetic oil (estimated from PVT Sim) are listed in Table 2.

**Table 1**
Mineral composition of berea sandstone cores.

| Mineral | Semi-quantitative (%) |
|---|---|
| Quartz | 94 |
| Kaolinite | 1 |
| Muscovite | 1 |
| Microline | 1 |

**Table 2**
Synthetic oil properties.

| Temperature °C | Viscosity (cP) | Density (g/ml) |
|---|---|---|
| 20 | 0.92 | 0.73 |
| 50 | 0.5802 | 0.7683 |
| 70 | 0.4812 | 0.7525 |

Zetasizer Nano ZSP from Malvern instruments was used to characterize the average size and zeta potential of the NPs. Scanning electron microscopy was performed on a Supra 35 V P SEM with an integrated EDXRF analyzer to visualize the adsorption of the NPs on the berea core pieces treated with NF. NP concentration during static isothermal adsorption tests and in the effluents from core floods were determined using a dual beam UV–vis 1700 spectrophotometer from Shimadzu Corporation. The schematic of the core flooding setup used in this study is shown in Fig. 1. The concentration of cations in effluents produced from core floodings was determined by a Dionex ICS-5000 Ion Chromatograph (IC) from Thermo Fisher Scientific.

### 2.1. Brines and nanofluid

Synthetic seawater (SSW) and Low Salinity Water (LSW) at 1:10 dilution of SSW were the used brines. Their ionic compositions are listed in Table 3. The particles size (average hydrodynamic diameters) and zeta potential exhibited by the NPs in NFs prepared in LSW and SSW are listed in Table 4. At the NPs concentration (1 g/l) used in this study, we did not observe any aggregation behavior. Particle size measurements made after 3 months of nanofluid preparation were within ± 5 nm of the original measurements for all nanofluids including in seawater (high salinity). Griffith, Ahmad, Daigle and Huh [20] made a similar observation (by observing particle size with time) only for very high concentration (200 g/l) in high salinity (20 wt.% API brine).

### 2.2. Adsorption of NPs on minerals

The adsorption behaviour of the NPs on the mineral surfaces in sandstones were investigated by two approaches: (1) static isothermal adsorption on individual mineral powders and (2) dynamic adsorption of NPs in berea core during low salinity flooding. A series of batch adsorption experiments were performed at room temperature to study the static isothermal adsorption of the used NPs on quartz and kaolinite mineral surface. The experiments were performed in DIW and SSW as the media to address the effect of salinity on NPs' adsorption. 0.15 g of mineral was added to NF prepared at a particular concentration and salinity. This fluid was then agitated (in a rotary agitator) for 24 h. Thereafter, the minerals were removed from the fluid. The remained concentration of NPs in the fluid was determined by measuring its absorption in a dual beam spectrophotometer at 240 nm wavelength, comparing it with the constructed calibration curve and making baseline corrections for the contribution of minerals [21].

The dynamic adsorption of NPs was addressed by injecting a slug of NPs with into a berea core. A dried berea core was vacuum saturated with LSW and loaded in to the core holder (Fig. 1). Confining pressure of 25 bar was applied on the core and the injection of the fluid was performed at a constant flow rate of 10 pore volumes (PV)/day at room temperature. The details of the core used is listed in Table 5. Multiple PV of LSW was injected into the core. Thereafter, 1.5 PV slug of NF (1 g/l DP in LSW + 0.1 mol/l LiCl tracer) was injected into the core followed by post flush with LSW. The produced effluents were collected at

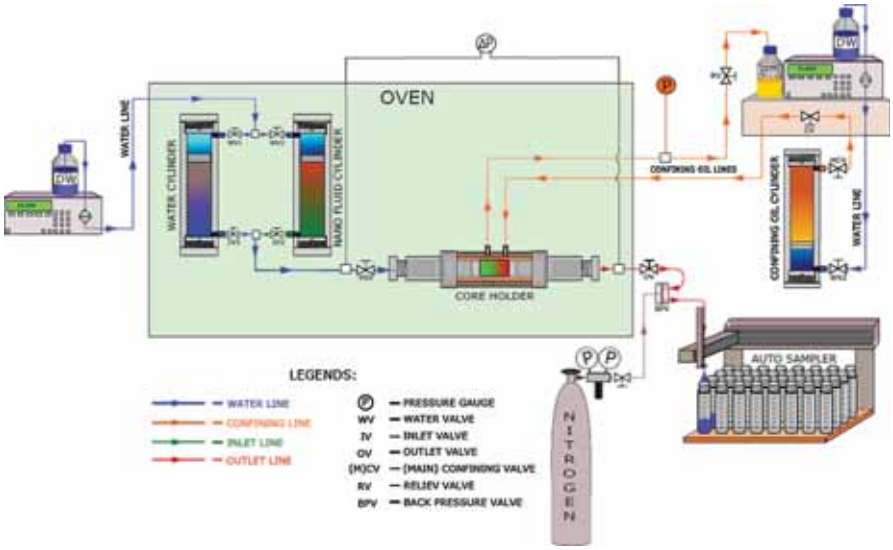


**Fig. 1.** Schematic of the core flooding setup.

**Table 3**
Ion concentration the brines.

| Ion | SSW (mol/l) | LSW (mol/l) |
|---|---|---|
| $HCO^{3-}$ | 0.002 | 0.0002 |
| Cl– | 0.525 | 0.0525 |
| $SO_4^{2-}$ | 0.0240 | 0.0024 |
| $Mg^{2+}$ | 0.045 | 0.0045 |
| $Ca^{2+}$ | 0.013 | 0.0013 |
| $Na^{+}$ | 0.450 | 0.045 |
| $K^{+}$ | 0.010 | 0.0010 |

**Table 4**
Particle size and zeta potential of silica NPs in different mediums.

| Dispersing fluid | Temperature (° C) | Average hydrodynamic diameters (nm) | Zeta-potential (mV) |
|---|---|---|---|
| DIW | 25 | 37.52 | −30.73 |
| DIW | 50 | 38.57 | N/A |
| DIW | 80 | 39.4 | N/A |
| LSW | 25 | 37.91 | −12.13 |
| LSW | 50 | 38.18 | N/A |
| LSW | 80 | 38.7 | N/A |
| SSW | 25 | 56.35 | −6.4 |
| SSW | 50 | 57.54 | N/A |
| SSW | 80 | 88.11 | N/A |

regular intervals. The effluents samples were analysed for NP concertation using the method outlined previously (UV–vis) and the pH was recorded. The concertation of cations produced was determined by IC.

### 2.3. Core preparation and oil recovery experiments

The berea cores were dried at 100 °C in a vacuum oven until the weights were stabilized. Then the cores were vacuum saturated with SSW and loaded in the core holder. The cores were flooded with model oil to establish initial water saturation (Swi). Thereafter the cores were aged in model oil for a period of two weeks at 50 °C to render them oil wet. The flooding experiments were performed at 70 °C under 25 bar confinement pressure and against 10 bar of back pressure in two stages: (1) primary recovery was done by flooding with the particular brine at two flowrates: 4 and 16 PV/day and (2) secondary recovery was done by switching the flood with NF, again the flooding was performed at 4 and 16 PV/day. The details of all the core flooding experiments are listed in Table 5. The amount of oil produced and the differential pressure drop (dP) across the core as flooding progressed were recorded. The concentration of NPs in the produced effluents was determined by the method outlined previously (UV–vis). The pH of the water produced was measured and the concentration of cations produced as flooding progressed was determined by IC.

**Table 5**
List of core properties and flooding details.

| Core Id | Porosity (%) | Permeability (mD) | Lenght (cm) | Dia (cm) | Type | Swi | Flooding sequence |
|---|---|---|---|---|---|---|---|
| BR1 | 20.25 | 200–220 | 9 | 3.78 | Dynamic adsorption | N/A | LSW - 1.5 PV Slug (DP 1 g/l + Tracer in LSW) - LSW |
| BR2 | 20.9 | 200–220 | 9 | 3.78 | Recovery | 0.250 | SSW - DP (1 g/l) in SSW |
| BR3 | 20.6 | 200–220 | 9 | 3.78 | Recovery | 0.293 | LSW - DP (1 g/l) in LSW |
| BR4 | 20.25 | 200–220 | 9 | 3.78 | Recovery | 0.218 | SSW - DP (1 g/l) in LSW |

### 2.4. Fines mineral interactions

Fines are solid mineral particles of sandstone that lose their coherence due to water-mineral interaction and become mobilized with the flowing fluids. The mobilization of fine particles is referred to as fine migration which can lead to formation damage in sandstone reservoirs. The theory of surface forces can be utilized to characterize the interaction between fine-mineral based on the Derjaguin-Landau-Verwey-Overbeek (DLVO) theory. The DLVO theory combines the effect of attraction due to van der Waals interaction and the electrostatic repulsion due to the double layer of counter ions around charged surfaces in a medium. Due to the size difference between the fine particles and the mineral surfaces, the curvature of the mineral surfaces may be neglected and the interactions can be modelled as Sphere - Plate collector geometry [18,22–25]. The net force acting on a fine particle approaching a mineral surface is the sum of van der Waals attraction, electric double layer repulsion and Born repulsion:

$$V_t(h) = V_{LVA}(h) + V_{EDLR}(h) + V_{BR}(h) \quad (1)$$

Where, $V$ is the potential of interaction as a function of separation distance ($h$) between the fine particle and the mineral surface. The subscripts *t, LVA, EDLR and BR* denote total, London-van der Waal interaction, electric double layer interaction and Born Repulsion, respectively. The interaction potential can be represented in non-dimensional (*ND*) form as follows:

$$V_{t,ND}(h) = \frac{V_t(h)}{k_B * T} \quad (2)$$

Where, $k_B$ is the Boltzmann constant ($1.38 \times 10^{-23}$ J $K^{-1}$) and T is temperature. The contributions due to the different types of interactions in Eq. (1) can be calculated as follows [18,22,23]:

$$V_{LVA}(h) = -\frac{A_{132}}{6}\left[\frac{2(1+H)}{H(2+H)} + ln\left(\frac{H}{2+H}\right)\right] \quad (3)$$

$$V_{EDLR}(h) = \left(\frac{\varepsilon_0\varepsilon_3 a_p}{4}\right)\left[2\zeta_p\zeta_s\, ln\frac{1+exp(-\kappa h)}{1-exp(-\kappa h)} + (\zeta_p^2+\zeta_F^2)\, ln(1-exp(-2\kappa h))\right] \quad (4)$$

$$V_{BR}(h) = \frac{A_{132}}{7560}\left(\frac{\sigma}{a_p}\right)^6\left[\frac{8+H}{(2+H)^7} + \frac{6-H}{H^7}\right] \quad (5)$$

Where,

$$H = \frac{h}{a_p} \quad (6)$$

And, $a_p$ is the particle radius (m). $A_{132}$ is the Hamaker's constant for the sphere and plate collector. For the mineral-fine system with water as the intervening medium, the Hamaker constant can be calculated based Lifshitz theory as follows [26,27]:

$$A_{132} \approx \frac{3}{4}K_b T\left(\frac{\varepsilon_1-\varepsilon_3}{\varepsilon_1+\varepsilon_3}\right)\left(\frac{\varepsilon_2-\varepsilon_3}{\varepsilon_2+\varepsilon_3}\right) + \frac{3h_{ov_e}}{8\sqrt{2}}\left(\frac{(\eta_1^2-\eta_3^2)(\eta_2^2-\eta_3^2)}{((\eta_1^2+\eta_3^2)(\eta_2^2+\eta_3^2))^{\frac{1}{2}}\left((\eta_1^2+\eta_3^2)^{\frac{1}{2}}+(\eta_2^2+\eta_3^2)^{\frac{1}{2}}\right)}\right) \quad (7)$$

Where $\varepsilon_1$, $\varepsilon_2$ and $\varepsilon_3$ represents the static dielectric constants and $\eta_1$, $\eta_2$ and $\eta_3$ represents the refractive index of the interacting species (mineral and fine) and the intervening media: water. $h_o$ is the Planck's constant ($6.626 \times 10^{-34}$ J s) and $v_e$ is the main electron adsorption frequency in the ultraviolet region and its value is between 3–5 $\times 10^{15} s^{-1}$ [26]. Berea sandstone used in this study is mostly composed of quartz (94%) which has a static dielectric constant ($\varepsilon_1$) of about 4.5 and refractive index ($\eta_1$):1.4298 [28,29]. The fine particles produced from berea sandstones mostly consist of clay particles mostly kaolinite mineral [23] which has a dielectric constant ($\varepsilon_2$) of about 11.8 and refractive index($\eta_2$): 1.362 [28,30]. The dielectric constant of water($\varepsilon_3$) equal to 78 [18,23] and its refractive index($\eta_3$):1.33. Based on Eq. (7), the Hamaker constant was calculated to: $2.3 \times 10^{-21}$ J). This value is in close agreement with Hamaker constant reported by Arab and Pourafshary [18] for a similar case. The permittivity of free space $\varepsilon_0$: $8.854 \times 10^{-12}$ $C^2$ $J^{-1}$ $m^{-1}$. $\zeta_p$ and $\zeta_s$ are the surface potentials of the particles and the surface respectively which can be considered as the zeta potential [23].The surface forces estimation in this study are performed at 70 °C. Therefore the measured zeta potential values at room temperature are corrected to 70 °C based on correlation for common minerals from previous studies [27,31]:

$$\zeta(T) = (0.01712(T-T_0) + 1)\bullet\zeta(T_0) \quad (8)$$

Where, $T$ and $T_o$ are interpolation and measurement temperature respectively in Kelvin. $\zeta(T_o)$ is the zeta potential measured at $T_o$. $\kappa$ is the inverse Debye length which is affected by the salinity of the intervening medium. For SSW and LSW, the inverse Debye length can be calculated by:

$$\kappa^{-1} = \sqrt{\frac{\varepsilon_0\varepsilon_3 k_B T}{2e^2 I}} \quad (9)$$

Where, $e$ is the elementary charge of an electron (C) and $I$ is the ionic strength of the medium:

$$I = \frac{1}{2}\sum c_i Z_i^2 \quad (10)$$

Where, $c_i$ is the ion concertation of the $i^{th}$ species and $Z_i$ is the valence number of the $i^{th}$ species. The concertation of the individual ion species in LSW and SSW is listed in Table 3. In Eq. (5), $\sigma$ is the atomic collision diameter and is equal to 0.5 nm [23]. The born repulsive potentials are formed when the particle approaches point of contact with the mineral resulting in overlap of electron clouds. Hence it is a short-range interaction and thus calculated only when the distance of separation is less than 1 nm.

## 3. Results and discussions

Experimental results are divided into three main sections. The first section deals with the static and dynamic adsorption of NP on the minerals. The second section addresses the synergy between NP and LSW for enhancing incremental oil recovery. The fluid/rock interaction with and without NPs and the salinity of the carrier fluid are discussed. The third section deals with surface modification of berea rock due to NP adsorption and its effect on interaction between the produced fines and minerals in presence of NPs. In this section DLVO theory was applied to address the different interaction potentials.

### 3.1. Adsorption of NP on mineral

Literature indicates some debatable with regards to Silica NP adsorption on sandstone minerals. Metin, Baran and Nguyen [32] reported that the adsorption of surface functionalized silica NPs on quartz mineral surfaces was insignificant. Other researchers reported significant adsorption of silica NPs on sandstones [33–36]. Isothermal static adsorption tests were carried out to investigate the adsorption of NPs on mineral powders (quartz and kaolinite). The effect of salinity was addressed in presence and absence of salt; SSW and DIW, respectively. The results are shown in Fig. 2.

Fig. 2 shows that the NPs have greater affinity to adsorb on quartz than on kaolinite surface and increasing NPs' concentration increases the adsorbed amount per unit surface area of the minerals. In all experiments, the volume of NF was kept at 30 ml and the added amount of mineral was kept at 0.15 g. It is also shown that higher adsorption occurred in SSW environment. The measured zeta potential of the NPs in SSW was -12.13 mV which is about 2.5 times less negative than that in the case of NPs in DIW (-30.73 mV) as shown in Table 4. The difference in the zeta potential may has been caused by compression of the double

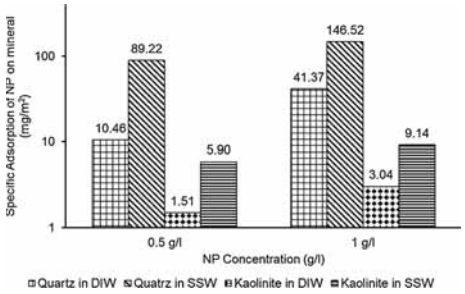


**Fig. 2.** Specific adsorption (mg/m$^2$) of two concentrations of NPs (0.5 and 1 g/l) on quartz and kaolinite minerals in DIW and SSW environment.

layer at higher ionic strength (SSW). Hence, the electrostatic repulsion between the NP and the mineral decreases causing more adsorption of NPs. Similar observation has been made previously for different modified silica NPs [33]. Zhang et al. [36] also identified that strong repulsion exists between NPs and sand particles at low salinity. They reported that adsorption of NPs increases with less clay content. The SEM image (Fig. 3) visually shows that more NPs adhere/adsorb on quartz surface compared to kaolinite. Thus increasing the clay content may affect the overall adsorption of NPs. The SEM image is for a berea core treated with 1 g/l NF prepared in DIW. The core was cleaved and imaged along the flooding plane. Adsorption of NPs on the mineral surface was shown to be well spread that may indicate a monolayer like coverage. There was some in situ aggregation of the NP which may be due to drying and handling processes of the core before taking the SEM image. However, the image did not show pore throat blockage hence permeability impairment is not expected. SEM image confirmed the preferential adsorption of NPs obtained by the static adsorption tests.

Dynamic adsorption of NPs dispersed in the low salinity water flooding of berea sandstone is shown in Fig.4(a): BR1. The core was saturated with LSW, loaded into the core holder and several PVs of LSW was injected into the core. Thereafter, 1.5 PV of NF (1 g/l DP in LSW with LiCl tracer) was injected into the core followed with post flush by LSW. The effluent samples were collected and analysed for NP concentration (UV/Vis spectrometry), pH and the produced relative cations concentration ($Na^+$ and $K^+$) as shown in Fig. 4(a), (b) and (c), respectively.

Fig. 4(a) shows that the breakthrough of the Li tracer and NPs occurred almost simultaneously. The NP concentration profile shows a longer tail compared to the tracer. This may indicate possible interaction of NPs with the core's minerals. The amount of NPs irreversibly adsorbed in the core was calculated from the mass balance by integrating the produced area under the NP concentration curve in

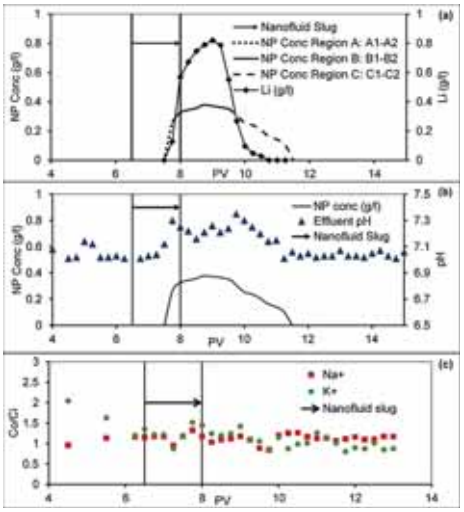


**Fig. 4.** (a) NP and tracer concertation (b) Effluent pH profiles and (c) Concertation of cations in effluents from flood BR1.

Fig. 4(a) and the known injected amount of NPs into the core. The produced concentration profile, may be divided into three regions: A, B and C. Table 6 shows the analysis of NP production in these three regions.

Where, $c_{inj}$ and $V_{sl}$ refers to the injected concentration and slug volume of the nanofluid. $c_{oA}(V)$, $c_{oB}(V)$ *and* $c_{oC}(V)$ are the produced NP concentration functions with respect to produced effluent volume ($V$) in regions A, B and C respectively. These were obtained from polynomial regression fitting of the concentration curves in Fig. 4(a). The $R^2$ for the fits varied between 1-0.99. *A1-A2*, *B1-B2* and *C1-C2* refer to the limits of region A, B and C respectively. In Fig. 4(a), the amount of NPs produced in region A is termed here as excess NP, since the breakthrough coincided with the breakthrough of the tracer, i.e. un-interacted with the rock minerals ($m_{Ao}$). In region B, almost a plateau of NP produced concentration is established. This may indicates that an equilibrium between the adsorbed NP on sandstone minerals and desorbed concentration in the flowing fluid. At equilibrium period by the end of region B, 43.49% of the total available NPs ($m_{NP}$) were estimated which may be considered to be equal to the adsorbed NPs on the sandstone minerals. In another way it may be considered as the maximum reversible adsorption up till that period of time (end of region B). During NPs' production region B, the tracer concentration reached a

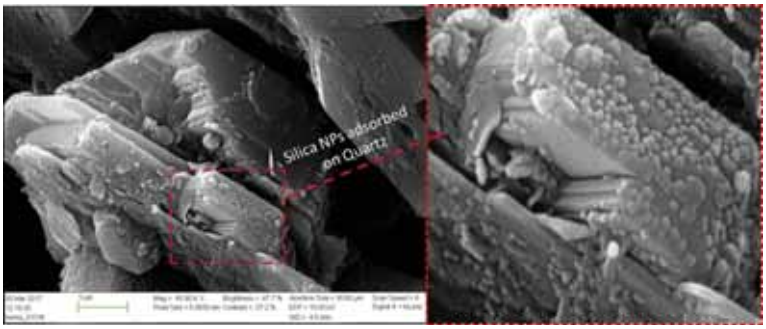


**Fig. 3.** SEM image of NP adsorbed on mineral surfaces on a berea core. Magnified view of the NP adsorbed on quartz surface on the right.

**Table 6**
Analysis of NPs production in Fig. 4 (a).

| | | | |
|---|---|---|---|
| **Total NP injected (g)** | $m_{NPi}$ | $m_{NPi} = c_{inj} * V_{sl}$ | 0.032715 |
| **Excess NP produced in region A (g)** | $m_{Ao}$ | $m_{Ao} = \int_{A1}^{A2} c_{oA}(V)dV$ | 0.000712 |
| **Total NP available for adsorption (g)** | $m_{NP}$ | $m_{NP} = m_{NPi} - m_{Ao}$ | 0.032003 |
| **Total NP produced in equilibrium region B (g)** | $m_{Bo}$ | $m_{Bo} = \int_{B1}^{B2} c_{oB}(V)dV$ | 0.013921 |
| **Total NP adsorbed in core till end of region A (g): reversibly adsorbed NP** | $m_{rev}$ | $m_{rev} = m_{NP} - m_{Bo}$ | 0.018082 |
| **Total NP produced during desorption phase in region C (g)** | $m_{Co}$ | $m_{Co} = \int_{C1}^{C2} c_{oC}(V)dV$ | 0.006767 |
| **Amount of NP irreversibly adsorbed in the core (g)** | $m_{irr}$ | $m_{irr} = (m_{rev} - m_{Co})$ | 0.011315 |
| **NP production in region B (%)** | $NP_{Bo}$ | $NP_{Bo} = \left(\frac{m_{Bo}}{m_{NP}}\right) * 100$ | 43.49 |
| **Desorption in region C (%)** | $Dsp_C$ | $Dsp_C = \left(\frac{m_{Co}}{m_{NP}}\right) * 100$ | 21.15 |
| **Total irreversible adsorption/ remained in core (%)** | $Ads_{irr}$ | $Ads_{irr} = \left(\frac{m_{irr}}{m_{NP}}\right) * 100$ | 35.36 |

peak, after which it declined. This indicates the injected NF slug with the tracer has passed through the core. Integrating the area under the tracer production curve showed that almost all the injected amount of the tracer was produced. Further, the tracer production stopped at 10.75 PV while the NP production continued up to 11.5 PV. Combining these two observations, it can be inferred that the NPs produced in region C were, most likely due to desorbed NPs. The NF slug injection length was 1.5 PV. The unreacted tracer production length was 2.75 PV (7.75 to 10.5 PV) and the NPs production length was 3.5 PV (7.75 to 11.25 PV). The ratio of NPs to tracer production volume was approximately 1.3. Thus NPs production takes approximately 30% longer time to cease production after the slug has passed through the core. This strengthens desorption of NPs during region C. As shown (Table 6), 21.15% or approximately $1/5^{th}$ of the available NPs were desorbed ($Dsp_c$) in region C. The maximum irreversible adsorption ($Ads_{irr}$) in the core was 35.36%. This indicates that irreversible adsorption of NPs exceeds the reversible adsorption of NPs.

The pH of the effluent is plotted along with the NP concentration as shown in Fig. 4(b). During the initial injection of LSW, the pH remained stable at about 7. The pH, then, increased after NP injection. Thereafter, the pH fell down in the region in which NP desorption is inferred from the difference in NP and Tracer concertation curves (region C). This may be related to the dissolution of adsorbed NPs in accordance with the following equations [37,38]:

$$SiO_2\,(s) + 2H_2O \leftrightarrow H_4SiO_4 \quad (11)$$

$$H_4SiO_4 \leftrightarrow H_3SiO_4^- + H_3O^+ \quad (12)$$

Eq. (11) shows the dissolution of $SiO_2$. Stumm and Morgan [37] stated that $SiO_2$ solubility increases at neutral to slightly alkaline pH ranges in accordance with the above equations, producing silicic acid. This weak acid further dissociates and reduces the pH (Eq. (12)) which was observed during desorption of NPs. The adsorption/desorption of silica NPs in low salinity environment in chalks showed similar behaviour [38]. Therefore it maybe concluded that the desorption of NPs is influenced by the pH wherein increased alkalinity favours the NP desorption.

The effluents were analysed for the produced cation concentrations for the different injection stages, Fig. 4(c). The concentration of cations in the effluent (Co) has been plotted relative to the injected concertation (Ci). Hamouda, Valderhaug, Munaev and Stangeland [39] have previously investigated mechanisms during LSW flooding. They stated that LSW injection leads to mineral dissolution such as for example K-feldspar as presented by the following equation:

$$4KAlSi_3O_8(s)(\text{orthoclase}) + 22H_20(aq) \rightarrow Al_4Si_4O_{10}(s)(\text{kaolinite}) + 8H_4SiO_4(aq) + 4K^+(aq) + 4OH^-(aq) \quad (13)$$

It is shown in Fig. 4(c) that during initial LSW injection, $K^+$ in the effluent was high (Co/Ci ≈2). This was followed by a decrease to ≈ 1.35 relative concertation. After injection of NF slug, $K^+$ increased to about 1.5, which coincides with the pH rise in the effluent, which may be explained based on Eq. (13). Thereafter, the $K^+$ concentration showed a downward trend which is accompanied the fall in pH. The pH reduction could be due to the contribution of NP dissolution as per Eqs. (11) and (12) and/or reduced mineral dissolution. During the post flush, the $K^+$ concentration stabilized at around 0.8 relative to injected concentration. This may indicate that, the in-situ adsorption of NPs on the berea rock surface may have reduced K-feldspar dissolution thus reducing fines production [23,39,40] therefore reduce formation damage. Hamouda, Valderhaug, Munaev and Stangeland [39] also stated that LSW injection leads to possible ion exchange represented by the following equation:

$$4KAlSi_3O_8(s)(\text{orthoclase}) + Na^+(aq) \rightarrow K^+ + NaAlSi_3O_8(s)(albite) \quad (14)$$

The above reaction leads to reduction of $Na^+$ during the initial LSW injection. However, after the NF slug injection, the $Na^+$ relative concentration in the effluent was about 1.1. This may indicate suppression of ion exchange based on Eq. (14). Thus, the investigated slug injection of NPs into the berea sandstone suggests that the NPs adsorb on the surface of berea and affect the fluid/rock interactions during low salinity flooding.

From the static and dynamic adsorption of NP, two main observation can be inferred: (1) Salinity enhances the adsorption of NPs on minerals and (2) Combining NPs with Low salinity may reduce fines migration and formation damage during low salinity flooding in berea sandstones. The validity of these effect of silica NPs during oil recovery from berea sandstone is investigated in the following section.

### 3.2. Effect of NPs on oil recovery during low salinity flooding

Many researchers have identified that, injection of low salinity brine may lead to enhanced release of fines which can cause formation damage [41–43]. In the previous section, adsorption of the NPs on sandstone minerals was addressed. In this section, the effect of NP adsorption during the recovery process and its effects on the mineral water interaction is addressed. The flooding was divided into two stages: primary recovery (brine alone) and secondary recovery (NP dispersed in brine). To systematically address the effect of NPs on low salinity flooding, three recovery schemes were compared. Table 5, summarizes, the followed flooding schemes for the three cases (BR2, BR3 and BR4). The flooding were performed at two flow rates 4 PV/day (0.06 ml/min) and 16 PV/day (0.24 ml/min). In the case of BR2, both primary and secondary flooding were done with SSW, however, in the secondary recovery, silica NPs at 1 g/l was mixed with SSW. For BR3, primary recovery was performed with LSW and secondary recovery flooding with silica NPs at 1 g/l prepared in LSW. Finally, for BR4, primary recovery was performed with SSW followed by secondary recovery with silica NPs at 1 g/l concentration in LSW. The obtained oil recovery profiles for floods BR 2-4 are plotted in Fig. 5.

It is shown in Fig. 5 that for all the flooding experiments, most of the oil was recovered within the first PV water injection at 4 PV/day injection rate. Increasing the rate to 16 PV/day led to increment in recovery (≈ 0.63%) in the BR2 experiment with SSW but not for experiments BR3 and BR4. For primary recovery (without NPs) SSW was more effective, BR2 and BR4, compared to primary recovery by LSW (BR3). However, when the flooding was switched to NF (1 g/l DP prepared in LSW) in BR3, incremental recovery of ≈0.69% was observed. Secondary recovery with NF in experiments BR2 and BR4 did not lead

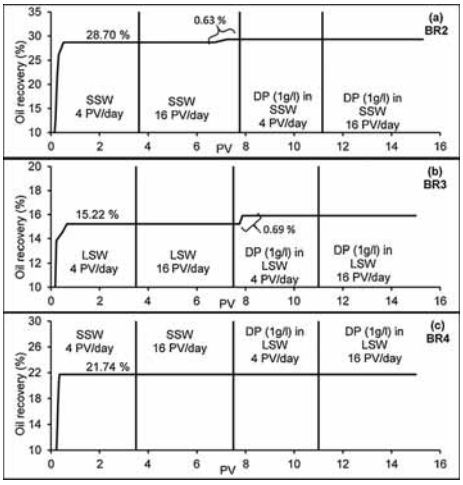


**Fig. 5.** Oil recovery profiles for floods (a) BR2, (b) BR3 and BR4.

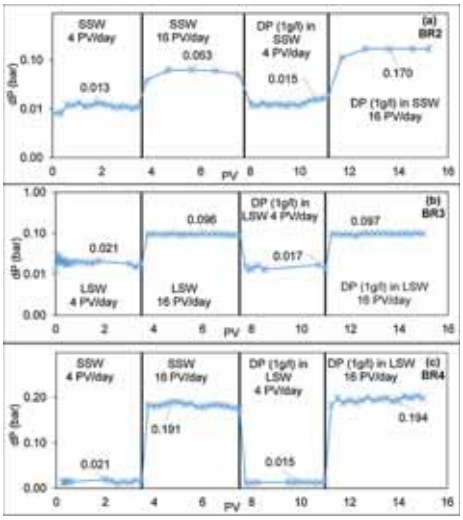


**Fig. 6.** Differential pressure drop profiles for floods (a) BR2, (b) BR3 and BR4.

to incremental recovery. Incremental recovery by silica NFs in sandstones have been reported previously by many studies [9,44,45]. These studies were performed at higher flow rates to enable better sweep of the used cores and address the incremental recovery by NFs. However, the objective of this study is to address the effect of NP adsorption on fluid/rock interactions during low salinity flooding. Therefore, the experimental design involved flooding performed at lower flowrates that is closer to real field cases and to give the injected fluid greater residence time in the core. However, a possible shortcoming of using lower flow rates is that it could lead to an un-swept zone, especially in a high permeability cores like berea as evidenced by the low overall recovery (average recovery of about 20%) shown in floods BR 2–4. The effluent fluid was analysed for: (1) pH (2) NP concertation and (3) concentration of cations produced due to fluid/rock interaction. In the previous section, it was indicated that combining LSW with silica NPs may reduce fines migration and formation damage. The differential pressure drop during the flooding was recorded (Fig. 6) to give a qualitative indication of the resistance to flow in the porous medium and thereby the fines migration.

It can be seen in Fig. 6 that the recorded pressure drop during primary recovery is lower for experiment BR2 (SSW) compared to BR3 (LSW). The cores were of similar dimension and PVs. Hence the flowrates at 4 and 16 PV/day for both the cores was similar. Previous studies have shown that lowering the salinity of brines may lead to release of fines and formation damage in berea sandstones [23,46]. Tang and Morrow [40] also suggested that low salinity water injection could lead to release of fines in sandstones. The higher observed pressure drop due to LSW injection could thus be an indication of increased release of fines. Hamouda and Valderhaug [13] made a similar observation of increased pressure drop during low salinity injection. On switching the flood to NF in BR2 at 4 PV/day, the pressure drop increases slightly to 0.015 bar from 0.013 bar. At 16 PV/day the recorded pressure drops with and without NPs were about the same: 0.097 and 0.096 bar, respectively. SEM imaging in Fig. 3 showed that the NP adsorption did not lead to blockage of pore throats. However, particle size measurements showed that the NP exhibit a higher size in SSW. The increased size could hinder the flow of NPs through the core and thus exhibit the slightly higher pressure drop in BR2. On switching the flood to NF in BR3, the pressure drop fluctuated between 0.013 and 0.017 bar, which was lower than the pressure drop during primary recovery at 4 PV/day, 0.021 bar. This may, qualitatively indicate reduction of the produced fines. Huang et al. [47] reported that for a sand pack treated with silica NPs, the pressure drop across was 10% lower (improving water injectivity) than of a sand pack without NP. In addition, Arab and Pourafshary [18] stated that porous media that has been treated with NPs adsorbs fines particles. Finally for combined flooding BR4 (Fig. 6(c)), the recorded pressure drops was lower than during NF injection at 4 PV/day. It was estimated that the water injectivity improved by 19 and 28% respectively for flood BR 3 and 4 respectively. At 16 PV/day, the pressure drops were almost equal. Thus the recorded pressure drops in Fig. 6 may indicate a reduction in the produced fines by combining low salinity and NPs. The NP concentration in the effluents during floods BR 2-4 is shown in Fig. 7.

It is shown in Fig. 7 that for BR2 (NF in SSW) that the effluent NP concentration reached a peak of 0.28 g/l as compared to the peak of 0.67 g/l for BR3 (NF in LSW). This indicates higher adsorption of NP in the core at elevated salinity similar to observations made in the previous section with static adsorption tests. Increasing NF injection rate to 16 PV/day, the effluent NP concentration fell for both BR2 and BR3 which suggests that NP adsorption increases with higher injection rate. This may be due to diversion of NPs to un-swept parts of the core. For combined flooding in BR4, the NP effluent concentration was around 0.5 g/l which is intermediate between BR 2-3. This may be due to the presence to residual SSW from the primary stage which enhanced the adsorption of NPs onto the core's minerals. The pH of the effluents during for the performed flooding is shown in Fig. 8.

During primary recovery by SSW (BR2), effluent pH was slightly lower than injected pH. This reduction in pH has been reported by other researchers earlier [48,49]. The pH observed during flood BR3 (all LSW) is slightly higher than the injected pH. This behaviour is typical to low salinity floods and has been reported previously [13]. On switching to NF in SSW in flood BR2, rise in pH was observed. A similar rise in pH was observed for flood BR3 with NF in LSW. For combined flood BR 4, the pH remain lower than injected pH for primary recovery by SSW. Thereafter, the pH rises when the flood is switched to NF prepared in LSW. The rise in pH after NP injection is similar to the observation made during NP slug injection (Fig. 4b). The cations produced during floods BR 2-4 are shown in Fig. 9.

The cation concentrations for experiment BR2, minor changes of the relative cations' concentrations ($Na^+$, $K^+$ and $Ca^{2+}$) at the different stages. For $Na^+$, $K^+$ and $Ca^{2+}$, the average relative concentrations are

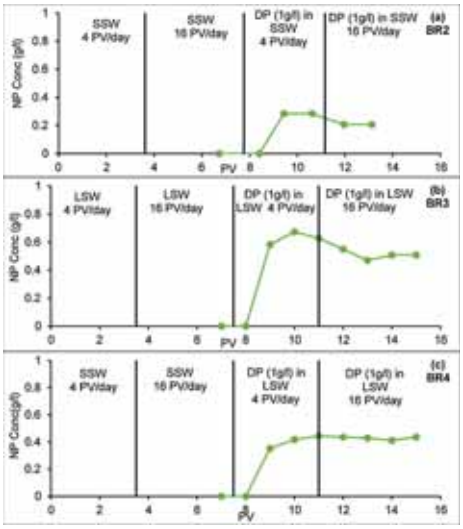


**Fig. 7.** Effluent NP concentration profile for floods (a) BR2, (b) BR3 and BR4.

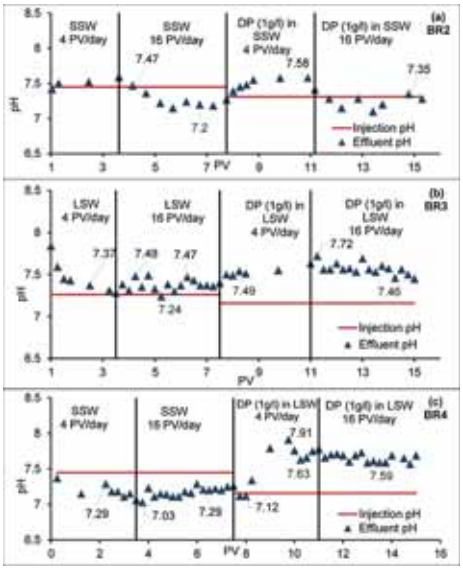


**Fig. 8.** Effluent pH profiles for flood (a) BR2, (b) BR3 and (c) BR4.

0.9, 0.5 and 0.4, respectively. The changes within the average concentration are extremely small to be explained within a reasonable accuracy.

In the case of experiment BR3 (LSW), initially high relative concentrations of $Na^+$, $K^+$ and $Ca^{2+}$ was produced perhaps due to residual SSW in the core during establishing initial water saturation. As the primary flood progressed, $K^+$ relative concentration stabilized at 1.6 and 1.37 at 4 and 16 PV/day respectively. Additionally, the increase in pH observed during these stages in Fig. 8(b) may suggest mineral dissolution of K-feldspar as per Eq. (13). During this stage the $Na^+$ concentration is lower than the injected concentration by about 0.2

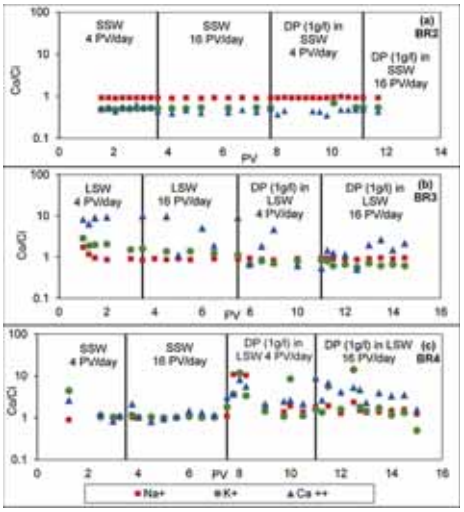


**Fig. 9.** Relative concertation of $K^+$ and $Na^+$ and $Ca^{2+}$ in effluents for floods (a) BR2, (b) BR3 and BR4.

relative. This suggests possible ion exchange by Eq. (14). However, when the flood was switched to NF, the $K^+$ relative concentration fell and stabilized at around 0.85 and 0.66 at injection rate of 4 and 16 PV/day respectively. Further the $Na^+$ relative concertation also rose to 0.94 and 0.95 at injection rate of 4 and 16 PV/day respectively. This may suggest that both mineral dissolution and ion exchange were reduced by the NF and this reduction was observed to be larger at higher flowrate. This coincides NP adsorption increases at the higher flowrate in Fig. 6(b).

Unlike BR2 (all SSW), high $Ca^{2+}$ production is observed during primary recovery by LSW in BR3. Hamouda and Valderhaug [13] reported the same observation and suggested the presence and dissolution of cementing material ($CaCO_3$) in the core. Previous work in our lab has shown that the used silica NPs can significantly lower the dissolution of calcite [38]. As the flood is switched to the NF, the $Ca^{2+}$ levels fell and fluctuated between 4.65 and 0.62. Further reduction in $Ca^{2+}$ levels was observed when NF injection rate was increased to 16 PV/day (fluctuation between 2.64 and 0.49). This confirms the previously stated observation of increasing effect of NP at higher flowrate. Thus combining LSW with the used NPs reduces the mineral dissolution induced by injecting LSW alone and also reduce loss of cementing mineral. This may explain the reduction in pressure drop observed in Fig. 5(b) due to reduction of fines caused by adsorption of NP of berea surface. During combined flooding in BR4, the relative concentrations of all the ions were close to 1 during primary recovery by SSW. During secondary recovery by NF in LSW, initially the ions are high perhaps due to residual SSW from previous stage. Thereafter both $K^+$ and $Ca^{2+}$ showed a decreasing trend. This confirms the conclusions made in the above cases.

### 3.3. Berea surface modification by NP adsorption

The adsorption of NPs modified the berea surface. The effect of the surface modification on the interaction between the fines and berea was modelled based on the DLVO theory. The zeta potential of berea powder aged in synthetic oil and dispersed in SSW and LSW corresponds to the primary recovery stages in floods BR2 and BR3 respectively. The oil aged berea was further treated with NF at 1 g/l concentration in SSW and LSW. The modified mineral was recovered and

**Table 7**
Zeta potential and size measurements of modified berea minerals and fines.

| Mineral | Zeta potential (mV) |
|---|---|
| Berea aged in oil and dispersed in SSW | −7.67 |
| Berea aged in oil and dispersed in LSW | −18.1 |
| Berea aged in oil and then treated with NP and dispersed in SSW | −8.91 |
| Berea aged in oil then treated with NP and dispersed in LSW | −21.2 |
| Fines in SSW | −5.89 |
| Fines in LSW | −13.7 |

| Size classes of the fine particles | |
|---|---|
| Radius of fine particles (nm) | Intensity (%) |
| 233.8 | 73.0 |
| 68.57 | 24.2 |
| 2687 | 2.8 |

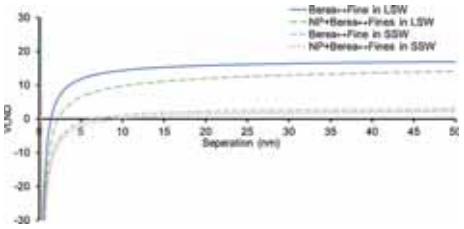


**Fig. 10.** Calculated interaction potential between the fines and the mineral at 70 °C.

dispersed in SSW and LSW after which zeta potential measurements were performed to correspond to the secondary recovery stage of floods BR2 and BR3. The size of the fines eluted from flooding berea has been reported by Abhishek and Hamouda [33]. The zeta potential and size measurement are listed in Table 7.

The interaction potential between the fine particles and the porous media was calculated assuming sphere plate collector model presented in Section 2.4. Since the fines have separate size classes, the interaction potential was calculated for each size class and summed on a weighted basis:

$$V_t(h) = \sum_{i=1}^{n} \{V_{t,i}(h) \times w_i\} \tag{15}$$

Where, $w_i$ is the weight intensity of each size class and $V_{t,i}(h)$ is the interaction potential calculated for the specific size class and finite distance of separation ($h$). Thereafter, the non-dimensional interaction energy was determined using Eq. (2). The calculated interaction potentials are plotted in Fig. 10.

The calculation done in Fig. 10 is to address the interaction between the fines and berea's minerals to illustrate the difference of the interaction in LSW and SSW. As it can be seen that the interaction is more repulsive in LSW compared to SSW, indicating that flooding with LSW could lead to greater fines release/migration. Further modifying the rock with NPs make the interaction energy less repulsive for both LSW and SSW. However, the change is greater in the case of LSW compared to SSW. This observation is supported by the lower pressure drop observed during secondary recovery in BR3 (NP + LSW) in Fig. 6(b). In addition, Fig. 6(c) shows that secondary recovery by LSW + NP has lower pressure drop than primary recovery by SSW. This may be due to adsorption of NPs on minerals. Thus the adsorption of silica NPs on the rock makes the interaction between fines and rock less repulsive.

## 4. Conclusions

This study addresses adsorption of silica NPs on the berea sandstone's minerals and its effect on fluid/rock interactions during low salinity water flooding. In summary, this work demonstrated the synergistic effect by combining the two technologies of LSW and nanoparticles by reducing the probability of formation damage. The following are the conclusions:

1 The silica NPs showed higher adsorption affinity towards quartz compared to kaolinite. Static adsorption and SEM images confirmed that the preferential adsorption affinity on quartz as well as the spread of NPs on the surface. In addition, it is shown that the adsorption of NPs on minerals was enhanced at higher salinity (SSW).
2 It is interesting to observe the dynamic adsorption behaviour of the dispersed silica NPs in LSW. Three regions were identified and correlated to the injected NPs' slug volume and the tracer profile. The adsorbed NPs on the berea surface was about 35% wt. The estimated desorption was about 21.2%wt. This may indicate a strong adherence of the nanoparticles on the mineral surface. It is also indicated that the adsorption/desorption of silica NPs is influenced by the pH wherein increased alkalinity favours the NP desorption as in low salinity environment.
3 During secondary recovery by NFs, it was shown that NP adsorption reduces mineral dissolution, ion exchange process and loss of cementing minerals caused by LSW injection. Lower pressure drop was observed during injection of NFs. These observations indicate that silica NPs may reduce formation damage associated with low salinity water injection in sandstone reservoirs.
4 Modifying the minerals with silica NPs make the interaction energy more attractive for both LSW and SSW. The change is more pronounced for the case of LSW compared to that with SSW.

## Acknowledgements

The authors thank the University of Stavanger (UiS), Norway for funding this study. We also thank Mona W. Minde (UiS) for helping with the SEM imaging and Lutz Eichacker (UiS) for arranging access to DLS equipment. The authors thank Inger Johanne M-K Olsen (UiS) for acquiring the chemical used in this study. In addition, the authors also thank Kim Andre Vorland (UiS) and Krzysztof I Nowicki (UiS) for helping with the core flooding setup.

## References

[1] S. Ayatollahi, M.M. Zerafat, Nanotechnology-assisted EOR techniques: new solutions to old challenges, SPE International Oilfield Nanotechnology Conference and Exhibition, Society of Petroleum Engineers, 2012.
[2] C.R. Miranda, L.Sd. Lara, B.C. Tonetto, Stability and mobility of functionalized silica nanoparticles for enhanced oil recovery applications, SPE International Oilfield Nanotechnology Conference and Exhibition, Society of Petroleum Engineers, 2012.
[3] L. Hendraningrat, S. Li, O. Torsæter, A coreflood investigation of nanofluid enhanced oil recovery, J. Pet. Sci. Eng. 111 (2013) 128–138.
[4] S. Li, O. Torsæter, Experimental investigation of the influence of nanoparticles adsorption and transport on wettability alteration for oil wet Berea sandstone, SPE Middle East Oil & Gas Show and Conference, Society of Petroleum Engineers, 2015.
[5] R. Abhishek, G.S. Kumar, R. Sapru, Wettability alteration in carbonate reservoirs using nanofluids, Pet. Sci. Technol. 33 (2015) 794–801.
[6] A. Dehghan Monfared, M.H. Ghazanfari, M. Jamialahmadi, A. Helalizadeh, Potential application of silica nanoparticles for wettability alteration of oil–wet calcite: a mechanistic study, Energy Fuel 30 (2016) 3947–3961.
[7] O. Torsater, S. Li, L. Hendraningrat, A coreflood investigation of nanofluid enhanced oil recovery in low-medium permeability Berea sandstone, SPE International Symposium on Oilfield Chemistry, Society of Petroleum Engineers, 2013.
[8] O.A. Alomair, K.M. Matar, Y.H. Alsaeed, Experimental study of enhanced-heavy-oil recovery in Berea sandstone cores by use of nanofluids applications, SPE Reservoir Eval. Eng. 18 (2015) 387–399.
[9] K.R. Aurand, G.S. Dahle, O. Torsæter, Comparison of oil recovery for six nanofluids in Berea sandstone cores, International Symposium of the Society of Core Analysts, (2014) September.
[10] B. Ju, T. Fan, M. Ma, Enhanced oil recovery by flooding with hydrophilic

nanoparticles, China Particuol. 4 (2006) 41–46.
[11] N. Morrow, J. Buckley, Improved oil recovery by low-salinity waterflooding, J. Pet. Technol. 63 (2011) 106–112.
[12] T. Austad, A. RezaeiDoust, T. Puntervold, Chemical mechanism of low salinity water flooding in sandstone reservoirs, SPE Improved Oil Recovery Symposium, Society of Petroleum Engineers, 2010.
[13] A.A. Hamouda, O.M. Valderhaug, Investigating enhanced oil recovery from sandstone by low-salinity water and fluid/rock interaction, Energy Fuel 28 (2014) 898–908.
[14] K.C. Khilar, H.S. Fogler, The existence of a critical salt concentration for particle release, J. Colloid Interface Sci. 101 (1984) 214–224.
[15] S. Kia, H. Fogler, M. Reed, Effect of pH on colloidally induced fines migration, J. Colloid Interface Sci. 118 (1987) 158–168.
[16] E. Rosenbrand, C. Kjøller, J.F. Riis, F. Kets, I.L. Fabricius, Different effects of temperature and salinity on permeability reduction by fines migration in Berea sandstone, Geothermics 53 (2015) 225–235.
[17] S. Bhattacharya, J. Paitaridis, A. Pedler, A. Badalyan, Y. Yang, T. Carageorgos, P. Bedrikovetsky, D. Warren, N. Lemon, Fines mobilisation by low-salinity water injection: 3-point-pressure tests, SPE International Conference and Exhibition on Formation Damage Control, Society of Petroleum Engineers, 2016.
[18] D. Arab, P. Pourafshary, Nanoparticles-assisted surface charge modification of the porous medium to treat colloidal particles migration induced by low salinity water flooding, Colloids Surf. A 436 (2013) 803–814.
[19] V.A. Tabrizy, R. Denoyel, A. Hamouda, Characterization of wettability alteration of calcite, quartz and kaolinite: surface energy analysis, Colloids Surf. A 384 (2011) 98–108.
[20] N. Griffith, Y. Ahmad, H. Daigle, C. Huh, Nanoparticle-stabilized natural gas liquid-in-water emulsions for residual oil recovery, SPE Improved Oil Recovery Conference, Society of Petroleum Engineers, 2016.
[21] A.D. Monfared, M.H. Ghazanfari, M. Jamialahmadi, A. Helalizadeh, Adsorption of silica nanoparticles onto calcite: equilibrium, kinetic, thermodynamic and DLVO analysis, Chem. Eng. J. 281 (2015) 334–344.
[22] N. Seetha, S. Majid Hassanizadeh, M. Kumar, A. Raoof, Correlation equations for average deposition rate coefficients of nanoparticles in a cylindrical pore, Water Resour. Res. 51 (2015) 8034–8059.
[23] K.C. Khilar, H.S. Fogler, Migrations of Fines in Porous media, Springer Science & Business Media, 1998.
[24] T. Zhang, M.J. Murphy, H. Yu, H.G. Bagaria, K.Y. Yoon, B.M. Nielson, C.W. Bielawski, K.P. Johnston, C. Huh, S.L. Bryant, Investigation of nanoparticle adsorption during transport in porous media, SPE J. 20 (04) (2015) 667–677.
[25] K.A. Dunphy Guzman, M.P. Finnegan, J.F. Banfield, Influence of surface potential on aggregation and transport of titania nanoparticles, Environ. Sci. Technol. 40 (2006) 7688–7693.
[26] J.N. Israelachvili, Intermolecular and Surface Forces, Academic press, 2011.
[27] O. Karoussi, A.A. Hamouda, Imbibition of sulfate and magnesium ions into carbonate rocks at elevated temperatures and their influence on wettability alteration and oil recovery, Energy Fuel 21 (2007) 2138–2146.
[28] A. Martinez, A.P. Byrnes, Modeling dielectric-constant values of geologic materials: an aid to ground-penetrating radar data collection and interpretation, Kansas, Geological Survey, University of Kansas Lawrence, KS, USA, 2001.
[29] I. Malitson, Interspecimen comparison of the refractive index of fused silica, Josa 55 (1965) 1205–1209.
[30] M. Querry, Optical Constants of Minerals and Other Materials from the Millimeter to the Ultraviolet, Chemical Research Development And Engineering Center Aberdeen Proving Groundmd, 1987.
[31] J. Schembre, G.-Q. Tang, A. Kovscek, Wettability alteration and oil recovery by water imbibition at elevated temperatures, J. Pet. Sci. Eng. 52 (2006) 131–148.
[32] C.O. Metin, J.R. Baran, Q.P. Nguyen, Adsorption of surface functionalized silica nanoparticles onto mineral surfaces and decane/water interface, J. Nanopart. Res. 14 (2012) 1246.
[33] R. Abhishek, A.A. Hamouda, Effect of various silica nanofluids: reduction of fines migrations and surface modification of berea sandstone, Appl. Sci. 7 (2017) 1216.
[34] S. Li, A.T. Kaasa, L. Hendraningrat, O. Torsæter, Effect of silica nanoparticles adsorption on the wettability index of Berea sandstone, Paper SCA2013-059 Presented at the International Symposium of the Society of core Analysts Held in Napa Valley, California, USA, (2013), pp. 16–19.
[35] B. Yuan, R.G. Moghanloo, D. Zheng, Analytical evaluation of nanoparticle application to mitigate fines migration in porous media, SPE J. 21 (2) (2016) 317-312,332.
[36] T. Zhang, M.J. Murphy, H. Yu, H.G. Bagaria, K.Y. Yoon, B.M. Nielson, C.W. Bielawski, K.P. Johnston, C. Huh, S.L. Bryant, Investigation of nanoparticle adsorption during transport in porous media, SPE J. 20 (2015) 667–677.
[37] W. Stumm, J.J. Morgan, Aquatic Chemistry; an Introduction Emphasizing Chemical Equilibria in Natural Waters, (1970).
[38] R. Abhishek, A. Hamouda, A. Ayoub, Effect of silica nanoparticles on fluid/rock interactions during low salinity water flooding of chalk reservoirs, Appl. Sci. 8 (2018) 1093.
[39] A. Hamouda, O. Valderhaug, R. Munaev, H. Stangeland, Possible mechanisms for oil recovery from chalk and sandstone rocks by low salinity water (LSW), SPE Improved Oil Recovery Symposium, Society of Petroleum Engineers, 2014.
[40] G.-Q. Tang, N.R. Morrow, Influence of brine composition and fines migration on crude oil/brine/rock interactions and oil recovery, J. Pet. Sci. Eng. 24 (1999) 99–111.
[41] V. Akhmetgareev, R. Khisamov, 40 Years of Low-Salinity Waterflooding in Pervomaiskoye Field, Russia: Incremental Oil, SPE European Formation Damage Conference and Exhibition, Society of Petroleum Engineers, 2015.
[42] A. Zeinijahromi, V. Ahmetgareev, P. Bedrikovetsky, Case study of 25 years of low salinity water injection, SPE/IATMI Asia Pacific Oil & Gas Conference and Exhibition, Society of Petroleum Engineers, 2015.
[43] A. Merdhah, A. Yassin, Scale formation due to water injection in Berea sandstone cores, J. Appl. Sci 9 (2009) 3298–3307.
[44] L. Hendraningrat, S. Li, O. Torsater, Effect of some parameters influencing enhanced oil recovery process using silica nanoparticles: an experimental investigation, SPE Reservoir Characterization and Simulation Conference and Exhibition, Society of Petroleum Engineers, 2013.
[45] E. Joonaki, S. Ghanaatian, The application of nanofluids for enhanced oil recovery: effects on interfacial tension and coreflooding process, Pet. Sci. Technol. 32 (2014) 2599–2607.
[46] R.N. Vaidya, H.S. Fogler, Formation damage due to colloidally induced fines migration, Colloids Surf. 50 (1990) 215–229.
[47] T. Huang, J. Han, G. Agrawal, P. Sookprasong, Coupling nanoparticles with waterflooding to increase water sweep efficiency for high fines-containing reservoir-lab and reservoir simulation results, SPE Annual Technical Conference and Exhibition, Society of Petroleum Engineers, 2015.
[48] A. RezaeiDoust, T. Puntervold, S. Strand, T. Austad, Smart water as wettability modifier in carbonate and sandstone: a discussion of similarities/differences in the chemical mechanisms, Energy Fuel 23 (2009) 4479–4485.
[49] I. Fjelde, S.M. Asen, A.V. Omekeh, Low salinity water flooding experiments and interpretation by simulations, SPE Improved Oil Recovery Symposium, Society of Petroleum Engineers, 2012.

**Effect of salinity on Silica Nanoparticle adsorption kinetics and mechanisms for fluid/rock interaction with calcite.**

A. A. Hamouda, Abhishek, R. (2019).

Nanomaterials, 9(2): 213. Special issue: Applications of Nano-Technology for Oil Recovery, MDPI Publications.

Paper IV

nanomaterials

MDPI

*Article*

# Effect of Salinity on Silica Nanoparticle Adsorption Kinetics and Mechanisms for Fluid/Rock Interaction with Calcite

**Aly A. Hamouda * and Rockey Abhishek**

Institute of Energy and Petroleum Technology, University of Stavanger, Stavanger-4036, Norway; rockey.abhishek@uis.no

* Correspondence: aly.hamouda@uis.no; Tel.: +47-957-026-04

Received: 19 December 2018; Accepted: 31 January 2019; Published: 6 February 2019

**Abstract:** This study addresses the kinetics of silica nanoparticle adsorption on calcite from a solution at three salinities: deionized water (DIW), synthetic seawater (SSW), and low salinity water (LSW). The nanoparticle adsorption mechanisms and the effects on calcite dissolution are addressed. It was shown that nanoparticle adsorption was best described with the second-order-kinetic model and that silica nanoparticle adsorption reduced calcite dissolution. This was confirmed by measuring the $Ca^{2+}$ ion concentration, the pH, and by estimating the amount of calcite dissolved. This is an important conclusion of this work, especially as LSW as an enhanced oil recovery technique is a candidate for use in chalk fields. Less formation damage/dissolution of chalk when silica nanoparticles are combined with LSW can lower the risk of reservoir subsidence. Intraparticle diffusion and the pseudo-second-order models, indicated a reduction in the adsorption rate with increasing nanoparticle concentration in LSW. This is explained by possible repulsive forces among the nanoparticles as they diffuse from the bulk fluid onto the calcite surface. Ion charges reduce the repulsion among the nanoparticles through shielding. However, an increasing nanoparticle concentration reduces the shielding efficiency by the ions. Estimates of the surface forces confirmed that nanoparticle–mineral interaction is less attractive in LSW as compared to SSW and DIW.

**Keywords:** chalk; silica NP; calcite dissolution; adsorption kinetics; intraparticle diffusion; kinetics of NP/chalk interaction; interaction forces in presence of salt

## 1. Introduction

Nanofluids are colloidal dispersions of nanoparticles with sizes below 100 nm dispersed in a suitable medium. Over the past decade, nanofluids have attracted a lot of attention for enhanced oil recovery (EOR) from petroleum reservoirs [1–4]. The effectiveness of nanoparticles (NP) for enhancing oil recovery has been investigated by many researchers [2,5–11]. Among the various metal oxide nanoparticles, silica has emerged as a promising material for EOR due to: (1) ease of surface functionalization, (2) good transport properties in the reservoir, and (3) wettability change due to adsorption of silica nanoparticles on the rock surface [12–14]. In addition, silica nanoparticles have found applications in fields such as $CO_2$ reforming [15], removal of organic and inorganic pollutants [16], drug delivery [17], environmental materials [18], among others. Since the incremental oil recovery obtained from the application of silica nanoparticles is generally attributed to the wettability alteration, the adsorption of nanoparticles on the rock surface is of primary importance for modifying the rock surface from an oil-wet to a water-wet state.

While some studies have addressed the adsorption behavior of nanoparticles in sandstone reservoirs [12,19–23], few investigations have addressed the applicability of nanoparticles to carbonate reservoirs [24–28]. Nazari Moghaddam et al. [29] addressed the applicability of nanoparticles in altering the wettability of carbonate reservoirs. Al-Anssari, et al. [30] reported that silica nanoparticle adsorption on the calcite surface is irreversible and it can cause wettability alteration from an oil/mixed-wet to water-wet state. Their research group also reported that the silica nanofluid treatment was more effective at elevated temperatures [24]. Monfared, et al. [31] studied silica nanoparticle adsorption on calcite surfaces and the effect of salinity and pH on the adsorption process. However, the adsorption of silica nanoparticles on the calcite mineral, which is the major constituent of chalk reservoirs, is not well understood.

Chalk reservoirs are highly porous but have low permeability. Chalk reservoirs have pore throats in the order of 0.2 μm [32]. The use of micro particles of silica could lead to a blockage of the pore throats and hence nanoparticles with particle size of less than 100 nm are ideal for chalk reservoirs. Previous work in our lab [33] addressed the adsorption of silica nanoparticles dispersed in different brines on chalk surfaces and their effect on fluid/rock interaction especially during combined nanoparticle and low salinity water injection. Low salinity water flooding has emerged as a cheap and environmentally friendly technique for improving oil recovery [34–41]. Increased calcite dissolution induced by the interaction between the injected low salinity water and calcite [42–45] during flooding may lead to a loss of rock integrity [46]. However, we found that silica nanoparticles could reduce calcite dissolution by ≈30% induced by low salinity flooding of chalk, in addition to increasing oil recovery that can be achieved by low salinity flooding alone [33]. The adsorption behavior of nanoparticles was studied during the flooding process. The present work focuses on the kinetic aspects of the adsorption process on the calcite mineral. Batch adsorption experiments were carried out at three salinities: deionized water (no added salts), seawater (high salinity) and low salinity water (at 1:10 seawater dilution). Additionally, the calcium ion concentration and pH were tracked during the batch adsorption experiments to address the effect of nanoparticle adsorption on calcite dissolution.

## 2. Materials and Methods

The silica nanoparticles (DP9711) were obtained at 30% weight (wt.) concentration from Nyacol Nano Technologies dispersed in deionized water (DIW). The nanofluids were prepared by diluting the stock dispersion with appropriate fluids. While aggregation is an issue with nanoparticles in general, the stability of the used nanoparticles (DP9711) in DIW, synthetic seawater (SSW), and low salinity water (LSW) with 1:10 SSW dilution has been investigated previously [33]. We found that after three months, particle size measurements were close to the initial measured values (within 5 nm). In addition, the nanofluids remained visually clear with no sign of sedimentation. Calcite mineral powder of analytical grade was acquired from Riedel-de Haen AG (Hannover, Germany). The specific surface area of the calcite powder (0.23 $m^2/g$) has been determined previously in our lab [34]. SSW (pH 7.45) and LSW (pH 7.32) were the brines used in this study. LSW at 1:10 dilution was used based on our previous work for the assessment of the best dilution performance as an EOR method [40,46]. The ionic composition of the brines is listed in Table 1.

**Table 1.** Ionic composition of brines.

| Ion | synthetic seawater (SSW) (mol/L) | low salinity water (LSW) (mol/L) |
|---|---|---|
| $HCO^{3-}$ | 0.002 | 0.0002 |
| $Cl^-$ | 0.525 | 0.0525 |
| $SO_4^{2-}$ | 0.0240 | 0.0024 |
| $Mg^{2+}$ | 0.045 | 0.0045 |
| $Ca^{2+}$ | 0.013 | 0.0013 |
| $Na^+$ | 0.450 | 0.045 |
| $K^+$ | 0.010 | 0.0010 |

The nanofluids were prepared at 1 g/L nanoparticle concentration in DIW, LSW, and SSW. The average particle size (hydrodynamic radius) and zeta potential (Smoluchowski model) of the silica nanoparticles were measured previously [33]. The zeta potential (Smoluchowski model) of calcite mineral powder dispersed in different fluids was also measured using a Zetasizer Nano ZSP from Malvern Instruments (Malvern, UK). The values are listed in Table 2.

**Table 2.** Particle size and Zeta potential of silica nanoparticles and calcite mineral. Deionized water—DIW.

| Material | Dispersing Fluid | Temperature (°C) | Hydrodynamic Radius (nm) | pH | Zeta-Potential (mV) |
|---|---|---|---|---|---|
| Silica nanoparticles | DIW | 25 | 18.76 | 6.0 | −30.7 |
| Silica nanoparticles | DIW | 50 | 19.29 | - | - |
| Silica nanoparticles | DIW | 80 | 19.7 | - | - |
| Silica nanoparticles | LSW | 25 | 18.96 | 7.2 | −12.1 |
| Silica nanoparticles | LSW | 50 | 19.1 | - | - |
| Silica nanoparticles | LSW | 80 | 19.35 | - | - |
| Silica nanoparticles | SSW | 25 | 28.18 | 7.3 | −6.4 |
| Silica nanoparticles | SSW | 50 | 28.77 | - | - |
| Silica nanoparticles | SSW | 80 | 44.06 | - | - |
| Calcite | DIW | 25 | - | 9.62 | −23.4 |
| Calcite | LSW | 25 | - | 8.39 | −8.0 |
| Calcite | SSW | 25 | - | 7.56 | −3.7 |

### *2.1. Adsorption Experiments*

Five grams of calcite powder was dispersed in 30 mL of nanofluid. The nanofluid was prepared at a predetermined nanoparticle concentration and dispersion fluid salinity. The nanofluid-calcite dispersion was placed in a 50 mL capped centrifuge tube. The tube containing the nanofluid and the mineral was then agitated on a rotary agitator for the desired length of time. At the end of the period, the mineral was removed from the fluid by centrifuging at 10,000 rpm and decanting the supernatant fluid. The supernatant fluid was then filtered through a 0.22 μm filter, which allowed the nanoparticles to pass through but not the larger calcite mineral particles. The remaining concentration of the nanoparticles in the supernatant was determined by their absorbance in a dual beam UV/Vis (Ultraviolet–visible) spectrophotometer (UV/Vis 1800 spectrophotometer from Shimadzu Corporation, Kyoto, Japan) at 240 nm wavelength against DIW, comparing it with the calibration curves and making baseline corrections. The supernatant nanoparticle concentration was then used to estimate the amount of nanoparticles (adsorbate) adsorbed on the known amount of calcite mineral (adsorbent). A series of adsorption experiments were performed with increasing time until equilibrium adsorption was reached. To address the extent of calcite mineral dissolution, the pH of the supernatant was measured using S220 SevenCompact™ pH/ion meter by Mettler-Toledo International Inc (Columbus, OH, USA) calibrated with buffers of pH 7 and 10.1. The concentration of the $Ca^{2+}$ in the supernatant fluid was determined by Ion Chromatography (IC) using a Dionex ICS-5000 ion chromatograph from Thermo Fisher Scientific (Waltham, MA, USA). Additionally, mineral

dispersions prepared in different fluids (without nanoparticles) were also analyzed for $Ca^{2+}$ concentration and pH to obtain a baseline for comparison.

### *2.2. Surface Forces*

The interaction energies between the nanoparticle and calcite minerals affect the adsorption of nanoparticle on the mineral. The theory of surface forces can be utilized to calculate the interaction energies between the nanoparticles and calcite minerals based on the Derjaguin–Landau–Verwey–Overbeek (DLVO) theory. As a result of the size difference between the nanoparticles and mineral, the curvature of the mineral surface may be neglected and the interactions can be modeled based on Sphere–Plate collector geometry. The net interaction ($V_t$) as a function of separation distance ($h$) is the sum of London–van der Waal interaction ($V_{LVA}$) and Electric double layer interaction ($V_{EDLR}$), which can be calculated as:

$$V_t(h) = V_{LVA}(h) + V_{EDLR}(h), \tag{1}$$

where $k_B$ is the Boltzmann constant ($1.38 \times 10^{-23}$ J K$^{-1}$) and $T$ is temperature. The contributions, as a result of the different interactions in Equation 1 based on the constant potential approach, can be calculated as follows [31,47,48]:

$$V_{LVA}(h) = -\frac{A_{132}}{6}\left[\frac{a_p}{h} + \frac{a_p}{h+2a_p} + ln\left(\frac{h}{h+2a_p}\right)\right], \tag{2}$$

$$V_{EDLR}(h) = \pi\varepsilon_0\varepsilon_3\kappa\left(\zeta_p^2 + \zeta_s^2\right)\int_0^{a_p}\left(-coth\left[\kappa\left(h + a_p - a_p\sqrt{1-\left(h/a_p\right)^2}\right)\right] + coth\left[\kappa\left(h + a_p + a_p\sqrt{1-\left(h/a_p\right)^2}\right)\right] + \frac{\zeta_p\zeta_s}{\zeta_p^2+\zeta_s^2}csch\left[\kappa\left(h + a_p - a_p\sqrt{1-\left(h/a_p\right)^2}\right)\right] - \frac{\zeta_p\zeta_s}{\zeta_p^2+\zeta_s^2}csch\left[\kappa\left(h + a_p + a_p\sqrt{1-\left(h/a_p\right)^2}\right)\right]\right) r.dr, \tag{3}$$

where $a_p$ is the silica particle radius (m) and $A_{132}$ is the Hamaker's constant calculated according to the Lifshitz theory based on the refractive indices, dielectric constants, and the temperature [48]:

$$A_{132} \approx \frac{3}{4}K_bT\left(\frac{\varepsilon_1-\varepsilon_3}{\varepsilon_1+\varepsilon_3}\right)\left(\frac{\varepsilon_2-\varepsilon_3}{\varepsilon_2+\varepsilon_3}\right) + \frac{3h_o\nu_e}{8\sqrt{2}}\left(\frac{(\eta_1^2-\eta_3^2)(\eta_2^2-\eta_3^2)}{((\eta_1^2+\eta_3^2)(\eta_2^2+\eta_3^2))^{\frac{1}{2}}((\eta_1^2+\eta_3^2)^{\frac{1}{2}}+(\eta_2^2+\eta_3^2)^{\frac{1}{2}})}\right), \tag{4}$$

where $\varepsilon_1(8)$, $\varepsilon_2(4.5,)$ and $\varepsilon_3(80)$ represent the static dielectric constants of the interacting species (mineral and nanoparticle) and the intervening media (water), respectively [49]. $\eta_1(1.66)$ [50], $\eta_2(1.45)$ [51], and $\eta_3(1.33)$ [52] represent the refractive indices at 0.5876 µm wavelength of the interacting species (mineral and nanoparticle) and the intervening media (water), respectively. The refractive index can vary by approximately $7.9 \times 10^{-3}$ between fresh water and salt water and its effect has been neglected [53]. Hence, in this study, the same value of refractive index is assumed for all mediums. $h_o$ is the Planck's constant ($6.626 \times 10^{-34}$ J s) and $\nu_e$ is the main electron absorption frequency in the ultraviolet region and its value is between 3–5 × $10^{15}$ s$^{-1}$ [50]. The permittivity of free space $\varepsilon_0$: $8.854 \times 10^{-12}$ C$^2$ J$^{-1}$ m$^{-1}$. $\zeta_p$ and $\zeta_s$ are the surface potentials of the nanoparticles and minerals, respectively, which can be considered as the zeta potential. The estimation of the surface forces in this study was performed at 25 °C. For DIW, the inverse Debye length can be taken as $(9.6 \times 10^{-7})^{-1}$ m$^{-1}$ [54]. For the saline mediums, the inverse Debye length ($\kappa^{-1}$) depends on the salinity of the intervening medium (LSW/SSW) and can be calculated as:

$$\kappa^{-1} = \sqrt{\frac{\varepsilon_0\varepsilon_w k_B T}{2e^2 I}}, \tag{5}$$

where $e$ is the elementary charge of an electron (C), $k_B$ is the Boltzmann constant, and $I$ is the ionic strength of the medium:

$$I = \frac{1}{2}\sum c_i Z_i^2, \tag{6}$$

where $c_i$ is the ion concentration of the i$^{th}$ species and $Z_i$ is the valence number of the i$^{th}$ species as listed in Table 1. The data used for the surface force calculation has been has been listed in Table 2. Finally, the total non-dimensionalized interaction energy ($V_{t,ND}$) can be calculated as follows:

$$V_{t,ND}(h) = \frac{(V_{LVA}(h)+V_{EDLR}(h))}{k_B \times T}. \quad (7)$$

## 3. Results and Discussions

Low salinity water injection has emerged as an EOR technique for chalk reservoirs [36–39]. LSW has also been shown to promote calcite dissolution [40,46] which can affect chalk matrix integrity and lead to subsidence. However, our previous work [33] showed that silica nanoparticles have a tendency to adsorb on calcite surface and reduce the solubility of calcite by about 30% during combined silica nanoparticles and low salinity flooding of chalk. This work addresses nanoparticle adsorption kinetics on calcite and its effect on fluid/mineral interaction. The adsorption of nanoparticles dispersed in water at three salinities (DIW, LSW, and SSW) and its influence on calcite dissolution mechanisms were investigated. The nanoparticle concentrations used were 1 g/L for all the fluids except an additional concentration of 1.5 g/L that was used in the case of LSW. The LSW used in this work was SSW diluted 1:10 by DIW. The selection of the LSW composition was based on our previous work as well as that of other researchers based on its performance as an EOR injection fluid.

### *3.1. Adsorption Kinetics*

The nanoparticle adsorption data obtained from the experiments described in section 2.1 were fitted to pseudo-first-order and pseudo-second-order models to address the order of the adoption process. The linearized form of the pseudo-first-order and second-order models can respectively be expressed as [31,55]:

$$\ln\left(q_{eq} - q(t)\right) = ln(q_{eq}) - k_1 t, \quad (8)$$

$$\frac{1}{q(t)} = \frac{1}{k_2 q_{eq}^2} + \frac{t}{q_{eq}}, \quad (9)$$

where $q(t)$ and $q_{eq}$ are the experimentally obtained data of nanoparticle adsorption (mg/g) on calcite at a given time ($t$) and equilibrium, respectively. $k_1$ (1/h) and $k_2$ (g/mg h) are the respective rate constants. The linear fits for kinetic adsorption data in DIW and SSW are shown in Figure 1. Figures 1 a,b, examine the linearity fit with the data by $ln(q_{eq}-q(t))$ vs. $t$ and $t/q(t)$ vs $t$, respectively, for pseudo-first and pseudo-second-order models. The slope and the intercept were used to estimate the rate constants and equilibrium adsorption for both models (Table 3). It is shown in Figure 1a and Table 3 that the $R^2$ correlation values of the linear fits are poor (0.88–0.94) for both DIW and SSW. Additionally, the model estimated equilibrium adsorption varies significantly from the experimentally observed level of equilibrium adsorption. Therefore, it may be concluded that the pseudo-first-order model does not describe the adsorption process well. However, the fits for adsorption in both DIW and SSW are excellent for the pseudo-second-order model (Figure 1b). The $R^2$ values are close to 1 and the model estimated equilibrium adsorption agrees well with the experimental data (Table 3). This indicates that the pseudo-second-order model best describes the adsorption of silica nanoparticle on the calcite surface. It is interesting to see that at elevated salinity, SSW, the adsorption rate is ≈3 times higher than that for DIW and the equilibrium adsorption almost doubled.

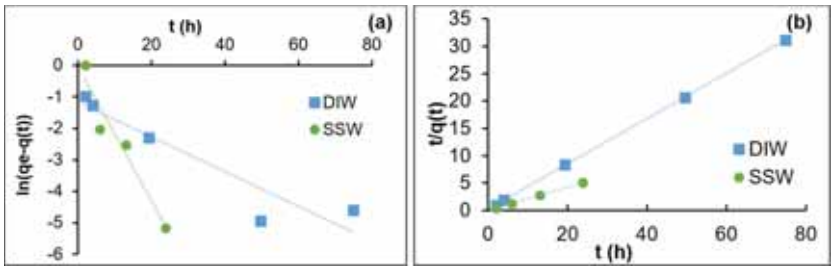


**Figure 1.** Data fit with kinetic models for the adsorption of nanoparticles on calcite in DIW and SSW: (**a**) pseudo-first-order (**b**) pseudo-second-order models.

**Table 3.** Summary of the fit parameters from the kinetic order data.

| **Pseudo-First-Order Model** | | | | |
|---|---|---|---|---|
| **Fluid** | **Exp $q_e$ (mg/g)** | **$R^2$** | **$k_1$ :(1/h)** | **Estimated $q_e$: (mg/g)** |
| DIW (nanoparticle conc 1 g/L) | 2.41 | 0.88 | 0.055 | 0.312 |
| SSW (nanoparticle conc 1 g/L) | 4.75 | 0.94 | 0.2132.5 | 0.971 |
| LSW (nanoparticle conc 1 g/L) | 4.4 | 0.9025 | 0.1149 | 1.09319 |
| LSW (nanoparticle conc 1.5 g/L) | 4.75 | 0.9378 | 0.0066 | 0.88923 |
| **Pseudo-Second-Order Model** | | | | |
| **Fluid** | **Exp $q_e$ (mg/g)** | **$R^2$** | **$k_2$: (g/mg h)** | **Estimated $q_e$: (mg/g)** |
| DIW (nanoparticle conc 1 g/L) | 2.41 | 0.99 | 0.73 | 2.41955 |
| SSW (nanoparticle conc 1 g/L) | 4.75 | 1 | 2.5 | 4.76644 |
| LSW (nanoparticle conc 1 g/L) | 4.4 | 1 | 0.191 | 4.44 |
| LSW (nanoparticle conc 1.5 g/L) | 4.75 | 0.99 | 0.11 | 5.68 |

To address the adsorption of nanoparticles in LSW, two sets of kinetic adsorption experiments were performed with two nanoparticle concentrations, 1 and 1.5 g/L, while the amount of the calcite was kept constant. It was shown that the adsorption data with the pseudo-second-order model for both nanoparticle concentrations fitted well. Figure 2a,b and Table 3 show the data fit, fitting coefficients, and the estimated equilibrium adsorption. It is shown in Figure 2a and Table 3 that $R^2$ for the first order are poor (0.9–0.93) for both concentration of nanoparticles in LSW and the model estimated equilibrium adsorption varies significantly from the experimentally observed level of equilibrium adsorption. It is therefore concluded that similar to the adsorption of nanoparticles from DIW and SSW, pseudo-second-order models describe the adsorption process well, as $R^2 \approx 1$ for both the concentrations and the model estimated equilibrium adsorption is close to the experimental equilibrium adsorption. It is interesting to note that as the nanoparticle concentration increases from 1 to 1.5 g/L, the rate of adsorption decreases from 0.191 to 0.11 *g/mg h*r. In addition, the adsorption rates in LSW (for both concentrations) are lower than the rate estimated for DIW and SSW. This observation is discussed in the following section. From the kinetic adsorption data discussed so far, it may be concluded that the adsorption for silica nanoparticles from the three dispersing fluids (DIW, SSW, and LSW) onto the calcite surface is a second-order process. The adsorption mechanism is discussed in the following section.

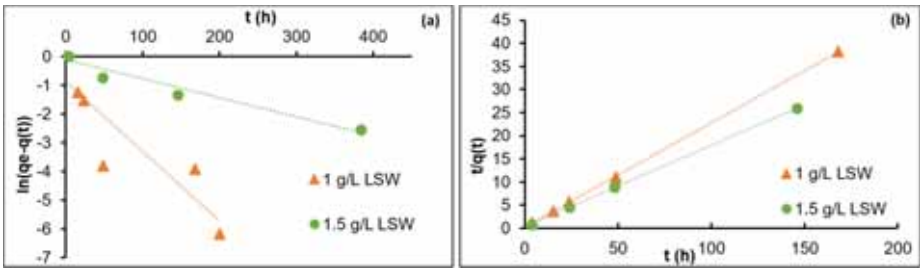


**Figure 2.** Data fit with kinetic models for the adsorption of nanoparticle on calcite in LSW: (**a**) pseudo-first-order (**b**) pseudo-second-order models.

### *3.2. Intraparticle Diffusion Model (IPD)*

The proposed model of Weber and Morris [56] has been applied in previous studies to understand adsorption mechanisms. The linear relationship between $q(t)$ and $t^{0.5}$ indicates the contribution of intraparticle diffusion. Wu et al. [57] used the fractional approach to equilibrium change to determine the IPD contribution to the adsorption kinetics as follows:

$$q_t = K\, t^{0.5} + C, \tag{10}$$

$$q_{eq} = K\, t_{eq}^{1.5} + C. \tag{11}$$

Rearrangement yields,

$$\frac{q_t}{q_{eq}} = 1 - R_i \left[1 - \left(\frac{t}{t_{eq}}\right)^{0.5}\right], \tag{12}$$

where

$$R_i = K \frac{t_{eq}^{0.5}}{q_{eq}}, \tag{13}$$

Here, $R_i$ is defined as the initial adsorption factor, $K$ (mg/g h$^{0.5}$), $q_t$ (mg/g), $q_{eq}$ (mg/g), t (hr), $t_{eq}$ (hr), and $C$ (mg/g) are the intraparticle diffusion rate, adsorbed amount at time t, adsorbed amount at equilibrium, time (h), the time to reach equilibrium, and initial adsorption amount (intercept). $R_i$ may also be expressed as the ratio of the initial adsorption to equilibrium adsorption amounts, which is used in this work

$$R_i = 1 - \frac{C}{q_{eq}}. \tag{14}$$

From Equation 14, if $C = 0$, that means there is no initial adsorption in the system.

Figure 3 shows the characteristic curves for DIW (nanoparticle conc 1 g/L), LSW (nanoparticle conc 1 g/L), LSW (nanoparticle conc 1.5 g/L), and SSW (nanoparticle conc 1 g/L) systems. Table 4 shows the classified adsorption characteristic according to Wu et al. [57]. In the case of DIW, LSW (1 g/L) and LSW (1.5 g/L) adsorption is classified as strong initial adsorption. That is, all the systems follow strong initial adsorption behavior except SSW (1 g/L), which is shown to be approaching complete initial adsorption, where $q_e$ is almost equal to C (initial adsorption amount). In addition, for SSW, the time to reach equilibrium is almost 50% less than that for the other systems.

**Table 4.** Summary of initial adsorption of intraparticle diffusion model (IPD) model.

| Fluid_ Nanoparticle Conc. | $C$ (mg/g) | $K$ (mg/g h$^{0.5}$) | $R_i$ | $t_{eq}$(hrs)_Adsorption Characterization |
|---|---|---|---|---|
| DIW_1.0 g/L | 1.8 | 0.16 | 0.25 | 49 (hrs)_ Strong initial adsorption |
| LSW_1.0 g/L | 2.13 | 0.51 | 0.52 | 49(hrs)_Strong initial adsorption |

| | | | | |
|---|---|---|---|---|
| LSW_1.5 g/L | 4.29 | 0.19 | 0.24 | 49(hrs)_Strong initial adsorption |
| SSW_1.0 g/L | 4.56 | 0.036 | 0.037 | 16(hrs)_near complete initial adsorption |

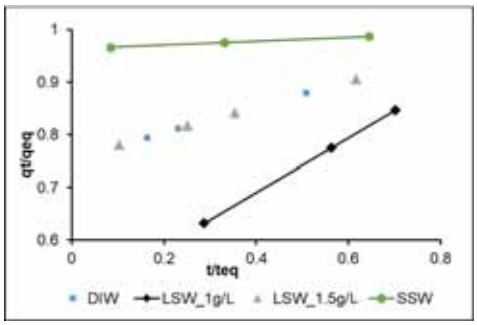


**Figure 3.** Non-dimensional intraparticle diffusion model for adsorption characteristic curves of the four tested systems with the dispersed silica nanoparticles.

The reduced *Ri* in LSW, as the nanoparticle concentration increases from 1 to 1.5 g/L to almost half may be explained by repulsive forces among the nanoparticles as they diffuse from the bulk fluid towards the calcite surface. In other words, the effect of ion charges could help to reduce the repulsive forces. However, the efficiency of the ion charges in shielding nanoparticles and reducing the repulsive forces among them is reduced as the nanoparticle concentration increases. This may also explain the lower adsorption rate observed for LSW with nanoparticles at 1.5 g/L during our investigation of the adsorption kinetic order in the earlier section.

Another interesting observation is that *Ri* is almost equal in both DIW and LSW (1.5 g/L), which may support the above hypothesis. That is to say, in the presence of dissolved salts, the ions work as a barrier reducing the adsorption rate and in the absence of salt ions (DIW) the repulsive force among the nanoparticles reduces the adsorption rate. This is an interesting phenomenon worth further investigation.

It is shown in Figure 4 that the total interaction energies, estimated by the DLVO theory, between nanoparticle and calcite mineral remain attractive at all separations in DIW and SSW. However, in the case of LSW, the interaction energy is shown to be less attractive and becomes slightly repulsive at around 30 nm separation. In other words, the LSW system involves more repulsive conditions compared to the SSW and DIW systems.

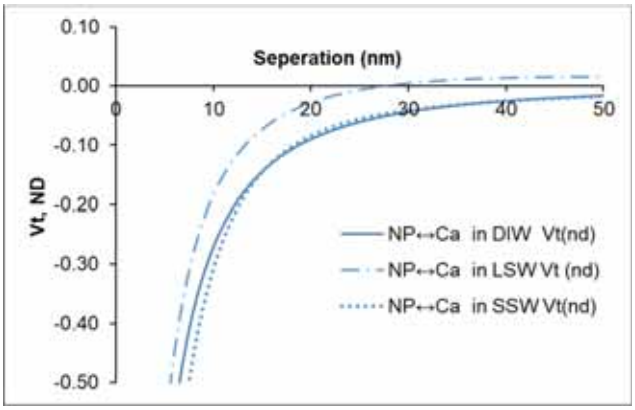


**Figure 4.** Total interaction energy between nanoparticles (1 g/L) and calcite (Ca) mineral in DIW, SSW, and LSW.

### *3.3. Fluid/Mineral Interaction*

Two main chemical processes may take place between fluids and mineral ($CaCO_3$). Those are dissolution and adsorption, as presented below:

$$CaCO_3 + H_2O \rightleftharpoons Ca^{2+} + HCO_3^- + OH^-, \quad (15)$$

$$2CaCO_3 + H_2O + NP \rightleftharpoons CaCO_3 - NP + Ca^{2+} + HCO_3^- + OH^-. \quad (16)$$

As shown in Equation 15, dissolution of calcite increases the pH. The adsorption process may be presented by Equation 16, where $OH^-$ and $HCO_3^-$ are among the reaction products. The above two reactions indicate an increase in the fluids' pH due to calcite dissolution.

The pH values with the dispersed nanoparticles in DIW, LSW, and SSW are 6.0, 7.2, and 7.3, respectively. The pH ranges vary depending on the fluid in which the adsorption and dissolution are taking place. That is, the pH is not controlled but the pH was monitored during the progression of the experiments. The changes in the pH with time during the experiments for the different dispersing fluids with and without nanoparticles are shown in Figure 5. The order of the pH values from highest to lowest for nanoparticle dispersing fluids are DIW > LSW(nanoparticle conc 1 g/L) > LSW(nanoparticle conc 1.5 g/L) > SSW. Generally, in all cases, during the dissolution/adsorption processes the pH declines. However, the changes are within about 0.3 pH units. The reduction may be explained by the formation of silanol, as a result of the dissociation of water molecules to form silanol groups and reduce the pH [58]:

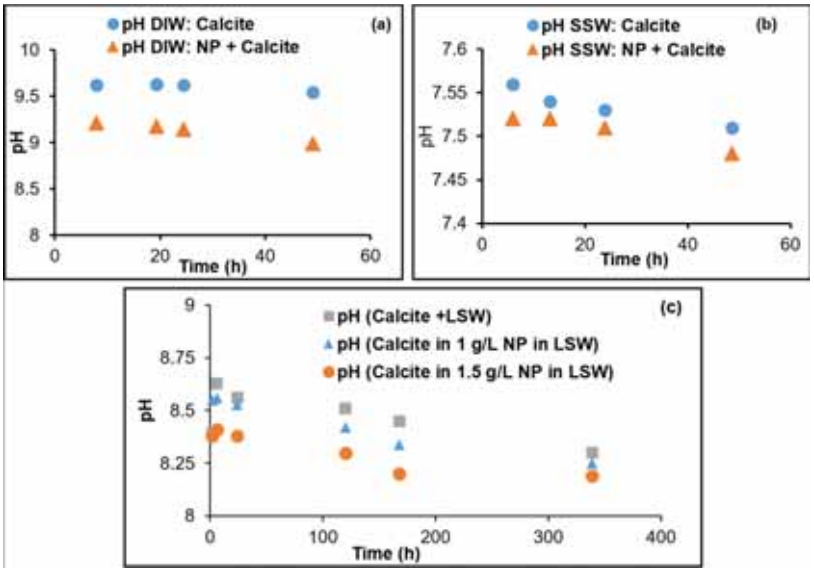


**Figure 5.** pHs of (**a**) DIW, (**b**) SSW, and (**c**) LSW (1 and 1.5 g/L) as a function of time during the kinetic adsorption tests.

$$-SiOH \rightleftharpoons -SiO^- + H^+. \quad (17)$$

In spite of the reduction of the pH, the dissolution of calcite is also reduced (this is discussed later), contrary to what is expected. There are two factors which contribute to less dissolution. The first is that the pH balance between calcite dissolution and formation of silanol shows an insignificant decrease in the pH, as discussed above. The second factor is the adsorption of the nanoparticles on the calcite surface which affects the dissolution and perhaps the formation of silanol.

Figure 6 shows the supernatant $Ca^{2+}$ and surface coverage with nanoparticles as a function of time in the cases of DIW and SSW. The contact barrier between the mineral and DIW is well demonstrated in Figure 6a. When the percentage coverage of the surface by the nanoparticles reached the equilibrium phase, the $Ca^{2+}$ concentrations reached a steady state at about 49 h. The $Ca^{2+}$ concentration was reduced (from ≈0.003 to ≈0.0015 mol/L) by about 50% with nanoparticle adsorption. In the case of SSW, Figure 6b demonstrates a reduction in $Ca^{2+}$ (≈ 0.0046 to 0.0041) of about 10% after 16 h, when the adsorption of the nanoparticle reached equilibrium for the percentage calcite surface coverage of about 27%. It is interesting to observe that the $Ca^{2+}$ concentrations decline rather than increase as a result of the solubility. Figure 7 for LSW (1 and 1.5 g/L nanoparticle concentration) shows similar observations as for SSW. The $Ca^{2+}$ concentrations decline after a concentration spike (without nanoparticles) reaching ≈0.011 mol/L compared to ≈0.0046 mol/L (with nanoparticles). The two most important observations are that $Ca^{2+}$ shows declining trends in both cases, LSW and SSW, as well as a higher initial spike in $Ca^{2+}$ concentration in the case of LSW compared to that of SSW. The reduction trend of $Ca^{2+}$ is difficult to explain. However, there are two possible mechanisms. The first is adsorption of $Ca^{2+}$ onto the silica surface according to the following equation [59]:

$$2\mathrm{SiOH} + \mathrm{Ca}^{2+} \rightleftharpoons (-\mathrm{SiO}^{-})_2\mathrm{Ca}^{2+} + 2\mathrm{H}^{+}. \quad (18)$$

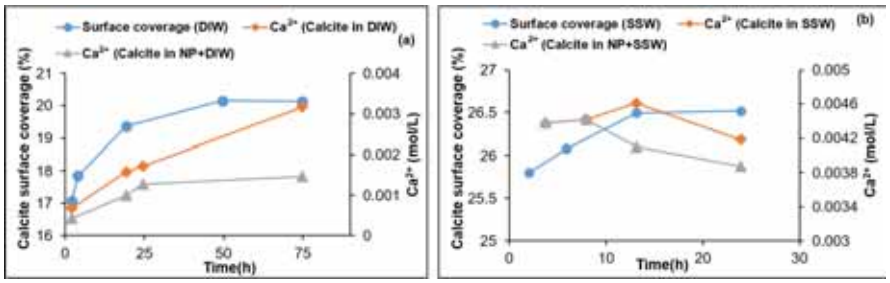


**Figure 6.** Supernatant $Ca^{2+}$ concentrations with and without nanoparticles and the estimated surface coverage by nanoparticles (**a**) DIW and (**b**) SSW fluids.

Equation 18 could support the reduction in $Ca^{2+}$. However, Janusz, Patkowski, and Chibowski [59] previously measured the $Ca^{2+}$ uptake by silica in solutions of ionic strength similar to the LSW used in the present study. They estimated an uptake capacity of ≈0.0016 µmol/L at a pH of 8. This reduction is much lower compared to the reductions in $Ca^{2+}$ concentrations in this study. Therefore, the uptake of calcium is not expected to be the main contributor to the observed $Ca^{2+}$ declining trend. The second hypothesis could be the formation of $CaSO_4$ due to possible reaction with $SO_4^{2-}$ ions present in both fluid cases (LSW and SSW). At the mineral–solution interface, assuming heterogeneous $Ca^{2+}$ distribution, the solubility product of the $CaSO_4$ may be exceeded. The smaller peak in the case of SSW (Figure 6b) may be the result of the higher $SO_4^{2-}$ ion concentration (65% higher than that with LSW). This would kinetically favor faster removal of $Ca^{2+}$ from the fluid in the form of $CaSO_4$, when the thermodynamic solubility product (Ksp) is reached. This may be supported by the case of the DIW, where $SO_4^{2-}$ is absent. We therefore believe that the second mechanism is the cause of this observation.

Figure 7 shows that as the nanoparticle concentration in LSW was increased from 1 to 1.5 g/L, the $Ca^{2+}$ concentration was further reduced at the onset of nanoparticle adsorption. As the adsorption progresses, the $Ca^{2+}$ concentration for the case of 1.5 g/L almost reached the same concentration as in the case of 1 g/L. Near the end of the experiment, in both cases the $Ca^{2+}$ concentration reached a level close to the $Ca^{2+}$ concentration in LSW. The observed decrease in $Ca^{2+}$ concentration may be related to the intraparticle diffusion phenomenon (discussed earlier) occurring after reaching the maximum calcite surface coverage by the nanoparticles. In both cases, $Ca^{2+}$ concentration reduction continues (Figure 7) reaching the lowest $Ca^{2+}$ concentration almost at the same rate until it reached the level of

$Ca^{2+}$ concentration in LSW. The $Ca^{2+}$ concentration after the nanoparticle surface coverage reached maximum (about 49 h, Table 4) was about 1.3 times higher for nanoparticle at 1 g/L (≈0.0032 mol/L) than that for 1.5 g/L (≈0.0024 mol/L). The amount of calcite dissolved was estimated from the areas under the produced $Ca^{2+}$ concentration curves in Figure 7 (with and without nanoparticles). The results are shown in Figure 8, where it demonstrates that an increasing nanoparticle concentration led to a lower amount of calcite dissolution. This can have profound implications when designing LSW flooding of chalk reservoirs.

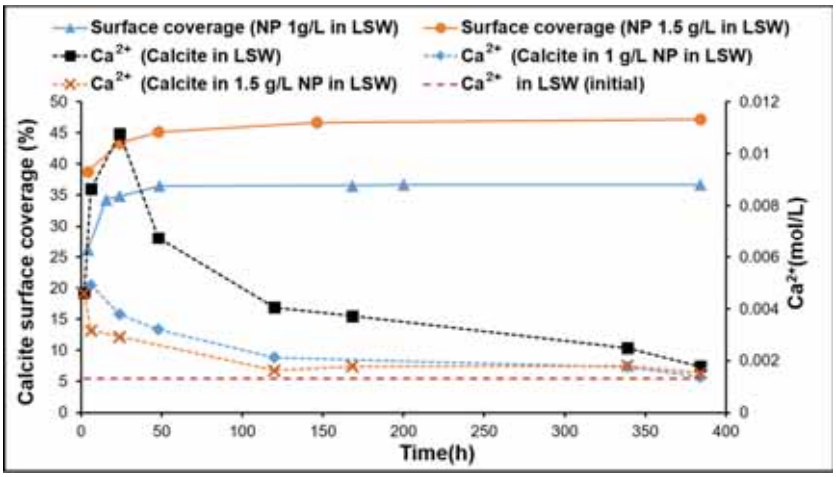


**Figure 7.** Supernatant $Ca^{2+}$ concentrations with and without nanoparticle and the estimated surface coverage by nanoparticles for LSW fluid.

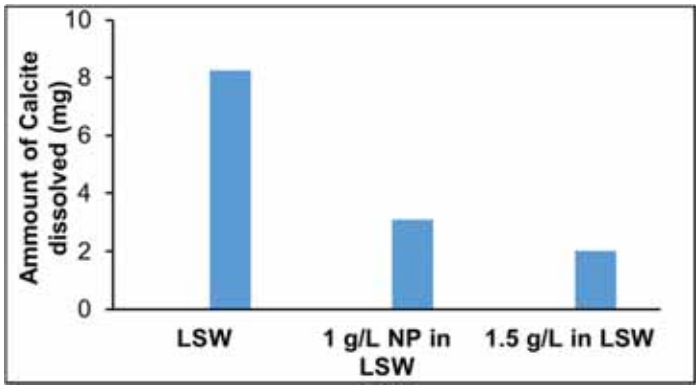


**Figure 8.** Amount on Calcite dissolved in LSW and with nanoparticle adsorption on calcite.

## 4. Conclusions

This study addressed the kinetics of silica nanoparticle adsorption dispersed in three saline waters (DIW, SSW, and LSW). Additionally, the dynamic calcite dissolution related to the progression of nanoparticle adsorption was addressed. On the basis of the observation and analysis made in this study, the following conclusions were made:

1. The adsorption of silica nanoparticles on calcite is best described with a pseudo-second-order model.
2. Both the rate of adsorption and the level of equilibrium adsorption increase substantially as the salinity increases from DIW to SSW.

3. The reduction by half of *Ri* in LSW as the nanoparticle concentration increases from 1 to 1.5 g/L may be explained by repulsive forces among the nanoparticles as they diffuse from the bulk fluid towards the calcite surface. This may also explain the lower adsorption rate observed for LSW with nanoparticles at 1.5 g/L during the investigation of adsorption kinetic order. The almost equal *Ri* in both DIW and LSW (1.5 g/L) supports the above hypothesis; where the presence of salt ions (in the LSW) acts as a barrier reducing the adsorption rate, and in the absence of salt ions (in the DIW), the repulsive forces among nanoparticles reduce the adsorption rate.
4. The estimation of the surface forces based on the DLVO theory showed that with nanoparticles in LSW, the interaction between nanoparticles and calcite mineral is less attractive in comparison with SSW and DIW.
5. Adsorption of silica nanoparticles reduces calcite dissolution. This was confirmed by the $Ca^{2+}$ ion concentration, pH, and lower dissolution observed at increased nanoparticle concentrations. Mass balance based on the analyzed $Ca^{2+}$ profile demonstrates the increased dissolution reduction with increasing nanoparticle concentration. This is an important outcome especially when LSW is a candidate for EOR in chalk fields, where less formation damage/dissolution of chalk is expected when silica nanoparticles are combined with LSW.

**Author Contributions:** A.A.H. and R.A. designed the study. The experiments were performed by R.A. The analysis was done by both authors. The manuscript was written by A.A.H. and R.A.

**Funding:** This research received no external funding.

**Acknowledgments:** The authors would like to thank the University of Stavanger (UiS), Norway, for funding this study. The authors thank Prof. Lutz Eichacker (UiS) for providing access to DLS equipment. Finally, the authors thank NYACOL® Nano Technologies Inc. for supplying DP9711 nanofluid used in this study.

**Conflicts of Interest:** The authors declare no conflict of interest. The funding sponsors had no role in the design of the study; in the collection, analyses, or interpretation of data; in the writing of the manuscript, and in the decision to publish the results.

## References

1. Ayatollahi, S.; Zerafat, M.M. In Nanotechnology-assisted eor techniques: New solutions to old challenges. In Proceedings of the SPE International Oilfield Nanotechnology Conference and Exhibition, Noordwijk, The Netherlands, 12–14 June 2012.
2. Zhang, H.; Nikolov, A.; Wasan, D. Enhanced oil recovery (eor) using nanoparticle dispersions: Underlying mechanism and imbibition experiments. *Energy Fuels* **2014**, *28*, 3002–3009.
3. Saboorian-Jooybari, H.; Dejam, M.; Chen, Z. Heavy oil polymer flooding from laboratory core floods to pilot tests and field applications: Half-century studies. *J. Pet. Sci. Eng.* **2016**, *142*, 85–100.
4. Chávez-Miyauchi, T.S.E.; Firoozabadi, A.; Fuller, G.G. Nonmonotonic elasticity of the crude oil–brine interface in relation to improved oil recovery. *Langmuir* **2016**, *32*, 2192–2198.
5. Behzadi, A.; Mohammadi, A. Environmentally responsive surface-modified silica nanoparticles for enhanced oil recovery. *J. Nanoparticle Res.* **2016**, *18*, 1–19.
6. Hendraningrat, L.; Torsæter, O. A stabilizer that enhances the oil recovery process using silica-based nanofluids. *Transp. Porous Media* **2015**, *108*, 679–696.
7. Ogolo, N.; Olafuyi, O.; Onyekonwu, M. Enhanced oil recovery using nanoparticles. In Proceedings of the SPE Saudi Arabia Section Technical Symposium and Exhibition, Al-Khobar, Saudi Arabia, 8–11 April 2012.
8. Shahrabadi, A.; Bagherzadeh, H.; Roostaie, A.; Golghanddashti, H. Experimental investigation of hlp nanofluid potential to enhance oil recovery: A mechanistic approach. In Proceedings of the SPE International Oilfield Nanotechnology Conference and Exhibition, Noordwijk, The Netherlands, 12–14 June 2012.
9. Ortega, D.J.S.; Kim, H.B.; James, L.A.; Johansen, T.E.; Zhang, Y. The effectiveness of silicon dioxide sio 2 nanoparticle as an enhanced oil recovery agent in ben nevis formation, hebron field, offshore eastern canada. In Proceedings of the Abu Dhabi International Petroleum Exhibition & Conference, Abu Dhabi, UAE, 7–10 November 2016.

10. Haroun, M.R.; Alhassan, S.; Ansari, A.A.; Al Kindy, N.A.M.; Abou Sayed, N.; Kareem, A.; Ali, B.; Sarma, H.K. Smart nano-eor process for abu dhabi carbonate reservoirs. In Proceedings of the Abu Dhabi International Petroleum Conference and Exhibition, Abu Dhabi, UAE, 11–14 November 2012.
11. Agista, M.; Guo, K.; Yu, Z. A state-of-the-art review of nanoparticles application in petroleum with a focus on enhanced oil recovery. *Appl. Sci.* **2018**, *8*, 871.
12. Hendraningrat, L.; Li, S.; Torsæter, O. A coreflood investigation of nanofluid enhanced oil recovery. *J. Pet. Sci. Eng.* **2013**, *111*, 128–138.
13. Maghzi, A.; Mohammadi, S.; Ghazanfari, M.H.; Kharrat, R.; Masihi, M. Monitoring wettability alteration by silica nanoparticles during water flooding to heavy oils in five-spot systems: A pore-level investigation. *Exp. Therm. Fluid Sci.* **2012**, *40*, 168–176.
14. Li, S.; Torsæter, O. Experimental investigation of the influence of nanoparticles adsorption and transport on wettability alteration for oil wet berea sandstone. In Proceedings of the SPE Middle East Oil & Gas Show and Conference, Manama, Bahrain, 8–11 March 2015.
15. Lovell, C.E.; Scott, J.; Amal, R. Ni-sio2 catalysts for the carbon dioxide reforming of methane: Varying support properties by flame spray pyrolysis. *Molecules* **2015**, *20*, 4594–4609.
16. Walcarius, A.; Mercier, L.J.J. Mesoporous organosilica adsorbents: Nanoengineered materials for removal of organic and inorganic pollutants. *J. Mater. Chem.* **2010**, *20*, 4478–4511.
17. Slowing, I.I.; Vivero-Escoto, J.L.; Wu, C.-W.; Lin, V.S. Mesoporous silica nanoparticles as controlled release drug delivery and gene transfection carriers. *Adv. Drug Deliv. Rev.* **2008**, *60*, 1278–1288.
18. Di Credico, B.; Bellobono, I.R.; Arienzo, M.; Fumagalli, D.; Redaelli, M.; Scotti, R.; Morazzoni, F. Efficacy of the reactive oxygen species generated by immobilized $TiO_2$ in the photocatalytic degradation of diclofenac. *Int. J. Photoenergy* **2015**, *2015*, 919217.
19. Zhang, T.; Murphy, M.J.; Yu, H.; Bagaria, H.G.; Yoon, K.Y.; Nielson, B.M.; Bielawski, C.W.; Johnston, K.P.; Huh, C.; Bryant, S.L. Investigation of nanoparticle adsorption during transport in porous media. *SPE J.* **2015**, *20*, 667–677.
20. Zhang, T.; Murphy, M.; Yu, H.; Huh, C.; Bryant, S.L. Mechanistic model for nanoparticle retention in porous media. *Transp. Porous Media* **2016**, *115*, 387–406.
21. Li, S.; Torsæter, O. The impact of nanoparticles adsorption and transport on wettability alteration of water wet berea sandstone. In Proceedings of the SPE/IATMI Asia Pacific Oil & Gas Conference and Exhibition, Muscat, Oman, 26–28 January 2015.
22. Abhishek, R.; Hamouda, A.A.; Murzin, I. Adsorption of silica nanoparticles and its synergistic effect on fluid/rock interactions during low salinity flooding in sandstones. *Colloids Surf. A Physicochem. Eng. Asp.* **2018**, *555*, 397–406.
23. Abhishek, R.; Hamouda, A.A. Effect of various silica nanofluids: Reduction of fines migrations and surface modification of berea sandstone. *Appl. Sci.* **2017**, *7*, 1216.
24. Al-Anssari, S.; Wang, S.; Barifcani, A.; Lebedev, M.; Iglauer, S. Effect of temperature and sio 2 nanoparticle size on wettability alteration of oil-wet calcite. *Fuel* **2017**, *206*, 34–42.
25. Roustaei, A.; Bagherzadeh, H. Experimental investigation of sio2 nanoparticles on enhanced oil recovery of carbonate reservoirs. *J. Pet. Explor. Prod. Technol.* **2015**, *5*, 27–33.
26. Abhishek, R.; Kumar, G.S.; Sapru, R. Wettability alteration in carbonate reservoirs using nanofluids. *Pet. Sci. Technol.* **2015**, *33*, 794–801.
27. Abhishek, R.; Bagalkot, N.; Kumar, G.S. Effect of transverse forces on velocity of nanoparticles through a single fracture in a fractured petroleum reservoir. *Int. J. OilGas Coal Technol.* **2016**, *12*, 379–395.
28. Nwidee, L.N.; Al-Anssari, S.; Barifcani, A.; Sarmadivaleh, M.; Lebedev, M.; Iglauer, S. Nanoparticles influence on wetting behaviour of fractured limestone formation. *J. Pet. Sci. Eng.* **2017**, *149*, 782–788.
29. Nazari Moghaddam, R.; Bahramian, A.; Fakhroueian, Z.; Karimi, A.; Arya, S. Comparative study of using nanoparticles for enhanced oil recovery: Wettability alteration of carbonate rocks. *Energy Fuels* **2015**, *29*, 2111–2119.
30. Al-Anssari, S.; Barifcani, A.; Wang, S.; Iglauer, S. Wettability alteration of oil-wet carbonate by silica nanofluid. *J. Colloid Interface Sci.* **2016**, *461*, 435–442.
31. Monfared, A.D.; Ghazanfari, M.; Jamialahmadi, M.; Helalizadeh, A. Adsorption of silica nanoparticles onto calcite: Equilibrium, kinetic, thermodynamic and dlvo analysis. *Chem. Eng. J.* **2015**, *281*, 334–344.
32. van Oort, E.; Van Velzen, J.; Leerlooijer, K. Impairment by suspended solids invasion: Testing and prediction. *SPE Prod. Facil.* **1993**, *8*, 178–184.

33. Abhishek, R.; Hamouda, A.; Ayoub, A. Effect of silica nanoparticles on fluid/rock interactions during low salinity water flooding of chalk reservoirs. *Appl. Sci.* **2018**, *8*, 1093.
34. Hamouda, A.A.; Rezaei Gomari, K.A. Influence of temperature on wettability alteration of carbonate reservoirs. In Proceedings of the SPE/DOE Symposium on Improved Oil Recovery, Tulsa, OK, USA, 22–26 April 2006.
35. Hamouda, A.; Valderhaug, O.; Munaev, R.; Stangeland, H. Possible mechanisms for oil recovery from chalk and sandstone rocks by low salinity water (lsw). In Proceedings of the SPE Improved Oil Recovery Symposium, Tulsa, OK, USA, 12–16 April 2014.
36. Zahid, A.; Shapiro, A.A.; Skauge, A. Experimental studies of low salinity water flooding carbonate: A new promising approach. In Proceedings of the SPE EOR Conference at Oil and Gas West Asia, Muscat, Oman, 16–18 April 2012.
37. Mahani, H.; Keya, A.L.; Berg, S.; Bartels, W.-B.; Nasralla, R.; Rossen, W.R. Insights into the mechanism of wettability alteration by low-salinity flooding (lsf) in carbonates. *Energy Fuels* **2015**, *29*, 1352–1367.
38. Al-Nofli, K.; Pourafshary, P.; Mosavat, N.; Shafiei, A. Effect of initial wettability on performance of smart water flooding in carbonate reservoirs—an experimental investigation with ior implications. *Energies* **2018**, *11*, 1394.
39. Wang, X.; Alvarado, V. Kaolinite and silica dispersions in low-salinity environments: Impact on a water-in-crude oil emulsion stability. *Energies* **2011**, *4*, 1763.
40. Hamouda, A.A.; Gupta, S. Enhancing oil recovery from chalk reservoirs by a low-salinity water flooding mechanism and fluid/rock interactions. *Energies* **2017**, *10*, 576.
41. Rezaei Gomari, S.; Joseph, N. Study of the effect of clay particles on low salinity water injection in sandstone reservoirs. *Energies* **2017**, *10*, 322.
42. Omekeh, A.V.; Friis, H.A.; Fjelde, I.; Evje, S. Modeling of ion-exchange and solubility in low salinity water flooding. In Proceedings of the SPE Improved Oil Recovery Symposium, Tulsa, OK, USA, 14–18 April 2012; p. 13.
43. Alagic, E.; Spildo, K.; Skauge, A.; Solbakken, J. Effect of crude oil ageing on low salinity and low salinity surfactant flooding. *J. Pet. Sci. Eng.* **2011**, *78*, 220–227.
44. Mahani, H.; Keya, A.L.; Berg, S.; Bartels, W.-B.; Nasralla, R.; Rossen, W. Driving mechanism of low salinity flooding in carbonate rocks. In Proceedings of the EUROPEC 2015, Madrid, Spain, 1–4 June 2015.
45. Patwardhan, S.D.; Singh, D.; Abhishek, R.; Suresh Kumar, G. Modelling of mineral precipitation in fractures with variable aperture. *ISH J. Hydraul. Eng.* **2017**, *23*, 203–211.
46. Hamouda, A.A.; Maevskiy, E. Oil recovery mechanism (s) by low salinity brines and their interaction with chalk. *Energy Fuels* **2014**, *28*, 6860–6868.
47. Bhattacharjee, S.; Elimelech, M.J.J. Surface element integration: A novel technique for evaluation of dlvo interaction between a particle and a flat plate. *J. Colloid Interface Sci.* **1997**, *193*, 273–285.
48. Dunphy Guzman, K.A.; Finnegan, M.P.; Banfield, J.F. Influence of surface potential on aggregation and transport of titania nanoparticles. *Environ. Sci. Technol.* **2006**, *40*, 7688–7693.
49. Israelachvili, J.N. *Intermolecular and Surface Forces*; Academic Press: Cambridge, MA, USA, 2011.
50. Ghosh, G. Dispersion-equation coefficients for the refractive index and birefringence of calcite and quartz crystals. *Opt. Commun.* **1999**, *163*, 95–102.
51. Malitson, I. Interspecimen comparison of the refractive index of fused silica. *JOSA* **1965**, *55*, 1205–1209.
52. Hale, G.M.; Querry, M.R. Optical constants of water in the 200-nm to 200-μm wavelength region. *Appl. Opt.* **1973**, *12*, 555–563.
53. Temple, S.J.J. Effect of salinity on the refractive index of water: Considerations for archer fish aerial vision. *J. Fish Biol.* **2007**, *70*, 1626–1629.
54. Khilar, K.C.; Fogler, H.S. *Migrations of Fines in Porous Media*; Springer Science & Business Media: New York, NY, USA, 1998; Volume 12.
55. Ho, Y.-S.; McKay, G.J.P. Pseudo-second order model for sorption processes. *Process Biochem.* **1999**, *34*, 451–465.
56. Weber, W.; Morris, J. In *Removal of biologically-resistant pollutants from waste waters by adsorption*, Proceedings of the First International Conference on Water Pollution Research, 1962; Pergamon Press Oxford: pp 231–266.
57. Wu, F.-C.; Tseng, R.-L.; Juang, R.-S. Initial behavior of intraparticle diffusion model used in the description of adsorption kinetics. *Chem. Eng. J.* **2009**, *153*, 1–8.

58. Iler, R.K. *Chemistry of Silica—Solubility, Polymerization, Colloid and Surface Properties, and Biochemistry*; Wily: Hoboken, NJ, USA, 1979.
59. Janusz, W.; Patkowski, J.; Chibowski, S. Competitive adsorption of $ca^{2+}$ and zn(ii) ions at monodispersed $sio_2$/electrolyte solution interface. *J. Colloid Interface Sci.* **2003**, *266*, 259–268.

**Adsorption kinetics and Enhanced Oil Recovery by Silica nanoparticles in sandstone.**

Abhishek, R., A. A. Hamouda and F. Abdulhameed.

Petroleum Science and Technology, Taylor and Francis.
DOI: 10.1080/10916466.2019.1587455

Paper V